UNIVERSIDAD NACIONAL AUTÓNOMA DE MÉXICO
PROGRAMA DE MAESTRÍA Y DOCTORADO EN INGENIERÍA
ENERGÍA – SOLAR FOTOVOLTAICA

ESTRUCTURA ELECTRÓNICA Y FOTOISOMERIZACIÓN DE CELDAS FOTOVOLTAICAS ORGÁNICAS: UN ESTUDIO DE TEORÍA DEL FUNCIONAL DE LA DENSIDAD.

TESIS
QUE PARA OPTAR POR EL GRADO DE:
DOCTOR EN INGENIERÍA

PRESENTA:
MER. CORNELIO DELESMA DIAZ

TUTOR PRINCIPAL
DR. MIGUEL ROBLES PEREZ, IER-UNAM

COMITÉ TUTOR
DRA. ANA KARINA CUENTAS GALLEGOS, IER-UNAM
DRA. HAILIN ZHAO HU, IER-UNAM
DR. CARLOS AMADOR BEDOLLA, FAC-QUIMICA
DR. JESÚS MUÑIZ SORIA, IER-UNAM

Temixco, Morelos, México, Enero 2023.

JURADO ASIGNADO:

Presidente: Dra. Zhao Hu Hailin

Secretario: Dr. Amador Bedolla Carlos

1er. Vocal: Dr. Robles Pérez Miguel

2do. Vocal: Dr. Muñiz Soria Jesús

3er. Vocal: Dr. De La Cruz Arreola Sergio

TEMIXCO, MORELOS, MÉXICO.

TUTOR DE TESIS:
NOMBRE

FIRMA

Dedicatoria

A Dios.
En memoria a mis padres.
A mi esposa Verónica por su amor, apoyo y comprensión.
A mis hijos Santigo, Melissa Alheli y Juan Luis por darme la alegría de vivir, ser el motivo y el aliento para seguir adelante.

Agradecimientos

A Dios.

A mis padres Cesar Delesma y Ursula Diaz, por darme la vida.

A mi hermano Jose T. que siempre me ha dado su apoyo incondicional.

A mi esposa Verónica, por su paciencia, su comprensión en todo momento de mi carrera. Mi suegros Abraham y Consuelo por sus sabios consejos y apoyo constante.

Al Dr. Jesús Muñiz por su amistad, por darme la oportunidad de trabajar con él, por haberme dado la confianza de compartir sus conocimientos y sobre todo por haberme inculcado el hábito a la investigación científica.

A mi tutor el Dr. Miguel Robles Pérez por su amistad, por la dirección de este trabajo, por su apoyo constante durante mis estudios de Doctorado.

A los integrantes de mi jurado, Dra. Hailin Zhao Hu, Dr. Carlos Amador Bedolla y Dr. Sergio De La Cruz Arreola por su empeño mostrado en la lectura, en sus comentarios y corrección del trabajo de tesis.

A mi sobrino Francisco A. por su motivación a seguir aprendiendo, por sus enseñanzas y comentarios. A mis amigos, Alfredo, Orlando y Jojhar por su gran amistad, por sus comentarios y sugerencias.

Al Instituto de Energías Renovables de la Universidad Nacional Autónoma de México (IER-UNAM) por permitirme hacer uso del Supercómputo para realizar los cálculos necesarios para el trabajo de tesis.

Al departamento de supercómputo de la Universidad Nacional Autónoma de México por los recursos computaciones otorgados dentro del proyecto No. LANCAD-UNAM-DGTIC-370 y LANCAD-UNAM-DGTIC-310.

Al Consejo Nacional de Ciencia y Tecnología (CONACYT) por haberme otorgado la beca de Doctorado No. 633818 para poder continuar mis estudios.

Acrónimos

ν_{XC} *Exchange Correlation Potential*, Potencial de intercambio y correlación. 18

$\boldsymbol{E}_{XC}$ *Exchange Correlation Energy*, Energía de intercambio y correlación. 18

FF *Fill Factor*, Factor de llenado. 23, 37, 38

$\boldsymbol{J}_{SC}$ *Short-circuit current*, Corriente en corto circuito. 23, 38, 39

$\boldsymbol{V}_{OC}$ *Open Circuit Voltage*, Voltaje en circuito abierto. 11, 23, 37–39

AIM *Atoms in Molecules*, Átomos en moléculas. 19, 20

BCP *Bond Critical Points*, Puntos críticos de enlace. 19, 20

BHJ *Bulk hetero-junction*, Heterounión. 9, 25, 37–39

CEP *Clean Energy Project*, Proyecto de energía limpia de Harvard. 23, 37

DFT *Density Functional Theory*, Teoría del Funcional de la Densidad. 7, 14, 17, 20, 21

DOS *Density of states*, Densidad de estados. 25, 41–43

HOMO *Highest Occupied Molecular Orbital*, Orbital ocupado más alto. 6, 10, 20, 29, 31

IR *Infrared radiation*, Radiación infrarroja. 27, 29, 31

IUPAC *International Union of Pure and Applied Chemistry*, Unión Internacional de Química Pura y Aplicada. 23

LHE *light-harvesting efficiency*, Eficiencia de generación de luz. 38, 39

LUMO *Lowest Unoccupied Molecular Orbital*, Orbital desocupado más bajo. 6, 10, 20, 25, 29, 31, 38

NDR *Negative differential resistance*, Resistencia diferencial negativa. 7, 8, 43, 44

NEGF *The Non-Equilibrium Green Function*, Función de Green de no equilibrio. 21

OFETs *Organic field-effect transistor*, Transistores orgánicos de efecto campo. 25

OPV *Organic Photovoltaics*, Orgánicos fotovoltaicos. 4–8, 20, 23, 24, 27, 44

PCBM *[6,6]-phenyl-C61-butyric acid methyl ester*, [6,6]fenil-C61-ácido butírico metil ester. 23, 24, 37, 38

PCE *Power Conversion efficiency*, Eficiencia de conversión de energía. 4–6, 23, 37–39

TDDFT *Time-Dependent Density Functional Teory*, Teoría del Funcional de la Densidad dependiente del tiempo. 6, 7, 18, 20, 27, 29

UV *Ultraviolet*, Radiación Ultravioleta. 27, 29

UV-vis *Ultraviolet-visible*, Radiación ultravioleta visible. 8, 20, 27

Resumen

En la actualidad la investigación en el campo de la energía solar, en donde la luz solar es convertida en energía eléctrica mediante el efecto fotovoltaico, se ha redirigido al diseño y manufactura de materiales fotovoltaicos flexibles, no contaminantes, económicos y de alta eficiencia. Los materiales orgánicos fotovoltaicos, son materiales novedosos que han revitalizado las tecnologías de energía solar. La importancia de los materiales orgánicos fotovoltaicos radica en su potencial para ser implementados como capa activa en una celda solar. Sin embargo, existe una gran lista de candidatos de materiales orgánicos fotovoltaicos, los cuales deben ser estudiados para conocer sus propiedades fotovoltaicas y de esta manera identificar los mejores candidatos. Estudiarlos experimentalmente resulta un arduo trabajo, pero esto se puede acelerar usando métodos computaciones, los cuáles han demostrado una gran precisión en la perdición de las propiedades fotovoltaica de los materiales. Por lo tanto, en este trabajo estudiamos un conjunto de materiales orgánicos fotovoltaicos usando métodos de la mecánica cuántica computacional, específicamente la teoría del funcional de la densidad. En el análisis de la estructura molecular del estado fundamental y del estado excitado del conjunto selecto de candidatos a materiales orgánicos fotovoltaicos, se observó que el estado fundamental de alguno de ellos fueron alterados radicalmente con respecto a la primera excitación. Un cambio muy significativo se encontró en los ángulos dihedrales en estos materiales los cuales pueden ser explicados mediante los mecanismos de fotoisomerización y además influenciados por las propiedades optoelectrónicas. En los cálculos de los espectros de absorción, las geometrías en estado fundamental y estado excitado mostraron cambios significativos en el pico máximo de absorción, esto podría ser debido a los cambios en su estructura molecular. Además, en los cálculos del momento dipolar se encontró una posible transferencia de carga de los materiales orgánicos fotovoltaicos hacia el aceptor en un celda solar. Adicionalmente, se desarrolló otro estudio basado en la teoría del funcional de la densidad y con la función de Green de no-equilibrio, denominado transporte electrónico, con el cual se puede comprender el comportamiento de estos materiales en una celda solar, simulando las condiciones de luz y sin luz solar. La metodología teórica utilizada y los datos computacionales obtenidos pueden ayudar al diseño de nuevos materiales donadores para la nueva generación de celdas solares.

Abstract

In recent years, research in the field of solar energy, where sunlight is converted into electrical energy through the photovoltaic effect, has been redirected to the design and manufacture of flexible, non-toxic, economical and highly efficient photovoltaic materials. Organic photovoltaic materials are novel materials that have revitalized solar energy technologies. The importance of organic photovoltaic materials lies in their potential to be implemented as an active layer in a solar cell. However, there is a large list of candidate organic photovoltaic materials, which must be studied to know their photovoltaic properties and thus identify the best ones. Studying them experimentally is an arduous task, but this can be accelerated by using computational methods, which have shown great accuracy in determining the photovoltaic properties of the materials. Therefore, in this work we study a set of organic photovoltaic materials using computational quantum mechanical methods, specifically density functional theory. In the analysis of the molecular structure of the ground state and the excited state of the selected set of candidate organic photovoltaic materials, it was observed that the ground state of some of them were radically altered with respect to the first excitation. A very significant change was found in the dihedral angles in these materials which can be explained by photoisomerization mechanisms and also influenced by optoelectronic properties. In the absorption spectra calculations, the ground state and excited state geometries showed a significant change in the absorption peak maximum, this could be due to the changes in their molecular structure. In addition, the dipole moment calculations showed us the possible charge transfer from the organic photovoltaic materials to the acceptor in a solar cell. Additionally, another study was developed based on the density functional theory and with the non-equilibrium Green's function, called electronic transport, with which it is possible to understand the behavior of these materials in a solar cell, simulating light and non-sunlight conditions. The theoretical methodology used, and the computational data obtained can help in the design of new donor materials for the new generation of solar cells.

Índice general

Capítulo 1

Introducción

El incremento constante de la demanda energética, principalmente el proveniente de los recursos convencionales como el petróleo, carbón y gas natural han incrementado la emisión de CO_2 (dióxido de carbono) en nuestro planeta, provocando la contaminación del medio ambiente. Solo en el año 2020 la demanda energética fue de 412.8 EJ (exajoules) y se tiene previsto de acuerdo a la política energética actual que para el año 2050 el consumo sea de 550.30 EJ (ver Fig. 1.1). En caso de continuar con la política energética actual se prevé un incremento de la temperatura de nuestro planeta de 1.5 °C para el año 2030 y de 2.6 °C. para el año 2100, lo que provocaría daños irreparables a nuestro ecosistema [1].

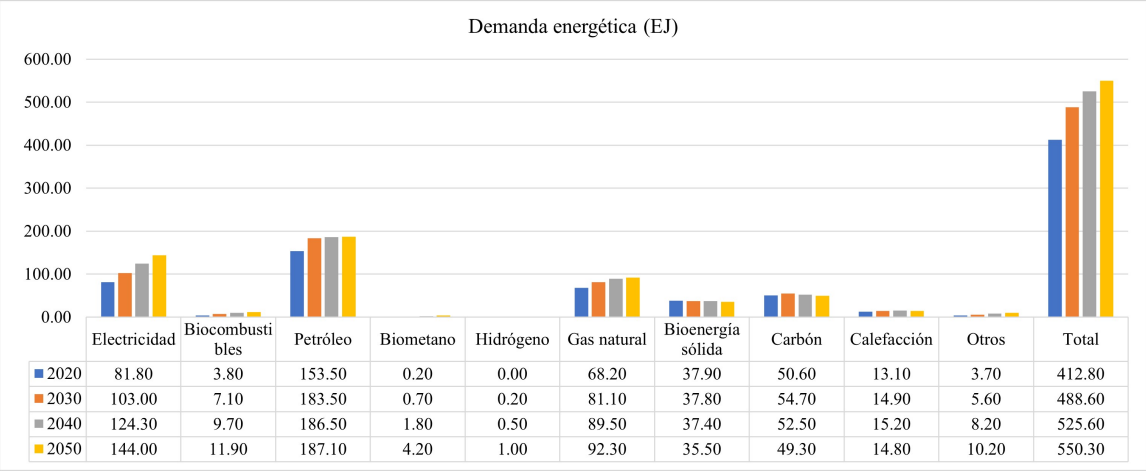

	Electricidad	Biocombustibles	Petróleo	Biometano	Hidrógeno	Gas natural	Bioenergía sólida	Carbón	Calefacción	Otros	Total
2020	81.80	3.80	153.50	0.20	0.00	68.20	37.90	50.60	13.10	3.70	412.80
2030	103.00	7.10	183.50	0.70	0.20	81.10	37.80	54.70	14.90	5.60	488.60
2040	124.30	9.70	186.50	1.80	0.50	89.50	37.40	52.50	15.20	8.20	525.60
2050	144.00	11.90	187.10	4.20	1.00	92.30	35.50	49.30	14.80	10.20	550.30

Fuente: IEA (2021), World Energy Outlook 2021, IEA, Paris https://www.iea.org/reports/world-energy-outlook-2021

Fig. 1.1: Demanda energética actual y futura.

Además de los tres recursos mencionados con anterioridad, la demanda de electricidad también ha ido en aumento. En el año 2020 el consumo fue de 81.8 EJ, y se tiene previsto la demanda de 103.00, 124.30 y 144.00 EJ, en los siguientes años 2030, 2040 y 2050, respectivamente (ver Fig. 1.1).

La electricidad cada día esta tomando un papel central en la vida de los consumidores, convirtiéndose en una fuente de energía cotidiana para la movilidad, cocina, iluminación, calefacción y refrigeración. La generación de electricidad con fuentes re-

novables como la eólica y la solar fotovoltaica, han aumentado su ritmo más rápido en la últimas dos décadas.

Actualmente los materiales que dominan el mercado en la fabricación de celdas fotovoltaicas, son el silicio y el teluro de cadmio. A pesar de tener una buena aceptación como fuente de energía renovable, sus altos costos en la fabricación, hace imposible competir con las fuentes de energía convencionales que generan electricidad. Por lo tanto, se han centrado los esfuerzos en encontrar materiales de bajo costo para su fabricación. Los estudios enfocados a la investigación, desarrollo y fabricación de celdas fotovoltaicas orgánicas (OPV por sus siglas en inglés, Organic Photovoltaics), han demostrado ser una alternativa para solucionar este problema (ver Fig. 1.2). Las celdas solares orgánicas son flexibles, pueden ser fabricadas por un proceso de recubrimiento por rodillo (roll-to-roll coating), es un método de fabricación que incrusta, recubre e imprime solución sobre un material de sustrado enrollado flexible. A medida que ese material se alimenta continuamente de un rodillo a otro, se forma una película sobre la superficie del sustrato. Esta técnica se aplica a materiales sobre el sustrato a medida que se mueve a lo largo de la red para crear una pieza. Por lo tanto, puede ser fabricado a bajo costo [2]. Además, los OPV pueden ser fabricados también con procesos de recubrimiento como la impresión por inyección de tinta, serigrafía y el recubrimiento por ranura [3]. Los OPV tienen la facilidad de ser integrados en otros productos [4] y presentan una adecuada eficiencia de conversión de energía (PCE por sus siglas en inglés, Power Conversion efficiency). Los OPV ofrecen un gran oportunidad en aplicaciones para móviles como fuentes de energía suplementaria y para energía fotovoltaica integrada escalable en edificios.

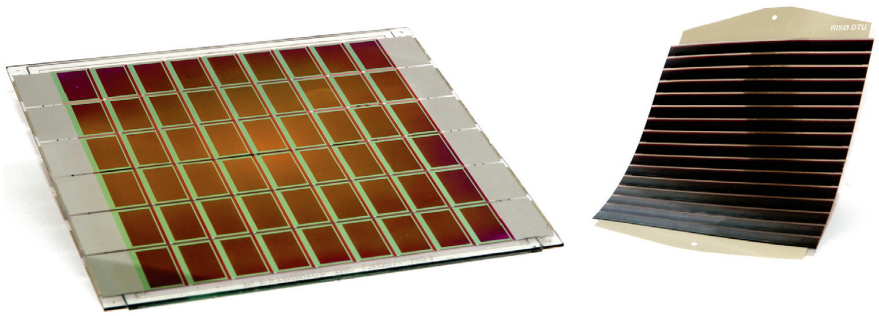

Fig. 1.2: Ejemplo de Celdas Solares Orgánicas, que comprende un sustrato de vidrio rígido, revestimiento por rotación, evaporación de metal, materiales absorbentes y un sello de vidrio con un contorno grueso de varios milímetros (izquierda) y un módulo de celda solar de polímero flexible completamente procesado en solución con un espesor de alrededor de cien micras (derecha). Materials Today (2012), Volume 15, Issues 1–2, with permission from Elsevier and Copyright Clearance Center. Licence No. 5306630121176

Eficiencia de conversión de energía de los OPVs.

Recientemente se ha reportado una PCE de 17.3 % en celdas solares en tandem [5] y de 16.7 % en celda de unión simple [6], [7]. A pesar de estos resultados es necesario realizar más investigación. El incremento de la PCE en los OPVs permitiría hacerlos más competitivos con otros materiales para fabricación del celdas solares. Es importante destacar que la capa activa de un sistema OPV está formado principalmente por un material donador de configuración polimérica y mezcla de varios polímeros. Además, la adecuada selección del material aceptor juega un papel importante en el rendimiento de los sistemas solares resultantes. Tal es el caso del aceptor fullereno bisaducto [8], [9] IC60BA and IC70BA, los cuales son capaces de alcanzar un rendimiento de 7.40 % de PCE. Xiao et al. [10] mostró que un bisaducto de fullereno libre de isómeros e-PPMF, a través de la ruta de síntesis de regioselectividad, es capaz de alcanzar un PCE de 8.11 %. Otro aceptor basado en una unidad copuente octacíclica COi8 [11], llamado COi8DFIC, demostró una bandgap aceptable de 1.26 eV y absorción en la longitud de onda visible, alcanzado una PCE de 14.08 %. La mezcla [12]-[14] del polímero Y6 y algunos copolimeros donadores con un band gap amplio de la forma donador-aceptor, permitieron una absorción más amplia en el rango de la luz visible, alcanzando una PCE de 15 % a 17 %. La PCE más alta que se conoce hasta la fecha es una mezcla de D18 y Y6 de los autores Liu et al. [15], alcanzando una eficiencia de 18.22 %, la cual corresponde a una PCE certificada de 17.6 %.

Las celdas solares OPV estan formadas por una celda heterounión entre semiconductores donadores y aceptores [16], [17]. El proceso de generación de foto-corriente en las celdas solares OPV inicia cuando la molécula donadora absorbe un fotón y se genera el excitón (par electrón-hueco). Éste se traslada a través del material donador hacia la interfase de la heterounión. Este proceso de transferencia de energía se le llama difusión del excitón. Posteriormente, el excitón se divide en portadores de cargas libres. El proceso de foto-generación finaliza cuando ocurre la disociación del excitón. Los portadores de carga son transportados a través de sus respectivas fases en los electrodos del dispositivo [18], [19].

En los materiales OPV, las moléculas donadoras tienen hibrización sp^2, debido que presentan enlaces de carbono-carbono. Estos monómeros se caracterizan por tener anillos con orbitales deslocalizados. En un esfuerzo para encontrar un conjunto de materiales órganicos de manera teórica, Olivares-Amaya et al [20] seleccionaron moléculas a las que le denominaron bloques de construcción. Usando descriptores físico-químicos y topológicos, tales como masa molar, número de anillos, número de enlaces de hidrógeno, densidad electrónica, electronegatividad de los orbitales π y σ, entre otros, se identificaron semiconductores orgánicos con propiedades deseadas de corriente-voltaje y de alta eficiencia en la conversión de energía. La metodología utilizada fue la informática química, la cual permite transformar datos en información y de información en conocimientos, metodología que actualmente es utilizado para seleccionar de forma rápida grandes compuestos con el potencial de una gran biblioteca, principalmente para aplicaciones farmacéuticas. Con esta metodología y la aplicación de técnicas relacionados con el aprendizaje automático (machine learning) y el reconocimiento de patrones, se descubrieron materiales solares orgánicos.

Los autores encontraron 2.6 millones de moléculas candidatas para ser utilizadas con donadores en los OPVs. De la base de datos generadas, se consideró seleccionar un conjunto de moléculas para realizar el presente trabajo, con la finalidad de entender las propiedades de su estructura electrónica y su posible relación con los parámetros fotovoltaicos, que nos permitan considerar para el diseño de las celdas solares.

Aunque las moléculas orgánicas con hibridación sp^2 pueden tener un estructura plana en estado excitado, tales moléculas pueden cambiar sus ángulos dihedrales [21], [22]. Estos efectos se observaron por primera vez en la molécula *azobenceno*. Este fenómeno es conocido como *fotoisomerización* [23], el cual puede ser atribuido a la absorción de un fotón en las moléculas de OPV. El cambio de los ángulos dihedrales se ha observado que disminuye la movilidad de transferencia de carga, y además los orbitales moleculares se vuelven localizados [24]. Por lo tanto, estos fenómenos en las moléculas orgánicas nos permiten ser capaces de predecir el posible comportamiento e identificar moléculas donadoras de alta eficiencia.

En otros estudios acerca de la PCE se han considerado parámetros tales como la aromaticidad, planaridad y HOMO-LUMO(Orbital molecular ocupado más alto y orbital molecular desocupado más bajo) gap, voltaje en circuito abierto y espectro de absorción. Esta serie de materiales muestran propiedades prometedores para ser implementados en aplicaciones fotovoltaicas [25].

Estudios de OPV con TD-DFT.

Utilizando TDDFT (por sus siglas en ingles, time-dependent Density Functional Teory), Teoría del Funcional de la Densidad Dependiente del Tiempo, se han llevado a cabo cálculos acerca de las propiedades ópticas no-lineales en este tipo de sistemas. En estos cálculos se consideraron las geometrías en estado fundamental, estado de mínima energía, de una serie de materiales [25], [26]. Los autores Wazzan e Irfan [27] llevaron a cabo un estudio con TDDFT, usando un colorante orgánico, la trifenilamina que encontraron de manera experimental. La usaron como un modelo para encontrar el espectro de absorción. TDDFT también se uso para modelar el espectro de luz visible para nuevos sistemas orgánicos, obtenida vía diseño rotacional de π-spacers en colorantes donador-π-spacer-aceptor [28]. Lo anterior, con el fin de encontrar nuevos colorantes para ser implementados en celdas solares. Bedoura et al. [29], estudiaron varias moléculas donadoras-aceptoras basados en triazol con π-conjugados, usando TDDFT, para simular los espectros de absorción de los moléculas donadoras-aceptoras. Fan et al. [30] presentaron un estudio de la molécula basado en 7H-benzo [6,7]indeno[1,2-b]tiofeno modificado con fracciones de tiofeno para obtener nuevas celdas solares sensibilizados con tintes de bajo band gap. Usando TDDFT, obtuvieron una buena aproximación del espectro de absorción. Notamos que los últimos trabajos se llevaron a cabo usando TDDFT para modelar espectros de absorción de estructuras geométricas en estado fundamental, pero no se desarrollaron estudios para obtener estructuras geométricas optimizadas en estado excitado para observar los posibles cambios en su geometría, respecto al estado fundamental. Respecto a la planaridad de estos sistemas, tampoco se llevó a cabo un estudio sistemático sobre la

conformación geométrica en estado excitado.

Estudio del transporte electrónico en OPV

El interés en diseñar sistemas que faciliten el transporte de carga a través de dos o más moléculas, ha tomado mucha importancia recientemente, sobre todo en los sistemas compuestos por moléculas orgánicas. El transporte de carga es una propiedad fundamental en el estudio de las moléculas donadores para ser implementados en celdas fotovoltaicas orgánicas de tipo hetero-unión.

Las moléculas orgánicas con enlaces π-conjugados mejoran el transporte electrónico, debido a su baja resonancia energética, inclusive más baja que el benceno. Además, si existe la presencia de átomos de azufre y orbitales π se obtiene mejor resultado en el transporte electrónico. El estudio del transporte electrónico en oligómeros puede darnos conocimiento fundamental dentro del área de la electrónica, óptica y comportamiento de transporte de carga en polímeros conjugados, beneficiando así en aplicaciones en transistores de película delgada y dispositivos electrónicos moleculares. [31].

La unión metal-molécula-metal es esencial para obtener las propiedades del transporte electrónico en conductores y semiconductores orgánicos.

Se han realizado estudios de transporte de carga en dispositivos tipo hetero-unión, tales como en los cortes moleculares hechos en nanotubos, también llamados "nanobelts". Este estudio se realizó en forma de dímeros, para comprender el efecto del enlace Carbono-Hidrógeno-Nitrógeno, entre los nanobelts, usando como electrodo un modelo de slab de Au(111) [32].

También se ha realizado estudios de transporte de carga para hilos de carbino (carbon wires) en una dimensión, usando como electrodo átomos de niquel [33] y carbino encapsulado en natotubo de carbono [34].

Un acercamiento más a las características del transporte electrónico en las moléculas orgánicas se realizaron en la aziridina bicíclica [35] para estudiar sus propiedades y su aplicación en interruptores moleculares. Se encontró que la fotosensibilidad puede cambiar entre abierto y cerrado, lo cual es provocado por la fotoexcitación. Además, fueron encontradas diferentes conformaciones geométricas, que le permite obtener la corriente máxima, usando como electrodo un slab de Au(111). Por otra parte, la conductancia eléctrica es el fenómeno de resistencia diferencial negativa (negative differential resistance (NDR)), esto ocurre cuando se aumenta el voltaje y la corriente disminuye, fenómeno observado por primera vez en el diodo Esaky [36].

Objetivos de la Investigación

El objetivo de este estudio fue identificar el efecto de los cambios en los parámetros estructurales en el comportamiento de los espectros de absorción e identificar sistemas con alto coeficiente de trasmisión. DFT y TDDFT nos permitieron observar este comportamiento en las moléculas OPV en estado fundamental y estado excitado, respectivamente. Presentamos los resultados obtenidos del estudio de un conjunto de

moléculas orgánicas donadoras, incluyendo las variables como band gap óptico teórico, momento dipolar eléctrico, orbitales moleculares y ángulos dihedrales. También, resultados de las propiedades de transporte electrónico. Además observamos cuales sistemas presentan el fenómeno de NDR. Dichas variables aún no se han estudiado sistemáticamente para entender la posible correlación con el espectro UV-vis en los materiales OPV, ni tampoco el efecto causado por la variación en la estructura molecular de los OPV en estado excitado.

Capítulo 2

Marco teórico

2.1. Celdas solares heterounión

Las celdas solares heterounión (BHJ) consisten esencialmente de una estructura multicapa (ver Fig. 2.1), cada capa del dispositivo puede ser depositado con técnicas de fabricación individual. La capa absorbedora está comprendida por dos componentes; un material donador y un material aceptor. La capa fotoactiva está intercalada entre el ánodo y el cátodo. Las capas interfaciales llamadas capas de transporte de huecos y capa de transporte de electrones, son colocadas en la interface entre el ánodo y cátodo fotoactivos, respectivamente. Esto permite mejorar el desarrollo y estabilidad de las celdas solares en heterounión [37]. El material comúnmente empleado en la capa transportadora de huecos es el PEDOT:PSS (Poli(3,4-etilendioxitiofeno)-poli(estireno sulfonato)), y para los portadores de electrones suele usarse LiF (fluoruro de litio) o Ca (Calcio) y ZnO (Óxido de zinc). Entre los conductores más utilizados para la elaboración de electrodos transparentes se encuentra el óxido de indio estaño (ITO, por sus siglas en ingles, Indium tin oxide) usado como ánodo y el Aluminio (Al) usado como Cátodo. El ITO es usado debido a su alta transmitancia en la región de luz visible, función de trabajo relativamente alta y alta conductividad [38].

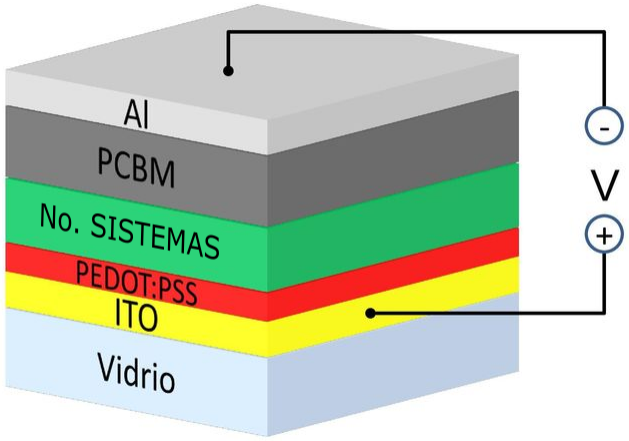

Fig. 2.1: Representación de una celda solar heterounión.

2.2. Principio de funcionamiento de una celda orgánica.

El principio de funcionamiento de una celda solar orgánica, puede ser descrito en cuatro pasos fundamentales:

1. Generación del excitón.
2. Difusión del excitón.
3. Disociación del excitón.
4. Transporte de portador de carga.

2.2.1. Generación del excitón.

Al ser iluminada la superficie de material activo, este absorbe un fotón. La luz generalmente es absorbida por el material donante, considerando siempre que el material tenga un alto coeficiente de absorción. Tras la absorción del fotón, un electrón es excitado desde el HOMO hasta el LUMO del material donante y un portador de carga positiva, denominado hueco, que permanece en el HOMO del material donante. Ambos portadores de carga se atraen entre sí y se unen por fuerzas coulombianas formando un excitón (par electrón-hueco).

2.2.2. Difusión del excitón.

El excitón generado se difunde dentro de la fase donante hasta la interfaz del material donante y aceptor. El excitón decae o puede recombinarse en caso de generarse demasiado lejos de la interfaz. En la celda solar de heterounión, el material donante y el aceptor se entremezclan, por tanto disminuyen la longitud de difusión comparado con la celdas bicapa. También reduce la velocidad del decaimiento del excitón. Las dimensiones entre las dos fases deberían estar en un rango determinado entre 4 nm a 20 nm [37] o más pequeño que la longitud de difusión de 7 ± 1 nm [39], 14 nm [40], 4.7-7.7 nm [41] o 7-17 nm [42]).

2.2.3. Disociación del excitón.

Los huecos fotogenerados y los electrones en la interfase donador-aceptor experimentan una fuerte energía de enlace coulombiana. Estos pares electrón-hueco unidos por la fuerza de Coulomb deben disociarse para obtener portadores de carga libres. La diferencia del HOMO y LUMO entre las capas del donante y aceptor genera una fuerza electrostática en la interfase. Tal diferencia forma un campo eléctrico que conduce a la separación de los excitones en electrones y huecos.

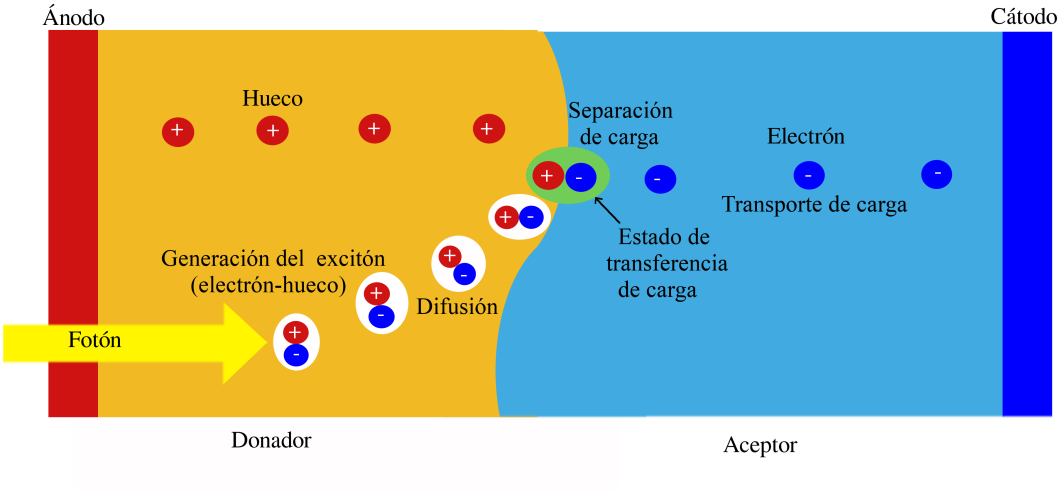

Fig. 2.2: Esquema de producción de fotocorriente.

2.2.4. Transporte de portadores de carga

Los portadores de carga libres están separados por un campo eléctrico interno, provocado por electrodos con diferentes función de trabajo. Generalmente, el ánodo tiene una alta función de trabajo y el cátodo tiene una baja función de trabajo. Con la creación del campo eléctrico interno podemos determinar el voltaje en circuito abierto (V_{OC}) del la celda. El transporte de portadores de carga ocurre a través del material donante y aceptor, donde los electrones se mueven hacia el cátodo y los huecos hacia el ánodo.

2.3. Breve introducción a la Mecánica Cuántica

La descripción de una celda solar hetero-unión, realizada en la sección anterior. Lo que nos permitió entender la generación de la foto corriente. En donde pudimos identificar los elementos que lo constituyen, material donante, aceptor, portadores de hueco y portadores de carga, y los electrodos. Nuestro estudio se centra esencialmente al material donador. En esta sección realizamos una acercamiento a la metodología teórica. Debido a que nuestro estudio describe la estructura electrónica, para entender el comportamiento, del material donador. Por lo tanto, es necesario conocer la bases que sustentan este estudio teórico, iniciamos describiendo los fundamentos de la mecánica cuantica.

Para describir el **estado** de un sistema en mecánica cuántica, se postula la existencia de una función de onda o función de estado. La función de onda contiene toda la información que es posible conocer acerca del sistema.

Para un sistema unidimensional de una sola partícula se postula la siguiente ecuación,

$$-\frac{\hbar^2}{2m}\frac{\partial\Psi^2(x,t)}{\partial x^2}+V(x,t)\Psi(x,t)=-\frac{\hbar}{i}\frac{\partial\Psi(x,t)}{\partial t} \tag{2.1}$$

en donde el primer término de la ecuación corresponde a la energía cinética y el segundo a la energía potencial del sistema. La constante de Planck $\hbar$ está definida como

$$\hbar\equiv\frac{h}{2\pi} \tag{2.2}$$

Esta ecuación es conocida como la ecuación de Schrödinger (descubierta en 1926 por el físico austríaco Erwin Schrödinger) dependiente del tiempo, $i=\sqrt{-1}$ y m es la masa de la partícula.

Una ecuación de onda no puede indicarnos exactamente el lugar en que se encuentra un electrón en un instante particular, ni lo rápido que se está moviendo; no nos permite dibujar una órbita precisa en torno a un núcleo. En cambio la ecuación de onda normalizada, nos revela la *probabilidad* de encontrar el electrón en cualquier lugar particular.

$$|\Psi(x,t)|^2dx \tag{2.3}$$

La región en el espacio en la que es probable que se encuentre un electrón se denomina **orbital**.

Cuando solo se necesitan los estados estacionarios, la mecánica cuántica no necesita utilizar la ecuación dependiente del tiempo, sino una ecuación independiente del tiempo. Por lo tanto, la ecuación 2.1, independiente del tiempo nos queda de la siguiente manera.

$$-\frac{\hbar^2}{2m}\frac{\partial\Psi^2(x)}{\partial x^2}+V(x)\Psi(x)=E\Psi(x) \tag{2.4}$$

Postulando que E es la energía total del sistema, para un átomo monoelectrónico la ecuación de Schrödinger tiene una solución exacta. Esto no aplica para átomos polielectrónicos, debido a los términos de repulsión interelectrónica . Así que debemos usar métodos de aproximación, uno de ellos es el de variaciones.

2.3.1. Método variacional

En este método de aproximación es necesario tratar a la ecuación de Schrödinger independiente del tiempo, la cual contiene partículas que interactúan entre sí.

El teorema de variaciones nos dice que, dado un sistema cuyo operador Hamiltoniano $\hat{H}$ es independiente del tiempo y cuyo valor propio de la energía más baja es E_1, si ϕ es cualquier función dependiente de las coordenadas del sistema, normalizada, que se comporta bien y que satisface las condiciones límite del problema, entonces

$$\int \phi^* \hat{H} \phi d\tau \geq E_1 \tag{2.5}$$

El teorema de variaciones nos permite calcular un límite superior a la energía del estado fundamental del sistema.

Supongamos que tenemos una función ϕ que no está normalizada. Para aplicar el teorema, multiplicamos ϕ por una constante de normalización N, de tal modo que $N\phi$ esté normalizada. Reemplazando ϕ por $N\phi$ en la ecuación 2.5 obtenemos

$$|N|^2 \int \phi^* \hat{H} \phi d\tau \geq E_1 \tag{2.6}$$

La constante N se determina mediante

$$\int (N\phi)^* N\phi d\tau = |N|^2 \int \phi^* \phi d\tau = 1$$

y nos queda de la siguiente forma

$$|N|^2 = \frac{1}{\int \phi^* \phi d\tau}$$

de tal manera que la ecuación 2.6 se transforma en

$$\frac{\int \phi^* \hat{H} \phi d\tau}{\int \phi^* \phi d\tau} \geq E_1 \tag{2.7}$$

La función ϕ se llama **función variacional de prueba**. Para obtener una buena aproximación a la energía del estado fundamental E_1, se utilizan diferentes funciones variacionales de prueba y se busca aquella que proporcione el valor más bajo en la integral de variación.

2.4. Teoría del funcional de la densidad

La teoría del funcional de la densidad DFT en un procedimiento computacional para cálculo de la estructura electrónica en moléculas y sólidos. La idea básica de este método es que la energía de un sistema electrónico puede escribirse en términos de la densidad de probabilidad electrónica ρ.

En esta sección nos centraremos en átomos y moléculas independientes del tiempo; es decir, nos centraremos en la ecuación de Schrödinger sin considerar el tiempo[43].

Para un sistema aislado de n-electrones atómicos o moleculares, la aproximación de Born-Oppenhaimer, estará dada por la ecuación

$$\hat{H}\Psi = E\Psi, \tag{2.8}$$

donde E es la energía electrónica, $\Psi = \Psi(x_1, x_2, ..., x_n)$ es la función de onda, y $\hat{H}$ es el operador Hamiltoniano,

$$\hat{H} = \sum_{i=1}^{N}(-\frac{1}{2}\nabla_i^2) + \sum_{i=1}^{N} v(r_i) + \sum_{i<j}^{N} \frac{1}{r_{ij}}. \tag{2.9}$$

El primer término de la ecuación es la energía cinética, el segundo es la energía de atracción del núcleo-electrón y el último término es la energía de repulsión del electrón-electrón.

En la cual

$$v(r_i) = -\sum_{\alpha} \frac{Z_\alpha}{r_{i\alpha}}. \tag{2.10}$$

es el potencial "externo" actuando sobre el i-ésimo electrón; es decir, el potencial debido a las cargas de los núcleos Z_α.

La energía total W es la energía electrónica más la energía de repulsión núcleo-núcleo.

$$V_{nn} = \sum_{\alpha<\beta} \frac{Z_\alpha Z_\beta}{R_{\alpha\beta}}. \tag{2.11}$$

Esto es,

$$W = E + V_{nn}. \tag{2.12}$$

La ecuación $\hat{H}\Psi = E\Psi$ debe resolverse sujeta a las condiciones de fronteras apropiadas. La función de onda Ψ debe comportarse de manera cuadrática integrable y continua en todas partes. Por otra parte $|\Psi|^2$ es una función de distribución de probabilidad en el sentido que

$|\Psi(r^N, s^N)|^2 dr^N =$ la probabilidad de encontrar el sistema con coordenadas de posición entre r^N y $r^N + dr^N$ y coordenas spin igual a s^N.

En este caso, $dr^N = dr_1, dr_2, ..., dr_N$. r^N representa el conjunto $r_1, r_2, ..., r_N$, y s^N representa el conjunto $s_1, s_2, ..., s_N$. Las coordenadas espaciales son continuas,

mientras que las coordenadas de spin son discretas. Debido a que los electrones son fermiones, Ψ también debe ser antisimétrico con respecto al intercambio de las coordenadas (ambas coordenadas espaciales y coordenadas de spin) de cualquiera de los dos electrones [43].

Hay muchas soluciones independientes aceptables de $\hat{H}\Psi = E\Psi$ para un sistema dado; esto es, las eigenfunciones Ψ_k, con sus correspondiente eigenvalores de energía E_k. Las Ψ_k forman un conjuto completo, y la Ψ_k siempre debe ser ortogonal y normalizada.

$$\int \Psi_k^* \Psi_l dx^N = \langle \Psi_k | \Psi_l \rangle = \delta_{kl}. \tag{2.13}$$

donde δ_{kl} es la delta de Kronecker.

Por otra parte, denotamos a la función de onda del estado base o fundamental, que se refiere al estado de menor energía por Ψ_0, y E_0 el valor de dicha energía. Aquí $\int dx^N$ significa la integración en $3N$ coordenadas espaciales y sumatoria en N coordenadas de spin.

Los valores observables está dado por la siguiente ecuación

$$\langle \hat{A} \rangle = \frac{\int \Psi^* \hat{A} \Psi dx}{\int \Psi^* \Psi dx} = \frac{\langle \Psi | \hat{A} | \Psi \rangle}{\langle \Psi | \Psi \rangle} \tag{2.14}$$

donde $\hat{A}$ es el operador lineal Hermitiano[1] para la observable A.

2.4.1. Teoremas de Hohenberg-Kohn

L. H. Thomas y E. Fermi (1927) intentaron demostrar que la energía cinética y potencial podrían estar directamente relacionadas a la densidad electrónica $\rho(r)$, más que por la función de onda electrónica. El método de Thomas-Fermi considera a un átomo confinado a una región cúbica de volumen L^3 y que cada uno contiene N electrones distribuidos uniformemente, para un total de N_e electrones. Lo anterior es conocido como el modelo de gas de electrones uniforme.

La prueba formal sobre la densidad electrónica lo realizaron de P. Hohenberg y W. Kohn (1964), concluyendo que la densidad electrónica determina las propiedades de las moléculas y sólidos, así como la energía exacta, la cual está dada por el principio variacional.

El teorema de existencia de Hohenberg y Kohn postula: *La energía del estado fundamental y todas las demás propiedades electrónicas estarán determinadas únicamente por la densidad electrónica.* Puesto que ρ determina el número de electrones, resulta que $\rho(\mathbf{r})$ también determina la función de onda Ψ del estado fundamental y todas las propiedades electrónicas del sistema.

Así, ρ determina el número de electrones y el potencial externo $v(r)$, por lo tanto, todas las propiedades del estado fundamental, por ejemplo la energía cinética $T[\rho]$, la energía potencial $V[\rho]$ y la energía total $E[\rho]$. Escribiendo E_v para E para hacer explícita la dependencia en v,

[1]Los eigenvalores de un operador hermitiano son reales. Las eigenfunciones correspondiente a diferentes eigenvalores de un operador hermitiano son ortogonales [44].

$$\begin{aligned} E_v[\rho] &= T[\rho] + V_{ne}[\rho] + V_{ee}[\rho] \\ &= \int \rho(\mathbf{r}) v(\mathbf{r}) d\mathbf{r} + F_{HK}[\rho], \end{aligned} \tag{2.15}$$

donde $V_{ne}[\rho]$, es la energía potencial núcleo-electrón, y $V_{ee}[\rho]$, es la energía potencial electrón-electrón, entonces

$$F_{HK}[\rho] = T[\rho] + V_{ee}[\rho], \tag{2.16}$$

podemos escribir a $V_{ee}[\rho]$

$$V_{ee}[\rho] = J[\rho] + TNC, \tag{2.17}$$

donde $J[\rho]$ es la repulsión clásica y TNC indica que es un término no clásico. El término no clásico es la parte más importante de la energía de intercambio y correlación. El término $F_{HK}[\rho]$ se le conoce como funcional de Hohenberg y Kohn.

Teorema variacional de Hohenberg y Kohn indica: *Para una densidad funcional de prueba $\rho^{'}(r)$, el funcional de energía $E_0[\rho^{'}]$ no puede ser menor que la verdadera energía del estado fundamental del sistema.*

$$E_0 \leq E_v[\tilde{\rho}], \tag{2.18}$$

donde $E_v[\tilde{\rho}]$ es el funcional de energía de la ecuación 2.15.

La densidad electrónica del estado fundamental debe satisfacer $\mu = \partial E[\rho]/\partial\rho(r)$, o

$$\mu = v(r) + \frac{\partial F_{HK}[\rho]}{\partial \rho(r)} \tag{2.19}$$

Donde μ es le conoce como el potencial químico. Esta es la ecuación fundamental de DFT.

2.4.2. Las ecuaciones de Kohn-Sham

Para obtener la densidad electrónica ρ, en primer lugar debemos resolver el conjunto de derivadas de la ecuación electrónica. Para la solución de conjunto de ecuaciones, W. Kohn y L. J. Sham consideraron un sistema de referencia hipotética, que consiste en N_e electrones que no interactúan dentro de un potencial externo $\nu_{ref}(r)$ seleccionado para que la densidad electrónica de referencia del sistema $\rho_{ref}(r)$ sea idéntica al verdadero valor de la densidad electrónica $\rho(r)$. El Hamiltoniano para el sistema de referencia es

$$h_{ref} = \sum_{i=1}^{N_e} h_i^{KS} \tag{2.20}$$

$$h_i^{KS} = -\frac{\hbar^2}{2m_e}\nabla^2 + \nu_{ref}(r_i) \tag{2.21}$$

Cuando los orbitales de Kohn-Sham Ψ_m^{KS} de un electrón son eigenfunciones del Hamiltoniano de Kohn-Sham h_i^{KS}, tenemos

$$h_i^{KS}\Psi_m^{KS} = \varepsilon_m^{KS}\Psi_m^{KS} \tag{2.22}$$

Introducción a los orbitales y la ecuaciones de Kohn-Sham

La energía del estado fundamental de un sistema mutielectrónico puede obtenerse como el mínimo de la energía funcional.

$$E[\rho] = \int \rho(\mathbf{r})v(\mathbf{r})d\mathbf{r} + F[\rho], \tag{2.23}$$

donde

$$F[\rho] = T[\rho] + V_{ee}[\rho]. \tag{2.24}$$

El funcional de energía total para la molécula, puede ser escrito en términos del funcional del sistema de referencia junto con los términos de corrección.

$$E[\rho] = T_{ref}[\rho_{ref}] + J_{ref}[\rho_{ref}] + \int \rho(\mathbf{r})\nu(\mathbf{r})d\mathbf{r} + \{F[\rho] - (T_{ref}[\rho_{ref}] + J_{ref}[\rho_{ref}])\} \tag{2.25}$$

Reescribiendo la ecuación tenemos

$$E[\rho] = T_{ref}[\rho] + J[\rho] + \int \rho(\mathbf{r})\nu(\mathbf{r})d\mathbf{r} + E_{XC}[\rho] \tag{2.26}$$

donde la energía de intercambio y correlación es

$$E_{XC}[\rho] = T[\rho] + V_{ee}[\rho] - (T_{ref}[\rho] + J[\rho]) \tag{2.27}$$

Debido a que en cualquier sistema con una distribución continua la densidad electrónica es la misma, se omite para $J[\rho]$ el subíndice ref.

La densidad electrónica en el estado fundamental es la densidad que minimiza $E[\rho]$ y por lo tanto satisface la ecuación de Euler (ver ecuación 2.19 ecuación fundamental de DFT)

$$\mu = \nu_{eff}(\mathbf{r}) + \frac{\partial T_{ref}[\rho]}{\partial \rho(\mathbf{r})}, \tag{2.28}$$

con

$$\nu_{eff} = \nu(\mathbf{r}) + \frac{\partial J[\rho]}{\partial \rho(\mathbf{r})} + \frac{\partial E_{XC}[\rho]}{\partial \rho(\mathbf{r})} \tag{2.29}$$

La derivada del funcional de $J[\rho]$ esta dada por

$$\frac{\partial J[\rho]}{\partial \rho(\mathbf{r})} = j_0 \int \frac{\rho(\mathbf{r}')}{|\mathbf{r} - \mathbf{r}'|} d\mathbf{r}' \tag{2.30}$$

y la energía de intercambio y correlación (E_{XC}) está definida por el potencial de intercambio y correlación (ν_{XC} ($\mathbf{r}$)):

$$\nu_{xc}\mathbf{r} = \frac{\partial E_{XC}[\rho]}{\partial \rho(\mathbf{r})} \tag{2.31}$$

Vemos que este potencial no es un funcional, sino una función ordinaria de posición. Por lo tanto el potencial efectivo queda de la siguiente forma

$$\nu_{eff}(\mathbf{r}) = \nu(\mathbf{r}) + j_0 \int \frac{\rho(\mathbf{r}')}{|\mathbf{r} - \mathbf{r}'|} d\mathbf{r}' + \nu_{XC}(\mathbf{r}) \tag{2.32}$$

Cambiando $\nu_{ref}(\mathbf{r})$ por $\nu_{eff}(\mathbf{r})$ en la ecuación 2.28, tenemos que para encontrar la densidad electrónica que minimice el funcional de energía, necesitamos resolver las **ecuaciones de Kohn-Sham**.

$$\left\{ h_1 + j_0 \int \frac{\rho(\mathbf{r}_2)}{|\mathbf{r}_1 - \mathbf{r}_2|} d\mathbf{r}_2 + \nu_{XC}(\mathbf{r}_1) \right\} \Psi_m^{KS}(\mathbf{r}_1) = \varepsilon_m^{KS} \Psi_m^{KS}(\mathbf{r}_1) \tag{2.33}$$

donde h_1, es el Hamiltoniano de un electrón.

$$h_1 = -\frac{\hbar^2}{2m_e}\nabla^2 + \nu(\mathbf{r}_1) \tag{2.34}$$

2.5. Teoría del Funcional de la Densidad Dependiente del Tiempo

Consideremos a la radiación electromagnética como una perturbación generada por el campo eléctrico y magnético oscilante. Ahora si solo tomamos en cuenta al campo eléctrico, y además al momento dipolar eléctrico de la molécula. Esto nos permite observar si nuestro sistema sufre alguna transición de un estado a otro estado, cuando esta expuesto a un potencial externo. Para describir al sistema expuesto a la radiación electromagnética, usamos la ecuación de Schrödinger independiente del tiempo.

$$-\frac{\hbar}{i}\frac{\partial \Psi(x,t)}{\partial t} = -\frac{\hbar^2}{2m}\frac{\partial \Psi^2(x,t)}{\partial x^2} + V(x,t)\Psi(x,t) \tag{2.35}$$

Por lo tanto, usando TDDFT, podemos determinar la polarizabilidad e hiperpolarizabildad, así como también la energía de excitación y espectro de absorción electrónica.

La ecuación de Kohn-Sham para TDDFT toma la siguiente forma:

$$\left\{ -\frac{\hbar^2}{2m_e}\nabla_1^2 - j_0 \sum_{I=1}^{N} \frac{Z_I}{r_{I1}} + j_0 \int \frac{\rho(\mathbf{r}_2, t)}{r_{12}} d\mathbf{r}_2 + V_{exc}(t) + V_{XC}(\mathbf{r}_1, t) \right\} \psi_i(\mathbf{r}_1, t) \tag{2.36}$$

$$= -\frac{\hbar}{i}\frac{\partial \psi(x,t)}{\partial t}$$

$$\rho(\mathbf{r},t) = \sum_{i=1}^{n} |\psi_i(\mathbf{r},t)|^2 \tag{2.37}$$

Donde V_{exc}, es el potencial externo, el cual corresponde a la interacción entre el campo eléctrico de la radiación y el momento dipolar eléctrico del sistema o molécula.

2.6. Teoría cuántica de átomos en moléculas

Es posible definir los enlaces en moléculas y sólidos con la ayuda de la Teoría de átomos en moléculas (AIM por sus siglas en inglés, Atoms In Molecules). Esta teoría es usada para conocer las interacciones covalentes y no covalentes de átomo-átomo en moléculas, clusters, y cristales. AIM usa la densidad de carga o densidad de electrones para estudiar la naturaleza de los enlaces en los sistemas moleculares. La densidad de electrones es afectada por las interacciones entre dos núcleos y por lo tanto también su enlace químico. Las propiedades topológicas de la densidad de electrones y sus derivados resultan útiles para describir el concepto de enlace a través de rutas de enlace y puntos críticos de enlace. AIM también nos permite conocer enlaces de hidrógeno, van der Waals y enlaces iónicos.

AIM calcula puntos críticos de enlace (BCP, por sus siglas en ingles, Bond Critical Points), indicando la existencia de una enlace químico. La densidad electrónica es nula ($\nabla\rho(r_c) = 0$) en el BCP. El signo en el Laplaciano de la densidad electrónica puede ser evaluado con la siguiente relación: $\nabla^2\rho(r_c) = \lambda_1 + \lambda_2 + \lambda_3$, en la cual λ_1, λ_2 y λ_3 representan tres valores del Hessiano (derivadas parciales de segundo orden) diferentes de cero. Si dos electrones son compartidos por dos centros atómicos, puede asumirse un enlace covalente ($\nabla^2\rho(r_c) < 0$). Si los electrones no están localizados en el BCP, pero centrado en cierto átomo, entonces corresponde a atracción de capa cerrada $\nabla^2\rho(r_c) > 0$. Si $\rho(r_c) > 0.1$ y $\nabla^2\rho(r_c) < 0$, se observa un enlace covalente. Cuando $\rho(r_c) < 0.01$ y $\nabla^2\rho(r_C) > 0$, es evidencia de un enlace de hidrógeno. Cuando $\rho(r_c) < 0.001$ y $\nabla^2\rho(r_c) > 0$, la metodología reporta una atracción de tipo van der Waals.

Capítulo 3

Métodos computacionales

3.1. Metodología teórica y comparaciones teóricas.

3.1.1. Síntesis de OPV y caracterización de bandgap

Para el conjunto de 33 sistemas OPV (Ver Esquema 1, Apéndice C) estudiados en este trabajo, un subconjunto de 8 sistemas (ver Tabla 4.1, Capítulo 4) se llevó a cabo una comparación entre los valores experimentales del bandgap ópticos y los valores teóricos. El subconjunto de sistemas fueron sintetizados y caracterizados por García, et al. [45], mientras que los bandgap ópticos fueron determinados por Sifuente-Vázquez et al. [46].

3.1.2. Detalles computacionales

Las optimizaciones geométricas de los sistema OPV se obtuvieron usando DFT, con el funcional PBE [47] y el conjunto base *def2-TZVP* [48], [49]. Calculamos los estados excitados para encontrar los espectros UV-vis, usando TDDFT. Además calculamos la estructura geométrica en estado excitado. Ambos cálculos nos permitieron comparar estructuralmente las geometrías en estado fundamental y estado excitado. Se consideraron los primero 10 estados excitados para encontrar el comportamiento completo del espectro de absorción. Además, obtuvimos el bandgap óptico teórico considerando la diferencia energética entre HOMO y LUMO. Todos los cálculos fueron desarrollados utilizando el código computacional TURBOMOLE [50]. Además, el suavizado de los datos de las gráficas se realizaron usando interpolación sobre funciones Gaussianas. En análisis gráfico de los sistemas se llevaron a cabo con el programa Tmolex [51].

Para conocer los valores de las distancias de enlace de los átomos de los sistemas OPV se realizó el cálculo usando la metodología AIM. AIM calcula BCP, indicando la existencia de una enlace químico.

El cálculo de los ángulos dihedrales en estado fundamental (θ_{Grd}) y el primer estado excitado singulete (θ_{Exc}) fueron calculados usando un código propio desarrollado en el lenguaje de programación Python2.7 [52]. Consideramos la ecuación del plano 3.1 para calcular en ángulo entre dos planos en las moléculas OPV, la cual es

necesario para obtener el ángulo dihedral. En la ecuación 3.1, θ representa a θ_{Grd} and θ_{Exc}. De acuerdo a la Fig. 3.1, el plano 1 corresponde a los átomos S1-C1-C2, el plano 2 por los átomos C1-C2-C3.

$$\cos\theta = \frac{|n_1.n_2|}{||n_1||||n_2||} \tag{3.1}$$

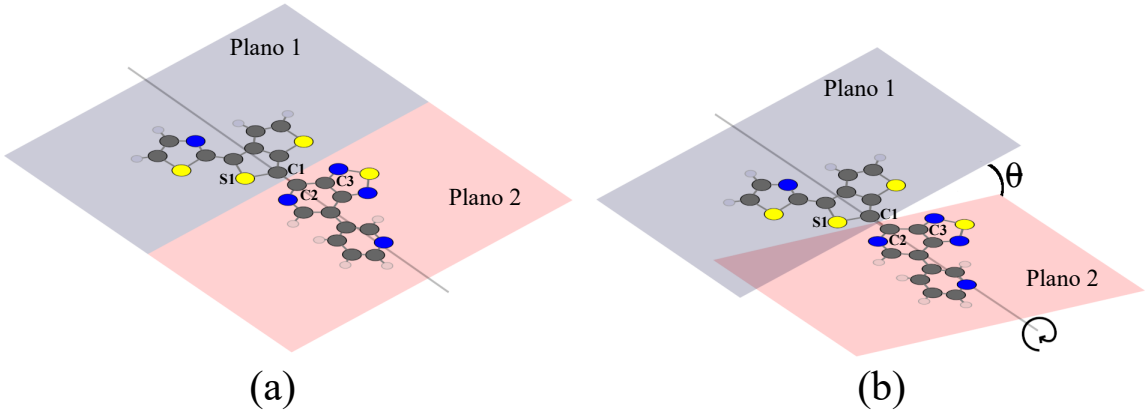

Fig. 3.1: Representación gráfica de dos planos usados para el cálculo del ángulo dihedral θ. (a) Estado fundamental, (b) estado excitado. La figura que muestra la imagen corresponde al sistema 23.

En la Ecuación 3.1, n_1 y n_2 representan los vectores normal perpendicular a los planos 1 y 2, respectivamente.

La simulación para el transporte electrónico se realizó utilizando la unión Au(100)-molécula-Au(100). Las condiciones periódicas se aplicaron en los ejes x, y y z. El valor del eje z se modificó de acuerdo al tamaño del sistema orgánico. Para el electrodo de Au(100) se realizó un arreglo periódico con 6 capas y un k-grid de $2 \times 2 \times 10$ (ver Fig. 3.2). La región de dispersión incluye moléculas orgánicas y dos capas de Au en cada contacto, tanto izquierdo como derecho, para simular los efectos de la perturbación de la región central. Se propusieron los enlaces de C-Au, eliminando el enlace de H debido a que no es un buen absorbedor en superficies metálicas [35], con una distancia de enlace de 2.09 Å. Dicha distancia fue obtenida ajustando los cálculos a un potencial de Morse (ver Fig. 3.3). La región de dispersión se llevo a cabo con un k-grid $2 \times 2 \times 2$.

Las propiedades de transporte electrónico se calcularon utilizando DFT combinado con el método de la función de Green de no equilibrio (NEGF, The Non-Equilibrium Green Function method) implementado en el modulo TranSIESTA [53] del paquete SIESTA [54]. Se utilizaron el funcional PBE [47], los pseudopotenciales de Troullier-Martins [55] y el conjunto base SZ (single-zeta). La energía de corte fue de 350 Ry.

Para obtener el perfil de corriente-voltaje (I-V) y el diferencial de conductancia (dI/dV) se usó el voltaje de polarización (*bias voltage*) entre -3.0 a 3.0 V. La corriente se obtuvo usando la formula de Landauer-Büttiker,

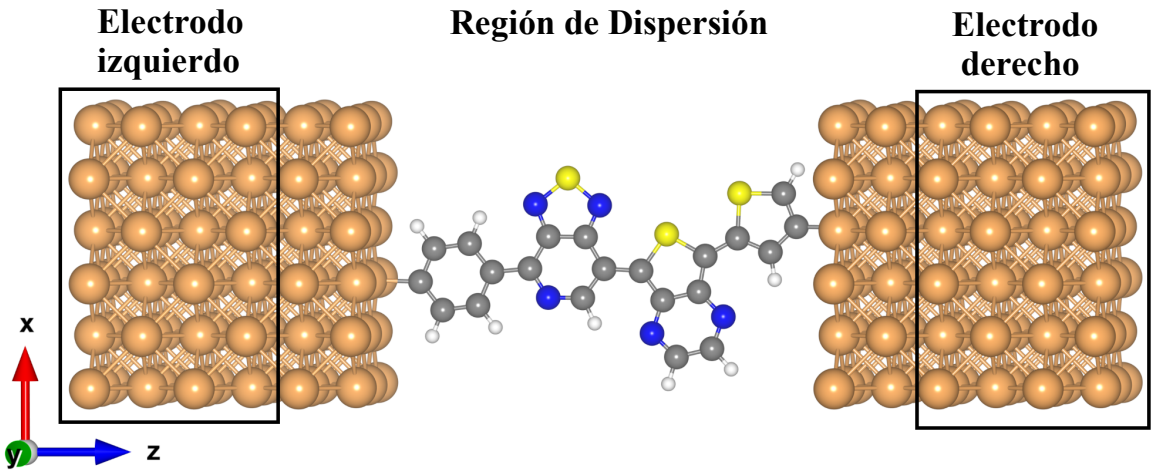

Fig. 3.2: Dispositivo correspondiente al sistema 11. Esfera de color amarillo corresponde al átomo de Au, blanco al H, gris al C, Azul al N y amarillo claro al S.

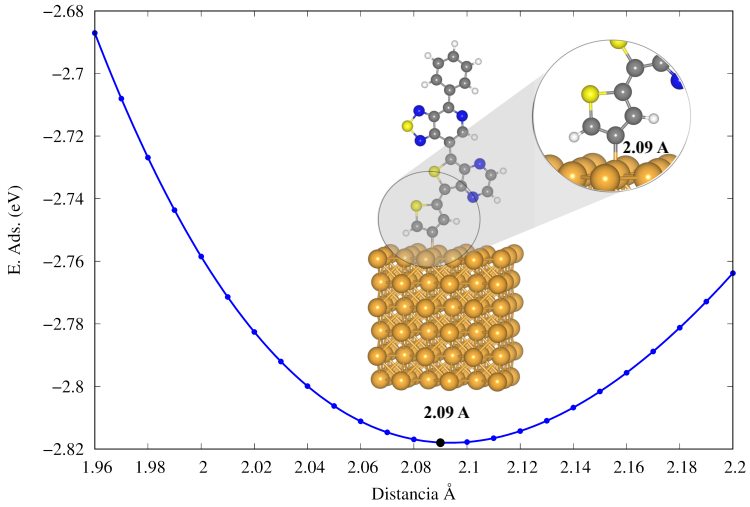

Fig. 3.3: Potencial de Morse, para obtener la distancia entre el Au y el sistema orgánico.

$$I(V_b) = \frac{2e^2}{h} \int_{\mu L}^{\mu R} T(E, V_b) \mathrm{d}E \tag{3.2}$$

donde μL y μR son el potencial químico de electrodo izquierdo y derecho, respectivamente. La diferencia del potencial químico está dado por eV_b con la aplicación del potencial de polarización (V_b), por ejemplo, $\mu_L(V_b) = \mu_L(0) - eV_b/2$ y $\mu_R(V_b) = \mu_R(0) + eV_b/2$. T(E,$V_b$) es la probabilidad de transmisión total de los electrones incidentes a una energía E a través del dispositivo dentro de un potencial de polarización (V_b).

Capítulo 4

Estructura electrónica de los OPV

4.0.1. Propiedades de la estructura electrónica de los OPV.

Los sistemas OPV del presente estudio se muestran en el Esquema 1, Apéndice C. Tales sistemas fueron estudiados por los autores Olivares-Amaya et al. [20] dentro de la iniciativa Harvard Clean Energy Proyect (CEP). Este estudio se basó en una combinación de 30 bloques moleculares (*building block*), del cual se obtuvieron una base de datos de 2.6 millones de moléculas con propiedadades fotovoltáicas deseables. En este trabajo se estudió un conjunto de 33 sistemas OPV, debido a que se reportaron valores altos en los descriptores usando *machine learning* e inteligencia artificial. Estos descriptores comprendían variables observables, tales como, PCE, voltaje en circuito abierto (V_{OC}), densidad de corriente en corto circuito (J_{SC}) y factor de llenado (FF). El CEP propuso oligómeros capaces de ser sintetizados, con buena capacidad de solubilidad, formación de películas y además que muestren excelentes propiedades para usar al [6,6]-fenil-C_{61}-ácido butírico metil ester (PCBM) como aceptor.

Estudiamos las propiedades de la estructura electrónica en estado fundamental y estado excitado para encontrar una posible relación con el cambio del ángulo de torsión. En el conjunto de sistemas orgánicos se identificaron 16 bloques de moléculas (ver Fig. 1, Apéndice C) los cuales corresponden a la nomenclatura de la IUPAC (ver Tabla 1, Apéndice C). Clasificamos las moléculas building block de manera ordenada iniciando con B01 hasta el B16.

De los 33 sistemas OPV, se seleccionaron un pequeño grupo de 8 moleculas (ver Tabla 4.1), las cuales fueron sintetizadas de acuerdo a la metodología presentada en la sección 3.1.1. Estos sistemas fueron caracterizados con la medición de los band gap experimentales. Por lo tanto, para indentificar la metodología teórica para modelar el estado fundamental y el estado excitado, se realizó un análisis comparativo con una serie de funcionales presentadas en la tabla 4.1. A pesar de que B3LYP [56]-[58] es un funcional con buena aproximación al valor de band gap (promedio) experimental, en los cálculos de optimización geométrica en estado excitado no nos permiten obtener la geometría final. En cambio, el funcional PBE si nos permite obtener las geometría tanto en estado fundamental y estado excitado, como se ha demostrado en estudios previos de OPV [25], usando el funcional PBE. Por lo tanto, se seleccionó PBE para realizar el estudio teórico.

Tabla 4.1: Tabla comparativa de la metodología usada en los calculos teóricos para obtener el band gap optico (eV). Notar que Δ denota la diferencia entre el valor experimental y el teórico (Modificada de [59])

Sistema	Exp	ΔPBE	ΔB3LYP	ΔPBE0 [41], [47]	ΔCAM-B3LYP	ΔM06 [60]
05	1.94	0.27	0.02	0.07	0.29	0.06
06	3.67	1.14	0.81	0.68	0.36	0.74
07	2.69	0.39	0.05	0.08	0.43	0.04
12	3.42	0.22	0.06	0.15	0.38	0.10
14	3.22	0.15	0.13	0.22	0.46	0.18
16	3.49	0.46	0.39	0.50	0.84	0.43
17	2.88	0.16	0.22	0.32	0.65	0.28
18	2.12	0.54	0.19	0.07	0.36	0.07
Δpromedio		0.41	0.23	0.26	0.47	0.24

Un valor aceptable para los cálculos de la energía del band gap óptico, para aplicaciones en celdas solares, están en un rango de 1.2 a 1.9 eV [61]. De acuerdo a los resultados que se presentan en la Tabla 4.2, para las geometrías en estado fundamental, en su mayoría los valores obtenidos se encuentre dentro del rango. Los sistemas 01, 02, 03, 06, 07, 09, 10, 12, 14, 16, 17 y 20 muestran valores más altos.

En el diseño de celdas solares se requiere una celda heterounión. Particularmente, las celdas orgánicas heterounión son una mezcla de un material aceptor de electrones tal como el PCBM y un material donador de electrones tales como los que se presentan en este trabajo. Usando al PCBM como aceptor, nos permitió obtener los valores de los parámetros químicos cuánticos como la dureza química [62], potencial químico y la electronegatividad, con la ayuda de la ecuación [63]:

$$\text{Dureza química: } \mu = (E_{LUMO} - E_{HOMO})/2 \tag{4.1}$$

$$\text{Potencial químico: } \eta = (E_{HOMO} + E_{LUMO})/2 \tag{4.2}$$

$$\text{Electronegatividad: } \chi = -(E_{HOMO} + E_{LUMO})/2 \tag{4.3}$$

La dureza química del PCBM es de 1.18 eV [63]. Si el valor de la dureza química de las moléculas donadoras es menor al del PCBM, entonces la transferencia de electrones puede ocurrir. En este sentido, los sistemas 02, 03, 12, 14 y 16 (ver Tabla 4.2), se encuentra fuera de este rango. El potencial químico del PCBM es de -4.93 eV [63], mientras que los sistemas OPV muestran valores más altos, por lo tanto la transferencia de electrones el posible. Respecto al valor de la electronegatividad del PCBM es de -5.93 eV [63], y nuestros sistemas muestran valores por debajo de ésta. Considerando este resultado, podemos decir que la atracción del electrón es fuerte.

Por otra parte, se obtuvo el cálculo del momento dipolar, debido a que es uno de los descriptores para la caracterización de las moléculas OPV dentro de este estudio. Los valores altos del momento dipolar nos indican que la separación de la carga es

factible en una mezcla de donador y aceptor [64], [65], además de que aumenta la transferencia de carga [66]. Los sistemas con momento dipolar en el rango entre 0.00 a 1.00 D son el 01, 05 y 07 (Grupo 1). En el rango entre 1.00 y 2.00 D son 03, 06, 08, 15, 18, 21 y 29-31 (Grupo 2). Un gran número de sistemas dentro de este estudio se localizaron en el rango de 2.00 a 3.00 D (09-12, 17, 19-20, 22, 24-28, y 33) y corresponde al grupo 3. Los sistemas localizados en el rango de 3.00 a 4.00 D son el 13, 14, 23 y 32 (Grupo 4). Tenemos moléculas en el rango de 4.00 y 6.00 D que son los sistemas 02, 04 y 06 (Grupo 5). De tal manera que, los resultados nos indican que los sistemas ubicados en el grupo 4, 5, y 6 pueden ser considerados como materiales con alta capacidad de transporte de carga.

De acuerdo con Friederich et al. [67], la presencia de un alto o permanente momento dipolar, induce a estados trampa que alteran la movilidad de portadores de carga del material. Este fenómeno particularmente adquiere fuerza cuando el LUMO de los materiales está localizado en una región específica del sistema molecular. En caso contrario, el sistema molecular con orbitales moleculares deslocalizados mitiga ese efecto. Adicionalmente, si tales orbitales están deslocalizados en enlaces dihedrales rotables en la moléculas, se observa un grado de desorden en los sistemas con alta energías, y consecuentemente un aumento intrínseco de la movilidad electrónica. Esto es válido en el comportamiento observado en algunos sistemas dentro del estudio. Después de la fotoisomerización en los sistemas 02, 03, 04, 14, 19, 22, 23, 27, 29, 30, 31 y 32, se observaron valores altos en los ángulos de rotación. Esto podría provocar un incremento en la movilidad de portadores de carga. Además, Sworakowski [68] identificó que sistemas con momento dipolar alto en cristales moleculares pueden ser considerados como trampas de portadores de carga. En consecuencia, la naturaleza polar de tales sistemas provoca una reducción en la profundidad de los estados trampas. En adición, la presencia de impurezas polares son también responsables por la alteración de energía de polarización, la cual incrementa el número de estados trampa en la vecindad de las moléculas. En este sentido, la presencia de especies polares amplía el tamaño de la densidad de estados electrónicos (DOS), induciendo una inminente reducción de la movilidad de transferencia de carga. Por otro lado, Toman et al. [69] desarrollaron un modelo atomístico de transporte de portadores de carga, basado en portadores en una cadena desordenada. En este modelo combinado se considera la perspectiva cuántica y una solución semi-clásica en la carga migrante a través de la cadena. El modelo también considera anisotropía local en los portadores de carga. Usando este modelo, puede ser explicado la degradación de la movilidad. Tal degradación está dirigida a la muy baja movilidad de carga en la interfase de la heterounión (BHJ). Este fenómeno ha sido observado, por ejemplo por Kim et al. [70] y Mottaghi et al. [71]. De acuerdo a este modelo, la fenomenología ocurre debido a la reducción de los estado de salto que podría usarse en grandes concentraciones de carga. Adicionalmente, esto también puede explicar el comportamiento eléctrico de sistemas orgánico como los diodos y transistores orgánico de efecto de campo (OFETs).

Tabla 4.2: Valores de la energía (eV) de: HOMO (E_{HOMO}), LUMO (E_{LUMO}), band gap óptico teórico (E_{gap}), dureza química (μ), potencial químico (η) y electronegatividad (χ). Momento dipolar (ρ) en Debye (D). Los valores corresponden al estado fundamental (Modificada de [59]).

Sistemas	E_{HOMO} (eV)	E_{LUMO} (eV)	E_{gap} (eV)	μ (eV)	i η (eV)	χ (eV)	ρ_{grd} (D)	ρ_{exc} (D)
1	-5.28	-3.52	1.91	0.88	-4.40	4.40	0.61	0.65
2	-4.44	-1.58	2.98	1.43	-3.01	3.01	4.18	5.60
3	-4.76	-1.19	3.66	1.78	-2.98	2.98	1.70	1.40
4	-4.59	-3.37	1.55	0.61	-3.98	3.98	4.43	2.04
5	-4.68	-3.42	1.67	0.63	-4.05	4.05	0.57	0.27
6	-5.42	-3.23	2.53	1.10	-4.32	4.32	1.27	1.16
7	-5.56	-3.59	2.30	0.98	-4.58	4.58	0.73	0.68
8	-5.26	-3.75	1.83	0.75	-4.50	4.50	1.19	1.19
9	-5.41	-3.30	2.36	1.06	-4.36	4.36	2.08	2.06
10	-5.16	-3.42	2.07	0.87	-4.29	4.29	2.57	2.56
11	-4.89	-3.77	1.56	0.56	-4.33	4.33	2.09	2.07
12	-5.38	-2.84	3.20	1.27	-4.11	4.11	2.00	2.04
13	-4.97	-3.60	1.70	0.68	-4.29	4.29	3.07	3.19
14	-5.63	-3.18	3.07	1.22	-4.40	4.40	3.12	4.88
15	-5.05	-3.56	1.86	0.75	-4.30	4.30	1.10	1.14
16	-5.72	-2.74	3.03	1.49	-4.23	4.23	5.73	4.97
17	-4.99	-2.70	2.72	1.15	-3.84	3.84	2.82	2.83
18	-4.86	-3.57	1.58	0.64	-4.22	4.22	1.01	0.80
19	-4.99	-3.64	1.69	0.68	-4.31	4.31	2.18	1.12
20	-5.41	-3.67	2.00	0.87	-4.54	4.54	2.70	1.73
21	-4.99	-3.54	1.67	0.72	-4.27	4.27	1.69	1.63
22	-5.04	-3.55	1.57	0.74	-4.30	4.30	2.13	2.27
23	-5.01	-3.68	1.78	0.66	-4.34	4.34	3.10	1.05
24	-5.01	-3.53	1.59	0.74	-4.27	4.27	2.20	2.00
25	-5.09	-3.66	1.65	0.71	-4.37	4.37	2.30	1.84
26	-5.04	-3.60	1.50	0.72	-4.32	4.32	2.63	2.35
27	-4.94	-3.61	1.59	0.67	-4.28	4.28	2.54	1.79
28	-4.92	-3.62	1.64	0.65	-4.27	4.27	2.46	2.61
29	-5.01	-3.54	1.60	0.74	-4.27	4.27	1.83	1.11
30	-5.03	-3.51	1.73	0.76	-4.27	4.27	1.69	0.88
31	-5.04	-3.53	1.79	0.76	-4.28	4.28	1.50	1.33
32	-4.98	-3.60	1.68	0.69	-4.29	4.29	3.10	2.31
33	-4.99	-3.71	1.61	0.64	-4.35	4.35	2.44	2.53
PCBM	-6.20 [72]	-4.26 [72]		1.18	-4.93	4.93		

4.0.2. Propiedades ópticas en estado fundamental y estado excitado.

Calculamos los espectros de absorción de los sistemas moleculares a nivel de la teoría de TDDFT/PBE previamente mencionada en la sección de Detalles Computacionales. En este caso, los cálculos se desarrollaron considerando la geometría en estado fundamental obtenido con el funcional PBE. De la radiación solar que nos llega a la Tierra, 40 % corresponde al espectro UV-vis (400-700 nm), 50 % corresponde al infrarrojo (IR) (700-1000 nm) y 10 % al ultravioleta (UV) [73]. Considerando los rangos mencionados, se clasificó en tres diferentes grupos los sistemas. El primer grupo corresponde a los sistemas por debajo de 400 nm (sistema 01-07, 12, 15, 16, 20 y 33), los cuales absorben en el rango de UV (ver Fig. 4.1 (a)); de 100 nm a 400 nm. Particularmente, esta serie requiere de mayor cantidad de energía para la excitación electrónica. La segunda serie se encuentran el rango de 400 a 700 nm, y corresponden a los sistemas 08-10, 13, 14, 17-19, 21-27, 29, 31 y 32. La absorción (ver Fig. 4.1 (b)) está localizado en la rango del UV-vis, permitiendo que la excitación electrónica sea más probable en condiciones experimentales. Este conjunto de sistemas absorben en el rango UV-vis, de tal manera que pueden ser considerados como materiales con posibilidades de participar en aplicaciones en dispositivos de celdas solares. Finalmente, como muestra la Fig. 4.1 (c), el tercer grupo se encuentra en el rango de 700 a 1000 nm (sistema 11, 28 y 30), en la cual la absorción se encuentra en el rango del IR.

Es importante destacar que los ángulos dihedrales en los sistemas en estudio son en algunos casos, significativamente desplazados de la planaridad en las geometría en estado fundamental. Además, es importante para el análisis de sus efectos en las propiedades en estado excitado. Clasificamos los sistemas de acuerdo a las magnitudes de los ángulos dihedrales. El primer grupo corresponde a los sistemas con dihedrales de 0 a 20°. El segundo grupo, en el rango de 20° a 40°. Finalmente, el tercer grupo en el rango de 40° a 60°.

De acuerdo a las propiedades estructurales, identificamos tres diferentes grupos de sistemas OPV. Esta clasificación esta directamente relacionada con sus propiedades. El primer grupo de sistemas con ángulos dihedrales entre 0° y 20°, en estado fundamental son 05, 08, 11, 12, 14, 15, 25, 27, 28 y 33. Después de los cálculos del estado excitado, los ángulos dihedrales de tales sistemas permanecieron constantes (excepto los sistemas 14 y 27).

El espectro UV-vis del sistema 05 en estado fundamental, mostró un máximo a 394.0 nm (rango en UV), mientras que el estado excitado, se localizó en un máximo de 430.7 nm (rango de UV-vis) (ver Fig. 4.2). Este carácter reveló su posible potencial para la absorción de luz y su posible aplicación como material para celdas solar. Esto es, un deplazamiento de 36.7 nm es el responsable de tal comportamiento. Un resultado análogo fue observado en el sistema 08 con un corrimiento de 24.2 nm.

La absorción máxima para el sistema 11 en estado fundamental se observó en 792.7 nm (región del IR). En la Fig. 4.2, el máximo en estado excitado se centró en 940.3 nm (también ubicado en la región del IR). Un desplazamiento de 147.6 nm, indicando que este sistema es adecuado para aplicaciones como material para celdas solares. En particular, la transición electrónica para el sistema 11 en su geometría

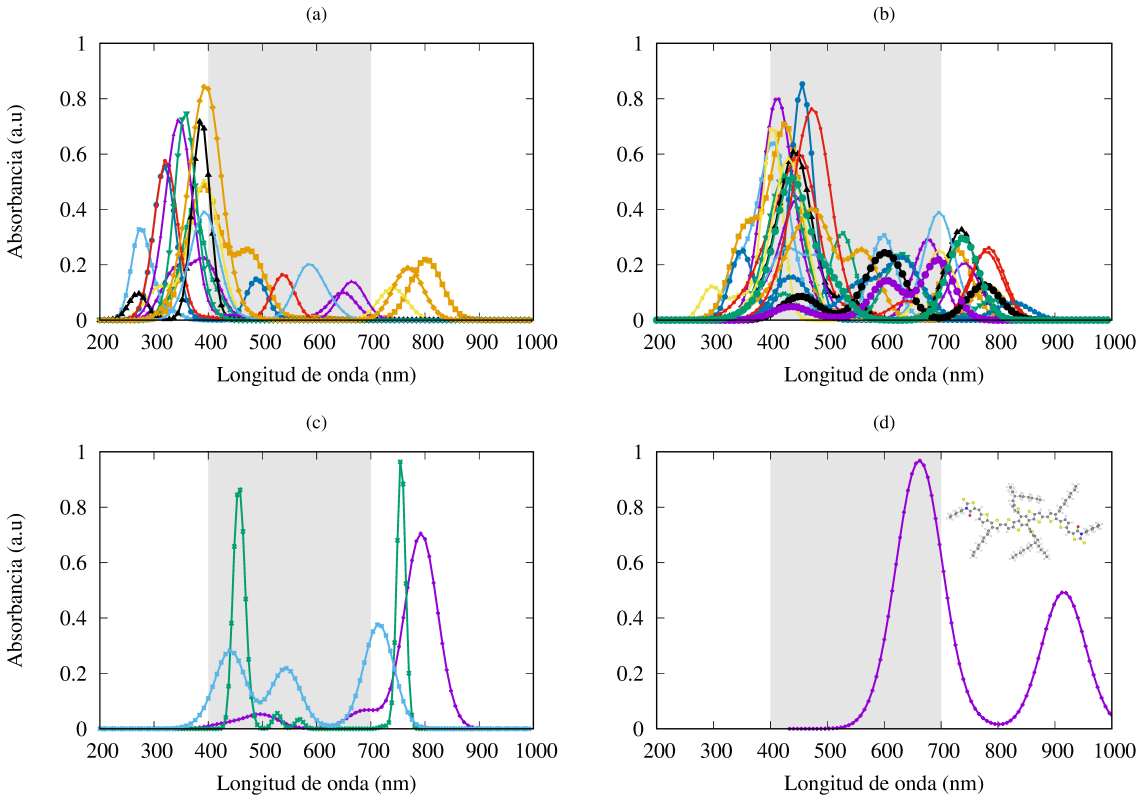

Fig. 4.1: Espectro de absorción de un subconjunto de sistemas con localización máxima: (a) por debajo de 400 nm; (b) en un rango de 400 nm a 700 nm; (c) en un rango de 700 nm a 1000 nm. (d) Optimización geométrica molecular y espectro de absorción del sistema molecular ZR1. La zona gris representa la región de la luz visible. Notar que las propiedades fueron obtenidas con el nivel de teoría TDDFT/PBE.

en estado fundamental, ocurrió del HOMO (-4.89 eV) al LUMO (-3.77 eV) con a 91.0 % de probabilidad (ver Fig. **2**, Apéndice C). Esto representa un alta probabilidad encontrada por el cálculo TDDFT. También el mismo comportamiento se identificó con un transición del HOMO al LUMO, en los sistemas 28 y 30. La máxima absorción de estos procesos se localizaron en la región de la longitud de onda del IR con una contribución de 92.8 % y 96.7 %, respectivamente (ver Fig. **2** y Tabla **36**, Apéndice C).

El segundo grupo es el conjunto de sistemas con ángulos dihedrales en estado fundamental en el rango de 20° a 40°, y corresponde a los sistemas 06, 07, 10, 13, 16-20, 23, 24 y 32. El sistema 20 mostró un pico en el rango del UV en estado fundamental y en el estado excitado se observó una variación de 320.0 nm. Esto permitió al sistema la absorción en la región del IR. Tal desplazamiento podría ser atribuido al cambio en los ángulos dihedrales, como se muestra en la Tabla **36**, Apéndice C, en la cual los ángulos θ_1 y θ_2 corresponde a 33.0° y 34.5°, respectivamente. Como consecuencia, en estado excitado se observó un geometría co-planar. Tal comportamiento indujo un desplazamiento hacia la región del IR, como se muestra en la Fig. 4.2 (a). Finalmente, se indentificó un tercer grupo de sistemas con ángulos dihedrales en el rango de 40° to 60° en estado fundamental; los sistemas son 01-04, 09, 21, 22, 26, 29, 30 y 31.

Las geometrías de las moléculas estudiadas también fueron optimizadas en estado excitado. Como se mencionó previamente, también se calculó sus espectros de absorción (ver Fig. 4.2). Estos resultados mostraron un cambio evidente en el promedio del cambio de sus ángulos dihedrales; tal como se reporta en las geometría en estado excitado en la Tabla **36**, Apéndice C. Esto es, claramente se identifica una isomerización en muchos de los sistemas en estudio. Este comportamiento aparente altera los espectros de absorción máxima induciendo un corrimiento hacia la región del IR en algunos casos, o un cambio en la región UV (ver tabla **36**, Apéndice C). Asignamos tal comportamiento como una fotoisomerización, la cual podría ser generada en presencia de la radiación solar, simulado con nuestras metodología teórica. La Fig. 4.2 muestra la localización del espectro de absorción máxima fuera del rango, en la cual la máxima originalmente se encontró en la geometría en estado fundamental.

4.1. Descripción estructural y su relación con la propiedades ópticas

Los resultados previos muestran una relación con los cambios de los ángulos dihedrales y los cambios en la geometría, al corrimiento de los espectros de absorción máxima. Esto se muestran en la gráfica de mapa de calor en la Fig. 4.3. El eje **x** corresponde a los sistemas estudiados, el eje **y** corresponde a la diferencia de los promedios de cambios entre el estado fundamental y excitado, columna (Δ Ave.)). La escala de colores del rojo al azul muestran el corrimiento que experimentan los sistemas en el espectro de absorción cuando cambia de estado (del estado fundamental al estado excitado). El color azul nos indica un corrimiento positivo, el color rojo indica un corrimiento negativo ($\Delta\lambda$). El caso de sistema 27, vemos un cambio del ángulo dihedral cercano a 90 grados, pero no presentan cambios en longitud de onda

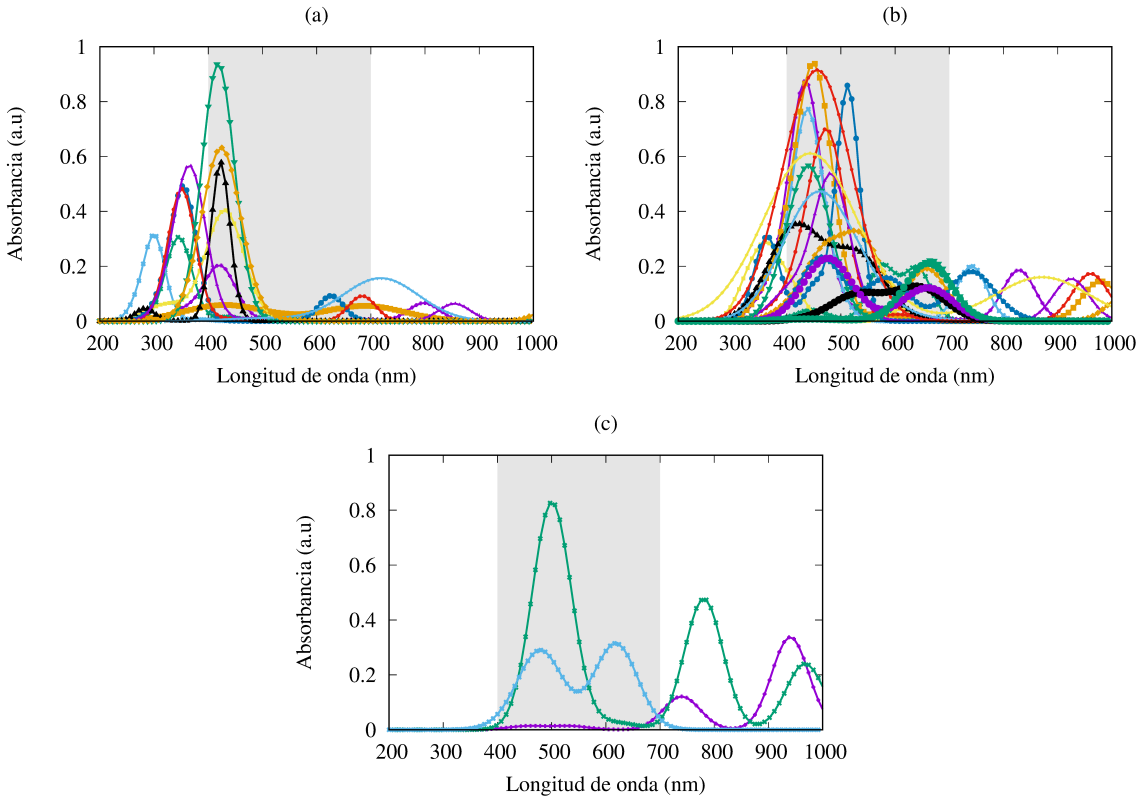

Fig. 4.2: Espectro de absorción en las geometría optimizadas en el primer estado excitado de los sistemas (a) 01-07, 12, 15, 16, 20, 33; (b) 08-10, 13, 14, 17-19, 21-27, 29, 31, 31; (c) 11, 28, 30. Las máxima fue localizado en comparación a la máxima obtenida en la geometría en estado excitado. Notar que la clasificación se adopto usando el estado fundamental para todo lo casos.

máxima, tal como se observa en la Fig. 4.3, un cuadro de color blanco. Como podemos observar los sistemas estudiados; en su mayoría, presentan cuadros de colores que van del celestes a azul oscuro. Es decir, en el estado excitado estos sistemas tienen un corrimiento hacia el IR (corrimiento positivo), lo cual mejora su rango de absorción .

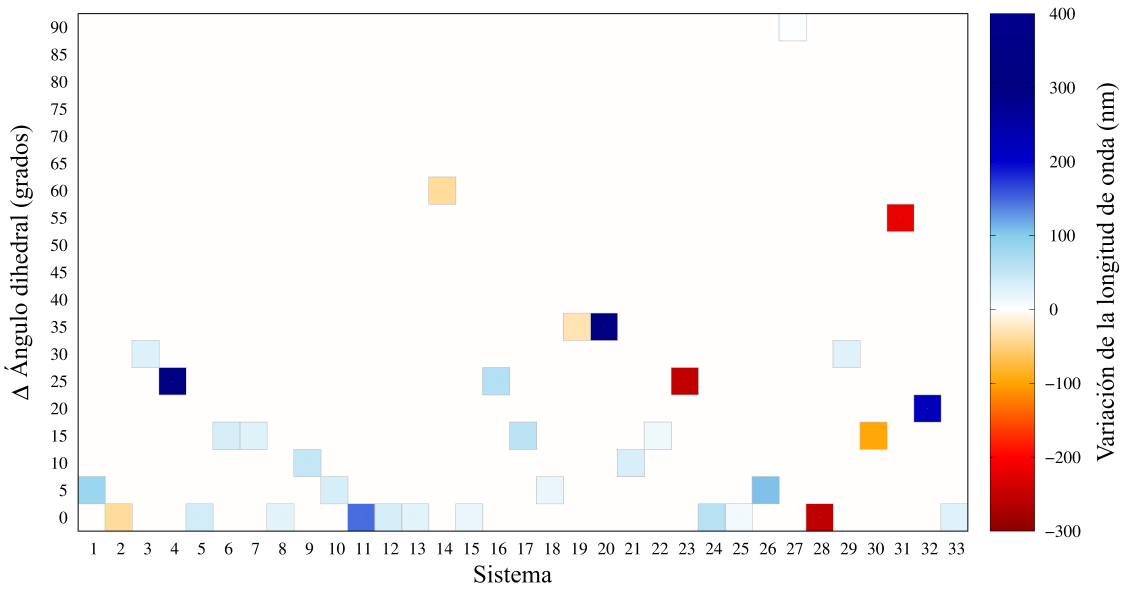

Fig. 4.3: Orgánicos fotovoltaicos en estudio.

Por otra parte, se observan sistemas sin cambios en sus ángulos dihedrales, pero con cambios en los espectros de absorción. Por ejemplo, el sistema **11** y el sistema **12** presentan cambios de 147.6 nm y 35.8 nm, respectivamente. Este comportamiento podría estar relacionado directamente con la transición electrónica de la transferencia de carga de los orbitales moleculares. De tal manera que estos sistemas en estado excitado presentan una re-distribución de carga (ver Fig. 4.4).

En la Fig. 4.4 (a) vemos los orbitales moleculares de las geometrías optimizadas en estado excitado de los sistemas 11 y 12 y las transiciones, que claramente se observan que van del HOMO al LUMO. La re-localización de las cargas del HOMO en estado excitado es evidente cuando se grafican los orbitales moleculares en 2D (ver Fig 4.4 (b y c)). La distribución de los electrones de los orbitales π en el HOMO del estado excitado se reduce para ambos sistemas. Esto podría ser atribuido en general a la curvatura que presenta la geometría en estado excitado. Es decir, las distancias de enlace se deforman en el plano xy; provocando tal distorsión. Los cambios de longitud de enlace entre el estado fundamental y estado excitado del sistema 11, se muestran en la Fig. 4.5 y la tabla 4.3. El enlace C11-C12, se redujo a 2.9 pm, N13-S14 aumento 3.4 pm y S14-N15 aumento 4.3 pm. También se observa que la interacción N15$\cdots$S17 disminuyó su distancia en 12.9 pm (interacción electrostática entre los átomos de N-S). Esta disminución hace que el sistema presente una curvatura. Estos cambios que presenta el sistema 11. En lo anterior, tienen participación los átomos de nitrógeno y azufre del building block 06 (thiadiazole[3,4-c]pyridine), los cuales juegan un papel

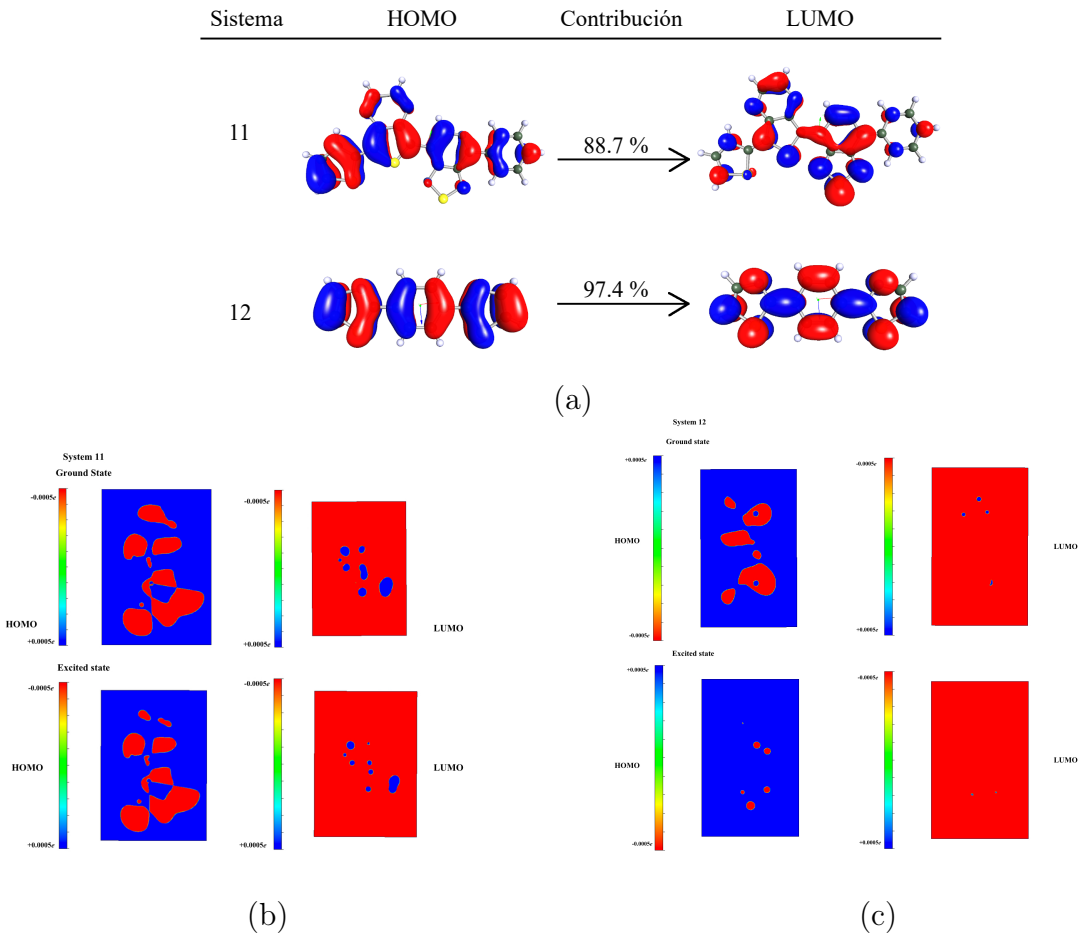

Fig. 4.4: Orbitales moleculares, (a) de los sistemas 11 y 12 en estado excitado, (b) en 2D respecto al eje *xy* del sistema 11 y (c) para el sistema 12.

muy importante en el cambio de geometría en estado excitado para ese sistema.

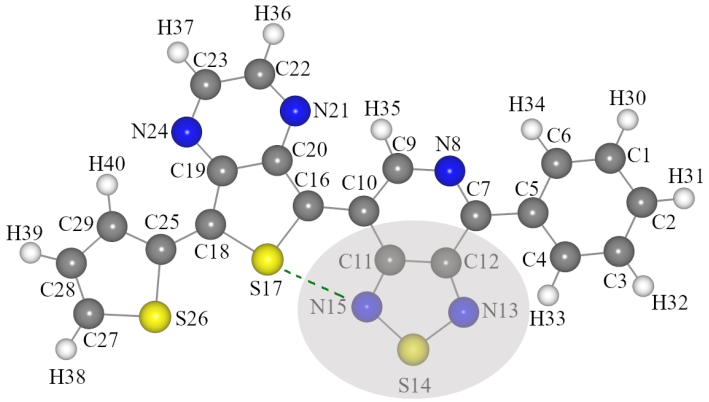

Fig. 4.5: Geometría correspondiente al sistema 11.

Tabla 4.3: Distancia de enlace correspondiente al sistema 11. Distancia de enlace en estado fundamental (Grd.), en estado excitado (Exc.) y la diferencia entre ambos (Diff.) medidos en picometros.

Enlace	Grd.	Exc.	Diff.	Enlace	Grd.	Exc.	Diff.
C1 - C2	139.9	140.0	-0.1	S14 - N15	162.7	167.0	-4.3
C1 - C6	139.0	138.8	0.2	C16 - S17	173.9	173.7	0.2
C1 - H30	109.2	109.2	0.0	C16 - C20	141.7	143.3	-1.6
C2 - C3	139.6	139.8	-0.2	S17 - C18	172.5	173.8	-1.3
C2 - H31	109.2	109.2	0.0	C18 - C19	141.3	141.6	-0.3
C3 - C4	139.5	139.2	0.3	C18 - C25	143.6	142.5	1.1
C3 - H32	109.2	109.1	0.1	C19 - C20	144.6	143.9	0.7
C4 - C5	141.0	141.4	-0.4	C19 - N24	135.9	135.9	0.0
C4 - H33	108.8	108.8	0.0	C20 - N21	136.0	135.2	0.8
C5 - C6	141.2	141.6	-0.4	N21 - C22	132.1	132.7	-0.6
C5 - C7	147.7	146.9	0.8	C22 - C23	142.3	141.8	0.5
C6 - H34	109.0	108.9	0.1	C22 - H36	109.5	109.4	0.1
C7 - N8	133.5	134.9	-1.4	C23 - N24	132.1	132.5	-0.4
C7 - C12	144.1	144.6	-0.5	C23 - H37	109.5	109.5	0.0
N8 - C9	134.5	133.8	0.7	C25 - S26	174.8	175.4	-0.6
C9 - C10	140.6	141.1	-0.5	C25 - C29	139.3	140.1	-0.8
C9 - H35	109.0	109.1	-0.1	S26 - C27	171.8	171.4	0.4
C10 - C11	143.2	142.1	1.1	C27 - C28	137.7	138.3	-0.6
C10 - C16	144.3	144.2	0.1	C27 - H38	108.6	108.7	-0.1
C11 - C12	145.0	142.1	2.9	C28 - C29	141.4	140.7	0.7
C11 - N15	134.7	136.2	-1.5	C28 - H39	108.9	108.9	0.0
C12 - N13	135.2	136.4	-1.2	C29 - H40	108.8	108.8	0.0
N13 - S14	162.2	165.6	-3.4	N15 ··· S17	284.3	271.4	12.9

En la Fig. 4.6 y la Tabla 4.4 se presentan las diferencias de distancias de enlace del sistema 12. Los enlaces de tiazoles que se conectan al benceno, C3-C12 y C6-C7 reducen sus distancias de enlace en 3.3 pm para ambos casos. Hay cambios de distancia de los tiazoles, sobre todo en los enlace de Carbono-Azufre. Los enlaces C12-S16 y C12-S16 aumentan sus distancias en 3.8 pm. Además del átomo de Azufre del tiozol, el Nitrógeno tiene un papel importante en la re-distribución de las cargas. Tal como se muestran en los enlaces C12-N13 y C7-N11, los cuales aumentan su distancia de enlace en 2.0 pm.

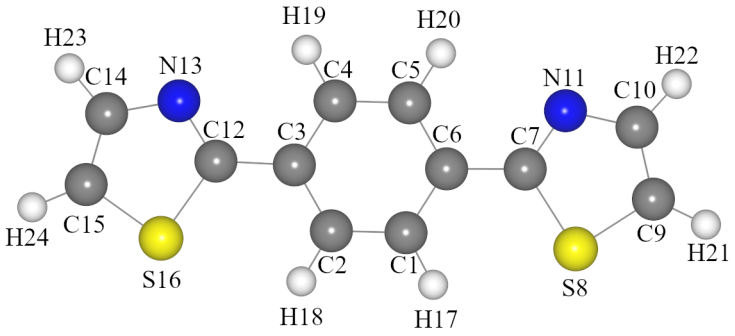

Fig. 4.6: Geometría correspondiente al sistema 12.

Tabla 4.4: Distancia de enlace correspondiente al sistema 12. Distancia de enlace en estado fundamental (Grd.), en estado excitado (Exc.) y la diferencia entre ambos (Diff.) medidos en picometros.

Enlace	Grd.	Exc.	Diff.	Enlace	Grd.	Exc.	Diff.
C1 - C2	138.8	137.8	1.0	C7 - N11	131.8	133.8	-2.0
C1 - C6	140.7	142.6	-1.9	S8 - C9	171.6	171.3	0.3
C1 - H17	109.2	109.2	0.0	C9 - C10	137.4	139.4	-2.0
C2 - C3	140.7	142.6	-1.9	C9 - H21	108.6	108.6	0.0
C2 - H18	109.2	109.2	0.0	C10 - N11	136.4	134.8	1.6
C3 - C4	140.9	143.1	-2.2	C10 - H22	109.0	109.1	-0.1
C3 - C12	146.1	142.8	3.3	C12 - N13	131.8	133.8	-2.0
C4 - C5	138.7	137.6	1.1	C12 - S16	175.9	179.7	-3.8
C4 - H19	109.0	109.0	0.0	N13 - C14	136.4	134.8	1.6
C5 - C6	140.9	143.1	-2.2	C14 - C15	137.4	139.4	-2.0
C5 - H20	109.0	109.0	0.0	C14 - H23	109.0	109.1	-0.1
C6 - C7	146.1	142.8	3.3	C15 - S16	171.6	171.3	0.3
C7 - S8	175.9	179.7	-3.8	C15 - H24	108.6	108.6	0.0

Orbitales moleculares

El comportamiento de los orbitales moleculares en los sistemas planos (ver figura 4.7) tales como el 05, 08, 11, 12, 15, 20, 25, 28 y 33, en su mayoría se observa

una distribución uniforme, excepto en los sistemas 20 y 25. El sistema 20, como mencionamos con anterioridad, en su estado fundamental se observaban torsiones en sus ángulos dihedrales y en estado excitado se convierten en ángulos coplanares. Aunque este sistema se vuelve coplanar, vemos que la distribución de sus orbitales no es uniforme. Tenemos orbitales localizados en la unión de los bloques B06 y B11. El sistema 25, es de geometría plana. Sin embargo, en la unión entre los bloques B06 Y B11, se observa localización de los orbitales. Dicha distribución ya no es uniforme.

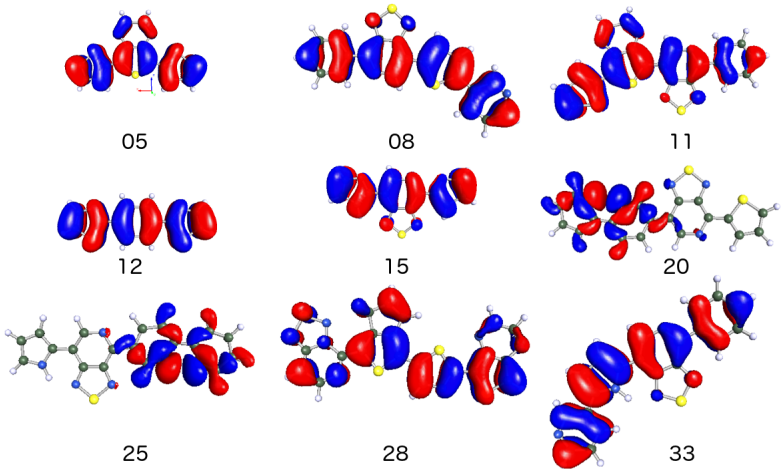

Fig. 4.7: Orbitales moleculares para los sistemas con ángulo dihedrales complanares.

Los orbitales moleculares de los sistemas ubicados entre 10° a 60° son el 01, 06, 07, 09, 10, 13, 16, 17, 18, 21, 24 y 26 (ver figura 4.8). En su mayoría presentan una distribución uniforme en sus orbitales moleculares. Con excepción de los sistemas 16, 24 y 26. En el sistema 16, en su estado fundamental, podemos observar que los tres ángulos dihedrales tienen torsiones. Sin embargo, en estado excitado, en dichos sistemas se disminuyen dichos ángulos. Estos cambios no tienen efectos sobre la distribución de los orbitales, se observa en unión de estos bloques B11 y B11, orbitales localizados. En el sistema 24 tampoco se observa orbitales moleculares uniformes entre la unión de los bloques B06 y B14. En el sistema 26, en la unión entre los bloques B06 y B14, también se observan orbitales localizados.

Los orbitales moleculares de los sistemas con ángulos dihedrales superiores a 60° son 02, 03, 04, 14, 19, 22, 23, 27, 29, 30, 31 y 32 (ver figura 4.9). Se observa que la distribución de los orbitales moleculares es estos sistemas no son uniformes. Estos sistemas son el 02, 03, 04, 14, 19, 22, 23, 27, 29, 30, 31 y 32, en los enlaces B10-B10, B10-B13, B06-B15, B03-B16, B06-B14, B05-B06, B06-B08, B06-B09, B04-B05 (también se encuentra el enlace B05-B06), B06-B08, B05-B06, B06-B16, respectivamente, es en donde se rompe la uniformidad de los orbitales moleculares.

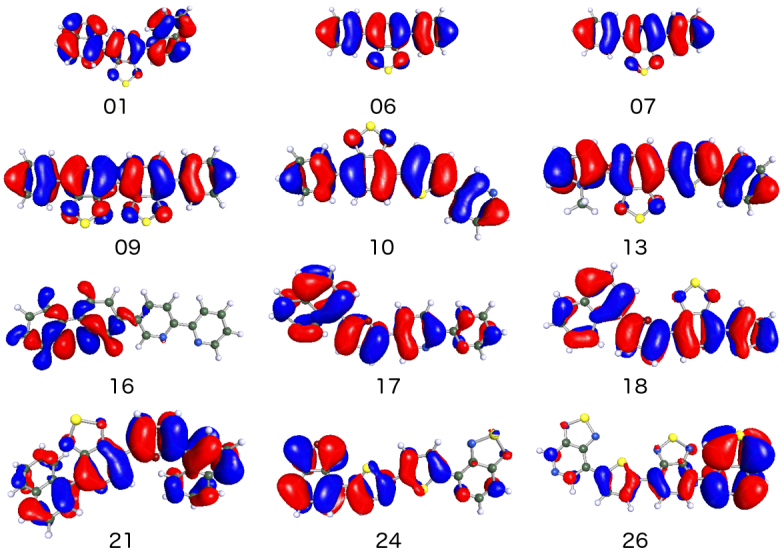

Fig. 4.8: Orbitales moleculares con ángulos dihedrales entre 10 a 60 grados.

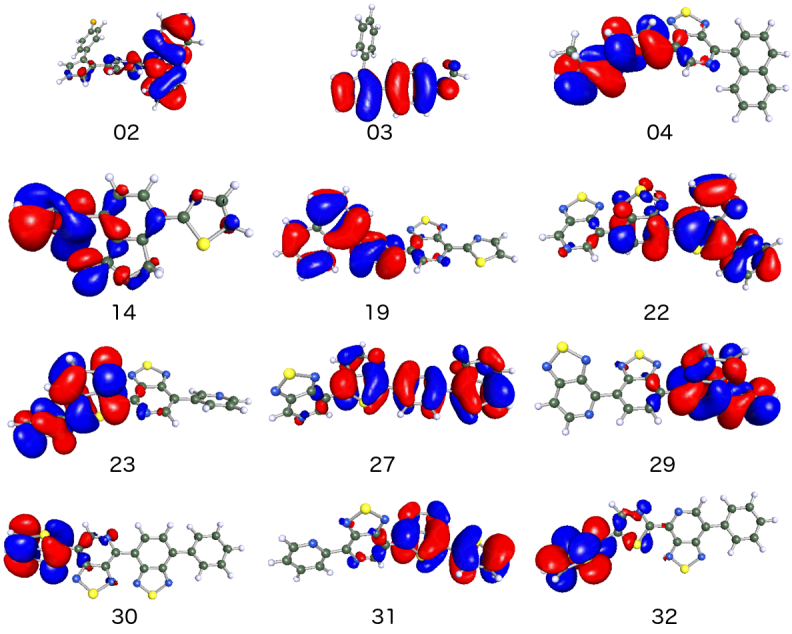

Fig. 4.9: Orbitales moleculares de los sistemas con ángulos dihedrales superiores a 60 grados

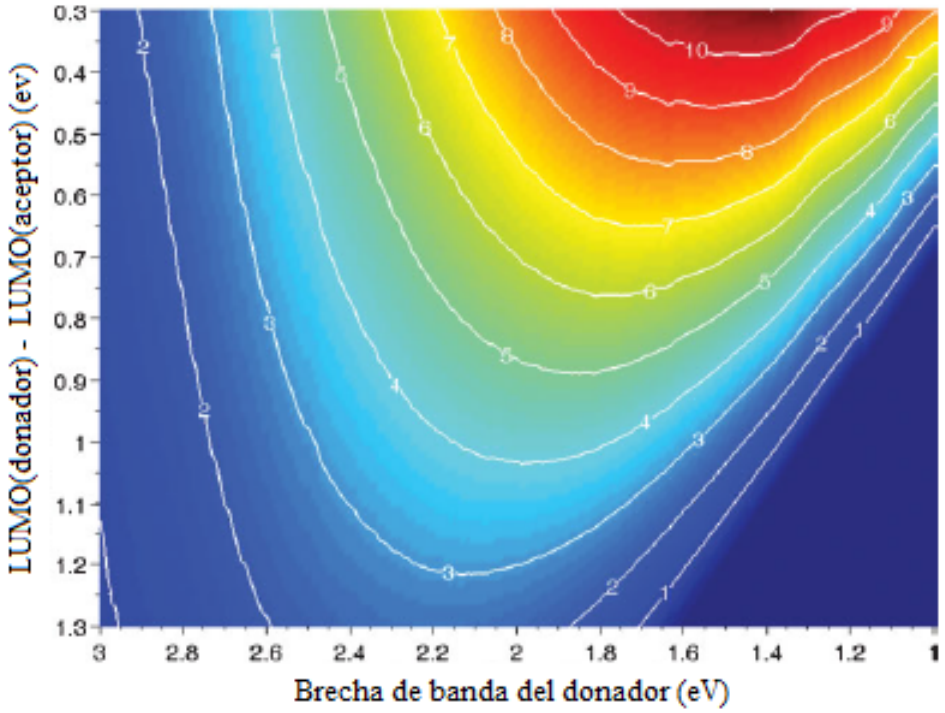

Fig. 4.10: Gráfica de contorno que muestra la eficiencia de conversión de energía de una celda solar BHJ con PCBM como material aceptor (el degradado de colores, el rojo representa mayor PCE y el azul menor PCE). John Wiley and Sons and Copyright Clearance Center, Número de licencia 5395001149820

4.1.1. Propiedades fotovoltaicas

Basado en una relación empírica para el V_{OC}, Scharber et al. concluyeron que la eficiencia de conversión de energía que podría alcanzar una celda orgánica BHJ seria de 10 % [74]. Usando una gráfica de contorno de un celda solar BHJ con PCBM como material aceptor,y considerando el valor de la eficiencia cuántica externa de 65 % y un factor de llenado (FF) de 65 % [75], podemos obtener la eficiencia empírica, la cual se encuentra esquematizada en la Fig. 4.10.

La PCE de los sistemas estudiados (ver Tabla 4.5) en su mayoría están dentro del rango de 5.50 % a 6.50 %. Los sistemas con valores más altos corresponde al 08, 10 y 20, con valores de 8.3 %, 8.2 % y 7.1 %, respectivamente. Los sistema que quedan fuera de la gráfica de contorno de Scharber son el 02, 03, 12, 16 y 17. Esto nos da una idea de la selección de la metodología para seleccionar sistemas moleculares de la base de datos de CEP con propiedades deseables y nos permite discriminar entre aquellos sistemas con propiedades no deseadas (como los sistemas 02, 03, 12, 16 y 17) obtenidos de métodos de estructura electrónica en estado fundamental y excitado.

En un estudio sistemático de un gran número de polímeros donadores combinados con PCBM como moléculas aceptoras, se observó que el V_{OC} puede ser calculado empíricamente por la siguiente ecuación [74]:

$$eV_{oc} = |E_H^D| - |E_L^A| - 0.3 \tag{4.4}$$

donde 0.3 se refiere a un factor de perdida relacionado a las BHJ. El valor experimental considerado para el LUMO del PCBM (E_L^A) fue de 4.26 eV [76].

Los resultados de la ecuación 4.4 para obtener el V_{OC}, se presentan en la Tabla 4.5, la cual se encuentran entre 0.12 eV y 1.16 eV, con excepción del sistema 02 y el 04 con valores de -0.12 eV y 0.03 eV, respectivamente. Los sistemas con valores de V_{OC} más altos con 0.53, 0.60, 0.70, 0.72, 0.82, 0.85, 0.85, 0.86, 1.00, 1.07 y 1.16 eV, corresponden a los sistema 25, 10, 08, 01, 12, 20, 09, 06, 07, 14 y 16, respectivamente.

La eficiencia de las celdas solares puede ser medida con los siguiente parámetros [77]: Considerando al V_{OC}, previamente descrito, la J_{SC} y el FF. El producto de estos tres valores corresponde al densidad máxima (P_{max}). La ecuación de la PCE se obtiene de acuerdo a la siguiente ecuación:

$$PCE = \frac{P_{max}}{P_{inc}} \tag{4.5}$$

donde P_{in} corresponde a la incidencia del fotón de la eficiencia de corriente. Este es un valor estándar de espectro de incidencia a AM1.5G (masa de aire global) con una intensidad de 1000 W/m^2 (100 mW/cm^2) a temperatura ambiente.

La estimación de J_{SC} puede obtenerse con la siguiente ecuación.

$$J_{sc} = \int_{\lambda} LHE(\lambda)\phi_{in}\mu_{collec}d\lambda \tag{4.6}$$

donde LHE(λ) es la eficiencia de captación de luz, que depende de la longitud de onda λ, la cual puede obtenerse con la ecuación:

$$LHE(\lambda) = 1 - 10^{-f} \tag{4.7}$$

donde f es el valor de la fuerza de oscilador de la longitud de onda máxima de absorción del material donador. El valor de ϕ_{in} corresponde a la eficiencia de inyección de electrón, el cual es relativo a la disponibilidad de inyección de electrón ΔG_{inj}, el cual se puede obtener de la siguiente ecuación

$$\Delta G_{inj} = E_{ox}^D - E_{0-0}^D - E_L^A \tag{4.8}$$

donde E_{ox}^D es la energía del potencial de ionización y E_{0-0} es la energía del primer estado excitado de la molécula donadora. El valor de μ_{collec} es la eficiencia de colección de electrón, la cual se considera una constante en nuestros cálculos.

El término E_{ox}^D se calcula con la siguiente ecuación

$$E_{ox}^D = E_0 - E_o^+ \tag{4.9}$$

donde E_0 es la energía total en estado neutro y E_0^+ es la energía total de catión

El ΔG_{inj} es una propiedad física que se refiere a la disponibilidad de una molécula de transferir electrones entre donador y aceptor. Todos los valores de ΔG_{inj} (ver Tabla 4.5) están en el rango de 0.50 eV a 3.56 eV, excepto los sistemas 02, 03

y 17, que tienen valores negativos o por debajo de 0.50 eV. Los valores más altos corresponden a los sistemas 05, 23, 20, 11, 25, 08, 07, 33, 15 y 16, las cuales podría ser usados como materiales donadores en una celda BHJ. Considerando la ecuación 4.6, para valores altos de ΔG_{inj} implica valores altos de J_{SC}. Además, para valores altos de LHE(λ) implica valores altos de J_{SC}. Los valores más altos para LHE(λ) son de 0.70, 0.71, 0.71, 0.75, 0.75, 0.76, 0.77, 0.79, 0.83, 0.83, 0.84 y 0.86, que correspoden a los sistemas 25, 06, 05, 13, 27, 15, 14, 08, 16, 17, 12 y 33, respectivamente.

Considerando los parámetros obtenidos en el presente trabajo de la estructura electrónica, tales como geometría molecular tanto en estado fundamental y estado excitado, se obtuvieron los parámetros empíricos tales como V_{OC}, J_{SC} y la PCE. De esta forma, es posible identificar sistemas orgánicos con posible aplicación en celdas solares BHJ como moléculas donadoras.

Tabla 4.5: Voltaje en circuito abierto (V_{OC}) en eV, Inyección de electrones (ΔG_{inj}) dado en eV, eficiencia de captación de luz (LHE), and PCE (%) de los sistemas OPV dentro del estudio. LHE es un parámetro adimensional que va desde 0.0 to 1.0.

Sistema	Grd				Exc		
	V_{oc} (eV)	ΔG_{inj} (eV)	LHE	PCE (%)	V_{oc} (eV)	ΔG_{inj} (eV)	LHE
01	0.72	0.83	0.35	6.5	0.59	1.07	0.47
02	-0.12	-0.98	0.49	–	-0.17	-0.35	0.42
03	0.20	-1.03	0.46	–	-0.35	-0.58	0.62
04	0.03	0.71	0.69	1.0	-0.27	1.48	0.17
05	0.12	1.01	0.71	3.0	-0.10	1.23	0.74
06	0.86	0.79	0.71	3.8	0.61	1.10	0.80
07	1.00	1.15	0.64	6.0	0.78	1.42	0.78
08	0.70	1.14	0.79	8.3	0.58	1.33	0.86
09	0.85	0.59	0.48	4.0	0.62	0.80	0.37
10	0.60	0.83	0.60	8.2	0.45	1.04	0.80
11	0.33	1.09	0.54	5.5	0.25	1.21	0.40
12	0.82	0.50	0.84	–	0.63	0.69	0.86
13	0.41	0.98	0.75	5.5	0.23	1.20	0.76
14	1.07	0.79	0.77	2.5	0.70	1.14	0.39
15	0.49	1.21	0.76	6.0	0.34	1.44	0.79
16	1.16	3.56	0.83	–	0.01	57.30	0.88
17	0.43	0.12	0.83	–	0.29	0.32	0.86
18	0.30	0.88	0.63	4.2	0.21	1.06	0.73
19	0.43	0.95	0.64	6.5	0.24	1.63	0.52
20	0.85	1.06	0.55	7.1	-0.15	8.32	0.42
21	0.43	0.77	0.55	6.0	0.29	0.97	0.67
22	0.48	0.96	0.52	6.0	0.37	1.33	0.73
23	0.45	1.03	0.56	6.0	0.20	1.73	0.55
24	0.45	0.89	0.51	6.0	0.34	1.17	0.48
25	0.53	1.10	0.70	6.5	-0.23	4.59	0.73
26	0.48	0.86	0.36	5.5	0.34	1.15	0.32
27	0.38	0.86	0.75	6.0	0.15	1.42	0.72
28	0.36	0.90	0.66	6.0	0.22	1.04	0.70
29	0.45	0.96	0.26	6.0	0.16	1.52	0.23
30	0.47	0.87	0.34	6.0	0.33	1.39	0.38
31	0.48	0.95	0.37	6.0	0.23	1.53	0.40
32	0.42	0.96	0.62	5.5	0.43	1.63	0.38
33	0.43	1.15	0.86	6.0	0.34	1.44	0.87
ZR1	0.14	0.14	0.99	2.0	0.06	0.26	0.97

Capítulo 5

Transporte electrónico

5.1. Estudio de transporte electrónico.

Los sistemas orgánicos que se seleccionaron para este estudio son el 06, 11 y 23 (ver Fig. 5.1), mostrado en la sección 4.0.1. De los tres sistemas, en dos de ellas se observa la fotoisomerización, lo que nos indica cambios en sus ángulos dihedrales del estado fundamental al estado excitado en presencia de la irradiación solar. En promedio los sistemas 06, 11 y 23 muestran cambios en sus ángulos dihedrales de 15°, 0° y 25°.

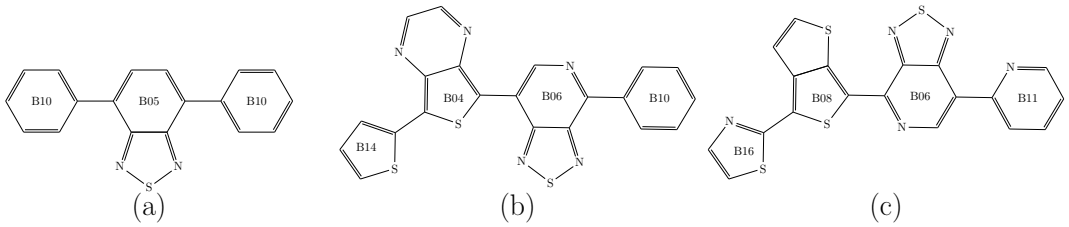

(a) (b) (c)

Fig. 5.1: Esquema de los sistemas orgánicos. (a) sistema 06, (b) sistema 11 y (c) sistemas 23.

En la Fig. 5.2 se muestra la relación del coeficiente de transmisión $T(E, V_b)$ y la energía del electrón a cero voltaje ($V_b = 0$). El promedio del nivel de Fermi representa el valor promedio del potencial químico de los dos electrodos y está ubicado en el cero del eje x. En el estado fundamental el sistemas 06 (ver Fig. 5.2 (a)) el sistema muestra picos de transmisión cercano al nivel de Fermi y por debajo del nivel de Fermi. En el estado excitado (ver Fig. 5.2 (b)) se observa un pico por arriba del nivel de Fermi, lo cual nos indica que mejoran las propiedades de transporte electrónico. Además una mayor densidad en las curvas de transmisión son indicativas de más canales de transmisión abiertos en el sistema debido a un fuerte acoplamiento entre la molécula y el electrodo. También podemos observar en la Fig. 5.2, la relación de las curvas de transmisión y la DOS. Este sistema muestra una fuerte correlación entre ambos,

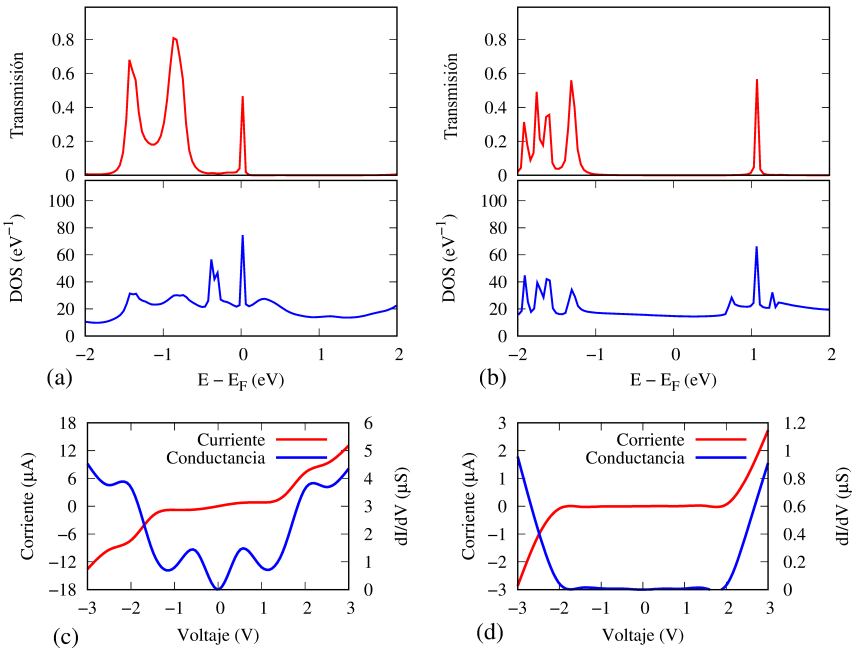

Fig. 5.2: Coeficiente de transmisión del sistema 06, (a) Estado fundamental y (b) Estado excitado. Corriente-Voltaje (I-V) y Conductancia-Voltaje (dI/dV). (c) Estado fundamental y (d) Estado excitado

la curva de transmisión y la DOS (ver Fig. 5.2 (c) y (d)), en estado fundamental y estado excitado.

En las curvas I-V y la conductancia del sistema 06 (ver Fig. 5.2), se observa una configuración simétrica debido a que el sistema 06 tiene una configuración simétrica (ver Fig. 5.1 (a)) entre los electrodos. En el estado fundamental (ver Fig. 5.2 (c)), a un intervalo entre 0.0 y 0.5 V, hay un pequeño aumento de corriente (0.71 μA), comportamiento que se puede observar también en el pico máximo de conductancia (1.42 μS). Otro aumento se observa entre 1.5 y 2.0 V, donde la corriente tiene un valor de 1.26 μA y un valor de conductancia de 3.63 μS. En estado excitado (ver Fig. 5.2 (d)), no se observan aumento de corriente sino hasta 2.0 V, lo que nos indica que requiere mayor energía para conducir la corriente.

En las curvas de transmisión y la DOS del sistema 11 (ver Fig. 5.3) se observa una fuerte correlación entre $T(E, V_b)$ y DOS. En el estado fundamental (ver Fig. 5.3 (a)) se observa un acoplamiento entre la molécula y el electrodo, debido a los picos de transmisión por arriba y por debajo de la energía de nivel de Fermi. En estado excitado (ver Fig. 5.3 (b)), las curvas de transmisión solo disminuyen su amplitud, pero se mantiene la propiedad de transporte de electrones.

En la Fig. 5.3 podemos observar los resultados de la curva I-V y la conductancia del sistema 11, donde podemos apreciar una gráfica asimétrica, probablemente debido a que por su estructura molecular no presenta simetría (ver Fig. 5.1 (b)), y por lo tanto, tampoco entre los electrodos. En estado fundamental vemos un incremento de

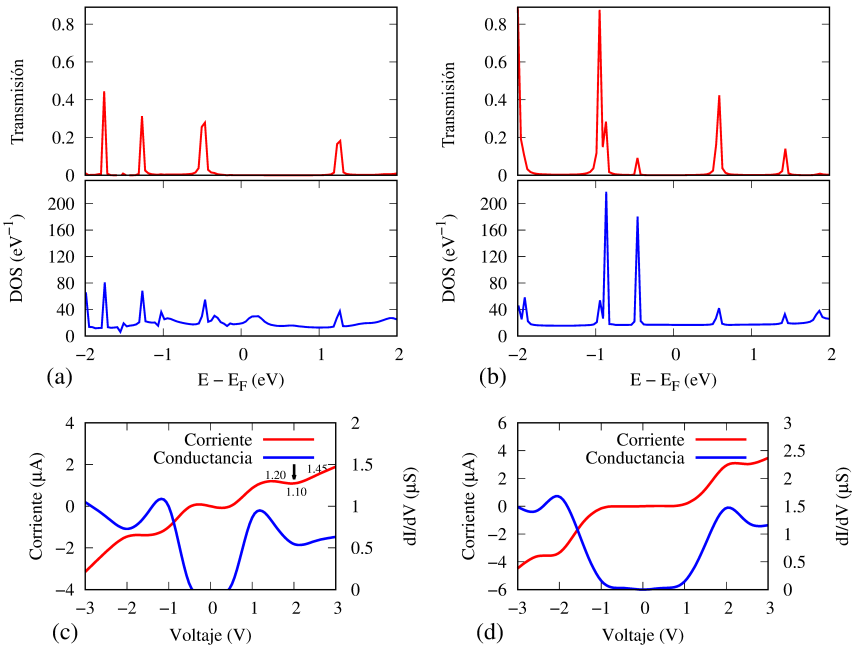

Fig. 5.3: Coeficiente de transmisión del sistema 11, (a) Estado fundamental y (b) Estado excitado. Corriente-Voltaje (I-V) y Conductancia-Voltaje (dI/dV). (c) Estado fundamental y (d) Estado excitado

corriente de 0.86 μA entre 0.5 y 1.0 V (ver Fig. 5.3 (c)). En este sistema podemos observar que entre 1.5 a 2.0 V, una disminución de la corriente. El valor de la corriente en 1.5 V es de 1.2 μA y en 2.0 V es de 1.1 μA y posteriormente vuelve a aumentar ubicándose en 1.45 μA a 2.5 V. Como se mencionó anteriormente, este fenómeno es conocido como NDR. En estado excitado se observa un incremento de la corriente de 0.1 μA en 0.5 V, después de 0.14 μA en 1.0 V y de 2.94 μA en 2.0 V (ver Fig. 5.3 (d)) Tal como se muestra en el pico máximo de conductancia con un valor de 1.5 μS a 2.0 V. Por lo tanto, este sistema tiene un buen comportamiento en sus propiedades de transporte de carga, además muestra una buena capacidad de conducir la corriente electrónica.

El sistema 23, de acuerdo a los resultados obtenidos de las curvas de transmisión y la DOS (ver Fig. 5.4), se observa que al igual que en los casos anteriores, hay una fuerte correlación entre el $T(E, V_b)$ y la DOS. De acuerdo a los resultados obtenidos vemos que en el estado fundamental (ver Fig. 5.4 (a)) se observa un pico máximo de transmisión, por arriba del nivel de Fermi, un coeficiente alto de 0.8. Por debajo del nivel de Fermi se observa una disminución del valor de transmisión.

En el estado excitado (ver Fig. 5.4 (b)) se observa valores de coeficiente de transmisión muy bajos, por ejemplo, valores por debajo de la energía de Fermi, con un valor máximo de 0.11 de coeficiente y por arriba del nivel Fermi un valor de 0.05 de coeficiente, de tal manera que disminuye sus propiedades de transporte electrónico, respecto al estado fundamental.

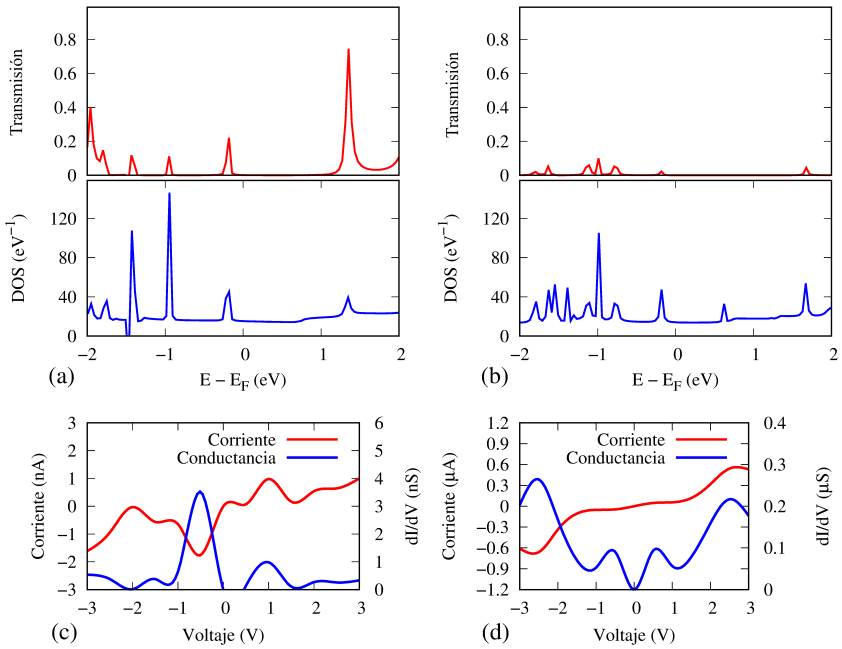

Fig. 5.4: Coeficiente de transmisión del sistema 23, (a) Estado fundamental y (b) Estado excitado. Corriente-Voltaje (I-V) y Conductancia-Voltaje (dI/dV). (c) Estado fundamental y (d) Estado excitado

En la Fig. 5.4 se muestran los resultados obtenidos de la curva I-V y la conductancia del sistema 23, la cual presenta un comportamiento asimétrico (ver Fig. 5.1 (c)). En estado fundamental se observa un incremento de corriente de 0.98 nA a un intervalo de 0.5 a 1.0 V (ver Fig. 5.4 (c)). Nuevamente en este sistema observamos el fenómeno NDR, a 1.5 V, donde vemos que pasó de 0.98 nA a 0.16 nA y después retoma el valor de 0.54 nA, en 1.0, 1.5 y 2.0 V, respectivamente. También podemos observar este fenómeno en -0.5 V. En estado excitado el comportamiento cambia (ver Fig. 5.4 (d)). Se pierde el fenómeno NDR y se observa un incremento de corriente de 0.05 μA entre el rango de 0.0 a 0.5 V. También la conductancia muestra un pico máximo en 0.5 V. Otro aumento de 0.54 μA se observa de 1.5 a 2.5 V. También se observa otro pico de conductancia máxima en ese punto.

La metodología utilizada para conocer las propiedades de transporte electrónico de los sistemas 06, 11 y 23, puede considerarse como una herramienta de guía para la selección de moléculas OPV. Además de que los parámetros de transmisión y la curva I-V podrian considerarse como descriptores para formar una base de datos para futuras aplicaciones en el diseño de materiales fotovoltaicos.

Conclusiones

En el estudio sistemático de las propiedades electrónicas de una serie de moléculas orgánicas, se identificaron cambios en sus ángulos dihedrales. Tales cambios se notaron al comparar las coordenadas geométricas en estado fundamental y en estado excitado, provocando un fenómeno llamado fotoisomerización. Tal comportamiento puede promover fácilmente la transferencia de electrones, cuando los cambios de los ángulos dihedrales son menores a 90 °. Esto debido a los valores obtenidos del momento dipolar en los cálculos teóricos. Esto también nos confirma la distribución uniforme de los orbitales moleculares. El cálculo de las propiedades ópticas y electrónicas revelan que los espectros UV-vis de tales sistemas presentan máximos locales cercanos a la región de luz visible, esto permite al grupo de sistemas OPV ser potenciales candidatos para el diseño de dispositivos de una celda solar. Los sistemas OPV con cambios dramáticos en estado excitado en sus angulos dihedrales, reducen considerablemente los parámetros de su estructura electrónica, tal como el momento dipolar, dificultando la movilidad de los electrones en los materiales. La distorsión estructural también fue la responsable del corrimiento hacia al infrarrojo de los espectros de absorción. Como resultado, los descriptores presentados en este trabajo, pueden ser usados como herramienta para la selección de materiales OPV con propiedades de estructura electrónica deseadas, en el diseño de dispositivos de celdas solares.

Del estudio sistemático basado en DFT y NEGF desarrollado para estudiar las propiedades de transporte electrónico de los sistemas OPV, que presentan el fenómeno de fotoisomerización, el sistema que ha presentado mejores propiedades es el 11, debido que tiene un buen coeficiente de transmisión, lo cual se puede comprobar en la curva I-V y la conductancia. También presenta el fenómeno de NDR. El sistema 06, a pesar de que en estado fundamental presenta propiedades de transmisión adecuadas, vemos que en el estado excitado disminuye, tal como se puede apreciar en la curva I-V y la conductancia. Lo anterior es indicativo de que requiere mayor energía para conducir la corriente electrónica. Respecto al sistema 23, el cual presenta un cambio en su geometría en estado excitado, se observa que tiene un buen coeficiente de transmisión en estado fundamental, pero en estado excitado disminuye.

Los sistemas orgánicos con altos valores de transmisión y con alta capacidad de conducción de corriente, son candidatos como materiales donadores en la aplicación de celdas solares tipo heterounión.

Bibliografía

[1] IEA. "World Energy Outlook 2021, IEA, Paris". (2021), dirección: https://www.iea.org/reports/world-energy-outlook-2021. (accessed: 10.02.2022).

[2] S. J. Lim, D. U. Kim, J.-H. Song y J.-W. Yu, "Enhanced performance of semi-transparent OPV with nanoparticle reflectors", *Organic Electronics*, vol. 59, págs. 314-318, 2018, ISSN: 1566-1199.

[3] H. Youn, T. Lee y L. J. Guo, "Multi-film roll transferring (MRT) process using highly conductive and solution-processed silver solution for fully solution-processed polymer solar cells", *Energy Environ. Sci.*, vol. 7, págs. 2764-2770, 8 2014.

[4] M. Scharber y N. Sariciftci, "Efficiency of bulk-heterojunction organic solar cells", *Progress in Polymer Science*, vol. 38, n.º 12, págs. 1929-1940, 2013, Topical issue on Conductive Polymers, ISSN: 0079-6700.

[5] L. Meng, Y. Zhang, X. Wan y col., "Organic and solution-processed tandem solar cells with 17.3 % efficiency", *Science*, vol. 361, n.º 6407, págs. 1094-1098, 2018, ISSN: 0036-8075.

[6] M.-A. Pan, T.-K. Lau, Y. Tang y col., "16.7 %-efficiency ternary blended organic photovoltaic cells with PCBM as the acceptor additive to increase the open-circuit voltage and phase purity", *J. Mater. Chem. A*, vol. 7, págs. 20 713-20 722, 36 2019.

[7] Y. Cui, H. Yao, J. Zhang y col., "Over 16 % efficiency organic photovoltaic cells enabled by a chlorinated acceptor with increased open-circuit voltages", *Nature Communications*, vol. 10, n.º 2515, pág. 1, 2019.

[8] Y. He, H.-Y. Chen, J. Hou e Y. Li, "Indene-C60 Bisadduct: A New Acceptor for High-Performance Polymer Solar Cells", *Journal of the American Chemical Society*, vol. 132, n.º 4, págs. 1377-1382, 2010.

[9] X. Guo, C. Cui, M. Zhang y col., "High efficiency polymer solar cells based on poly(3-hexylthiophene)/indene-C70 bisadduct with solvent additive", *Energy Environ. Sci.*, vol. 5, págs. 7943-7949, 7 2012.

[10] Z. Xiao, X. Geng, D. He, X. Jia y L. Ding, "Development of isomer-free fullerene bisadducts for efficient polymer solar cells", *Energy Environ. Sci.*, vol. 9, págs. 2114-2121, 6 2016.

[11] Z. Xiao, X. Jia, D. Li y col., "26mAcm^{-2} J_{sc} from organic solar cells with a low-bandgap nonfullerene acceptor", *Science Bulletin*, vol. 62, n.º 22, págs. 1494-1496, 2017.

[12] J. Yuan, Y. Zhang, L. Zhou y col., "Single-Junction Organic Solar Cell with over 15 % Efficiency Using Fused-Ring Acceptor with Electron-Deficient Core", *Joule*, vol. 3, n.º 4, págs. 1140-1151, 2019.

[13] J. Xiong, K. Jin, Y. Jiang y col., "Thiolactone copolymer donor gifts organic solar cells a 16.72 % efficiency", *Science Bulletin*, vol. 64, n.º 21, págs. 1573-1576, 2019.

[14] T. Wang, J. Qin, Z. Xiao y col., "A 2.16 eV bandgap polymer donor gives 16 % power conversion efficiency", *Science Bulletin*, vol. 65, n.º 3, págs. 179-181, 2020.

[15] Q. Liu, Y. Jiang, K. Jin y col., "18 % Efficiency organic solar cells", *Science Bulletin*, vol. 65, n.º 4, págs. 272-275, 2020.

[16] S. Gélinas, A. Rao, A. Kumar y col., "Ultrafast Long-Range Charge Separation in Organic Semiconductor Photovoltaic Diodes", *Science*, vol. 343, n.º 6170, págs. 512-516, 2014, ISSN: 0036-8075.

[17] A. A. Bakulin, A. Rao, V. G. Pavelyev y col., "The Role of Driving Energy and Delocalized States for Charge Separation in Organic Semiconductors", *Science*, vol. 335, n.º 6074, págs. 1340-1344, 2012, ISSN: 0036-8075.

[18] T. M. Clarke y J. R. Durrant, "Charge Photogeneration in Organic Solar Cells", *Chemical Reviews*, vol. 110, n.º 11, págs. 6736-6767, 2010.

[19] S. D. Collins, N. A. Ran, M. C. Heiber y T.-Q. Nguyen, "Small is Powerful: Recent Progress in Solution-Processed Small Molecule Solar Cells", *Advanced Energy Materials*, vol. 7, n.º 10, pág. 1 602 242, 2017.

[20] R. Olivares-Amaya, C. Amador-Bedolla, J. Hachmann y col., "Accelerated computational discovery of high-performance materials for organic photovoltaics by means of cheminformatics", *Energy Environ. Sci.*, vol. 4, págs. 4849-4861, 12 2011.

[21] B. Bai, M. Zhang, N. Ji, J. Wei, H. Wang y M. Li, "E-Z isomerization of the -C=N- bond in anthracene-based acylhydrazone derivatives under visible light", *Chem. Commun.*, vol. 53, págs. 2693-2696, 18 2017.

[22] V. Hernández and J. T. López Navarrete, "Ab initio study of torsional potentials in 2,2'-bithiophene and 3,4'- and 3,3'-dimethyl-2,2'-bithiophene as models of the backbone flexibility in polythiophene and poly(3-methylthiophene)", *The Journal of Chemical Physics*, vol. 101, n.º 2, págs. 1369-1377, 1994.

[23] P. Bortolus y S. Monti, "Cis-trans photoisomerization of azobenzene. Solvent and triplet donors effects", *The Journal of Physical Chemistry*, vol. 83, n.º 6, págs. 648-652, 1979.

[24] D. L. Meyer, R. Matsidik, M. Sommer y T. Biskup, "Electronic Structure Trumps Planarity: Unexpected Narrow Exciton Delocalization in PNDIT2 Revealed by Time-Resolved Electron Paramagnetic Resonance (EPR) Spectroscopy", *Advanced Electronic Materials*, vol. 4, n.º 3, pág. 1 700 385, 2018.

[25] A. Guillén-López, C. Delesma, C. Amador-Bedolla, M. Robles y J. Muñiz, "Electronic structure and nonlinear optical properties of organic photovoltaic systems with potential applications on solar cell devices: a DFT approach", *Theoretical Chemistry Accounts*, vol. 137, n.º 6, pág. 85, 2018.

[26] H. Brahim, "DFT/TD-DFT investigation on the UV–vis absorption and phosphorescence spectra of platinum(II) and palladium(II) complexes with Schiff-base ligands", *Journal of Luminescence*, vol. 210, págs. 96-103, 2019.

[27] N. Wazzan y A. Irfan, "Theoretical study of triphenylamine-based organic dyes with mono-, di-, and tri-anchoring groups for dye-sensitized solar cells", *Organic Electronics*, vol. 63, págs. 328-342, 2018.

[28] Q. Arooj y F. Wang, "Switching on optical properties of D-π-A DSSC sensitizers from π-spacers towards machine learning", *Solar Energy*, vol. 188, págs. 1189-1200, 2019.

[29] S. Bedoura, H.-W. Xi, H. W. Goh y K. H. Lim, "DFT/TDDFT Investigation on donor-acceptor triazole-based copolymers for organic photovoltaics", *Journal of Molecular Structure*, vol. 1248, pág. 131 406, 2022, ISSN: 0022-2860.

[30] S. Fan, Z.-R. Sun, H. Shi, W.-J. Fan, D.-Z. Tan e Y.-G. Chen, "Modification of benzoindenothiophene-based organic dye with fused thiophenes for efficient dye-sensitized solar cells", *Journal of Molecular Graphics and Modelling*, pág. 108 214, 2022, ISSN: 1093-3263.

[31] Q. Bao, Z. Lu, J. Li, K. P. Loh y C. M. Li, "Theoretical and Experimental Studies of Electronic Transport of Dithienothiophene", *The Journal of Physical Chemistry C*, vol. 113, n.º 28, págs. 12 530-12 537, 2009.

[32] L. O. Jones, M. A. Mosquera, G. C. Schatz y M. A. Ratner, "Molecular Junctions Inspired by Nature: Electrical Conduction through Noncovalent Nanobelts", *The Journal of Physical Chemistry B*, vol. 123, n.º 38, págs. 8096-8102, 2019.

[33] D. Ferreira, M. Moura-Moreira, S. Corrêa, C. da Silva Jr y J. Del Nero, "Electronic transport in 1D system with coupling atomic-size nickel electrodes and carbon wires", *Materials Science and Engineering: B*, vol. 262, pág. 114 681, 2020, ISSN: 0921-5107.

[34] G. Berdiyorov, G. Eshonqulov y H. Hamoudi, "Electronic transport of CNT-encapsulated carbyne", *Computational Materials Science*, vol. 183, pág. 109 809, 2020, ISSN: 0927-0256.

[35] A. Kanaani, M. Vakili y D. Ajloo, "Electronic transport properties of 2-nIiitro-4-(6-(4-nitrophenyl)-4-phenyl-1,3-diaza-bicyclo[3.1.0]hex-3-en-2-yl)phenol: A light-driven molecular switch", *Optik*, vol. 219, pág. 165 295, 2020, ISSN: 0030-4026.

[36] L. Esaki, "New Phenomenon in Narrow Germanium $p - n$ Junctions", *Phys. Rev.*, vol. 109, págs. 603-604, 2 ene. de 1958.

[37] S. Rafique, S. M. Abdullah, K. Sulaiman y M. Iwamoto, "Fundamentals of bulk heterojunction organic solar cells: An overview of stability/degradation issues and strategies for improvement", *Renewable and Sustainable Energy Reviews*, vol. 84, págs. 43-53, 2018, ISSN: 1364-0321.

[38] C. Li, C. Kwong, A. Djurišić y col., "Improved performance of OLEDs with ITO surface treatments", *Thin Solid Films*, vol. 477, n.º 1, págs. 57-62, 2005, ICMAT 03, ISSN: 0040-6090.

[39] J. J. M. Halls, K. Pichler, R. H. Friend, S. C. Moratti y A. B. Holmes, "Exciton diffusion and dissociation in a poly(p-phenylenevinylene)/C60 heterojunction photovoltaic cell", *Applied Physics Letters*, vol. 68, n.º 22, págs. 3120-3122, 1996.

[40] A. Haugeneder, M. Neges, C. Kallinger y col., "Exciton diffusion and dissociation in conjugated polymer/fullerene blends and heterostructures", *Phys. Rev. B*, vol. 59, págs. 15 346-15 351, 23 1999.

[41] J. P. Perdew, M. Ernzerhof y K. Burke, "Rationale for mixing exact exchange with density functional approximations", *The Journal of Chemical Physics*, vol. 105, n.º 22, págs. 9982-9985, 1996.

[42] J. Piris, T. E. Dykstra, A. A. Bakulin y col., "Photogeneration and Ultrafast Dynamics of Excitons and Charges in P3HT/PCBM Blends", *The Journal of Physical Chemistry C*, vol. 113, n.º 32, págs. 14 500-14 506, 2009.

[43] R. G. Parr y W. Yang, *Density-functional theory of Atoms and Molecules*, I. series of monographs on chemistry, ed. Oxford University Press, Inc. USA, 1994.

[44] P. Atkins y F. Ronald, *Molecular quantum mechanics*, Fourth, O. U. Press, ed. ,Great Britain: OXFORD University Press, 2005.

[45] H. García, N. Farfán y M. Hernández, "Communication", *Personal communication*, Facultad de Química UNAM, 2019.

[46] L. D. Sifuentes-Vázquez, E. Martínez-González, R. A. Toscano y col., "Experimental and theoretical exploration of aryl substituent effects on the electronic properties of asymmetric 4,7-di(thiophene-2-yl)-benzo[c][2,1,5]thiadiazole.", *Polycyclic Aromatic Compounds*, DOI: 10.1080/10406638.2020.1749858, 2020.

[47] J. P. Perdew, K. Burke y M. Ernzerhof, "Generalized Gradient Approximation Made Simple", *Phys. Rev. Lett.*, vol. 77, n.º 18, págs. 3865-3868, 1996.

[48] F. Weigend, M. Häser, H. Patzelt y R. Ahlrichs, "RI-MP2: optimized auxiliary basis sets and demonstration of efficiency", *Chemical Physics Letters*, vol. 294, n.º 1, págs. 143-152, 1998, ISSN: 0009-2614.

[49] F. Weigend y R. Ahlrichs, "Balanced basis sets of split valence, triple zeta valence and quadruple zeta valence quality for H to Rn: Design and assessment of accuracy", *Phys. Chem. Chem. Phys.*, vol. 7, págs. 3297-3305, 18 2005.

[50] *TURBOMOLE V6.6 2014, a development of University of Karlsruhe and Forschungszentrum Karlsruhe GmbH, 1989-2007, TURBOMOLE GmbH, since 2007; available from*
`http://www.turbomole.com`.

[51] C. Steffen, K. Thomas, U. Huniar, A. Hellweg, O. Rubner y A. Schroer, "TmoleX—A graphical user interface for TURBOMOLE", *Journal of Computational Chemistry*, vol. 31, n.º 16, págs. 2967-2970, 2010.

[52] G. Rossum, "Python Reference Manual", Python Software Foundation, Amsterdam, The Netherlands, The Netherlands, inf. téc., 1995.

[53] K. STOKBRO, J. TAYLOR, M. BRANDBYGE y P. ORDEJÓN, "TranSIESTA: A Spice for Molecular Electronics", *Annals of the New York Academy of Sciences*, vol. 1006, n.º 1, págs. 212-226, 2003.

[54] J. M. Soler, E. Artacho, J. D. Gale y col., "The SIESTA method forab initioorder-Nmaterials simulation", *Journal of Physics: Condensed Matter*, vol. 14, n.º 11, págs. 2745-2779, mar. de 2002.

[55] N. Troullier y J. Martins, "A straightforward method for generating soft transferable pseudopotentials", *Solid State Communications*, vol. 74, n.º 7, págs. 613-616, 1990, ISSN: 0038-1098.

[56] A. D. Becke, "Density-functional exchange-energy approximation with correct asymptotic behavior", *Phys. Rev. A*, vol. 38, págs. 3098-3100, 6 1988.

[57] C. Lee, W. Yang y R. G. Parr, "Development of the Colle-Salvetti correlation-energy formula into a functional of the electron density", *Phys. Rev. B*, vol. 37, págs. 785-789, 2 1988.

[58] A. D. Becke, "Density-functional thermochemistry. III. The role of exact exchange", *The Journal of Chemical Physics*, vol. 98, n.º 7, págs. 5648-5652, 1993.

[59] C. Delesma, C. Amador-Bedolla, M. Robles y J. Muñiz, "Photoisomerization and its effect in the opto-electronic properties of organic photovoltaic materials: A quantum chemistry study", *Journal of Photochemistry and Photobiology A: Chemistry*, vol. 409, pág. 113 155, 2021, ISSN: 1010-6030.

[60] Y. Zhao y D. G. Truhlar, "The M06 suite of density functionals for main group thermochemistry, thermochemical kinetics, noncovalent interactions, excited states, and transition elements: two new functionals and systematic testing of four M06 functionals and 12 other functionals", *Theoretical Chemistry Accounts*, vol. 119, n.º 5, pág. 525, 2008.

[61] N. Blouin, A. Michaud, D. Gendron y col., "Toward a Rational Design of Poly(2,7-Carbazole) Derivatives for Solar Cells", *Journal of the American Chemical Society*, vol. 130, n.º 2, págs. 732-742, 2008.

[62] R. G. Parr y R. G. Pearson, "Absolute hardness: companion parameter to absolute electronegativity", *Journal of the American Chemical Society*, vol. 105, n.º 26, págs. 7512-7516, 1983.

[63] R. El Mouhi, S. El Khattabi, M. Hachi y col., "DFT and TD-DFT calculations on thieno[2,3-b]indole-based compounds for application in organic bulk heterojunction (BHJ) solar cells", *Research on Chemical Intermediates*, vol. 45, n.º 3, págs. 1327-1340, 2019.

[64] B. Carsten, J. M. Szarko, H. J. Son y col., "Examining the Effect of the Dipole Moment on Charge Separation in Donor–Acceptor Polymers for Organic Photovoltaic Applications", *Journal of the American Chemical Society*, vol. 133, n.º 50, págs. 20 468-20 475, 2011.

[65] H. D. de Gier, R. Broer y R. W. A. Havenith, "Non-innocent side-chains with dipole moments in organic solar cells improve charge separation", *Phys. Chem. Chem. Phys.*, vol. 16, págs. 12 454-12 461, 24 2014.

[66] Q. Arooj y F. Wang, "Switching on optical properties of D-π-A DSSC sensitizers from π-spacers towards machine learning", *Solar Energy*, vol. 188, págs. 1189-1200, 2019, ISSN: 0038-092X.

[67] P. Friederich, A. Fediai, J. Li y col., "The influence of impurities on the charge carrier mobility of small molecule organic semiconductors", *arXiv preprint arXiv:1908.11854*, 2019.

[68] J. Sworakowski, "Effect of polar molecules on the transport and localization of charge carriers in molecular materials", *Brazilian Journal of Physics*, vol. 29, págs. 318-331, 1999.

[69] P. Toman, M. Menšík, W. Bartkowiak y J. Pfleger, "Modelling of the charge carrier mobility in disordered linear polymer materials", *Phys. Chem. Chem. Phys.*, vol. 19, págs. 7760-7771, 2017.

[70] C. H. Kim, Y. Bonnassieux y G. Horowitz, "Charge Distribution and Contact Resistance Model for Coplanar Organic Field-Effect Transistors", *IEEE Transactions on Electron Devices*, vol. 60, págs. 280-287, 2013.

[71] Mohammad Mottaghi and Gilles Horowitz, "Field-induced mobility degradation in pentacene thin-film transistors", *Organic Electronics*, vol. 7, págs. 528-536, 2006.

[72] D. M. Lyons, J. Kesters, W. Maes, C. W. Bielawski y J. L. Sessler, "Improving efficiencies by modulating the central metal ion in porphyrin-oligothiophene-mediated P3HT/PCBM organic solar cells", *Synthetic Metals*, vol. 178, págs. 56-61, 2013, ISSN: 0379-6779.

[73] Q. Fu, "Radiation (SOLAR)", en *Encyclopedia of Atmospheric Sciences*, J. R. Holton, ed., Oxford: Academic Press, 2003, págs. 1859-1863, ISBN: 978-0-12-227090-1.

[74] M. C. Scharber, D. Mühlbacher, M. Koppe y col., "Design Rules for Donors in Bulk-Heterojunction Solar Cells—Towards 10 % Energy-Conversion Efficiency", *Advanced Materials*, vol. 18, n.º 6, págs. 789-794, 2006.

[75] G. Dennler, M. C. Scharber y C. J. Brabec, "Polymer-Fullerene Bulk-Heterojunction Solar Cells", *Advanced Materials*, vol. 21, n.º 13, págs. 1323-1338, 2009.

[76] I.-J. Chang, Y.-S. Jeon y K.-J. Hwang, "Synthesis and Band Gap Analysis of Designed Porphyrin Derivatives Containing Electron Donating and Accepting Group", *Bulletin of the Korean Chemical Society*, vol. 40, n.º 2, págs. 173-179, 2019.

[77] W.-L. Ding, D.-M. Wang, Z.-Y. Geng, X.-L. Zhao y W.-B. Xu, "Density functional theory characterization and verification of high - performance indoline dyes with D–A–π–A architecture for dye-sensitized solar cells", *Dyes and Pigments*, vol. 98, n.º 1, págs. 125-135, 2013, ISSN: 0143-7208.

Apéndice A

Journal of Photochemistry & Photobiology, A: Chemistry 409 (2021) 113155

Contents lists available at ScienceDirect

Journal of Photochemistry & Photobiology, A: Chemistry

journal homepage: www.elsevier.com/locate/jphotochem

Photoisomerization and its effect in the opto-electronic properties of organic photovoltaic materials: A quantum chemistry study

Cornelio Delesma [a], Carlos Amador-Bedolla [b], Miguel Robles [a], Jesús Muñiz [a,*]

[a] Instituto de Energías Renovables, Universidad Nacional Autónoma de México, Priv. Xochicalco s/n, Col. Centro, Temixco, Morelos CP 62580, Mexico
[b] Facultad de Química, Universidad Nacional Autónoma de México, Ciudad de México 04510, Mexico

ARTICLE INFO

Keywords:
Density functional theory
Organic photovoltaic
Photoisomerization
Excited state

ABSTRACT

A density functional theory study was performed on a series of organic photovoltaic materials with a promising potential to be implemented as the active layer in a solar cell device. A thorough analysis on the molecular structure at ground and excited state revealed that some of the systems in the series of molecules observed in the ground state is dramatically altered in the first excitation. The dihedral deviations could be addressed as a ruling mechanism behind isomerization and its influence in the opto-electronic properties. The computation of absorption spectra at ground and excited state geometries showed a significant shift in the absorption maxima, presumably due to such geometrical changes. Furthermore, the computation of dipole moments gave us insights into the possible charge transfer from the OPV material to an acceptor in a solar cell device. This is critical when the system is implemented in such a device. Additionally, relevant photovoltaic parameters were collected, and a candidate series of OPV systems was proposed as potential materials for the heterojunctions of a solar cell device. The given theoretical methodology and the photovoltaic data computationally obtained may aid in the *in silico* design of novel donor materials for the new generation of solar cells.

1. Introduction

Conventional resources of energy such as petroleum, carbon and natural gas, represent major sources of contamination to the environment. Therefore, it is necessary to find out new alternatives of energy consumption. Although inorganic photovoltaic cells based on silicon and cadmium telluride are adequate choices, they cannot compete with the conventional energies, due to high cost of production. In this regard, many efforts have been focused to find low cost materials, such as the organic photovoltaic (OPV) materials. That is, they present low-cost manufacturing and flexibility, with low weight and semi-transparency. Furthermore, they are manageable with easy integration into other products [1] and present an adequate power conversion efficiency (PCE). Although it has recently been reported a 17.3% efficiency when they are incorporated in tandem cells [2] and 16.7% in single-junction solar cell devices [3,4], further investigation is still necessary. The increase of PCE would allow OPV materials to be more competitive with other renewable energy materials. It is important to highlight that the active layer of OPV systems is formed of donor materials mainly composed of polymers, and also several blends of such polymers. Moreover, the adequate selection of the acceptor material also plays an important role on the performance of the resulting solar cell systems. That is, it was shown [5,6] that fullerene bisadduct acceptor IC60BA and IC70BA are capable to yield a PCE of 7.40%. Xiao et al. [7] also showed that an isomer-free fullerene bissaduct e-PPMF, through the route of regioselectivity synthesis, is able to reach a PCE of 8.11%. An acceptor based on an octacyclic co-bridged unit COi8 [8], namely COi8DFIC, shows an adequate bandgap of 1.26 eV and an absorption at the visible wavelength. This gives to ternary solar cells formed of COi8DFIC, remarkable photovoltaic (PV) parameters with a PCE of 14.08%. The mixture [9–11] of the polymer Y6 and some wide-band gap copolymer donors of the form donor–acceptor (D–A), allows a wide range of visible light to be absorbed. This indicates an outstanding PCE of 15–17%. Furthermore, to the best of our knowledge, Liu et al. [12] reported the highest PCE known to date for an organic solar cell. They used a mixture of D18 and Y6, producing a PCE of 18.22%, which also corresponds to a certified 17.6% of PCE.

OPV solar cells are formed of a heterojunction between donor and acceptor semiconductors [13,14]. The charge photo-generation process in the OPV cells begins when the donor molecules absorb a photon and generate the exciton. It migrates through the material towards the interface of the heterojunction. This energy transfer process is termed

* Corresponding author.
E-mail address: jms@ier.unam.mx (J. Muñiz).

https://doi.org/10.1016/j.jphotochem.2021.113155
Received 23 September 2020; Received in revised form 17 December 2020; Accepted 13 January 2021
Available online 19 January 2021

exciton diffusion. The exciton is subsequently split into a free charge carrier. The photo-generation process finalizes with the dissociation of the exciton. The charge carriers are then transported through their respective phases into the electrodes of the device [15,16].

OPVs, which are considered to be polymer-based materials present advantages over inorganic solar cells; such as CIGS or CdTe, since they are flexible materials with a reduced weight in the solar cell, and also with an affordable cost of fabrication [17]. The adequate selection of donor/acceptor materials in the bulk heterojunction (BHJ) is an important issue to be considered in the development of polymer-based solar cells (PSC) to improve the PCE. In accordance to Zhou et al. [17], the improvement of PCE is feasible by promoting some parameters, such as (a) the selection of appropriate structural arrangements of donor–acceptor (D–A) polymers. This may give narrow band gaps with an enhanced electron-accepting character [18]. (b) The full width at half-maximum (FWHM) of the conjugated polymers (which is approximately 200 nm), is in most of the cases small. As a consequence, the increase of FWHM is an alternative to improve PCE by random copolymerization to bind several monomers at the backbone of the polymers with conjugation [19]. (c) Selecting *n*-type systems that are capable to absorb the complementary section of solar spectrum. This may strengthen the light conversion into the active layer [20]. (d) The enhancement of the external quantum efficiency (EQE), which typically ranges from 50% to 80%, is another alternative (for instance see [21]). This is complementary to the well-known high internal quantum efficiencies (IQE) reported. (e) The search of fullerene-free new acceptors. This may increase the lowest unoccupied molecular orbitals (LUMO) levels to give higher V_{OC} values. (f) The increase of the fill factor (FF) by controlling and optimizing the morphology of the thin film to improve electric contacts [17]. This would form new paths to allow charge transport. In this respect, Firdaus et al. [22] performed a theoretical/experimental study on those parameters required in fullerene-free acceptors. An energy conversion efficiency higher than 20% was obtained if charge mobility is higher than $10^{-3}\,cm^2\,V^{-1}\,s^{-1}$. A thickness higher than 200 nm and a constant recombination rate smaller than $1 \times 10^{-13}\,cm^3\,s^{-1}$ are also required.

Particularly, OPV materials are formed of donor molecules with a sp^2 hybridization, in which the presence of carbon-carbon bonding is dominant. These monomers are characterized by rings with delocalized orbitals. From the theoretical point of view, an effort to find a set of OPV materials based on molecular building blocks was previously performed by Olivares-Amaya et al. [23]. In that study, 2.6 million OPV molecules were found by using machine learning techniques and drug-discovery methodologies. From such data base, a reduced set of molecular systems was chosen in the present work, in order to understand their electronic structure properties and their possible relations with photovoltaic parameters that could be considered in the design of a solar cell device.

Although the organic molecules with sp^2 hybridization may have a planar structure, in the excited state configuration, such molecules are subjected to changes in the dihedral angles [24,25]. The effect was observed for the first time in the azobenzene molecules. Such phenomena is known as photoisomerization [26], which could be attributed to photon absorption in OPV molecules. Moreover, it has been observed that the changes of dihedral angle decrease the charge transfer mobility and allows orbital localization [27]. For this reason, it is important to study the electronic structure of such molecules to permit the prediction of these changes and to be able to identify high efficiency donor molecules.

Some other studies on the PCE have also been performed by considering parameters such as aromaticity, planarity, HOMO (highest occupied molecular orbital) – LUMO (lowest unoccupied molecular orbital) gap, open circuit voltage and absorption spectra. The results showed promissory properties in the material series under study to be implemented in photovoltaic material applications [28]. In other studies, the evaluation of the energy gap magnitude, planarity, and aromaticity of π-conjugated systems, showed that OPVs are potential materials to be implemented in electronic and photonic applications [29]. Additionally, using the combined replica-exchange molecular dynamics (REMD) with density functional tight binding (DFTB) [30] and steady-state UV–vis and nuclear magnetic resonance spectroscopy, the geometrical conformations of organic materials to identify torsion and planarization [31], were disclosed. Additionally, time-dependent DFT (TDDFT) calculations were also performed to elucidate non-linear optical properties (NLO), by considering the ground state geometries of a series of OPV systems [28,32]. Wazzan and Irfan [33] performed a TDDFT study by using the optimized geometries in ground state in a group of triphenylamine-based organic dyes to model the absorption spectra found in the experiment. Additionally, TDDFT was also used to model UV–vis spectra of novel organic systems obtained via rational design of π-spacers in the donor-π-spacer-acceptor dyes [34]. This was done to find new dyes with improved performance for solar cell devices. Note that the last works were carried out with TDDFT to model absorption spectra in the ground state geometries, but no study has been performed to obtain the optimized geometries in the excited state and elucidate possible changes from those found in the ground state. Despite the disposition of such studies on planarity, no systematic analysis on geometrical conformation in the excited state has been performed. The aim of this study was to identify the effect of changes in structural parameters in the behavior of absorption spectra. Density Functional Theory (DFT) and Time Dependent DFT (TDDFT) allowed us to observe the behavior of OPV molecules in the ground and excited states, respectively. We present the results obtained for a set of organic donor molecules, in which variables such as theoretical optical band gap, electric dipole moment, molecular orbitals and dihedral angles were studied. Such variables have not been yet systematically studied to understand the possible correlation with UV-spectra in OPV materials. This contribution presents a description of the theoretical methodologies; a thorough discussion of the results regarding the geometrical structure of the molecular systems under study, electronic structure properties and their relation to photovoltaic properties and efficiency. A conclusions section with future perspectives for further work is also provided.

2. Theoretical methodologies and experimental comparisons

2.1. OPV synthesis and band gap characterization

For a subset of the compounds mentioned in this paper (8 out of 33), a comparison was made between experimental measurements of their optical band gaps and their corresponding theoretical values. Compounds in this subset were synthesized and characterized by García et al. [35], while optical band gaps were determined by Sifuentes-Vázquez et al., using methods described in [36].

2.2. Computational details

We performed the geometrical optimization of the OPV systems using DFT at the PBE [37] level of theory and the basis set *def2-TZVP* [38,39]. We used the PBE functional since it has been previously observed in our group that it adequately models excited state properties for OPVs [28]. We calculated the excited states to find UV–vis spectra, using the Time Dependent DFT (TDDFT) scheme at the same level. Furthermore, we computed the optimized geometrical structure for the excited state. Both calculations allowed us to structurally compare the geometries at ground and excited states. The first ten excited states were considered in order to find the full behavior of the absorption spectra. Moreover, it is known that the optical gap could be approximated with the computation of the HOMO-LUMO gap difference. Nevertheless, it often underestimates the experimental value. As an alternative, Jacquemin et al. [40] stated that the computation of the first excitation energy adequately approaches the experimental band gap. Such excitations were computed in accordance to the TDDFT methodology

described above. All calculations were performed using TURBOMOLE computational code [41]. Moreover, we smoothed data on the graphical representations using a Gaussian fitting. The graphical analysis of the systems was carried out with the TmoleX suite [42].

The calculations of the dihedral angles at the ground state (θ_{Grd}) and the first singlet excited state (θ_{Exc}) were performed with a home-made code developed with Python2.7 programming language [43]. We considered Eq. (1) to calculate the angle between two planes in the OPV molecules, which is necessary to further compute the dihedral angles. In Eq. (1), θ stands for θ_{Grd} and θ_{Exc}. According to Fig. 1, plane **1** was generated by the atoms S1-C1-C2, while plane **2** was formed by atoms C1-C2-C3.

$$cos\theta = \frac{|n_1 . n_2|}{||n_1||||n_2||} \tag{1}$$

In Eq. (1), n_1 and n_2 represent normal vectors perpendicular to the planes **1** and **2**, respectively.

3. Results and discussion

3.1. Electronic structure properties

The OPV systems under study are depicted in Fig. 2 and Scheme 1 in Ref. [44]. Such systems were disclosed by Olivares-Amaya et al. [23] with the aid of the Harvard Clean Energy Project (CEP) initiative. This study was based on the combination of 30 building blocks from which they obtained a data base of 2.6 million molecules with desirable photovoltaic properties. We screened a set of 33 OPV systems from that data set (see Fig. 2 and Scheme 1 in Ref. [44]), due to the high values reported in the descriptors disclosed via machine learning and artificial intelligence. Such descriptors comprised observable variables such as PCE, open circuit voltage (V_{OC}), short circuit current density (J_{SC}) and fill factor (*FF*). It is worth mentioning that, firstly, the CEP proposed oligomers were designed to correspond to synthesizable compounds with potential capabilities for solubility and film formation, and with PCBM as the acceptor counterpart; and, secondly, that ever since their predicted parameters were published, some of the most promising ones have been actually synthesized, and films have been produced [36,45,46]. Measurements of electronic properties, i.e. HOMO, LUMO, electrochemical and optical gaps, have been in accord with original predictions, even though OPV figures of merit, J_{SC}, V_{OC}, *FF* and power efficiency have not shown improvements, thus reflecting the limitation in the scope of the original Scharber model.

The group of OPV materials under study belong to a wider group of OPV systems, which were initially tailored by a known theoretical screening methodology [23]. It has been known that OPV materials, designed with such *in silico* method, can be easily synthesized with a straightforward procedure, based on the parent molecules from which they were initially obtained. Moreover, such materials present advantages with respect to polymers due their mono-dispersed nature and

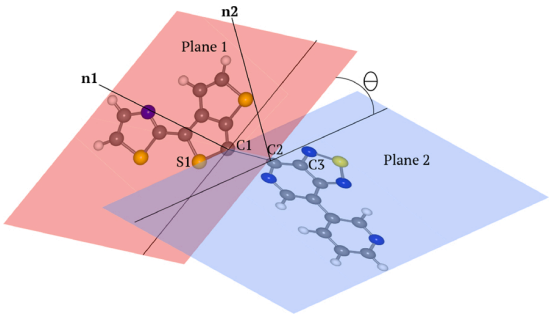

Fig. 1. Graphical representation of the two planes used to compute the dihedral angle θ. The molecule depicted in the figure corresponds to system **23**.

feasible synthetic routes [36,45,46]. For instance, Sokolov et al. [47] used the methodology of the CEP to predict the OPV system dianthracen-[2,3-b:2′,3′-f]thieno[3,2-b]thiophene (DTT). In that work it was shown that the solubility of this type of systems could not be adequate and it may be challenging to obtain, since DTT did not present the sufficient solubility in organic solvents to conduct an optical characterization in solution. Considering the poor solubility, the purification of the derivatives during the synthesis can be achieved with selective precipitation. Furthermore, OPV materials typically report acceptable crystal growth with no degradation. The route of film fabrication is performed by evaporation, and atomic force microscopy shows adequate 2D growth, which is related to high charge transport [47]. Additionally, an enhanced stability with long periods of time is also corroborated when the thin film is incorporated to a transistor device, and the performance remains unaltered. It is worth mentioning that if the thin film fabrication is performed via sublimation, the yield could be low. This implies that it is not possible to perform more than two steps of the sublimation purification, and extra steps of the sublimation procedure should be executed to keep the performance of the device [47,48].

We studied the electronic structure properties at the ground and excited state to find a possible relation with the changes of torsional angle. In our series of OPV systems, we were able to identify 16 building blocks that are shown in Fig. 1 in Ref. [44]. The corresponding IUPAC nomenclature of such systems is presented in Table 1 in Ref. [44]. We classified those building blocks with labels ranging from B01 to B16.

From the screened 33 OPV systems, we selected a reduced group of 8 molecules (see Table 1) which were synthesized in accordance to the methodology presented in Section 2.1. Such systems were characterized with the measurement of the experimental band gap; as it is reported in Table 1. In order to identify the adequate theoretical methodology to model ground and excited state properties, we performed a benchmark analysis with the series of GGA functionals presented in Table 1. Despite B3LYP [49–51] functional is in good agreement with the experimental band gaps (in average), we found that the PBE functional was not suitable for the computation of the optimized geometries of OPV systems in excited state; while CAM-B3LYP functional [52] gives a poor performance not suitable for further studies. Consequently, the PBE functional was selected to perform further computations. The PBE functional has shown to give reliable results on analogous OPV systems [28]. As it was previously suggested, all molecular systems under study were optimized at the ground and excited states, in accordance to the methodology described in the Computational details section. Note that the Cartesian coordinates of both, ground and excited states are presented in Tables 2–34 of Ref. [44].

A reasonable value for the calculated optical band gap energy, accepted in a solar cell application, ranges from 1.2 to 1.9 eV [55]. According to the results presented in Table 2 for the ground state geometries, a significant number of the systems under study are in this range; but systems 01, 02, 03, 06, 07, 09, 10, 12, 14, 16, 17, and 20, which showed high energy values. Note that the Table 2 comprises the complete set of OPV systems under study.

Bulk heterojunctions (BHJ) are required in the design of a solar cell. Particularly, organic BHJ for solar cells are a mixture of an electron acceptor material such as (6,6)-phenyl-C_{61}-butyric acid methyl ester (PCBM) and an electron donor material such as our organic systems presented in this work. Consequently, considering the PCBM as an acceptor, we computed quantum-chemical parameters such as chemical hardness [56], chemical potential, and electronegativity, with the aid of the following equations [57]:

$$\text{Chemical hardness} : \mu = \frac{E_{\text{LUMO}} - E_{\text{HOMO}}}{2} \tag{2}$$

$$\text{Chemical potential} : \eta = \frac{E_{\text{HOMO}} + E_{\text{LUMO}}}{2} \tag{3}$$

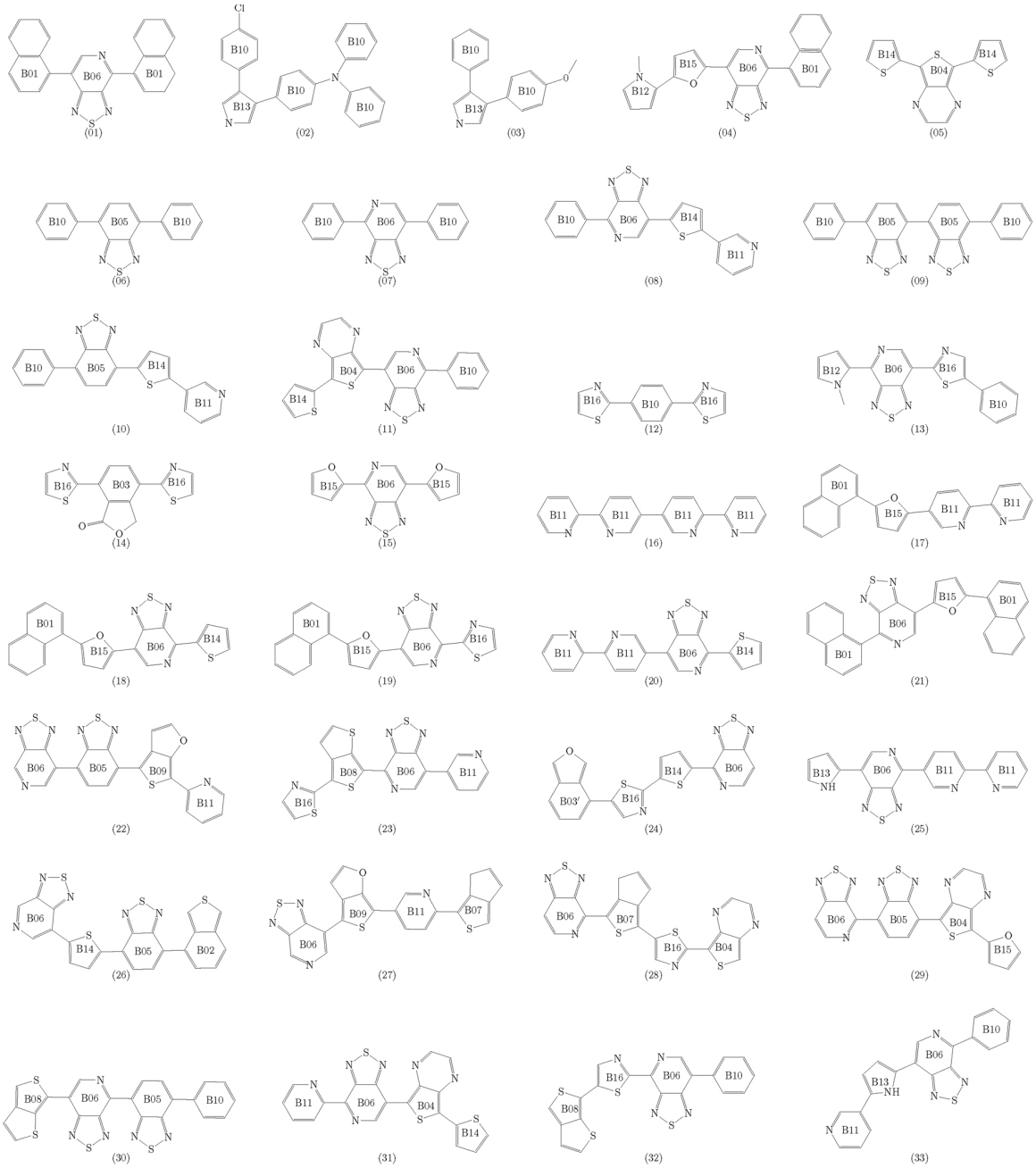

Fig. 2. The complete set of 33 molecular systems used in the present work. Note that the H-atoms were omitted for clarity.

Table 1
Benchmark on the methodology used to compute the theoretical optical band gap (eV). Note that Δ denotes the difference between experiment and theory.

System	Exp	ΔPBE	ΔB3LYP	ΔPBE0 [37, 53]	ΔCAM-B3LYP	ΔM06 [54]
05	1.94	0.27	0.02	0.07	0.29	0.06
06	3.67	1.14	0.81	0.68	0.36	0.74
07	2.69	0.39	0.05	0.08	0.43	0.04
12	3.42	0.22	0.06	0.15	0.38	0.10
14	3.22	0.15	0.13	0.22	0.46	0.18
16	3.49	0.46	0.39	0.50	0.84	0.43
17	2.88	0.16	0.22	0.32	0.65	0.28
18	2.12	0.54	0.19	0.07	0.36	0.07
Δaverage		0.41	0.23	0.26	0.47	0.24

$$\text{Electronegativity} : \chi = -\frac{E_{\text{HOMO}} + E_{\text{LUMO}}}{2} \tag{4}$$

The chemical hardness of the PCBM is 1.18 eV [57]. In order to be able to transfer electrons between donor and acceptor molecules, the donor hardness should be lower than this value. In this sense, the systems 02, 03, 12, 14 and 16 (see Table 2), are out of this range. At the ground state, the broadening in their energy gaps of both systems, exclude them from photovoltaic applications (see Table 2). Moreover, the PCBM chemical potential amounts to −4.93 eV [57], while our OPV systems showed higher values. Consequently, electron transfer could be feasible. Since the PCBM electronegativity is −5.93 eV [57], and our systems showed lower values, it is then possible electron attraction to be strong.

Table 2
Energy values (eV) of: HOMO (E_{HOMO}), LUMO (E_{LUMO}), theoretical optical band gap (E_{gap}), chemical hardness (μ), chemical potential (η) and electronegativity (χ). Dipole moment (ρ) in Debye (D). The values are given at ground state.

System	E_{HOMO} (eV)	E_{LUMO} (eV)	E_{gap} (eV)	μ (eV)	η (eV)	χ (eV)	ρ_{grd} (D)	ρ_{exc} (D)
1	−5.28	−3.52	1.91	0.88	−4.40	4.40	0.61	0.65
2	−4.44	−1.58	2.98	1.43	−3.01	3.01	4.18	5.60
3	−4.76	−1.19	3.66	1.78	−2.98	2.98	1.70	1.40
4	−4.59	−3.37	1.55	0.61	−3.98	3.98	4.43	2.04
5	−4.68	−3.42	1.67	0.63	−4.05	4.05	0.57	0.27
6	−5.42	−3.23	2.53	1.10	−4.32	4.32	1.27	1.16
7	−5.56	−3.59	2.30	0.98	−4.58	4.58	0.73	0.68
8	−5.26	−3.75	1.83	0.75	−4.50	4.50	1.19	1.19
9	−5.41	−3.30	2.36	1.06	−4.36	4.36	2.08	2.06
10	−5.16	−3.42	2.07	0.87	−4.29	4.29	2.57	2.56
11	−4.89	−3.77	1.56	0.56	−4.33	4.33	2.09	2.07
12	−5.38	−2.84	3.20	1.27	−4.11	4.11	2.00	2.04
13	−4.97	−3.60	1.70	0.68	−4.29	4.29	3.07	3.19
14	−5.63	−3.18	3.07	1.22	−4.40	4.40	3.12	4.88
15	−5.05	−3.56	1.86	0.75	−4.30	4.30	1.10	1.14
16	−5.72	−2.74	3.03	1.49	−4.23	4.23	5.73	4.97
17	−4.99	−2.70	2.72	1.15	−3.84	3.84	2.82	2.83
18	−4.86	−3.57	1.58	0.64	−4.22	4.22	1.01	0.80
19	−4.99	−3.64	1.69	0.68	−4.31	4.31	2.18	1.12
20	−5.41	−3.67	2.00	0.87	−4.54	4.54	2.70	1.73
21	−4.99	−3.54	1.67	0.72	−4.27	4.27	1.69	1.63
22	−5.04	−3.55	1.57	0.74	−4.30	4.30	2.13	2.27
23	−5.01	−3.68	1.78	0.66	−4.34	4.34	3.10	1.05
24	−5.01	−3.53	1.59	0.74	−4.27	4.27	2.20	2.00
25	−5.09	−3.66	1.65	0.71	−4.37	4.37	2.30	1.84
26	−5.04	−3.60	1.50	0.72	−4.32	4.32	2.63	2.35
27	−4.94	−3.61	1.59	0.67	−4.28	4.28	2.54	1.79
28	−4.92	−3.62	1.64	0.65	−4.27	4.27	2.46	2.61
29	−5.01	−3.54	1.60	0.74	−4.27	4.27	1.83	1.11
30	−5.03	−3.51	1.73	0.76	−4.27	4.27	1.69	0.88
31	−5.04	−3.53	1.79	0.76	−4.28	4.28	1.50	1.33
32	−4.98	−3.60	1.68	0.69	−4.29	4.29	3.10	2.31
33	−4.99	−3.71	1.61	0.64	−4.35	4.35	2.44	2.53
PCBM	−6.20 [66]	−4.26 [66]		1.18	−4.93	4.93		

We computed molecular dipole moments as another descriptor to characterize the OPV molecules under study. Large dipole moments allow charge separation more easily in a donor and acceptor mixture [58,59], enhancing charge transfer [60]. The systems with dipole moments ranging from 0.00 to 1.00 D are 01, 05, and 07 (Group **1**). Those systems with dipole moments ranging from 1.00 and 2.00 D are 03, 06, 08, 15, 18, 21, and 29–31 (Group **2**). A large number of the systems under study are located in a range from 2.00 to 3.00 D (09–12, 17, 19–20, 22, 24–28, and 33), and corresponds to Group **3**. The system located on the range from 3.00 to 4.00 D are 13,14, 23, and 32 (Group **4**). Those molecules ranging from 4.00 to 6.00D are 02, 04, and 06 (Group **5**). Consequently, these results indicated that the systems in Groups **4** and **5** could be considered as materials with high availability for charge transport. It is important to highlight that the theoretical optical band gap of such systems (see Table 2), are also in adequate ranges to achieve the requirements of a solar cell material.

On the other hand, according to Friederich et al. [61], the presence of a high or a permanent dipole moment, induces trap states that alter the charge carrier mobility in the host material. This phenomena is particularly strengthened when the LUMO of the materials is localized at a specific region of the molecular system. On the contrary, molecular systems with delocalized frontier molecular orbitals mitigate such effect. Additionally, if such orbitals are delocalized on rotatable dihedral bonds in the molecule, a degree of disorder in the system is observed with higher energies, and consequently an enhanced intrinsic electron mobility. This is certainly a behavior observed in some of the systems under study, since after the photoisomerization in systems 02, 03, 04, 14, 19, 22, 23, 27, 29, 30, 31, 32 (see Table 36) in Ref. [44], large angles of rotation were observed. This could promote an improved charge carrier mobility. Moreover, Sworakowski [62] identified that molecules with high dipole moments at molecular crystals can be considered as traps of charge carriers. Consequently, the polar nature of such systems provokes a reduction in the depth of the trap states. In addition, the presence of polar impurities are also responsible for the alteration in polarization energy, which increases the number of trap states on the molecules of the vicinity. In this sense, the presence of polar species widens the size of the electronic density of states (DOS), inducing the imminent reduction of the mobility of charge carriers. On the other hand, Toman et al. [63] performed an atomistic model of charge carrier transport, based on the carriers in a disordered chain. Such a model combines the quantum perspective and a semi-classical solution in the charge hopping through the chain. The model also considers local anisotropy of the charge carriers. By using this model, the mobility degradation could also be explained. Such degradation is addressed to the lower charge mobility at the BHJ interface. This phenomena has been observed, for instance by Kim et al. [64] and Mottaghi et al. [65]. According to such a model, the phenomenology occurs due to the reduction of hopping states which could be used in large charge concentrations. Additionally, this could also explain the electrical behavior of organic-based systems such as diodes and organic field effect transistors (OFETs).

3.2. Optical properties in ground and excited states.

We computed the absorption spectra of the molecular systems under study at the TDDFT/PBE level of theory as previously stated in the Computational Details section. In this case, the computations were performed by considering the ground state geometries obtained with the PBE functional. From sun radiation reaching the Earth, 40% corresponds to the UV–vis spectrum (400–700 nm), 50% is infrared (700–1000 nm) and 10% is ultraviolet radiation [67]. Considering such radiation ranges, we classified three different groups of systems. The first group corresponds to those systems below 400 nm (system 01–07, 12, 15, 16, 20 and 33), absorbing in the UV range (see Fig. 3(a)); from 100 to 400 nm.

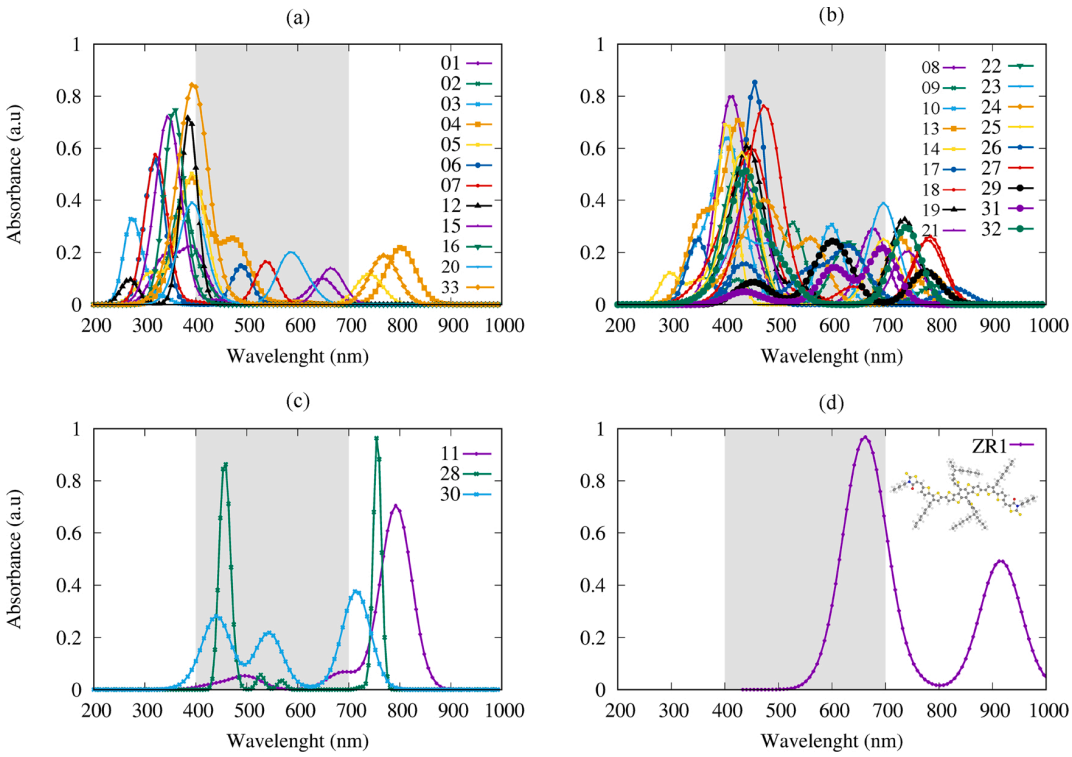

Fig. 3. Absorption spectra of subsets of systems with maxima located: (a) below 400 nm; (b) in a range from 400 to 700 nm; (c) in a range from 700 to 1000 nm. (d) Optimized molecular geometry and absorption spectrum of ZR1 molecular system. The gray zones represent the visible light region. Note that the profiles were obtained at the TDDFT/PBE level of theory.

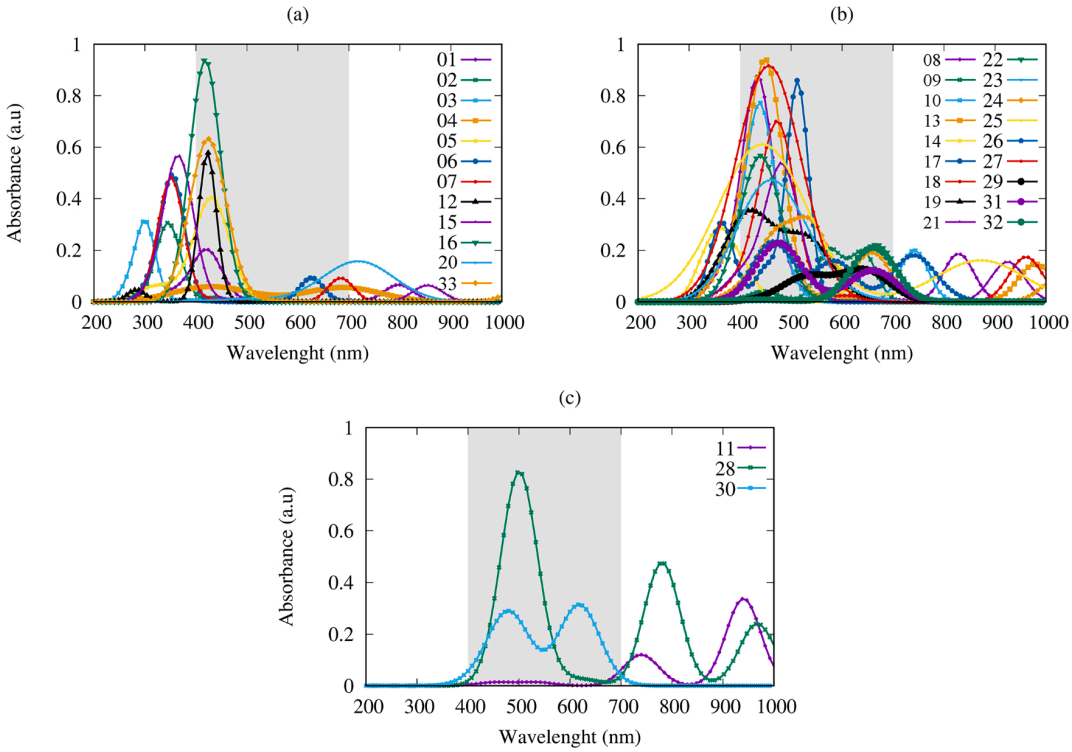

Fig. 4. Absorption spectra in the optimized geometries at the first excited state of systems (a) 01–07, 12, 15, 16, 20, 33; (b) 08–10, 13, 14, 17–19, 21–27, 29, 31, 31; (c) 11, 28, 30. The maxima was relocated in comparison to the maxima obtained in the excited state geometries. Note that the classification adopted in the ground state for all cases was also used.

Particularly, this series require a large amount of energy to perform the electronic excitation. The second series ranges from 400 to 700 nm, and corresponds to systems 08–10, 13, 14, 17–19, 21–27, 29, 31 and 32. The absorption (see Fig. 3(b)) is localized at the visible range, allowing such electronic excitation to be very likely in experimental conditions. Since this set of systems absorb in the UV–vis range, they could be addressed as materials which may likely participate in a solar cell device. Finally, as it is depicted in Fig. 3(c), the third group ranges from 700 to 1000 nm (systems 11, 28 and 30), in which the absorption is at the infrared range.

It is important to highlight that the dihedral angles in the systems under study, are in some cases, significantly shifted from planarity at the ground state geometries. Furthermore, it is important to analyze its possible effect on the excited state properties. We classified the systems in accordance to the magnitude of the dihedral angles. The first group corresponds to those systems with dihedrals from 0 to 20°. The second group, ranges from 20° to 40°. Finally, the third group ranges from 40° to 60°.

In accordance to the structural features disclosed with our methodology, we identified three different groups of OPV systems, whose classification is directly related to those properties. The first group of systems with dihedral angles between 0° and 20° at the ground state are 05, 08, 11, 12, 14, 15, 25, 27, 28 and 33. After computation of the excited state, the dihedral angles of such systems remained constant (except systems 14 and 27). The UV–vis spectrum of system 05 in ground state, showed a maximum located at 394.0 nm (UV range), while in the excited state, a maximum located at 430.7 nm (UV–vis range) was found (see Fig. 4). This character revealed its possible potential to absorb light and possible performance as a solar cell material. That is, a displacement of 36.7 nm was responsible for such behavior. An analogous result was obtained for system 08 with a shift of 24.2 nm.

The absorption maximum for system 11 at the ground state was observed at 792.7 nm (infrared region). In Fig. 4, the excited state maximum was centered at 940.3 nm (also at the infrared region). A displacement amounting to 147.6 nm was assessed, indicating that the system is adequate for a solar cell material application. In particular, the electronic transition for system 11 at the ground state geometry, occurred from the HOMO (−4.89 eV) to the LUMO (−3.77 eV) with a 91.0% of probability (see Fig. 2 of Ref. [44]). This represents the most likely transition found via the TDDFT calculation. The same behavior was also identified with transitions coming from the HOMO to the LUMO, as observed in systems 28 and 30. The maxima of these processes are located in the infrared wavelength region with 92.8% and 96.7% contributions, respectively (see Fig. 2 and Table 36 in Ref. [44]).

The second group is the set of systems with the dihedral angles in ground state ranging from 20° to 40°, and corresponds to systems 06, 07, 10, 13, 16–20, 23, 24 and 32. System 20 showed a peak in the UV range at the ground state, and in the excited state a shift of 320.9 nm was observed. This allowed the system to absorb in the infrared range. Such displacement could be attributed to the change in the dihedral angles, as it is shown in Table 36 in Ref. [44], in which the angles θ_1 and θ_2 corresponded to 33.0° and 34.5°, respectively. As a consequence, a co-planar geometry in the excited state was observed. Such behavior induced a shift to the infrared region, as it is depicted in Fig. 4(a). Finally, a third group was identified and corresponds to the systems with dihedral angles ranging from 40° to 60° in ground state geometries; namely, systems 01–04, 09, 21, 22, 26, 29, 30 and 31.

Furthermore, all molecular geometries of the systems under study were also optimized at the first excited state. As previously stated, their absorption spectra were also computed (see Fig. 4). The results showed an evident change in the average of the dihedral angles as reported in the excited state geometries presented in Table 36 in Ref. [44]. That is, an isomerization was clearly identified in most of the systems under study. This behavior appeared to alter the absorption spectra maxima by inducing a red-shift in some cases, or a change to the UV-region (see Table 36 in Ref. [44]). We assigned such behavior as a photoisomerization, which could be generated in the presence of solar irradiation, as simulated with our theoretical methodologies. Fig. 4 depicts the absorption maxima located out of the ranges in which the maxima were originally found at the ground state geometries. This could represent an insight into the determination of the absorption maxima from the information available on the possible isomerization mechanisms. In this regard, we present in Section 3.3, a theoretical method to identify potential OPV systems in which absorption maxima are shifted after photoisomerization occurs.

3.3. Structural description and its relation with the optical properties

Previous results suggested that a relationship could be present; exerting an influence, between the change in the dihedral angles observed from the ground to the excited state geometries (which is directly ascribed to the photoisomerization), and the shift in the absorption spectra maxima observed also from the ground to the excited state.

According to the results presented in Table 36 of Ref. [44], the systems could be grouped into a classification of 3 sets: (a) Group **A** comprises those OPV systems in which a red-shift is exhibited in the absorption maximum, from the ground to the excited state. (b) Group **B** revealed a set with an evident blue-shift of the absorption maxima from the ground to the excited state. Finally, a third Group **C** was also identified, in which the planarity of the molecules is their main feature, with no dihedral angles in both states. A red-shift is also reported in this group of systems. The heat graph shown in Fig. 5 depicts such a behavior, in which the *x*-axis corresponds to the molecular system label, while the *y*-axis shows the difference of the average in the dihedral angles from the ground to the excited state. The color scale indicates the value of $\Delta\lambda$. That is, the final red or blue-shift after the photoisomerization is evidenced in the first excited state. Consequently, those systems colored in blue in Fig. 5, are characteristic of a red-shift; while those colored in brown and reddish, represent those systems that are blue-shifted after photoisomerization.

The systems in Group **B** showed that the blue-shift is formed in those cases in which a small (2° and 16°) or a large (ranging from 23° to 62°) dihedral angle difference (in average) is observed. It is important to highlight that as a criterion, the dihedral angles smaller than 5° were omitted from the average, as they were considered to present no distortion. Note that we addressed photoisomerization in this work to those systems in which $\Delta\theta_{avg}$ in Fig. 5 is larger than 5°. That is, the systems reduced their potential to absorb light if the dihedral angles are subjected to slight deviations in their dihedral angles. Additionally, this property was also found when those variations are sufficiently large to modify the original structure and to increase the overall energy in the excited state. The variations in the dihedral angles with an intermediate magnitude (10–34°) gave as a consequence, a red-shift comprising Group **A**. Such behavior is of high relevance since it is expected that such systems are more susceptible to absorb a broader range of the visible light spectrum. This gave to several systems in Group **A**, a high potential to act as absorber materials in a solar cell device.

Moreover, systems in Group **C** showed the particular behavior of red-shift with no dihedral variation (systems **11** and **12**); in which a red-shift of more than 30 nm was observed. Note that systems with a shift of smaller values, were omitted from this classification. The behavior observed on systems **11** and **12** could be directly related to a one-electron transition coming from a charge transfer in the frontier molecular orbitals (MO), in which the charge distribution is re-allocated in the excited state. That is, as depicted in Fig. 2 in Ref. [44], the transitions comes from the HOMO to the LUMO; and in the excited state, the most likely transition corresponded to the same excitation (see Fig. 3 in Ref. [44]). The charge re-allocation at the HOMO in the excited state was evidenced from the 2D slices of the frontier MOs performed for both, systems **11** and **12**, as depicted in Figs. 4 and 5 in Ref. [44], respectively. The electron distribution of the π-orbitals in the HOMO at the excited state is reduced for both systems. This could be attributed to an overall

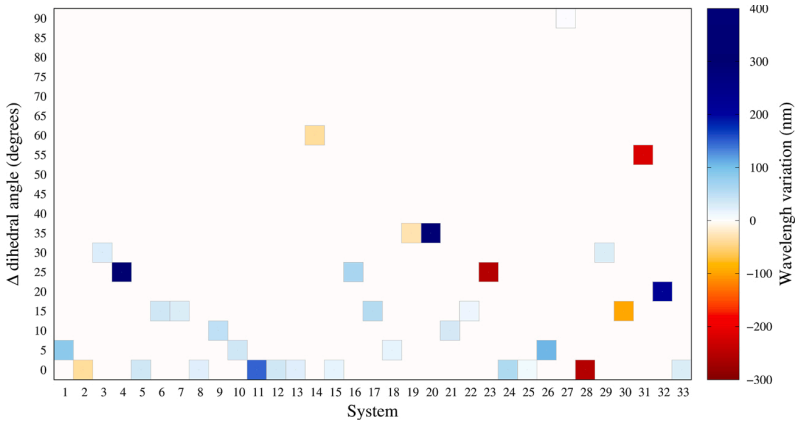

Fig. 5. Dihedral angle variation $\Delta\theta_{avg}$ (in average) for all organic photovoltaic materials under study. The heat scale represents the corresponding wavelength variation in nm ($\Delta\lambda$).

structural bending disclosed in the geometry of the molecules at the excited state. That is, the bonding distances are deformed in the *xy*-plane of the molecules; which induced such distortion. The structural changes are presented in the Cartesian coordinates of systems **11** and **12** (and also all systems under study) in ground and excited state. Such geometries are listed in Ref. [44]. Despite the shape of the tridimensional isosurfaces appeared to be equivalent, the electron distributions (see Figs. 4 and 5 in Ref. [44]) are significantly altered. Consequently, the electron distribution of the LUMO at the excited state in system **11** is reduced, and the mechanism of charge transfer to produce the absorption spectrum is modified. As previously suggested, this behavior may be the responsible for the shift of the absorption maxima observed in system **11**. An analogous mechanism could be also associated to system **12**, due to the electron distribution observed in the frontier MOs from the ground to the excited state (see Fig. 5 in Ref. [44]).

Our theoretical results may be used as a predictive tool to tune the opto-electronic properties of OPV systems from the structural modifications observed in the excited state. That is, the maxima in the absorption spectra; which is expected in experimental conditions, could be anticipated from the structural changes of the molecular system in the excited state. This could be convenient to tailor OPV materials intended to be implemented as absorbers in a solar cell device.

3.4. Molecular orbital analysis

The electronic charge distribution at the frontier molecular orbitals (MO) represents an important tool to elucidate the phenomena related to charge transfer in the systems under study at the excited state. That is, the isosurfaces of the highest occupied molecular orbitals (HOMO) are presented in Fig. 6. Such surfaces corresponded to planar molecules (systems 5, 08, 11, 12, 15, 20, 25, 28 and 33) with π-orbitals uniformly distributed on the rings of all fragments. Systems 20 and 25 are exceptions in this set owing to the torsion observed in dihedral angles, which are subsequently co-planar in the excited state (see Table 36 of Ref. [44]). Despite this system is coplanar, the distribution of the MOs is not uniform. The contributions can be located at the region between blocks B06 and B11 (see Fig. 6), breaking the uniformity of the distribution.

With respect to those systems in which the changes in dihedral angles at the ground state, ranged from 10° to 60°, a uniform distribution in the frontier MOs could also be observed. This behavior was absent in systems 6, 24 and 26. In system 16, three dihedral angles were distorted (see Table 36 of Ref. [44]). Moreover, the orbital distribution was not affected and the electronic charge resides at the peripheral of the B11-B11 blocks. The same behavior could be assessed from the MOs located at the region between blocks B06 and B14. That is, the location of the MOs is mainly found at the region of this linkage. Moreover, the linkage between blocks B06 and B14 in system 26 were mainly formed of bonding π-orbitals (see Fig. 7).

The MOs of the group corresponding to dihedral angles larger than 60° are depicted in Fig. 8. The lack of planarity breaks the symmetry of the π-orbitals previously observed at the former groups. In this case, the MOs are virtually found at the intermediate regions linking the building blocks. The systems with changes in the dihedral angles at the excited states (systems 02, 14 and 22) showed a clear increasing in the dipole moment, as it is shown in Table 2. This could be addressed as an additional descriptor to select molecular systems with changes in the dihedral angle in which the charge mobility is expected to be improved. That

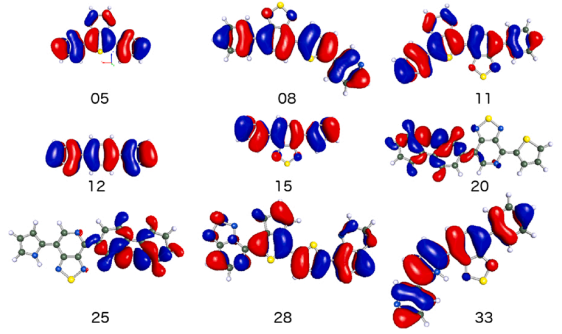

Fig. 6. Frontier molecular orbitals of OPV systems with co-planar dihedral angles.

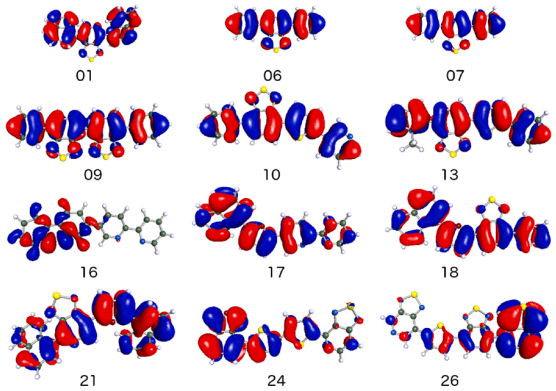

Fig. 7. Frontier molecular orbitals of OPV systems with dihedral angles ranging from 10° to 60°.

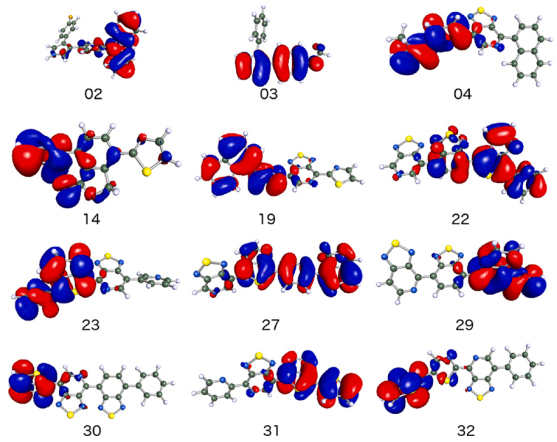

Fig. 8. Frontier molecular orbitals of OPV systems with dihedral angles larger than 60°.

is, the geometrical changes observed in the excited state could be associated as a parameter to predict an improvement in the electron transport in a photovoltaic device.

3.5. Photovoltaic properties

We determined the maximum efficiency of a BHJ in a solar cell device with the estimation values under heat mapping at AM1.5G illumination for a single-junction device [1,68]. Such values were presented in a graph with band gap values of donor versus $E_L^D - E_L^A$ (eV), in which E_L^D is the LUMO energy of the donor and E_L^A is the LUMO energy of the acceptor. The efficiency of a solar cell may be measured with the parameters: open-circuit voltage (V_{OC}), short-circuit current (J_{sc}) and fill factor (*FF*). The product of these values corresponds to the maximum output power (P_{max}). In this work, we computed the PCE in accordance to Eq. (5):

$$\mathrm{PCE} = \frac{P_{\max}}{P_{\mathrm{inc}}} \tag{5}$$

In which P_{inc} corresponds to the input power. This is a standard value of incident spectrum at AM1.5G with an intensity of 1000 W/m^2 (100 mW/cm^2) at room temperature. Note that the PCE for the systems under study was calculated in accordance to the methodology given by Scharber et al. [1,68], which is based on a heat map where the PCE of a molecular system may be estimated by considering that the band gap of the donor should be in a range from 1.0 to 3.0 eV. Moreover; as a second criterion, the quantity ($E_L^D - E_L^A$) should range from 0.3 to 1.3 eV. Consequently, the systems under study that remain out of such ranges could not be considered in the computation of PCE. In this respect, the PCE values are absent in the systems that do not fulfill the requirements of the criteria (see Table 3). The theoretical V_{OC} values were calculated with the aid of Eq. (6) [69], in which 0.3 refers to the loss factor related to the BHJ. The LUMO value of the PCBM (E_L^A) was used in Eq. (6). That is, the experimental value of 4.26 eV was considered [66]:

$$\mathrm{eV_{oc}} = |E_H^D| - |E_L^A| - 0.3 \tag{6}$$

The J_{SC} values could be estimated in accordance to Eq. (7), in which $LHE(\lambda)$ is the light-harvesting efficiency at a given wavelength λ. This value was obtained using Eq. (8). The f parameter is the oscillator strength of the maximum wavelength absorption of the donor material. The ϕ_{in} value refers to the electron injection efficiency, which is related to the availability of electron injection ΔG_{inj} (Eq. (9)) from the excited state of the donor to the LUMO of the acceptor. E_{ox}^D is the ionization potential energy, while E_{o-o}^D is the energy of the first excited state (HOMO–LUMO gap); in both cases, of the donor molecule. The μ_{collec} term is the electron collection efficiency, which is considered constant in our computations:

$$J_{\mathrm{sc}} = \int_{\lambda} \mathrm{LHE}(\lambda)\phi_{\mathrm{in}}\mu_{\mathrm{collec}}\, d\lambda \tag{7}$$

$$\mathrm{LHE}(\lambda) = 1 - 10^{-f} \tag{8}$$

$$\Delta G_{\mathrm{inj}} = E_{\mathrm{ox}}^D - E_{0-0}^D - E_L^A \tag{9}$$

The E_{ox}^D term is known as the oxidation potential and it was calculated using Eq. (10), in which E_0 is the total energy of the neutral state and E_0^+ is the total energy of the cation. Both energies were computed in the ground state geometries:

$$E_{\mathrm{ox}}^D = E_0 - E_0^+ \tag{10}$$

The results on the assessment of Eq. (10) are presented in Table 3. Note that the Table 3 comprises the complete set of OPV systems under study. Moreover, the values for V_{OC} are also presented in Table 3, which range from 0.12 to 1.16 eV, with the exception of systems 02 and 04 with values amounting −0.12 and 0.03 eV, respectively. As it is presented in Table 3, those systems with the largest V_{OC} values corresponded to 01, 06–10, 12, 14, 16, 20, 25. Moreover, the electron injection ΔG_{inj} is a physical property that suggests the susceptibility of the molecular system to transfer electrons in a donor/acceptor arrangement. All ΔG_{inj} values ranged from 0.50 to 3.56 eV, except systems 02, 03 and 17 (see Table 3). The largest values reported for ΔG_{inj} revealed that particularly, the series of OPV systems 05, 07, 08, 11, 15, 16, 20, 23, 25 and 33, could be used in heterojunctions for donor/acceptor dispositions. Moreover, in

Table 3
Open circuit voltage (V_{OC}) in eV, electron injection (ΔG_{inj}) given in eV, light-harvesting efficiency (LHE), and PCE (%) of the OPV systems under study. Note that LHE is a dimensionless parameter ranging from 0.0 to 1.0.

System	Ground state				Excited state		
	V_{oc} (eV)	ΔG_{inj} (eV)	LHE	PCE (%)	V_{oc} (eV)	ΔG_{inj} (eV)	LHE
01	0.72	0.83	0.35	6.5	0.59	1.07	0.47
02	−0.12	−0.98	0.49	–	−0.17	−0.35	0.42
03	0.20	−1.03	0.46	–	−0.35	−0.58	0.62
04	0.03	0.71	0.69	1.0	−0.27	1.48	0.17
05	0.12	1.01	0.71	3.0	−0.10	1.23	0.74
06	0.86	0.79	0.71	3.8	0.61	1.10	0.80
07	1.00	1.15	0.64	6.0	0.78	1.42	0.78
08	0.70	1.14	0.79	8.3	0.58	1.33	0.86
09	0.85	0.59	0.48	4.0	0.62	0.80	0.37
10	0.60	0.83	0.60	8.2	0.45	1.04	0.80
11	0.33	1.09	0.54	5.5	0.25	1.21	0.40
12	0.82	0.50	0.84	–	0.63	0.69	0.86
13	0.41	0.98	0.75	5.5	0.23	1.20	0.76
14	1.07	0.79	0.77	2.5	0.70	1.14	0.39
15	0.49	1.21	0.76	6.0	0.34	1.44	0.79
16	1.16	3.56	0.83	–	0.01	57.30	0.88
17	0.43	0.12	0.83	–	0.29	0.32	0.86
18	0.30	0.88	0.63	4.2	0.21	1.06	0.73
19	0.43	0.95	0.64	6.5	0.24	1.63	0.52
20	0.85	1.06	0.55	7.1	−0.15	8.32	0.42
21	0.43	0.77	0.55	6.0	0.29	0.97	0.67
22	0.48	0.96	0.52	6.0	0.37	1.33	0.73
23	0.45	1.03	0.56	6.0	0.20	1.73	0.55
24	0.45	0.89	0.51	6.0	0.34	1.17	0.48
25	0.53	1.10	0.70	6.5	−0.23	4.59	0.73
26	0.48	0.86	0.36	5.5	0.34	1.15	0.32
27	0.38	0.86	0.75	6.0	0.15	1.42	0.72
28	0.36	0.90	0.66	6.0	0.22	1.04	0.70
29	0.45	0.96	0.26	6.0	0.16	1.52	0.23
30	0.47	0.87	0.34	6.0	0.33	1.39	0.38
31	0.48	0.95	0.37	6.0	0.23	1.53	0.40
32	0.42	0.96	0.62	5.5	0.43	1.63	0.38
33	0.43	1.15	0.86	6.0	0.34	1.44	0.87
ZR1	0.14	0.14	0.99	2.0	0.06	0.26	0.97

accordance to Eq. (7), large values of the ΔG_{inj} increases J_{sc}. Additionally, large $LHE(\lambda)$ results also allow J_{sc} to increase. That is, the systems with highest $LHE(\lambda)$ were 05, 06, 08, 12–17, 25, 27 and 33. The PCE of our systems were estimated in accordance to the graphic efficiency given by Scharber et al. [68], in which the majority of the systems ranged from 5.50% to 6.50%. The systems 08, 10 and 20 presented the largest efficiencies, namely 8.3%, 8.2% and 7.1%, respectively. Owing systems 02, 03, 12, 16 and 17 appeared to be out of the range of the Scharber graphic efficiency.

In accordance to Table 3, the OPV systems 08, 10 and 20 showed the highest values. This gives us insights into the selection of the methodology to screen molecular systems from the CEP data base with desirable properties and allows us to discriminate among those systems with poor properties (such as systems 02, 03, 12 and 17) as obtained from electronic structure methods in ground and excited state. It is important to highlight that in the systems presented in this work, the maximum theoretical PCE values are around 8%. Zhou et al. [70] reported the synthesis of DTBDT-based small-molecule donor, ZR1, and fabricated all-small-molecule organic solar cells (SM-OSC) by individually mixing it with Y6 and IDIC-4Cl, as acceptors. They found that for ZR1, the UV–vis absorption spectra was located at 675 nm. The medium optical bandgap value was 1.84 eV. The HOMO and LUMO energy levels amounted −5.32 and −3.53 eV, respectively. For the IDIC-4Cl, the UV–vis maximum was located at 810 nm, with an optical bandgap of 1.53 eV. The HOMO and LUMO energy levels amounted −5.72 and −4.10 eV, respectively. For Y6, the UV–vis maximun was located at 930 nm. The optical bandgap was 1.33 eV, and the HOMO and LUMO energy levels were −5.91 and −4.10 eV, respectively. Zhou et al., used organic nonfullerene acceptor (NFA) molecules to design and synthesize the organic solar cells. They found that the ZR1:Y6 blend presented a certified PCE of 14.1%. In our PCE calculation, we used the heat mapping at AM1.5G illumination for a single-junction device presented by Scharber [69], using the PCBM as acceptor and they presented a maximum for PCE of 10%. It is likely that the systems presented in this work could increase the PCE by using fullerene-free acceptors.

As a further experimental/theoretical work, it is critical to consider the separation in a donor-acceptor arrangement of a bulk heterojunction for a solar cell, to advantage higher charge transport efficiencies [71]. This is related to the length limitation of exciton diffusion. Moreover, the thickness of the organic film should be such that light is effectively absorbed. This is challenging in the design of a binary blend for a BHJ. Nevertheless, there are experimental techniques to overcome such issue such as *in situ* photoisomerization [71], in which the PCE of a single junction device could be increased up to 8.47%. Other small donor molecules [72] such as *p*-DTS(FBTTh$_2$)$_2$, are able to achieve different crystallization morphologies, which allow such systems to reach PCE values up to 7% with PCBM-derived acceptor blends.

Note that we also considered the ZR1 donor material [70] as a reference molecule in order to compare with the electronic structure properties of the rest of systems presented in this work. ZR1 was used due to its large PCE of 14% experimentally found. That is, such efficiency could be reached due to the blends in which ZR1 molecules participate [70]. Furthermore, the use of fullerene-free acceptors in the blends are also one of the keys giving rise to such enhanced PCE. Fig. 3 (d) depicts the optimized molecular structure of ZR1, which appears to be planar at the center of the backbone with slight deviations at the end of the branches. That is, ZR1 shows an absence of dihedral angles such as those found in the series of OPV systems presented in this work. Moreover, the UV–vis simulated spectrum (Fig. 3(d)) revealed a peak centered close to 700nm, which would allow ZR1 an effective visible light absorption in accordance with experimental results. This could be considered as one of the key features that make ZR1 an excellent donor material. According to the results shown in Fig. 4(c); for the UV–vis spectra at the excited state, it would only be expected that some of our molecules in the series of compounds (systems **28** and **30**) are capable to behave such as ZR1 system. Moreover, although the PCE and LHE values reported in Table 3 for ZR1 are larger than those of the series, some of the systems in our group remained close to such parameters, and could be of interest to participate as units in blends of organic compounds to yield improved efficiencies as components in a solar cell. Nevertheless, after the theoretical PCE computation was performed, a poor performance for ZR1 was disclosed (see Table 3). This could be explained by considering that originally, the ZR1 was synthesized to perform with non-fullerene blends. Consequently, its use with PCBM (based on the Scharber's method [1,68], results in a low theoretical efficiency, since it was conceived to be a donor functioning with a fullerene-free acceptor. Additionally, this analysis could be used to screen potential molecules in OPV data bases (such as CEP) with improved electronic structure properties that give to such molecules an ameliorated performance in a solar cell device.

4. Conclusions

A systematic study on the electronic structure properties at ground and excited state in a series of OPV materials was thoroughly performed. Surprisingly, the dihedral angles were changed at the excited state from those initially found at the ground state, triggering the photoisomerization phenomena. Such behavior may promote a more facile electron transfer when the dihedral angles were altered by less than 60°, owing to their dipole moments computed with the corresponding theoretical methodology. This was indeed confirmed by the uniform distribution observed in their frontier molecular orbitals. Furthermore, the opto-electronic properties calculations revealed that the UV–vis spectra of such systems presented maxima located around the visible light region. This allows such group of OPV systems to be potential candidates to participate in the design of a solar cell device. Moreover, those OPV systems with dramatic changes reported at the excited state for the dihedral changes, considerably reduced some electronic structure parameters such as the dipole moments which could hinder electron mobility in the material. The structural distortion was also responsible of an imminent red-shift in the absorption spectra. This gives those OPV molecules in the series, possible photovoltaic applications. As a consequence, the descriptors theoretically obtained in the present work may aid as a tool to discriminate OPV materials with desirable electronic structure properties from those which are not necessarily relevant in the design of a solar cell device.

Authors' contribution

C.D.: investigation, computational simulation, writing-original draft preparation. C.A.B. and M.R.: conceptualization, visualization, reviewing & editing. J.M.: computational simulation, writing-original draft preparation.

Declaration of Competing Interest

The authors report no declarations of interest.

Acknowledgements

The authors would like to acknowledge the financial support given by DGAPA (Dirección General de Asuntos del Personal Académico) under Project No. PAPIIT-IA102820 and PAPIIT-IN109319. C.D. wants to acknowledge the Ph.D. scholarships provided by Consejo Nacional de Ciencia y Tecnología (CONACYT) with No. 633818. J.M. would like to acknowledge the computational infrastructure provided by Laboratorio Nacional de Conversión y Almacenamiento de Energía (CONACYT) under Project No. 270810; the Supercomputing Department of Universidad Nacional Autónoma de México for the computing resources under Project Nos. LANCAD-UNAM-DGTIC-370 and LANCAD-UNAM-DGTIC-310; and the support given by Fondo Sectorial de Investigación para la Educación-CONACYT under Project No. A1-S-13294.

References

[1] M. Scharber, N. Sariciftci, Efficiency of bulk-heterojunction organic solar cells, Prog. Polym. Sci. 38 (12) (2013) 1929–1940. Topical Issue on Conductive Polymers.

[2] L. Meng, Y. Zhang, X. Wan, C. Li, X. Zhang, Y. Wang, X. Ke, Z. Xiao, L. Ding, R. Xia, H.-L. Yip, Y. Cao, Y. Chen, Organic and solution-processed tandem solar cells with 17.3% efficiency, Science 361 (6407) (2018) 1094–1098.

[3] M.-A. Pan, T.-K. Lau, Y. Tang, Y.-C. Wu, T. Liu, K. Li, M.-C. Chen, X. Lu, W. Ma, C. Zhan, 16.7%-efficiency ternary blended organic photovoltaic cells with pcbm as the acceptor additive to increase the open-circuit voltage and phase purity, J. Mater. Chem. A 7 (2019) 20713–20722.

[4] Y. Cui, H. Yao, J. Zhang, T. Zhang, Y. Wang, L. Hong, K. Xian, B. Xu, S. Zhang, J. Peng, Z. Wei, F. Gao, J. Hou, Over 16% efficiency organic photovoltaic cells enabled by a chlorinated acceptor with increased open-circuit voltages, Nat. Commun. 10 (2515) (2019) 1.

[5] Y. He, H.-Y. Chen, J. Hou, Y. Li, Indene-C60 bisadduct: a new acceptor for high-performance polymer solar cells, J. Am. Chem. Soc. 132 (4) (2010) 1377–1382.

[6] X. Guo, C. Cui, M. Zhang, L. Huo, Y. Huang, J. Hou, Y. Li, High efficiency polymer solar cells based on poly(3-hexylthiophene)/indene-C70 bisadduct with solvent additive, Energy Environ. Sci. 5 (2012) 7943–7949.

[7] Z. Xiao, X. Geng, D. He, X. Jia, L. Ding, Development of isomer-free fullerene bisadducts for efficient polymer solar cells, Energy Environ. Sci. 9 (2016) 2114–2121.

[8] Z. Xiao, X. Jia, D. Li, S. Wang, X. Geng, F. Liu, J. Chen, S. Yang, T.P. Russell, L. Ding, 26 mA cm^{-2}J_{sc} from organic solar cells with a low-bandgap nonfullerene acceptor, Sci. Bull. 62 (22) (2017) 1494–1496.

[9] J. Yuan, Y. Zhang, L. Zhou, G. Zhang, H.-L. Yip, T.-K. Lau, X. Lu, C. Zhu, H. Peng, P. A. Johnson, M. Leclerc, Y. Cao, J. Ulanski, Y. Li, Y. Zou, Single-junction organic solar cell with over 15% efficiency using fused-ring acceptor with electron-deficient core, Joule 3 (4) (2019) 1140–1151.

[10] J. Xiong, K. Jin, Y. Jiang, J. Qin, T. Wang, J. Liu, Q. Liu, H. Peng, X. Li, A. Sun, X. Meng, L. Zhang, L. Liu, W. Li, Z. Fang, X. Jia, Z. Xiao, Y. Feng, X. Zhang, K. Sun, S. Yang, S. Shi, L. Ding, Thiolactone copolymer donor gifts organic solar cells a 16.72% efficiency, Sci. Bull. 64 (21) (2019) 1573–1576.

[11] T. Wang, J. Qin, Z. Xiao, X. Meng, C. Zuo, B. Yang, H. Tan, J. Yang, S. Yang, K. Sun, S. Xie, L. Ding, A 2.16 eV bandgap polymer donor gives 16% power conversion efficiency, Sci. Bull. 65 (3) (2020) 179–181.

[12] Q. Liu, Y. Jiang, K. Jin, J. Qin, J. Xu, W. Li, J. Xiong, J. Liu, Z. Xiao, K. Sun, S. Yang, X. Zhang, L. Ding, 18% Efficiency organic solar cells, Sci. Bull. 65 (4) (2020) 272–275.

[13] S. Gélinas, A. Rao, A. Kumar, S.L. Smith, A.W. Chin, J. Clark, T.S. van der Poll, G. C. Bazan, R.H. Friend, Ultrafast long-range charge separation in organic semiconductor photovoltaic diodes, Science 343 (6170) (2014) 512–516.

[14] A.A. Bakulin, A. Rao, V.G. Pavelyev, P.H.M. van Loosdrecht, M.S. Pshenichnikov, D. Niedzialek, J. Cornil, D. Beljonne, R.H. Friend, The role of driving energy and delocalized states for charge separation in organic semiconductors, Science 335 (6074) (2012) 1340–1344.

[15] T.M. Clarke, J.R. Durrant, Charge photogeneration in organic solar cells, Chem. Rev. 110 (11) (2010) 6736–6767.

[16] S.D. Collins, N.A. Ran, M.C. Heiber, T.-Q. Nguyen, Small is powerful: recent progress in solution-processed small molecule solar cells, Adv. Energy Mater. 7 (10) (2017) 1602242.

[17] H. Zhou, L. Yang, W. You, Rational design of high performance conjugated polymers for organic solar cells, Macromolecules 45 (2) (2012) 607–632.

[18] H. Zhou, L. Yang, A.C. Stuart, S.C. Price, S. Liu, W. You, Development of fluorinated benzothiadiazole as a structural unit for a polymer solar cell of 7% efficiency, Angew. Chem. Int. Ed. 50 (13) (2011) 2995–2998.

[19] Y. Liang, S. Xiao, D. Feng, L. Yu, Control in energy levels of conjugated polymers for photovoltaic application, J. Phys. Chem. C 112 (21) (2008) 7866–7871.

[20] M.M. Wienk, J.M. Kroon, W.J.H. Verhees, J. Knol, J.C. Hummelen, P.A. van Hal, R. A.J. Janssen, Efficient methano[70]fullerene/MDMO-PPV bulk heterojunction photovoltaic cells, Angew. Chem. Int. Ed. 42 (29) (2003) 3371–3375.

[21] R.C. Coffin, J. Peet, J. Rogers, G.C. Bazan, Streamlined microwave-assisted preparation of narrow-bandgap conjugated polymers for high-performance bulk heterojunction solar cells, Nat. Chem. 1 (2009) 657–661.

[22] Y. Firdaus, V.M. Le Corre, J.I. Khan, Z. Kan, F. Laquai, P.M. Beaujuge, T. D. Anthopoulos, Key parameters requirements for non-fullerene-based organic solar cells with power conversion efficiency > 20%, Adv. Sci. 6 (9) (2019) 1802028.

[23] R. Olivares-Amaya, C. Amador-Bedolla, J. Hachmann, S. Atahan-Evrenk, R. S. Sanchez-Carrera, L. Vogt, A. Aspuru-Guzik, Accelerated computational discovery of high-performance materials for organic photovoltaics by means of cheminformatics, Energy Environ. Sci. 4 (2011) 4849–4861.

[24] B. Bai, M. Zhang, N. Ji, J. Wei, H. Wang, M. Li, E-Z isomerization of the –C=N– bond in anthracene-based acylhydrazone derivatives under visible light, Chem. Commun. 53 (2017) 2693–2696.

[25] V. Hernández, J.T. López Navarrete, Ab initio study of torsional potentials in 2,2′-bithiophene and 3,4′- and 3,3′-dimethyl-2,2′-bithiophene as models of the backbone flexibility in polythiophene and poly(3-methylthiophene), J. Chem. Phys. 101 (2) (1994) 1369–1377.

[26] P. Bortolus, S. Monti, Cis-trans photoisomerization of azobenzene. Solvent and triplet donors effects, J. Phys. Chem. 83 (6) (1979) 648–652.

[27] D.L. Meyer, R. Matsidik, M. Sommer, T. Biskup, Electronic structure trumps planarity: unexpected narrow exciton delocalization in PNDIT2 revealed by time-resolved electron paramagnetic resonance (EPR) spectroscopy, Adv. Electron. Mater. 4 (3) (2018) 1700385.

[28] A. Guillén-López, C. Delesma, C. Amador-Bedolla, M. Robles, J. Mu niz, Electronic structure and nonlinear optical properties of organic photovoltaic systems with potential applications on solar cell devices: a DFT approach, Theoret. Chem. Acc. 137 (6) (2018) 85.

[29] J. Roncali, Molecular engineering of the band gap of π-conjugated systems: facing technological applications, Macromol. Rapid Commun. 28 (17) (2007) 1761–1775.

[30] R. Petraglia, A. Nicolaï, M.D. Wodrich, M. Ceriotti, C. Corminboeuf, Beyond static structures: putting forth REMD as a tool to solve problems in computational organic chemistry, J. Comput. Chem. 37 (1) (2016) 83–92.

[31] J. Maciejewski, A. Sobczuk, A. Claveau, A. Nicolai, R. Petraglia, L. Cervini, E. Baudat, P. Mieville, D. Fazzi, C. Corminboeuf, G. Sforazzini, Photochromic torsional switch (PTS): a light-driven actuator for the dynamic tuning of π-conjugation extension, Chem. Sci. 8 (2017) 361–365.

[32] H. Brahim, DFT/TD-DFT investigation on the UV–vis absorption and phosphorescence spectra of platinum(II) and palladium(II) complexes with Schiff-base ligands, J. Luminesc. 210 (2019) 96–103.

[33] N. Wazzan, A. Irfan, Theoretical study of triphenylamine-based organic dyes with mono-, di-, and tri-anchoring groups for dye-sensitized solar cells, Org. Electron. 63 (2018) 328–342.

[34] Q. Arooj, F. Wang, Switching on optical properties of D-π-A DSSC sensitizers from π-spacers towards machine learning, Solar Energy 188 (2019) 1189–1200.

[35] H. García, N. Farfán, M. Hernández, Communication, Personal communication, 2019 (Facultad de Química UNAM).

[36] L.D. Sifuentes-Vázquez, E. Martínez-González, R.A. Toscano, R. Gavi no, J. Cárdenas, C.A. Rius-Alonso, C. Amador-Bedolla, G.A. García de la Mora, V. M. Ugalde Saldivar, Experimental and theoretical exploration of aryl substituent effects on the electronic properties of asymmetric 4,7-di(thiophene-2-yl)-benzo[c][2,1,5]thiadiazole, Polycyclic Aromatic Compounds (2020), https://doi.org/10.1080/10406638.2020.1749858.

[37] J.P. Perdew, K. Burke, M. Ernzerhof, Generalized gradient approximation made simple, Phys. Rev. Lett. 77 (18) (1996) 3865–3868.

[38] F. Weigend, M. Häser, H. Patzelt, R. Ahlrichs, RI-MP2: optimized auxiliary basis sets and demonstration of efficiency, Chem. Phys. Lett. 294 (1) (1998) 143–152.

[39] F. Weigend, R. Ahlrichs, Balanced basis sets of split valence, triple zeta valence and quadruple zeta valence quality for H to Rn: design and assessment of accuracy, Phys. Chem. Chem. Phys. 7 (2005) 3297–3305.

[40] D. Jacquemin, I. Duchemin, X. Blase, Benchmarking the Bethe-Salpeter formalism on a standard organic molecular set, J. Chem. Theory Comput. 11 (7) (2015) 3290–3304.

[41] TURBOMOLE V6.6 2014, A Development of University of Karlsruhe and Forschungszentrum Karlsruhe GmbH, 1989–2007, TURBOMOLE GmbH, since 2007. Available from http://www.turbomole.com.

[42] C. Steffen, K. Thomas, U. Huniar, A. Hellweg, O. Rubner, A. Schroer, TmoleX – a graphical user interface for TURBOMOLE, J. Comput. Chem. 31 (16) (2010) 2967–2970.

[43] G. Rossum, Python Reference Manual, Tech. Rep., Python Software Foundation, Amsterdam, The Netherlands, 1995.

[44] C. Delesma, C. Amador-Bedolla, M. Robles, J. Muñiz, Electronic structure data at ground and excited state of the structural and opto-electronic properties of organic photovoltaic materials, Data in Brief (2021) (submitted for publication).

[45] M. Jayakannan, P.A. van Hal, R.A.J. Janssen, Synthesis and structure-property relationship of new donor-acceptor-type conjugated monomers and polymers on the basis of thiophene and benzothiadiazole, J. Polym. Sci. Part A: Polym. Chem. 40 (2) (2002) 251–261.

[46] A. Mishra, P. Bäuerle, Small molecule organic semiconductors on the move: promises for future solar energy technology, Angew. Chem. Int. Ed. 51 (9) (2012) 2020–2067.

[47] A.N. Sokolov, S. Atahan-Evrenk, R. Mondal, R.S. Akkerman, B. Hylke, S. Sánchez-Carrera, J. Granados-Focil, S.C. Schrier, A.P. Mannsfeld, Z. Zoombelt, A. Bao, Aspuru-Guzik, From computational discovery to experimental characterization of a high hole mobility organic crystal, Nat. Commun. 2 (2011) 437.

[48] O.D. Jurchescu, J. Baas, T.T.M. Palstra, Effect of impurities on the mobility of single crystal pentacene, Appl. Phys. Lett. 84 (2004) 3061–3063.

[49] A.D. Becke, Density-functional exchange-energy approximation with correct asymptotic behavior, Phys. Rev. A 38 (1988) 3098–3100.

[50] C. Lee, W. Yang, R.G. Parr, Development of the Colle-Salvetti correlation-energy formula into a functional of the electron density, Phys. Rev. B 37 (1988) 785–789.

[51] A.D. Becke, Density-functional thermochemistry. III. The role of exact exchange, J. Chem. Phys. 98 (7) (1993) 5648–5652.

[52] T. Yanai, D.P. Tew, N.C. Handy, A new hybrid exchange-correlation functional using the Coulomb-attenuating method (CAM-B3LYP), Chem. Phys. Lett. 393 (1) (2004) 51–57.

[53] J.P. Perdew, M. Ernzerhof, K. Burke, Rationale for mixing exact exchange with density functional approximations, J. Chem. Phys. 105 (22) (1996) 9982–9985.

[54] Y. Zhao, D.G. Truhlar, The M06 suite of density functionals for main group thermochemistry, thermochemical kinetics, noncovalent interactions, excited states, and transition elements: two new functionals and systematic testing of four M06 functionals and 12 other functionals, Theoret. Chem. Acc. 119 (5) (2008) 525.

[55] N. Blouin, A. Michaud, D. Gendron, S. Wakim, E. Blair, R. Neagu-Plesu, M. Belletête, G. Durocher, Y. Tao, M. Leclerc, Toward a rational design of poly(2,7-carbazole) derivatives for solar cells, J. Am. Chem. Soc. 130 (2) (2008) 732–742.

[56] R.G. Parr, R.G. Pearson, Absolute hardness: companion parameter to absolute electronegativity, J. Am. Chem. Soc. 105 (26) (1983) 7512–7516.

[57] R. El Mouhi, S. El Khattabi, M. Hachi, A. Fitri, A.T. Benjelloun, M. Benzakour, M. Mcharfi, M. Bouachrine, DFT and TD-DFT calculations on thieno[2,3-b]indole-based compounds for application in organic bulk heterojunction (BHJ) solar cells, Res. Chem. Intermed. 45 (3) (2019) 1327–1340.
[58] B. Carsten, J.M. Szarko, H.J. Son, W. Wang, L. Lu, F. He, B.S. Rolczynski, S.J. Lou, L.X. Chen, L. Yu, Examining the effect of the dipole moment on charge separation in donor-acceptor polymers for organic photovoltaic applications, J. Am. Chem. Soc. 133 (50) (2011) 20468–20475.
[59] H.D. de Gier, R. Broer, R.W.A. Havenith, Non-innocent side-chains with dipole moments in organic solar cells improve charge separation, Phys. Chem. Chem. Phys. 16 (2014) 12454–12461.
[60] Q. Arooj, F. Wang, Switching on optical properties of D-π-A DSSC sensitizers from π-spacers towards machine learning, Solar Energy 188 (2019) 1189–1200.
[61] P. Friederich, A. Fediai, J. Li, A. Mondal, N. Kotadiya, G. D'Avino, F. Symalla, G.-J. Wetzelaer, D. Andrienko, D. Beljonne, P. Blom, J.-L. Brédas, W. Wenzel, The Influence of Impurities on the Charge Carrier Mobility of Small Molecule Organic Semiconductors, 2019. arXiv:1908.11854.
[62] J. Sworakowski, Effect of polar molecules on the transport and localization of charge carriers in molecular materials, Braz. J. Phys. 29 (1999) 318–331.
[63] P. Toman, M. Menšík, W. Bartkowiak, J. Pfleger, Modelling of the charge carrier mobility in disordered linear polymer materials, Phys. Chem. Chem. Phys. 19 (2017) 7760–7771.
[64] C.H. Kim, Y. Bonnassieux, G. Horowitz, Charge Distribution and Contact Resistance Model for Coplanar Organic Field-Effect Transistors, IEEE Transactions on Electron Devices 60 (2013) 280–287.
[65] Mottaghi Mohammad, Horowitz Gilles, Field-induced mobility degradation in pentacene thin-film transistors, Org. Electron. 7 (2006) 528–536.
[66] D.M. Lyons, J. Kesters, W. Maes, C.W. Bielawski, J.L. Sessler, Improving efficiencies by modulating the central metal ion in porphyrin-oligothiophene-mediated p3ht/pcbm organic solar cells, Synth. Metals 178 (2013) 56–61.
[67] Q. Fu, Radiation (solar), in: J.R. Holton (Ed.), Encyclopedia of Atmospheric Sciences, Academic Press, Oxford, 2003, pp. 1859–1863.
[68] G. Dennler, M.C. Scharber, C.J. Brabec, Polymer-fullerene bulk-heterojunction solar cells, Adv. Mater. 21 (13) (2009) 1323–1338.
[69] M.C. Scharber, D. Mühlbacher, M. Koppe, P. Denk, C. Waldauf, A.J. Heeger, C. J. Brabec, Design rules for donors in bulk-heterojunction solar cells-towards 10% energy-conversion efficiency, Adv. Mater. 18 (6) (2006) 789–794.
[70] R. Zhou, Z. Jiang, C. Yang, J. Yu, J. Feng, M.A. Adil, D. Deng, W. Zou, J. Zhang, K. Lu, W. Ma, F. Gao, Z. Wei, All-small-molecule organic solar cells with over 14% efficiency by optimizing hierarchical morphologies, Nat. Commun. 10 (5393) (2019) 1.
[71] L. Zhang, X. Xing, L. Zheng, Z. Chen, L. Xiao, B. Qu, Q. Gong, Vertical phase separation in bulk heterojunction solar cells formed by *in situ* polymerization of fulleride, Sci. Rep. 4 (2014) 5071.
[72] J.A. Love, C.M. Proctor, J. Liu, C.J. Takacs, A. Sharenko, T.S. van der Poll, A. J. Heeger, G.C. Bazan, T.-Q. Nguyen, Film morphology of high efficiency solution-processed small-molecule solar cells, Adv. Funct. Mater. 23 (40) (2013) 5019–5026.

Apéndice B

Journal of Photochemistry & Photobiology, A: Chemistry 433 (2022) 114182

Contents lists available at ScienceDirect

Journal of Photochemistry & Photobiology, A: Chemistry

journal homepage: www.elsevier.com/locate/jphotochem

Electronic transport in organic photovoltaic materials subjected to dark and light irradiation conditions: A first principles study

Cornelio Delesma [a], Carlos Amador-Bedolla [b], Miguel Robles [a], Jesús Muñiz [a,*]

[a] Instituto de Energías Renovables, Universidad Nacional Autónoma de México, Priv. Xochicalco s/n, Col. Centro, Temixco, 62580, Morelos, Mexico
[b] Facultad de Química, Universidad Nacional Autónoma de México, Ciudad de México, 04510, Mexico

ARTICLE INFO

Keywords:
Organic photovoltaics
DFT
Renewable energy
Electron transport

ABSTRACT

Organic solar cell nanomaterials are molecular systems that have been recently incorporated in devices with remarkable properties and high efficiencies. A systematic theoretical study based on density functional theory and non-equilibrium Green's functions was performed to elucidate the electron transport behavior on solar cell materials. The $I-V$ profiles based on the transmission obtained from the electronic density revealed an appropriate performance in simulated conditions of sunlight irradiation, while in dark conditions such systems may behave as a diode. The current methodology may represent a tool to select and design high performance materials for the new generation of solar cell devices.

1. Introduction

The design of organic molecular systems with facile electronic transport has been the subject of intense research. It is of fundamental interest in donor molecules implemented in an organic cell heterojunction.

It is known that in organic materials with π-conjugation, the electronic transport is improved due to a low energetic resonance, which is smaller than that of benzene [1]. Moreover, if the organic molecule contains a sulfur atom, an enhancement is also obtained [2–6]. This was observed in the organic semiconductor dithienothiophene, used as a building block in organic cells, in which a high charge mobility was disclosed. An Au(111) slab was used as the model electrode [7]. The bonding $M-O-M$ (M=metal, O=organic) is crucial to study the electronic transport properties. Furthermore, its understanding in organic materials may directly improve efficiency. Heterojunction devices have been explored, in which a section of a nanotube was considered to understand the effect of the bond carbon–hydrogen–nitrogen (C–H ··· N) within those nanotube sections [8]. Ferreira et al. studied 2D carbon wires using as an electrode model a nickel atom [9], and Berdiyorov et al. [10] analyzed carbyne encapsulated in a carbon nanotube. Bicyclic aziridine was also studied as a molecular switch [11]. Photosensibility properties can be changed between opened and closed states by photo-excitation effects. Open geometry states allowed to obtain a larger current using a Au(111) electrode, unlike the case for Ag(111) and Pt(111) slabs.

Moreover, it is important to note that solar cell devices show a phenomenon termed negative differential resistance (NDR) that is characterized by the increase of voltage with a decrease of current [12]. This effect could be detrimental for a solar cell, but beneficial in other devices, such as diodes. Pyrene-based molecule with a Au(111) slab as an electrode model [13] was also studied. A simulation was performed on two different contacts of pyrene-based molecules by using Au(111) as the electrode. This results show that asymmetrical anchoring groups play an important role to evidence the NDR. On the other hand, from the theoretical point of view, a previous study based on density functional theory (DFT) and time-dependent DFT (TDDFT) in organic molecules, reported photo-sensibility when the systems changed between ground and excited states [14]. The absorption spectra in these molecular systems revealed a close dependence on a photoisomerization effect that is related to the geometry changes from the ground to the excited state. As a consequence, more insights into the structural changes in molecular organic photovoltaic OPV systems and its relationship with electron mobility appears to be a subject of fundamental interest. In this regard, organic solar cells represent a new generation of photovoltaic devices, which are light and versatile with interesting efficiencies up to 18% [15]. Nevertheless, the photophysics and chemical mechanisms behind the organic solar cells have been partially unknown. Consequently, a deeper understanding is still required to achieve higher efficiencies and more photostable solar cells. In this respect, the electron transport at the molecular level has not been explored in OPV systems that present the photoisomerization phenomena. The aims of this work is to elucidate the behavior of electron transport in OPV systems in which the photoisomerization rules the electronic

* Corresponding author.
E-mail address: jms@ier.unam.mx (J. Muñiz).

https://doi.org/10.1016/j.jphotochem.2022.114182
Received 24 February 2022; Received in revised form 4 July 2022; Accepted 26 July 2022
Available online 30 July 2022

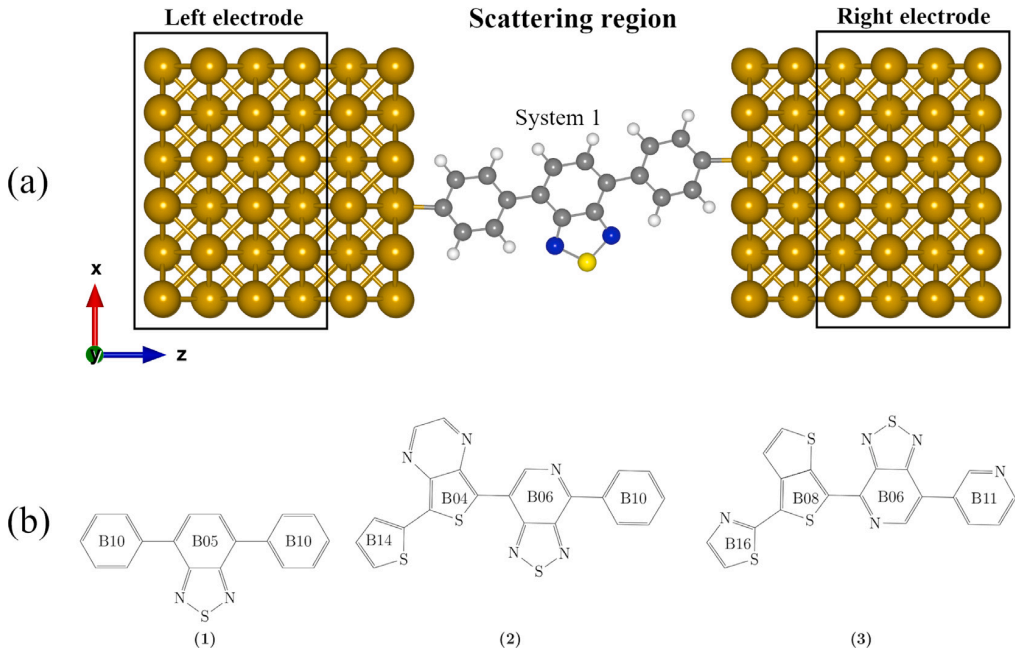

Fig. 1. (a) Electronic device used to compute transmission properties with the NEGF. The Au(100) electrodes were set up with periodic conditions as given in the computational details section. The three molecular systems under study were interchanged at the scattering region. Dark yellow, white, gray, blue and light yellow balls correspond to Au, H, C, *N* and S atoms, respectively. The intermolecular distance between the molecular systems and the Au electrodes is 2.09 Å. (b) Molecular representation of the OPV systems under study. The hydrogen atoms were omitted for clarity in this scheme.

structure properties, and also to build fundamental understanding of charge carrier photogeneration in a solar device formed of an OPV material.

In this work, a theoretical study was performed to identify systems with high transmission coefficients. Additionally, the study of the NDR phenomena was also considered. Novel descriptors are proposed to evaluate organic systems with potential applications in cell heterojunctions as donor materials.

2. Computational details

Electronic transport calculations were performed by using Au electrodes to allow an adequate conduction. The system Au(100)-OPV-Au(100) was implemented as the device. Periodic conditions were imposed at the x, y and z axis. The size of z was modified according to the magnitude of the organic system. For the periodicity of the Au(100) electrode, four layers were used with a k-grid of $2 \times 2 \times 10$ (see Fig. 1(a)). The Au(100) model was selected due to its large number of states available for electron conduction.

The scattering region included the OPV system and 2 layers of Au(100) in the left and right directions. Such layers simulate the perturbation effect in the central region. The Au–C bond was proposed by omitting the H bonding in the OPV, since H is not efficiently adsorbed on the metallic surfaces [11]. The distance between C and the Au electrode amounted to 2.09 Å, computed by using a Morse potential fitting, as depicted in Fig. **S1** of Supplementary Information (SI). Such a distance is in agreement with the typical Au–C bonding distance previously calculated somewhere else [16]. At the scattering region, a k-grid of $2 \times 2 \times 2$ was imposed.

The calculations were performed at the DFT/PBE (Perdew–Burke–Ernzerhof) level [17]. The core electrons were modeled with the Troullier–Martins pseudopotential [18] and the valence electrons with a SZ basis set. The cutoff energy was fixed to 350 Ry. The non-equilibrium Green's function (NEGF) method was employed in the TranSIESTA module [19] of the SIESTA code [20]. The current–voltage ($I - V$) profiles and the NDR phenomenon was also studied with a bias voltage from −3.0 to +3.0 V. The current was calculated with the Landauer–Büttiker equation [21–23]:

$$I(V_b) = \frac{2e^2}{h} \int_{\mu_L}^{\mu_R} T(E, V_b) \mathrm{d}E \tag{1}$$

in which μ_L and μ_R represent the chemical potentials of the left and right electrodes, respectively. The chemical potential difference is given by eV_b, with the application of polarization potential (V_b). That is, $\mu_L(V_b) = \mu_L(0) - eV_b/2$ and $\mu_R(V_b) = \mu_R(0) + eV_b/2$. The term $T(E, V_b)$ represents the total transmission probability of incident electrons with energy E throughout the device, and within the range of the polarization potential (V_b).

It is important to highlight that the OPV molecules subjected to excited state calculations were previously performed in a work by our group [14]. In those calculations, the molecular geometries were optimized in the excited state in accordance with the TDDFT methodology [24] by using the same basis set than in this work, as implemented in the TURBOMOLE computational code [25].

3. Results and discussion

The systems under study (compounds 1, 2 and 3 in Fig. 1(b)) were selected as the most representative compounds following the findings reported in a previous work [14] (compounds 6, 11 and 23 in that work). The IUPAC notation for the systems under study are: 4,7-diphenylbenzo[*c*][1,2,5]thiadiazole (compound **1**), 4-phenyl-7-(7-(thiophen-2-yl)thieno[3,4-*b*]pyrazin-5-yl)-[1,2,5]thiadiazolo[3,4-*c*] pyridine (compound **2**) and 7-(pyridin-3-yl)-4-(4-(thiazol-2-yl)thieno [3,4-*b*]thiophen-6-yl)-[1,2,5]thiadiazolo[3,4-*c*]pyridine (compound **3**). A screening was performed from the data base since at the excited state, two of the title systems showed photoisomerization, and one presented no changes at all. Photoisomerization is indicative of changes in the dihedral angles from the ground to the excited state in the presence of solar irradiation. Systems **1**, **2** and **3** showed an average change in the dihedral angles at the excited state of 15°, 0°and 25°, respectively [14]. System **2** was screened since no dihedral variation was evidenced

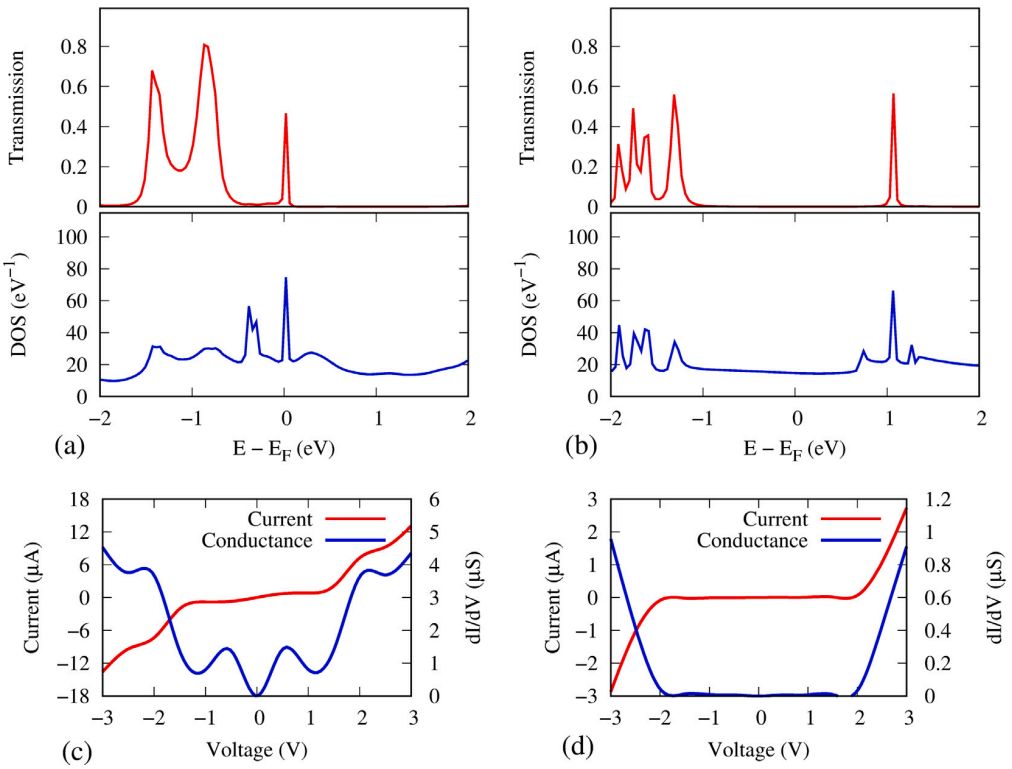

Fig. 2. Density of states (DOS) with respect to the transmission coefficients of system **1**: (a) at ground state and (b) at the excited state. Energy values were displaced with respect to the Fermi level (E_F), indicating that the E_F is located at a null energy. Note that the transmission was assessed in accordance to the NEGF methodology. Current (I in Amperes) and conductance (dI/dV in S) profiles with respect to applied voltage of system **1**: (c) at ground state and (d) at excited state.

at the excited state, showing, instead, a red-shift absorption. It was addressed to a frontier molecular orbital (MO) re-distribution at the excited state [14]. Moreover, such systems absorbed in the range of visible light in accordance to TDDFT calculations.

Fig. 2 shows the relationship of transmission coefficient $T(E, V_b)$ and the electron energy at a zero voltage ($V_b = 0$). The Fermi level is located at zero. In the ground state (see Fig. 2(a)), system **1** shows transmission below the Fermi level, with no contributions beyond. In the excited state (see Fig. 2(b)) a peak above E_F (located at the conduction band) suggests the enhancement of electronic transport. This could be attributed to the presence of states at the conduction band. Such states may be related to the change of geometry in the excited state and to the formation of modified unoccupied molecular orbitals. That is, those states at the conduction band may be related to the changes in the lowest unoccupied molecular orbital (LUMO) distribution of system **1**. The LUMO corresponds to an unoccupied molecular orbital that formally presents the absence of electron density. Nevertheless, it can be interpreted as those regions surrounding the molecule where an electron transfer could be feasible. In this respect, the 2D slices in Fig. 3(c) depict the probable regions in which electrons could be transferred. Indeed, an electronic phase change was evidenced in the LUMO of the ground and excited states. Particularly, the contribution located at the benzo[1,2,5]thiadiazole group in system **1**, as presented in Fig. 3(c). In the ground state, the negative distribution revealed sites of low probability to be occupied by electrons (red regions), while the LUMO of the excited state showed regions of likely sites to be occupied by electrons (blue regions). Such a behavior could be directly related to the formation of states at the conduction band. As a consequence, it is likely that upon light irradiation, the system enhances electronic transmission, and a more effective conductance. The rising of additional contributions in transmission indicates the formation of new opened channels in which the charge is allowed to be tracked. Consequently, a close relationship among the transmission profile and the density of states may play an important role in electron transport.

Ground state geometries could be addressed as states in which a solar cell device is evaluated under dark conditions. Moreover, the excited state could simulate illumination conditions upon solar cell irradiation.

The high symmetry of **1** at ground state allowed the interaction with the two Au-electrodes (see Fig. 1(a) and (b)). Its $I - V$ curve and conductance values are both presented in Fig. 2(c). In the range from 0.0 to 0.5 V, there is a small current increase to 0.71 μA. The increase was identified in the full range of the potential energy. This character clearly represents the J-shaped curve observed in organic solar cells [26]. The excited state geometry of system **1** was also located at the interface of the Au electrodes to elucidate the conduction properties, simulating the material in the presence of solar irradiation. No current contribution was found in the range from 0.0 V to 2.0 V (see Fig. 2(d)), but a J-shaped curve was disclosed up to 3.0 V. This suggests that the OPV would adequately operate [26] as a solar material in the active layer in the presence of a heterojunction. The conductance is analogous to the $I-V$ curve, revealing a constant electron transport. In this case, the S-shaped character is absent. As a consequence, system **1** may represent an active layer with an effective electron mobility. This may be related to the high symmetric distribution of the frontier molecular orbitals with sp^2 hybridization (see Fig. 3), allowing an efficient electron transport throughout the molecular system.

Fig. **S2** (a) shows the DOS/transmission of system **2** at ground state. Localized states at the conduction band address the probability of electron transmission in accordance to the presence of a sharp peak shown at the same energy level (approximately 1.25 eV). The profiles for system **2** at the excited state geometry (see Fig. **S2** (b)) showed a larger number of states which virtually doubled transmission. It could be understood in terms of the $I-V$ and conductance profiles as depicted

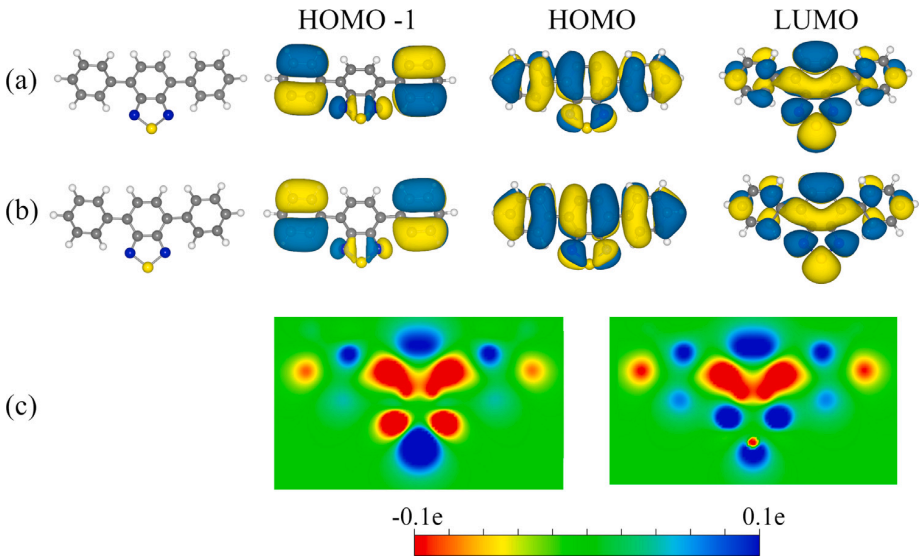

Fig. 3. Frontier molecular orbitals of system **1** at (a) ground state, and (b) excited state. (c) Isosurface 2D slices of the LUMO. The left side represents the ground state LUMO, and the right side that of the excited state.

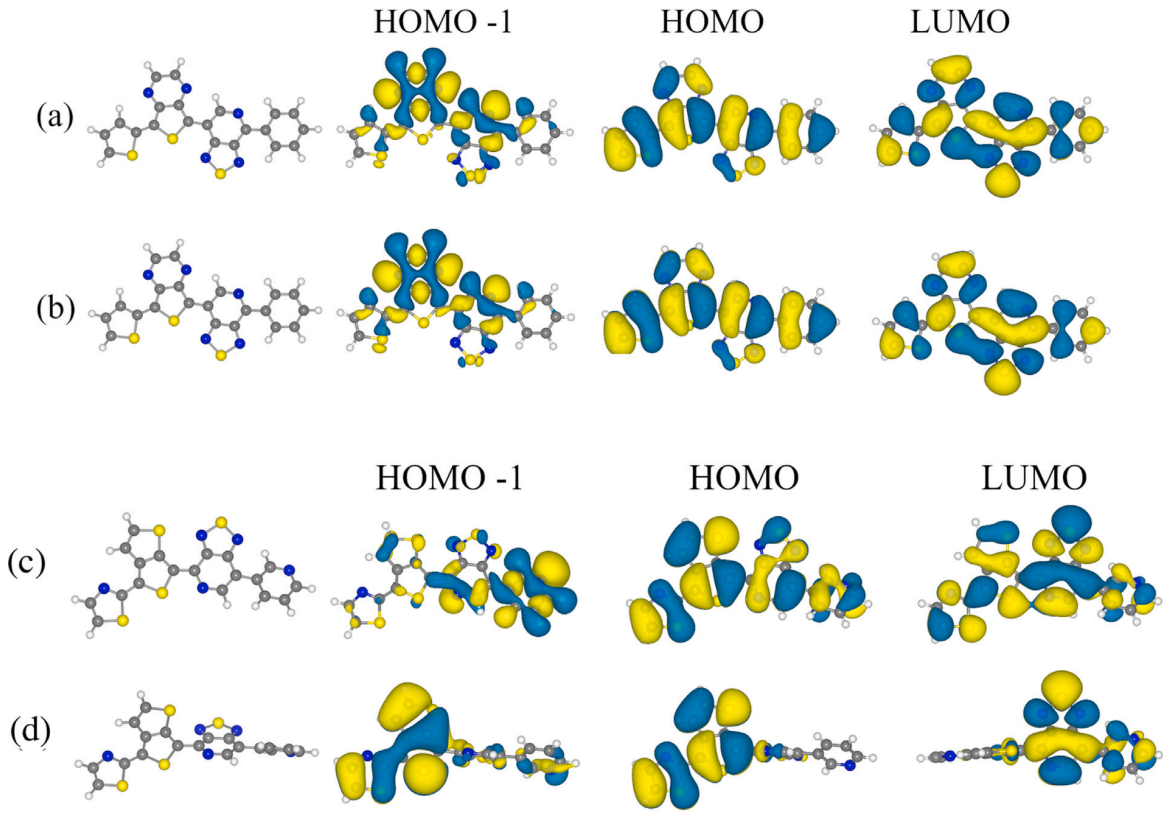

Fig. 4. Frontier molecular orbitals of system **2** at (a) ground state, and (b) excited state. Frontier molecular orbitals of system **3** at (c) ground state, and (d) excited state.

in Fig. **S2** (c) and (d). The $I - V$ profile of system **2** at the ground state showed a different character at the first quadrant, indicating the electron mobility could be challenging through the sp^2 bonding of the frontier molecular orbitals. Unlike system **1**, the asymmetrical distribution of the π-orbitals at the HOMO and HOMO-1 (see Fig. 4) was probably provoked by the BO4 ring unit (Fig. 1(b)).

The system **2** at ground state also showed a diode-like behavior (see Fig. **S2** (c)). In the range from 1.5 to 2.0 V, the current was decreased. The current at 1.5 V is 1.2 μA, at 2.0 V corresponds to 1.1 μA and for 2.5 V, the current is 1.45 μA. This could be addressed as the NDR. Unlike a positive resistance in which power is exhausted, a negative resistance could amplify the power of an electrical signal. Such a device could be implemented as a tunnel or Gunn diode [27]. This system would be

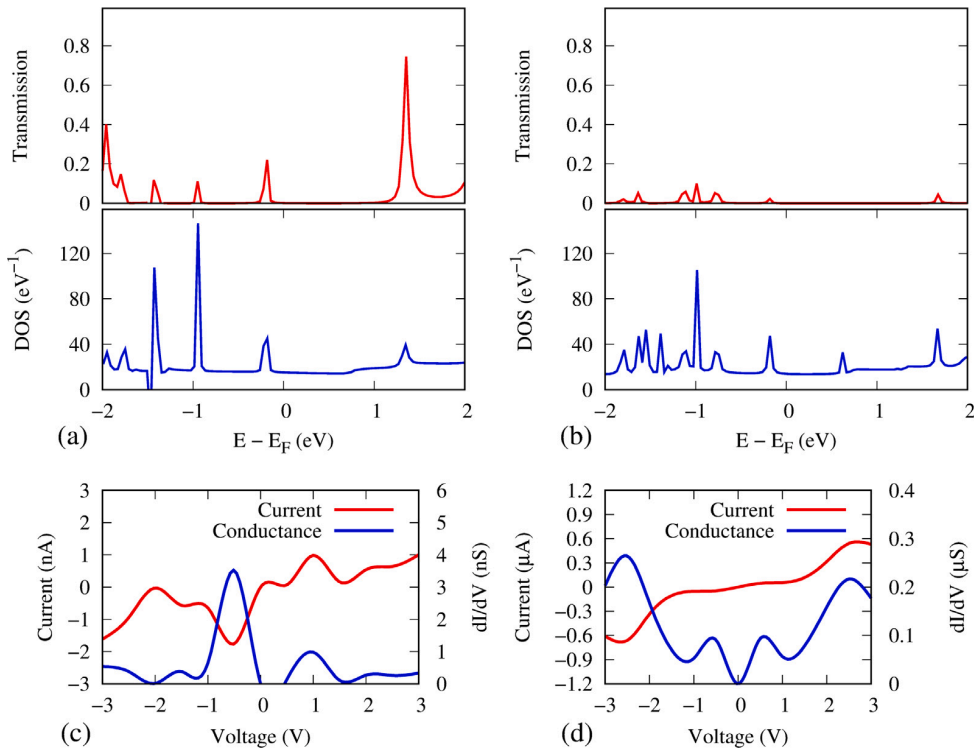

Fig. 5. Density of states (DOS) with respect to the transmission coefficients of system **3**: (a) at ground state and (b) at the excited state. Energy values were displaced with respect to the Fermi level (E_F), indicating that the E_F is located at a null energy. Note that the transmission was assessed in accordance to the NEGF methodology. Current (I in Amperes) and conductance (dI/dV in S) profiles with respect to applied voltage of system **3**: (c) at ground state and (d) at excited state. Note that amplifications of (c) and (d) are depicted in Fig. **S4** of SI.

significantly affected by the electron mobility at the excited state, due to the rise of a *S*-shaped character beyond 2.0 V.

Such a behavior was strengthened by the structural changes in the excited state, limiting the electron mobility at the frontier molecular orbitals (see Fig. 4) due to the lack of symmetry among the HOMO/HOMO-1 and the LUMO of **2**. As a consequence, system **2** could be a possible organic compound with a limited electron mobility upon light irradiation.

The transmission/DOS profiles of system **3** for the ground state are depicted in Fig. 5(a). The formation of unoccupied states at the conduction band is indicative of transmission formation through the molecular system. It was also identified in the excited state with a smaller contribution for transmission, as depicted in Fig. 5(b). As a consequence, a marginal conductance rules at the window potential from 0.0 to 3.0 V (see Fig. 5(c)), resulting in an oscillatory behavior that may not be favorable in heterojunctions. Nonetheless, conduction is fully rectified at the excited state, increased up to 2.5 V (as depicted in Fig. 5(d)). Moreover, the $I-V$ profile revealed a dominant J-shape behavior. The improvement of current with the applied voltage in the excited state could be related to the modified torsional angles at the excited state, allowing a facile electron mobility along the molecular system. As it is presented in Fig. 4, HOMO and HOMO-1 would permit a more effective electron transport to the LUMO. Such geometrical configuration is virtually absent at the ground state (see Fig. 4). As a consequence, system **3** could be a potential candidate for the active layer of a solar cell upon light irradiation. Moreover, in the ground state the current is increased to 0.98 nA in the range from 0.5 to 1.0 V. (see Fig. 5(c)). As previously addressed in system **2**, system **3** also announces NDR. However, in the excited state, this phenomenon is virtually lost (see Fig. 5(d)). That is, an incipient current increase of 0.05 μA is observed between the range from 0.0 to 0.5 V. Also an increase up to 0.54 μA was assessed in the (1.5–2.5 V) range.

Based on the DFT/NEGF methodology presented in this work, it was identified that systems **1** and **3** could result in an enhanced efficiency if implemented in a solar cell device. Such improvement could be predicted from the improved transmission at excited state, which simulates the conditions of light irradiation. The electronic structure properties of system **2** suggests the material to a different application, since the $I-V$ profile revealed a behavior that would be more favorable if it were used as a diode. Transmission and $I-V$ profiles could be considered as novel descriptors to be implemented in order to elucidate the performance of an OPV material intended to be applied in a solar cell device. The descriptors may represent a practical tool to tailor the organic cell materials of the new generation of photovoltaic systems.

It is important to highlight that OPVs, as the systems 1–3 of this work, represent small oligomers with enhanced properties with respect to polymers. They exhibit stable chemical structures, and behave as mono-dispersive materials. The feasibility of such systems to be synthesized has been previously reported [28–30]. In those works, the synthesis and reproducibility do not represent a challenge. A representative case is given by 4,7- di(thiophene-2-yl)-benzo[c][2,1,5]thiadiazole materials. Since the size of their band gap is capable to be tuned, the systems are implemented to tailor monomers and polymers with the required band gap [28,29]. Since the property may be modified, it is possible to screen the donor material to be implemented. The adequate solubility has also been tested with the measurement of the HOMO–LUMO gap by applying cyclic voltammetry with aprotic solvents, which play the role of the supporting electrolyte. The systems 1–3 also show the possibility to be fabricated as thin films, since adequate routes have been performed to optimize such materials as polymer mixtures. In this respect, Lagner et al. [31] implemented a methodology to produce more than 6,000 films per day, and quaternary OPV mixtures are efficiently obtained.

4. Conclusions

A systematic study based on DFT and NEGF was performed by the first time to elucidate the electron transport properties on OPV systems, in which photoisomerization rules their opto-electronic properties. The transmission revealed the current behavior of the systems at ground and excited states. The theoretical $I-V$ profiles showed that system **1**, and **3** could finely operate as a nanomaterial at the active layer of a solar cell device upon solar light irradiation conditions. System **2** may be a potential candidate to be used as a diode due to current variation with respect to applied voltage. Particularly, the electron transport was assessed by using Au slab models as conductive electrodes with the molecular systems **1**-**3** as the scattering region, where the electrons are transported. The conduction nature of system **1** may be intimately related to the formation of states at the conduction band, and to the presence of localized regions in the LUMO of the molecular system in which the electronic charge may be allowed to track. The transmission of system **2** is enhanced at the excited state, giving as a consequence the NDR behavior. It may then be considered as an OPV with limited electron mobility upon light irradiation. Despite a small transmission in the excited state for system **3**, the disposition of the frontier molecular orbitals would allow a facile electron transport to the LUMO. This would be feasible due to the resulting torsional angle caused by the photoisomerization effect at the excited state. As a consequence, system **3** would act as an excellent active layer in a solar cell with light irradiation. The present theoretical methodology may be considered as a guiding tool to screen adequate OPV molecules to be applied in the design of high performance solar cell systems. Transmission and $I-V$ profiles could be considered as descriptors to form data bases for further applications in the design of photovoltaic materials implemented in solar cell systems.

CRediT authorship contribution statement

Cornelio Delesma: Investigation, Methodology, Writing – original draft. **Carlos Amador-Bedolla:** Conceptualization, Writing – review & editing, Resources. **Miguel Robles:** Validation, Data curation, Writing – review & editing, Methodology. **Jesús Muñiz:** Supervision, Project administration, Funding acquisition, Writing – review & editing, Formal analysis.

Declaration of competing interest

The authors declare that they have no known competing financial interests or personal relationships that could have appeared to influence the work reported in this paper.

Data availability

Data will be made available on request.

Acknowledgments

The authors would like to acknowledge the financial support given by DGAPA-UNAM (Dirección General de Asuntos del Personal Académico), Mexico under Project No. PAPIIT-(IG100720, IA102820, IN106122). J.M. would like to acknowledge the Supercomputing Department of Universidad Nacional Autónoma de México for the computing resources under Project No. LANCAD-UNAM-DGTIC-370, LANCAD-UNAM-DGTIC-310, and the support given by Fondo Sectorial de Investigación para la Educación-CONACYT, Mexico under Project No. A1-S-13294; and Fronteras de la Ciencia-CONACYT, Mexico under Project No. 21077. Project No. 270810 (Laboratorio Nacional de Conversión y Almacenamiento de Energía-CONACYT, Mexico) is also acknowledged. C.D. wants to acknowledge CONACYT, Mexico for the PhD fellowship.

Appendix A. Supplementary data

Supplementary material related to this article can be found online at https://doi.org/10.1016/j.jphotochem.2022.114182.

References

[1] Q. Bao, Z. Lu, J. Li, K.P. Loh, C.M. Li, Theoretical and experimental studies of electronic transport of dithienothiophene, J. Phys. Chem. C 113 (28) (2009) 12530–12537.
[2] R.P. Ortiz, M.C. Ruiz Delgado, J. Casado, V. Hernández, O.-K. Kim, H.Y. Woo, J.T. López Navarrete, Electronic modulation of dithienothiophene (DTT) as p-center of D-p-D chromophores on optical and redox properties:? Analysis by UV-vis-NIR and Raman spectroscopies combined with electrochemistry and quantum chemical DFT calculations, J. Am. Chem. Soc. 126 (41) (2004) 13363–13376.
[3] O.-K. Kim, K.-S. Lee, Z. Huang, W.B. Heuer, C.S. Paik-Sung, Oligothiophene as photonic/electronic property modulator, Opt. Mater. 21 (1) (2003) 559–564.
[4] O.-K. Kim, K.-S. Lee, H.Y. Woo, K.-S. Kim, G.S. He, J. Swiatkiewicz, P.N. Prasad, New class of two-photon-absorbing chromophores based on dithienothiophene, Chem. Mater. 12 (2) (2000) 284–286.
[5] R.E. Martin, F. Diederich, Linear monodisperse p-conjugated oligomers: Model compounds for polymers and more, Angew. Chem. Int. Edition 38 (10) (1999) 1350–1377.
[6] T. Otsubo, Y. Aso, K. Takimiya, Functional oligothiophenes as advanced molecular electronic materials, J. Mater. Chem. 12 (2002) 2565–2575.
[7] Q. Bao, Z. Lu, J. Li, K.P. Loh, C.M. Li, Theoretical and experimental studies of electronic transport of dithienothiophene, J. Phys. Chem. C 113 (28) (2009) 12530–12537.
[8] L.O. Jones, M.A. Mosquera, G.C. Schatz, M.A. Ratner, Molecular junctions inspired by nature: Electrical conduction through noncovalent nanobelts, J. Phys. Chem. B 123 (38) (2019) 8096–8102.
[9] D. Ferreira, M. Moura-Moreira, S. Corrêa, C. da Silva Jr, J. Del Nero, Electronic transport in 1D system with coupling atomic-size nickel electrodes and carbon wires, Mater. Sci. Eng. B 262 (2020) 114681.
[10] G. Berdiyorov, G. Eshonqulov, H. Hamoudi, Electronic transport of CNT-encapsulated carbyne, Comput. Mater. Sci. 183 (2020) 109809.
[11] A. Kanaani, M. Vakili, D. Ajloo, Electronic transport properties of 2-niiitro-4-(6-(4-nitrophenyl)-4-phenyl-1,3-diaza-bicyclo[3.1.0]hex-3-en-2-yl)phenol: A light-driven molecular switch, Optik 219 (2020) 165295.
[12] L. Esaki, New phenomenon in narrow germanium $p-n$ junctions, Phys. Rev. 109 (1958) 603–604.
[13] C.-J. Xia, D.-S. Liu, H.-C. Liu, X.-J. Zhai, Large negative differential resistance in a molecular device with asymmetric contact geometries: A first-principles study, Physica E 43 (8) (2011) 1518–1521.
[14] C. Delesma, C. Amador-Bedolla, M. Robles, J. Muñiz, Photoisomerization and its effect in the opto-electronic properties of organic photovoltaic materials: A quantum chemistry study, J. Photochem. Photobiol. A: Chem. 409 (2021) 113155.
[15] Q. Liu, Y. Jiang, K. Jin, J. Qin, J. Xu, W. Li, J. Xiong, J. Liu, Z. Xiao, K. Sun, S. Yang, X. Zhang, L. Ding, 18% Efficiency organic solar cells, Sci. Bull. 65 (4) (2020) 272–275.
[16] P. Pyykkö, M. Atsumi, Molecular single-bond covalent radii for elements 1–118, Chem.: Eur. J. 15 (2009) 186–197.
[17] J.P. Perdew, K. Burke, M. Ernzerhof, Generalized gradient approximation made simple, Phys. Rev. Lett. 77 (18) (1996) 3865–3868.
[18] N. Troullier, J. Martins, A straightforward method for generating soft transferable pseudopotentials, Solid State Commun. 74 (7) (1990) 613–616.
[19] K. Stokbro, J. Taylor, M. Brandbyge, P. Ordejón, TranSIESTA: A spice for molecular electronics, Ann. New York Acad. Sci. 1006 (1) (2003) 212–226.
[20] J.M. Soler, E. Artacho, J.D. Gale, A. García, J. Junquera, P. Ordejón, D. Sánchez-Portal, The SIESTA method forab initioorder-nmaterials simulation, J. Phys.: Condens. Matter 14 (11) (2002) 2745–2779.
[21] M. Büttiker, Four-terminal phase-coherent conductance, Phys. Rev. Lett. 57 (1986) 1761–1764.
[22] M. Büttiker, Absence of backscattering in the quantum hall effect in multiprobe conductors, Phys. Rev. B 38 (1988) 9375–9389.
[23] M. Büttiker, Y. Imry, R. Landauer, S. Pinhas, Generalized many-channel conductance formula with application to small rings, Phys. Rev. B 31 (1985) 6207–6215.
[24] U. Carsten, Time-Dependent Density-Functional Theory: Concepts and Applications, first ed., Oxford University Press, 2012.
[25] TURBOMOLE V6.6 2014, a development of University of Karlsruhe and Forschungszentrum Karlsruhe GmbH, 1989–2007, TURBOMOLE GmbH, since 2007; available from http://www.turbomole.com.
[26] J. Xue, Perspectives on organic photovoltaics, Polymer Rev. 50 (4) (2010) 411–419.

[27] L. Esaki, New phenomenon in narrow germanium $p-n$ junctions, Phys. Rev. 109 (1958) 603–604.

[28] A. Mishra, P. Bäuerle, Small molecule organic semiconductors on the move: Promises for future solar energy technology, Angew. Chem. Int. Edition 51 (9) (2012) 2020–2067.

[29] M. Jayakannan, P.A. van Hal, R.A.J. Janssen, Synthesis and structure-property relationship of new donor-acceptor-type conjugated monomers and polymers on the basis of thiophene and benzothiadiazole, J. Polym. Sci. A 40 (2) (2002) 251–261.

[30] L.D. Sifuentes-Vázquez, E. Martínez-González, R.A. Toscano, R. Gaviño, J. Cárdenas, C.A. Rius-Alonso, C. Amador-Bedolla, G.A. García de la Mora, V.M. Ugalde Saldivar, Experimental and theoretical exploration of aryl substituent effects on the electronic properties of asymmetric 4,7-di(thiophene-2-yl)-benzo[c][2,1,5]thiadiazole, Polycycl. Aromat. Compd. (2020).

[31] S. Langner, F. Häse, J.D. Perea, T. Stubhan, J. Hauch, L.M. Roch, T. Heumueller, A. Aspuru-Guzik, C.J. Brabec, Beyond ternary OPV: High-throughput experimentation and self-driving laboratories optimize multicomponent systems, Adv. Mater. 32 (14) (2020) 1907801.

Apéndice C

Data in Brief 35 (2021) 106952

Contents lists available at ScienceDirect

Data in Brief

journal homepage: www.elsevier.com/locate/dib

Data Article

Electronic structure data at ground and excited state of the structural and opto-electronic properties of organic photovoltaic materials

Cornelio Delesma[a], Carlos Amador-Bedolla[b], Miguel Robles[a], Jesús Muñiz[a,*]

[a] *Instituto de Energías Renovables, Universidad Nacional Autónoma de México, Priv. Xochicalco s/n, Col. Centro, Temixco, Morelos CP 62580, México*
[b] *Facultad de Química, Universidad Nacional Autónoma de México, Ciudad de México, CP 04510, México*

ARTICLE INFO

Article history:
Received 22 January 2021
Revised 5 March 2021
Accepted 8 March 2021
Available online 16 March 2021

Keywords:
Density functional theory
Organic photovoltaic
Photo-isomerization
Excited state

ABSTRACT

This work presents data coming from electronic structure calculations at the Density Functional Theory level, performed in a series of organic photovoltaic materials. The data represents the Cartesian coordinates of such molecular systems at the lowest energy geometry and at the first excited state. Data evidencing the nature of the photo-isomerization in the OPV systems was also obtained. Additionally, the highest probabilities of the molecular electronic transitions giving rise to the absorption spectra observed in excited state were also computed. These data may aid to estimate photovoltaic parameters, and to tailor materials intended to be implemented in solar cell devices. They may also be used as input to design a training set for machine learning analysis and artificial intelligence.

DOI of original article: 10.1016/j.jphotochem.2021.113155
* Corresponding author.
E-mail address: jms@ier.unam.mx (J. Muñiz).
Social media: (J. Muñiz)

https://doi.org/10.1016/j.dib.2021.106952

Specifications Table

Subject	Organic Chemistry Physical and Theoretical Chemistry Renewable Energy, Sustainability and the Environment
Specific subject area	Computational Chemistry
Type of data	Table Graph Figure
How data were acquired	Data obtained with TURBOMOLE computational code at the DFT/PBE level. Data processing using gnuplot and molecular viewer TmoleX.
Data format	Raw data At Supplementary information
Parameters for data collection	Data was acquired from electronic structure properties coming from the computational evaluation of electron density at ground and excited states in a series of organic photovoltaic materials.
Description of data collection	The data collected corresponds to structural and optoelectronic parameters, which are presented in tables (raw data) and graphs (secondary data). Additionally, all Cartesian coordinates are given at an electronic data base located at: http://dx.doi.org/10.17632/k9fts9zjd6.1 They can also be accessed at the Supplementary information of this article.
Data source location	http://dx.doi.org/10.17632/k9fts9zjd6.1 Data collected at Instituto de Energías Renovables, Universidad Nacional Autónoma de México, Priv. Xochicalco s/n Col. Centro, Temixco, Morelos, Mexico.
Data accessibility	Dataset published on Mendeley Data: (http://dx.doi.org/10.17632/k9fts9zjd6.1)
Related research article	C. Delesma, C. Amador-Bedolla, M. Robles, J. Muñiz, Photoisomerization and its effect in the opto-electronic properties of organic photovoltaic materials: A quantum chemistry study, Journal of Photochemistry and Photobiology A: Chemistry (2021) 409, 113155 [1]

Value of the Data

- The electronic structure data of the organic photovoltaic (OPV) series in this study may aid to select descriptors to tailor heterojunctions for solar cell devices.
- The data may be used as a tool for organic chemists and materials scientists to identify potential OPV materials, acting as an active layer in a solar cell device.
- The data obtained at ground and excited states for this series of OPV materials may be implemented as training sets for machine-learning and artificial intelligence methodologies to search novel OPV materials with enhanced photovoltaic properties.
- The structural data could be directly related to understand the mechanisms behind photoisomerization.

1. Data Description

The data collected corresponds to structural and optoelectronic parameters, which are presented in tables (raw data) and graphs (secondary data). Additionally, all Cartesian coordinates are given at an electronic data base located at: http://dx.doi.org/10.17632/k9fts9zjd6.1. They can also be accessed at the Supplementary information of this article. The data show the electronic structure properties of a series of 33 OPV materials with potential to be implemented as a component in a solar cell device. The data was obtained considering ground state geometries (lowest energy geometries), and also excited states at the Density Functional Theory (DFT) level by using the PBE/def2-TZVP methodology. Scheme 1 presents the molecular representations of the OPV materials under study. Fig. 1 depicts the molecular building blocks forming the OPV systems. Fig. 2 presents the molecular orbital (MO) representations of the most likely excitations in the title molecules; while Fig. 3 shows the most likely transitions at the first-excited state for

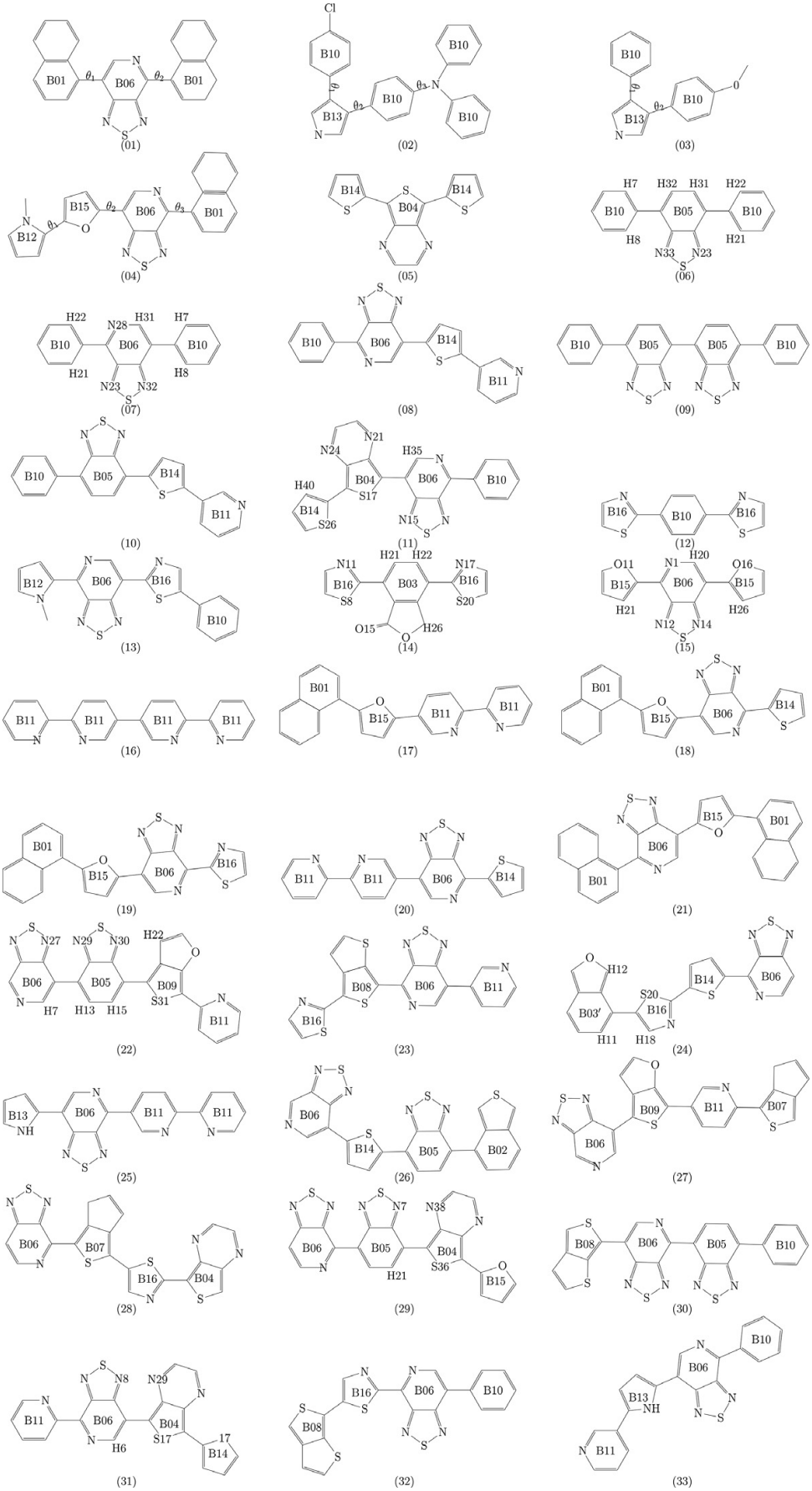

Scheme 1. Organic photovoltaic materials under study.

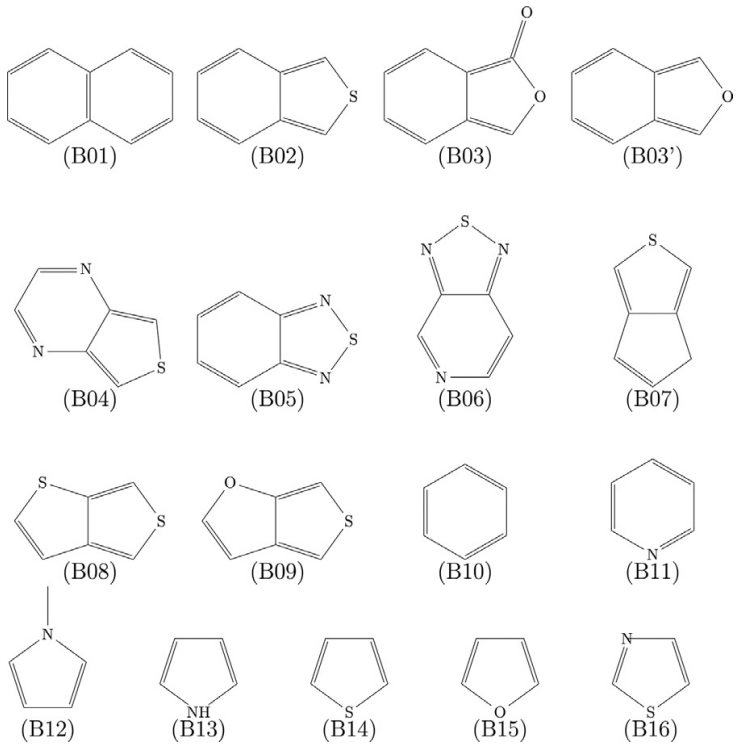

Fig. 1. Building blocks forming the OPV series.

Table 1
IUPAC nomenclature used for the building blocks.

Building Blocks	IUPAC Name
B01	Naphthalene
B02	Benzo(c)thiophene
B03	2-benzofuran-1(3H)-one
B03′	Benzo[c]furan
B04	Thieno[3,4-b]pyrazine
B05	Benzo[1,2,5]thiadiazole
B06	Thiadiazolo[3,4-c]pyridine
B08	Thieno[3,4-b]thiophen
B09	Thieno[3,4-b]furan
B10	Benzene
B11	Pyridine
B13	Pyrrole
B12	1-Methyl-1H-pyrrole
B14	Thiophene
B15	Furan
B16	Thiazole

selected OPV systems. Figs. 4 and 5 show the electron occupation with 2D plots of the frontier molecular orbitals in selected systems. Moreover, Table 1 presents the IUPAC nomenclature of the building blocks forming the OPV systems. Tables 2–34 show the Cartesian coordinates of the optimized molecular structure at ground and excited states. Table 35 shows the probabilities in the electronic transitions giving rise to the absorption spectra obtained via Time-Dependent DFT (TDDFT) calculations. Finally, in Table 36, the shifting in the absorption spectra maxima from the geometries at ground and excited state are presented. Additionally, the changes from ground to excited state in the average of dihedral angles, are also shown.

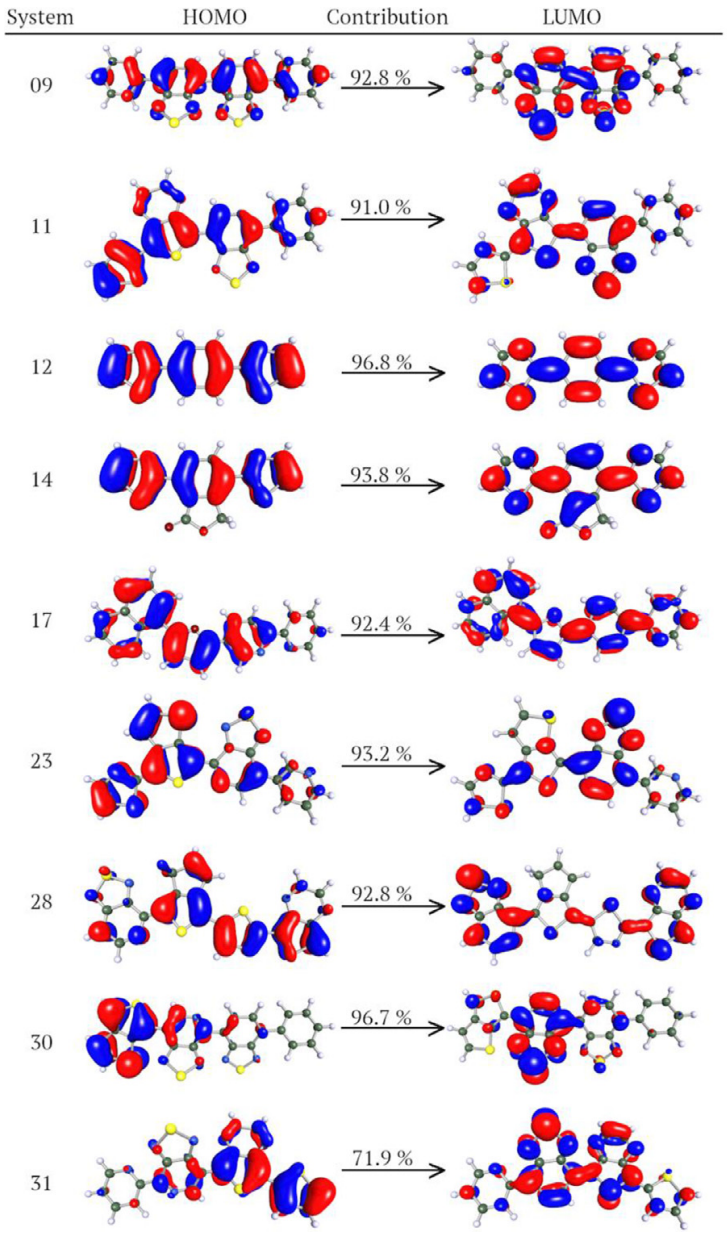

Fig. 2. Contributions with highest probability corresponding to one-electron HOMO-LUMO electronic transitions, in accordance to Table 35.

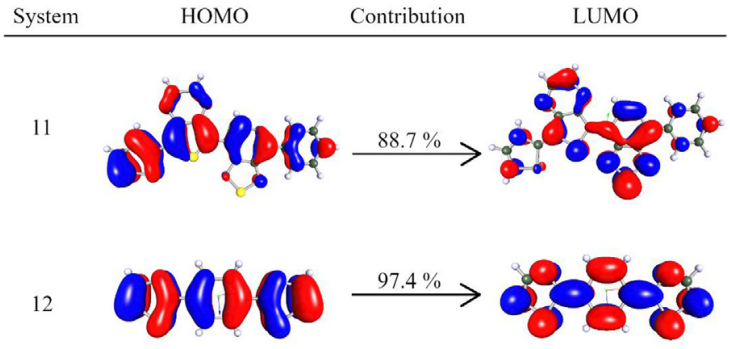

Fig. 3. Contributions with highest probability corresponding to one-electron HOMO-LUMO electronic transitions in excited state.

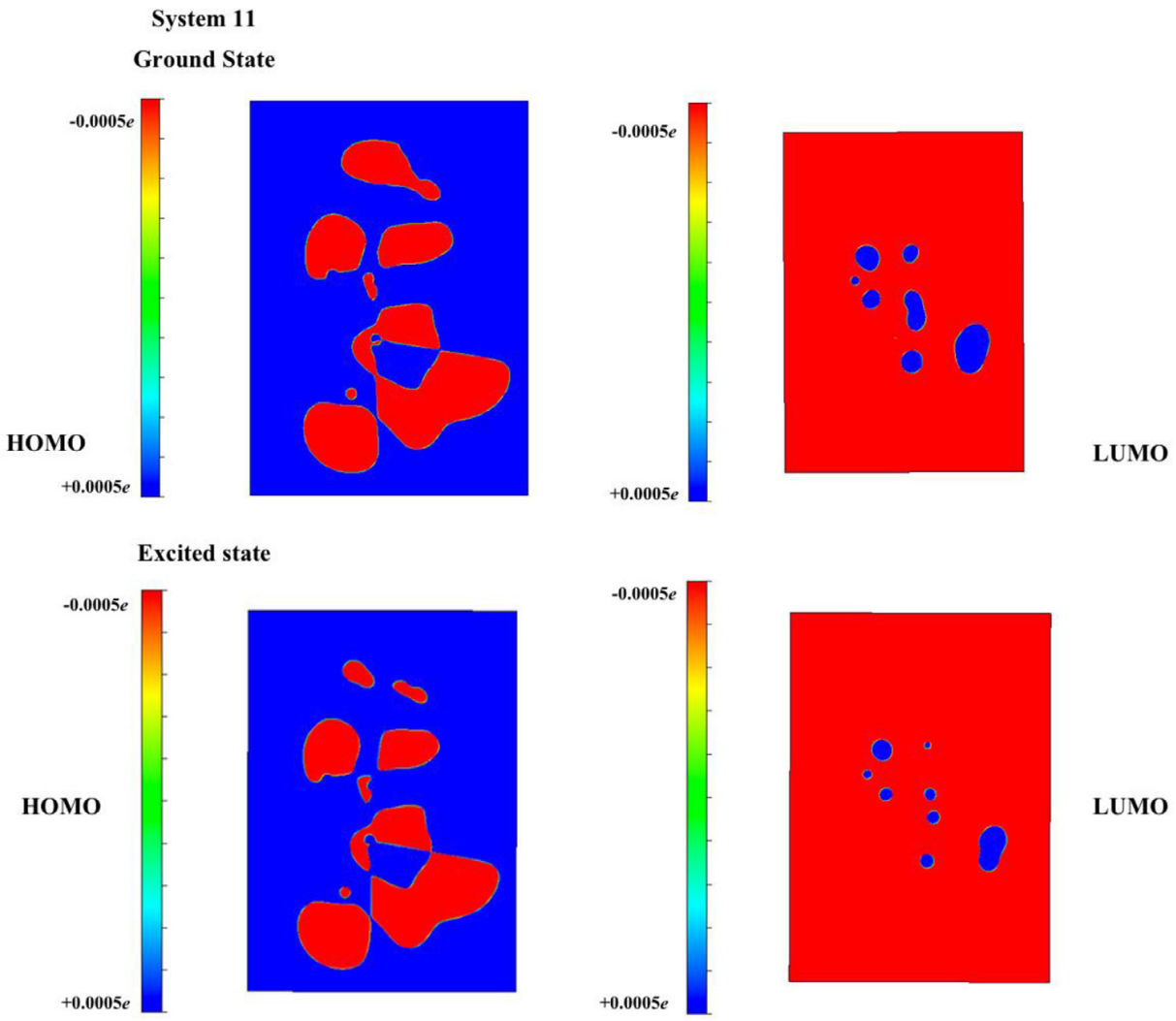

Fig. 4. 2D slices of the frontier molecular orbitals at the xy-plane of system 11. Note that both contributions (HOMO and LUMO) were evaluated at ground and excited state. The heat scale is given in electrons.

2. Experimental Design, Materials and Methods

All electronic structure data was found by implementing DFT calculations on a series of OPV systems. Such calculations were performed by considering ground and excited states of the molecular systems under study. The ground state geometries were disclosed at the Perdew-Becke-Ernzerhof (PBE) [2] functional level and using the basis set functions *def2*-TZVP [3,4]. Note that a benchmark study is a comparative process in which different functionals are tested. The theoretical results obtained with the functional that is in closer agreement with available experimental evidence, is used through the investigation. In this work, the comparative study was performed to compute the HOMO-LUMO gap with different functionals, such as B3LYP, PBE0, CAM-B3LYP, M06 and B97-3C. In this regard, the PBE functional appeared to show the smallest energy differences in band gap energy with respect to a set of OPV systems experimentally synthesized (see Table 1 in [1]).

The one-electron excitations were calculated using TDDFT with the same basis set *def2*-TZVP. Moreover, the geometries of the systems under study were also optimized at the first excited state. The electronic structure calculations were performed using the computational code TURBOMOLE version 7.3 [5]. The visualization of the molecular systems and isosurfaces mapping were performed using the TmoleX suite [6].

The analysis of dihedral angles at ground and excited states (θ_{Grd} and θ_{Exc}, respectively) was performed using a computational code developed in Python 2.7 programming language [7]. The

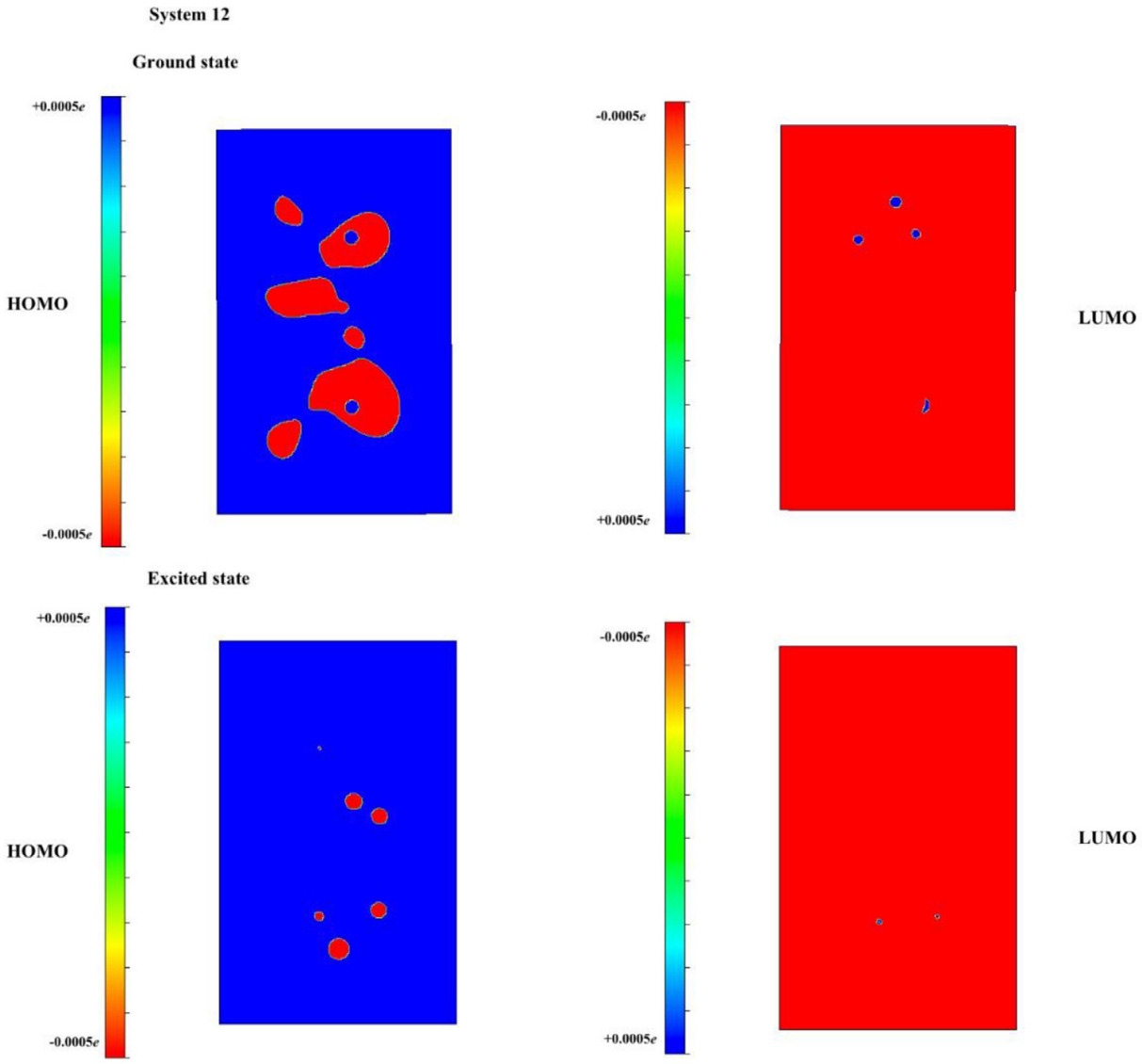

Fig. 5. 2D slices of the frontier molecular orbitals at the *xy*-plane of system 12. Note that both contributions (HOMO and LUMO) were evaluated at ground and excited state. The heat scale is given in electrons.

Table 2
Molecular system 01: Cartesian coordinates of the optimized molecular structure at ground and excited states.

	Ground state geometry				Excited state geometry			
No.	Atom	X	Y	Z	Atom	X	Y	Z
1	C	0.560523	-1.074601	5.941410	C	0.343144	-0.933834	5.752700
2	C	0.674049	-1.433892	4.579097	C	0.555458	-1.339888	4.426087
3	C	1.302771	-0.024565	6.436102	C	1.112522	0.090120	6.288260
4	C	1.502624	-0.725297	3.733043	C	1.506338	-0.698717	3.636816
5	C	2.175214	0.718491	5.596492	C	2.097101	0.753349	5.512031
6	C	2.263880	0.381179	4.199771	C	2.270959	0.386615	4.133326
7	C	2.970433	1.772219	6.114722	C	2.933350	1.741182	6.082378
8	C	3.144285	1.146340	3.359171	C	3.245559	1.081377	3.334270
9	C	3.837649	2.463597	5.296955	C	3.936689	2.332251	5.322305
10	C	3.923847	2.147290	3.926273	C	4.096619	2.000737	3.973999
11	H	-0.103427	-1.637706	6.599511	H	-0.405502	-1.435544	6.367350
12	H	0.106252	-2.282668	4.193796	H	-0.014995	-2.172393	4.011963

(*continued on next page*)

Table 2 (*continued*)

	Ground state geometry				Excited state geometry			
No.	Atom	X	Y	Z	Atom	X	Y	Z
13	H	1.239763	0.250288	7.491707	H	0.976935	0.393806	7.328829
14	H	1.588238	-1.028589	2.689609	H	1.694196	-1.054195	2.624339
15	H	2.888913	2.018343	7.175944	H	2.798234	2.009620	7.132302
16	H	4.455332	3.267159	5.701396	H	4.599699	3.071023	5.775362
17	H	4.602897	2.714882	3.289418	H	4.884595	2.467821	3.385532
18	C	0.628152	2.772841	-3.740263	C	0.528129	2.686247	-3.612962
19	C	0.582741	2.406631	-5.103974	C	0.400082	2.275187	-4.953433
20	C	1.435204	2.091452	-2.851397	C	1.428885	2.062290	-2.763014
21	C	1.365145	1.367135	-5.556179	C	1.199304	1.253190	-5.430616
22	C	2.248327	1.006638	-3.277069	C	2.247881	0.991677	-3.208681
23	C	2.215445	0.651168	-4.671780	C	2.140951	0.602152	-4.589460
24	C	3.132371	0.277039	-2.404006	C	3.209342	0.323068	-2.369182
25	C	3.037838	-0.400282	-5.151537	C	2.988873	-0.407834	-5.104101
26	C	3.935418	-0.727287	-2.935901	C	4.053913	-0.630580	-2.945654
27	C	3.884603	-1.074478	-4.299744	C	3.939407	-1.003028	-4.293357
28	H	0.016184	3.603364	-3.383355	H	-0.084007	3.507849	-3.236645
29	H	-0.065348	2.949706	-5.794102	H	-0.315448	2.768428	-5.613459
30	H	1.439798	2.373306	-1.800994	H	1.511083	2.385627	-1.728163
31	H	1.351643	1.078374	-6.609846	H	1.127475	0.934822	-6.473372
32	H	2.989194	-0.661300	-6.211393	H	2.892555	-0.693529	-6.154225
33	H	4.605752	-1.276552	-2.275971	H	4.813517	-1.096941	-2.320554
34	H	4.516032	-1.882890	-4.671695	H	4.604453	-1.768494	-4.696812
35	C	2.098079	0.918306	1.079391	C	2.181251	0.876120	1.085523
36	N	2.079176	0.736927	-0.265267	N	2.151528	0.740010	-0.243811
37	C	3.201137	0.531155	-0.947780	C	3.314789	0.575291	-0.912793
38	C	4.450457	0.542762	-0.231621	C	4.565907	0.600072	-0.230766
39	N	5.690454	0.408078	-0.753672	N	5.805273	0.456368	-0.794995
40	S	6.716300	0.514138	0.499747	S	6.875353	0.634472	0.465828
41	N	5.694090	0.734654	1.742749	N	5.821639	0.866564	1.745565
42	C	4.453326	0.741246	1.203337	C	4.586951	0.804059	1.189058
43	C	3.220803	0.917974	1.899884	C	3.342355	0.887413	1.881501
44	H	1.116467	1.089052	1.530674	H	1.209687	1.037794	1.563381

Table 3
Molecular system 02: Cartesian coordinates of the optimized molecular structure at ground and excited states.

	Ground state geometry				Excited state geometry			
No.	Atom	X	Y	Z	Atom	X	Y	Z
1	C	-2.169082	2.759604	-1.029992	C	-2.175851	2.853616	-0.992660
2	C	-1.382239	3.916827	-1.178860	C	-1.375446	4.038301	-1.014651
3	C	-1.542983	4.769441	-2.269165	C	-1.624609	5.073853	-1.904365
4	C	-2.508038	4.475540	-3.234228	C	-2.689134	4.978461	-2.813986
5	C	-3.306256	3.337320	-3.116414	C	-3.513253	3.836354	-2.813717
6	C	-3.128234	2.489864	-2.023625	C	-3.259210	2.807753	-1.920810
7	H	-0.637970	4.159438	-0.419411	H	-0.573635	4.155083	-0.284652
8	H	-0.929627	5.665072	-2.369482	H	-1.009849	5.975246	-1.887181
9	Cl	-2.715012	5.538954	-4.602165	Cl	-2.993006	6.278881	-3.951898
10	H	-4.050670	3.112861	-3.880564	H	-4.337001	3.762241	-3.524876
11	H	-3.735168	1.585395	-1.947607	H	-3.889389	1.915733	-1.955777
12	C	5.004728	0.129040	-1.546211	C	5.003545	-0.020714	-1.289090
13	C	5.303960	1.500494	-1.462652	C	5.462893	1.319887	-1.273972
14	C	6.227013	2.049095	-2.370824	C	6.574922	1.679254	-2.080346
15	C	6.838091	1.241782	-3.328700	C	7.226500	0.714682	-2.835277
16	C	6.533690	-0.119769	-3.412632	C	6.794424	-0.616220	-2.808343
17	C	5.610477	-0.666700	-2.517275	C	5.678668	-0.972080	-2.035057
18	H	4.292308	-0.306800	-0.844661	H	4.128931	-0.282371	-0.696160
19	N	4.683463	2.316034	-0.482652	N	4.776788	2.269671	-0.524618

(*continued on next page*)

Table 3 (*continued*)

	Ground state geometry				Excited state geometry			
No.	Atom	X	Y	Z	Atom	X	Y	Z
20	H	6.460845	3.113214	-2.319454	H	6.872826	2.724664	-2.150132
21	H	7.548889	1.687480	-4.027246	H	8.062262	1.005980	-3.472314
22	H	7.009645	-0.746873	-4.167650	H	7.307635	-1.369561	-3.406665
23	H	5.366620	-1.729793	-2.564177	H	5.332390	-2.005857	-2.022311
24	C	0.573319	1.723740	0.487193	C	0.616651	1.650065	0.378692
25	C	1.529266	2.002110	1.482126	C	1.644601	1.421030	1.346269
26	C	2.874328	2.184127	1.172948	C	2.985604	1.620739	1.062681
27	C	3.315845	2.118213	-0.159081	C	3.364812	2.050992	-0.221218
28	C	2.368635	1.853277	-1.163454	C	2.392127	2.284849	-1.203584
29	C	1.030112	1.651317	-0.842437	C	1.049132	2.097188	-0.910169
30	H	1.206965	2.081102	2.522598	H	1.364014	1.117496	2.356259
31	H	3.592689	2.392435	1.967087	H	3.741909	1.457255	1.833886
32	H	2.692172	1.796219	-2.203704	H	2.689195	2.607617	-2.204321
33	H	0.319772	1.433130	-1.641142	H	0.308326	2.266797	-1.688887
34	C	4.845089	4.571769	0.466351	C	4.614029	4.594762	0.156857
35	C	5.576930	5.557205	1.126824	C	5.213427	5.747266	0.640104
36	C	6.903698	5.328368	1.501950	C	6.576985	5.760227	0.968592
37	C	7.488788	4.092462	1.212801	C	7.341174	4.599128	0.814109
38	C	6.760912	3.095307	0.565596	C	6.762433	3.440626	0.311917
39	C	5.428072	3.324541	0.179924	C	5.391501	3.431101	-0.044752
40	H	3.813572	4.761085	0.166702	H	3.553682	4.569988	-0.088930
41	H	5.107354	6.520140	1.336883	H	4.612964	6.648273	0.767637
42	H	7.475000	6.104106	2.013499	H	7.034979	6.667141	1.364606
43	H	8.521170	3.893743	1.507034	H	8.390827	4.590386	1.109959
44	H	7.220961	2.129424	0.353211	H	7.342764	2.520780	0.245294
45	N	-2.613128	0.634567	1.905102	N	-2.512184	0.245708	1.529829
46	C	-1.243965	0.709542	1.923417	C	-1.168819	0.432538	1.653181
47	C	-0.833289	1.475907	0.839471	C	-0.765964	1.369519	0.678816
48	C	-2.031579	1.879589	0.140368	C	-1.981357	1.794847	-0.020941
49	C	-3.105009	1.333851	0.834440	C	-3.025136	1.041326	0.534388
50	H	-0.656743	0.171953	2.660689	H	-0.578750	-0.183631	2.323057
51	H	-4.172020	1.448516	0.673725	H	-4.094421	1.103668	0.364375
52	H	-3.177024	0.138462	2.583405	H	-3.059564	-0.386809	2.099028

Table 4
Molecular system 03: Cartesian coordinates of the optimized molecular structure at ground and excited states.

	Ground state geometry				Excited state geometry			
No.	Atom	X	Y	Z	Atom	X	Y	Z
1	C	-5.094181	2.836552	3.841470	C	-5.372523	2.184640	3.734550
2	C	-4.375491	1.908137	4.609780	C	-4.319752	1.833706	4.635884
3	C	-3.399226	1.137982	3.945678	C	-2.985131	1.819854	4.120681
4	C	-3.149788	1.291196	2.587533	C	-2.715545	2.141042	2.812896
5	C	-3.882348	2.223348	1.836885	C	-3.777397	2.498768	1.943726
6	C	-4.861610	2.997842	2.473349	C	-5.106914	2.513813	2.421662
7	H	-5.849958	3.458100	4.323984	H	-6.399107	2.163934	4.101788
8	H	-2.838759	0.389360	4.509703	H	-2.154072	1.552138	4.772606
9	H	-2.396224	0.686546	2.080486	H	-1.699929	2.130917	2.416814
10	O	-3.571917	2.298086	0.505087	O	-3.413367	2.800413	0.686008
11	H	-5.442999	3.733839	1.919046	H	-5.933701	2.775978	1.763441
12	C	-9.894838	1.875509	5.390061	C	-9.892818	2.293565	5.357399
13	C	-9.520414	2.611354	6.516767	C	-9.236757	3.243228	6.231890
14	C	-8.196779	2.596015	6.958119	C	-7.923735	2.955640	6.656448
15	C	-7.216244	1.836668	6.291994	C	-7.243080	1.814165	6.248517

(*continued on next page*)

Table 4 (*continued*)

	Ground state geometry				Excited state geometry			
No.	Atom	X	Y	Z	Atom	X	Y	Z
16	C	-7.610455	1.099073	5.159713	C	-7.906234	0.855112	5.370758
17	C	-8.931663	1.121227	4.714086	C	-9.231009	1.141557	4.968200
18	H	-10.928543	1.890722	5.040207	H	-10.912017	2.478609	5.013222
19	H	-10.261265	3.210199	7.050523	H	-9.738928	4.151971	6.558770
20	H	-7.905524	3.195500	7.823430	H	-7.408970	3.665680	7.312841
21	H	-6.870127	0.494841	4.633747	H	-7.442507	-0.102540	5.136248
22	H	-9.213263	0.537185	3.835570	H	-9.750969	0.420245	4.329461
23	N	-4.138991	1.590636	8.243747	N	-4.156826	1.101877	8.158504
24	C	-3.574704	1.638795	6.994021	C	-3.572333	1.242327	6.960510
25	C	-4.593969	1.763236	6.058352	C	-4.592718	1.535503	6.007991
26	C	-5.834734	1.788868	6.797916	C	-5.865119	1.552429	6.729758
27	C	-5.502531	1.682719	8.143389	C	-5.543784	1.273296	8.032369
28	H	-2.498125	1.639688	6.858102	H	-2.498328	1.143582	6.843251
29	H	-6.142274	1.605787	9.016546	H	-6.195372	1.182644	8.894974
30	C	-4.304818	3.224433	-0.288514	C	-4.428355	3.174251	-0.262598
31	H	-3.913670	3.122489	-1.307410	H	-3.893360	3.372472	-1.196263
32	H	-4.155934	4.261616	0.056990	H	-4.954589	4.081002	0.067576
33	H	-5.383925	2.994808	-0.287016	H	-5.145331	2.354011	-0.408783
34	H	-3.625070	1.497436	9.110381	H	-3.669785	0.893965	9.022622

Table 5
Molecular system 04: Cartesian coordinates of the optimized molecular structure at ground and excited states.

	Ground state geometry				Excited state geometry			
No.	Atom	X	Y	Z	Atom	X	Y	Z
1	N	-0.696245	2.212344	1.475705	N	-0.857081	0.159008	1.159561
2	N	-0.592818	2.285736	-1.037154	N	-0.928458	0.425566	-1.392946
3	C	-1.908008	2.101909	0.889521	C	-1.962162	0.762560	0.682870
4	C	-1.849438	2.136846	-0.560531	C	-2.022496	0.924901	-0.753014
5	C	-3.179485	1.976505	1.539047	C	-3.053961	1.249029	1.444146
6	C	-3.057190	2.049343	-1.335469	C	-3.147883	1.575662	-1.337967
7	C	-4.269196	1.933860	0.660074	C	-4.112280	1.864011	0.760127
8	S	0.375715	2.356498	0.263353	S	0.059296	-0.186480	-0.205508
9	N	-4.219078	1.968337	-0.684790	N	-4.167567	2.031827	-0.559018
10	H	-5.278426	1.857606	1.074951	H	-4.972727	2.240872	1.325320
11	O	-2.279886	1.978985	3.788963	O	-2.531866	2.080191	3.667221
12	C	-3.376312	1.901952	2.963338	C	-3.077132	1.093506	2.898457
13	C	-4.510693	1.753679	3.742548	C	-3.565781	0.089130	3.729730
14	C	-4.092089	1.740165	5.092580	C	-3.304756	0.468868	5.050623
15	C	-2.710189	1.880767	5.087039	C	-2.657378	1.711275	4.987157
16	H	-5.530987	1.660538	3.384399	H	-4.043694	-0.819673	3.382623
17	H	-4.735234	1.637487	5.958224	H	-3.550823	-0.088829	5.946991
18	C	-0.639504	1.959863	8.066942	C	-1.529825	3.572293	7.848264
19	C	0.346807	2.106092	7.103782	C	-1.137687	4.456715	6.828347
20	C	-0.291911	2.097222	5.846738	C	-1.505695	3.879640	5.622989
21	C	-1.665755	1.944876	6.068334	C	-2.130538	2.630579	5.915820
22	N	-1.858366	1.862320	7.441800	N	-2.125259	2.477250	7.298854
23	H	1.410269	2.207825	7.295809	H	-0.638399	5.407584	6.979259
24	H	0.165577	2.189246	4.866804	H	-1.361652	4.266131	4.620380
25	C	-3.118491	1.699075	8.139161	C	-2.646750	1.352232	8.060915
26	H	-0.575939	1.916837	9.149846	H	-1.419390	3.655404	8.925243
27	C	-5.895955	4.267047	-3.875577	C	-4.640121	5.236974	-3.296139
28	C	-5.856903	4.109600	-5.279011	C	-4.808010	5.271638	-4.699110
29	C	-5.006188	3.592508	-3.063672	C	-4.158970	4.104236	-2.671287

(*continued on next page*)

Table 5 (*continued*)

	Ground state geometry				Excited state geometry			
No.	Atom	X	Y	Z	Atom	X	Y	Z
30	C	-4.908148	3.287165	-5.845448	C	-4.469202	4.168347	-5.450960
31	C	-4.021203	2.725444	-3.608915	C	-3.811708	2.939169	-3.410062
32	C	-3.968826	2.587982	-5.041083	C	-3.957591	2.990332	-4.842039
33	C	-3.048899	2.018800	-2.813320	C	-3.280812	1.742505	-2.805229
34	C	-2.974248	1.769826	-5.635610	C	-3.573956	1.875280	-5.630841
35	C	-2.079644	1.252315	-3.454431	C	-2.892087	0.694974	-3.634333
36	C	-2.043670	1.119102	-4.855706	C	-3.042769	0.753456	-5.034265
37	H	-6.639020	4.928971	-3.426662	H	-4.893757	6.115941	-2.699569
38	H	-6.571047	4.643140	-5.908869	H	-5.196529	6.170414	-5.182478
39	H	-5.064497	3.709787	-1.984029	H	-4.053966	4.080822	-1.589019
40	H	-4.854903	3.164355	-6.929914	H	-4.579078	4.182379	-6.538502
41	H	-2.957765	1.671424	-6.723646	H	-3.696913	1.930630	-6.715351
42	H	-1.341777	0.721298	-2.854519	H	-2.462158	-0.197540	-3.182048
43	H	-1.278586	0.491177	-5.315253	H	-2.737739	-0.101925	-5.640531
44	H	-3.797046	2.540301	7.934599	H	-3.727167	1.241551	7.898086
45	H	-3.613761	0.760831	7.848902	H	-2.133601	0.423620	7.777878
46	H	-2.917947	1.667864	9.216145	H	-2.468829	1.542791	9.124351

Table 6
Molecular system 05: Cartesian coordinates of the optimized molecular structure at ground and excited states.

	Ground state geometry				Excited state geometry			
No.	Atom	X	Y	Z	Atom	X	Y	Z
1	S	-2.454968	0.508086	3.565883	S	-2.373756	0.521205	3.611993
2	C	-1.158159	0.459270	2.395345	C	-1.115511	0.458601	2.382337
3	C	-1.680843	0.428806	1.105201	C	-1.689212	0.423529	1.098296
4	C	-3.092921	0.444171	1.069671	C	-3.089180	0.446824	1.117522
5	C	-3.648713	0.486424	2.329053	C	-3.594452	0.499535	2.409530
6	H	-1.052996	0.396748	0.214606	H	-1.087966	0.382499	0.190341
7	H	-3.679126	0.425133	0.152090	H	-3.714837	0.426218	0.226470
8	H	-4.701308	0.506812	2.598397	H	-4.640396	0.526545	2.706283
9	S	5.473524	0.396023	3.536967	S	5.392929	0.408205	3.583746
10	C	6.657046	0.338117	2.291417	C	6.603693	0.351336	2.372372
11	C	6.090984	0.309308	1.036198	C	6.087657	0.313611	1.084073
12	C	4.679292	0.334180	1.082072	C	4.687479	0.331038	1.075084
13	C	4.167203	0.382072	2.375964	C	4.124443	0.382432	2.363307
14	H	7.711782	0.328908	2.553027	H	7.652136	0.347858	2.661485
15	H	6.669648	0.271756	0.114385	H	6.705928	0.274974	0.188464
16	H	4.044201	0.318031	0.196159	H	4.078655	0.307761	0.171539
17	C	0.806204	0.570974	6.338334	C	0.823234	0.563387	6.291602
18	C	2.235247	0.550984	6.333222	C	2.217771	0.542912	6.286609
19	N	2.950092	0.501331	5.224973	N	2.983587	0.492977	5.161504
20	C	2.233801	0.469934	4.070173	C	2.212567	0.465152	4.031629
21	C	2.791232	0.416157	2.781249	C	2.758502	0.412522	2.716307
22	S	1.501202	0.392590	1.621882	S	1.500862	0.389024	1.509498
23	C	0.221169	0.453115	2.790468	C	0.253246	0.448967	2.725371
24	C	0.789189	0.490512	4.075356	C	0.809981	0.485572	4.036680
25	N	0.082407	0.541724	5.235207	N	0.048247	0.535903	5.172044
26	H	0.267614	0.612184	7.290452	H	0.292525	0.604223	7.246960
27	H	2.781616	0.577267	7.281434	H	2.756286	0.567810	7.238140

Table 7
Molecular system 06: Cartesian coordinates of the optimized molecular structure at ground and excited states.

	Ground state geometry				Excited state geometry			
No.	Atom	X	Y	Z	Atom	X	Y	Z
1	C	-1.174118	2.718694	-1.640288	C	-1.224941	2.595801	-1.586525
2	C	0.022774	2.396161	-0.972029	C	0.023663	2.403593	-0.928447
3	C	1.138020	2.030072	-1.748857	C	1.169024	2.197475	-1.747154
4	C	1.050269	1.974022	-3.139179	C	1.058565	2.162051	-3.130458
5	C	-0.145829	2.290895	-3.787408	C	-0.181756	2.351545	-3.753114
6	C	-1.257970	2.667425	-3.030549	C	-1.322484	2.577594	-2.968813
7	H	-2.040846	3.041320	-1.060183	H	-2.118726	2.801927	-0.998422
8	H	2.076909	1.783143	-1.255311	H	2.134590	2.073719	-1.261337
9	H	1.925309	1.678773	-3.721118	H	1.949828	1.988269	-3.735784
10	H	-0.209225	2.251354	-4.876183	H	-0.260652	2.330323	-4.841492
11	H	-2.193860	2.932798	-3.525703	H	-2.289195	2.745356	-3.446423
12	C	-1.230568	2.702608	6.991557	C	-1.296365	2.608930	6.930616
13	C	-0.115588	2.326978	7.744668	C	-0.151581	2.387434	7.710293
14	C	1.076145	2.002793	7.092007	C	1.085453	2.194050	7.082313
15	C	1.156735	2.050659	5.700947	C	1.188678	2.221068	5.698258
16	C	0.038449	2.415535	4.927985	C	0.039045	2.422242	4.884320
17	C	-1.153898	2.745671	5.600586	C	-1.206065	2.618680	5.547752
18	H	-2.163077	2.973458	7.490113	H	-2.260524	2.779843	7.412250
19	H	-0.173312	2.293987	8.833976	H	-0.224797	2.372724	8.799174
20	H	1.953290	1.708130	7.671061	H	1.979861	2.023863	7.684011
21	H	2.092167	1.797801	5.203824	H	2.151681	2.094307	5.208151
22	H	-2.022662	3.067496	5.023081	H	-2.102894	2.821334	4.963092
23	N	2.386288	3.312112	3.224868	N	2.536115	2.944381	3.251434
24	C	1.229062	2.847883	2.701676	C	1.325661	2.654704	2.688413
25	C	1.225205	2.843132	1.245103	C	1.321866	2.650057	1.259068
26	C	0.081880	2.429746	3.451566	C	0.112060	2.420414	3.428005
27	C	0.074129	2.419861	0.504015	C	0.104377	2.411001	0.527442
28	C	-1.009014	2.033118	2.688955	C	-1.064181	2.164461	2.671839
29	S	3.338223	3.686698	1.965195	S	3.575650	3.164020	1.966073
30	C	-1.012699	2.028331	1.275070	C	-1.067846	2.160011	1.291462
31	H	-1.900032	1.669203	3.203759	H	-1.985826	1.907773	3.192135
32	H	-1.906483	1.661093	0.767480	H	-1.992286	1.900175	0.777727
33	N	2.379621	3.304203	0.712912	N	2.529291	2.936028	0.687735

Table 8
Molecular system 07: Cartesian coordinates of the optimized molecular structure at ground and excited states.

	Ground state geometry				Excited state geometry			
No.	Atom	X	Y	Z	Atom	X	Y	Z
1	C	-1.110306	2.940628	-1.541458	C	-1.203742	2.768300	-1.471230
2	C	0.051110	2.417435	-0.939649	C	0.048513	2.418394	-0.885375
3	C	1.048039	1.878154	-1.775011	C	1.125045	2.110200	-1.765735
4	C	0.878207	1.849811	-3.158269	C	0.946274	2.134813	-3.140806
5	C	-0.282650	2.364742	-3.740372	C	-0.296268	2.477503	-3.692614
6	C	-1.275278	2.913836	-2.925034	C	-1.367914	2.802605	-2.845755
7	H	-1.878595	3.399435	-0.916434	H	-2.039543	3.049098	-0.831025
8	H	1.957791	1.474447	-1.332552	H	2.093558	1.869502	-1.331528
9	H	1.660141	1.420049	-3.786959	H	1.783037	1.890113	-3.796993
10	H	-0.410058	2.345061	-4.824024	H	-0.429646	2.498547	-4.775579
11	H	-2.179482	3.333848	-3.369246	H	-2.331533	3.088077	-3.270443
12	C	-1.339269	2.100764	6.841143	C	-1.371458	2.238161	6.787824
13	C	-0.258802	2.361302	7.690633	C	-0.289313	2.531819	7.628592
14	C	0.993202	2.640618	7.140641	C	0.984787	2.732848	7.079664
15	C	1.172496	2.661041	5.757352	C	1.186419	2.646652	5.707784
16	C	0.092518	2.400050	4.890770	C	0.101032	2.357420	4.842124
17	C	-1.167238	2.119557	5.461486	C	-1.182693	2.148654	5.416993

(*continued on next page*)

Table 8 (*continued*)

	Ground state geometry				Excited state geometry			
No.	Atom	X	Y	Z	Atom	X	Y	Z
18	H	-2.323177	1.880133	7.259446	H	-2.362884	2.070552	7.212226
19	H	-0.393668	2.346103	8.773754	H	-0.436192	2.595170	8.708603
20	H	1.843251	2.846809	7.793590	H	1.828762	2.957233	7.734235
21	H	2.154793	2.881007	5.345431	H	2.174204	2.796305	5.274761
22	H	-2.002706	1.917993	4.791683	H	-2.007807	1.910060	4.747321
23	N	2.676214	2.815120	3.182922	N	2.727955	2.492382	3.231763
24	C	1.437804	2.609812	2.680545	C	1.478674	2.385639	2.673075
25	C	1.413842	2.611876	1.227898	C	1.467169	2.437000	1.246757
26	C	0.211998	2.411336	3.415099	C	0.241434	2.285412	3.385975
27	C	0.185323	2.418611	0.528080	C	0.206449	2.380491	0.558667
28	N	-0.903754	2.221890	2.714290	N	-0.930458	2.138268	2.707456
29	S	3.665623	2.993678	1.910456	S	3.767438	2.626767	1.939947
30	C	-0.910113	2.219463	1.363823	C	-0.937716	2.200682	1.387213
31	H	-1.886543	2.019661	0.912475	H	-1.909816	2.026923	0.918346
32	N	2.628800	2.827954	0.673890	N	2.685750	2.576634	0.664160

Table 9
Molecular system 08: Cartesian coordinates of the optimized molecular structure at ground and excited states.

	Ground state geometry				Excited state geometry			
No.	Atom	X	Y	Z	Atom	X	Y	Z
1	C	1.371568	2.454372	-3.924816	C	1.370589	2.461491	-3.907493
2	C	-0.020247	2.471238	-4.131243	C	-0.030626	2.469425	-4.092932
3	C	-0.452951	2.481929	-5.476582	C	-0.487922	2.480732	-5.438744
4	N	0.360673	2.473785	-6.534105	N	0.308588	2.482243	-6.504514
5	C	1.682897	2.455814	-6.303313	C	1.635795	2.473310	-6.291838
6	C	2.229899	2.446900	-5.018512	C	2.206578	2.463911	-5.013644
7	H	1.777725	2.444651	-2.910797	H	1.791261	2.452074	-2.899833
8	H	-1.522403	2.498777	-5.705189	H	-1.560758	2.490779	-5.649160
9	H	2.328228	2.448672	-7.186426	H	2.266996	2.473486	-7.184727
10	H	3.311881	2.433231	-4.878767	H	3.290868	2.457363	-4.895250
11	C	-1.383859	2.519034	7.102656	C	-1.395338	2.512595	7.072919
12	C	-2.569567	2.494943	7.844775	C	-2.593830	2.507056	7.797766
13	C	-3.795189	2.471562	7.177048	C	-3.815540	2.494512	7.116517
14	C	-3.844695	2.471506	5.783207	C	-3.851269	2.487480	5.725552
15	C	-2.657394	2.495255	5.023298	C	-2.648997	2.492871	4.978387
16	C	-1.425673	2.518811	5.713035	C	-1.419753	2.505597	5.685175
17	H	-0.419267	2.537468	7.613373	H	-0.438806	2.522422	7.598643
18	H	-2.536614	2.494980	8.935815	H	-2.574405	2.512502	8.889443
19	H	-4.726881	2.452581	7.745455	H	-4.751881	2.490158	7.677366
20	H	-4.808372	2.452677	5.279420	H	-4.800454	2.477789	5.192772
21	H	-0.507191	2.536695	5.127200	H	-0.497217	2.509707	5.106330
22	N	-5.098550	2.460101	3.074617	N	-5.089824	2.467021	3.084697
23	C	-3.801627	2.476417	2.693528	C	-3.786820	2.473773	2.665572
24	C	-3.644080	2.474284	1.248861	C	-3.631283	2.467940	1.249301
25	C	-2.637889	2.494564	3.545383	C	-2.619141	2.485834	3.510076
26	C	-2.335241	2.489595	0.667806	C	-2.312568	2.474348	0.706311
27	N	-1.443604	2.511947	2.951657	N	-1.378800	2.491486	2.960390
28	S	-5.983055	2.442961	1.716623	S	-5.995414	2.454052	1.693009
29	C	-1.306828	2.509584	1.614945	C	-1.255321	2.485892	1.637384
30	H	-0.268826	2.524282	1.265140	H	-0.222628	2.491017	1.266193
31	N	-4.819073	2.454638	0.584394	N	-4.790645	2.456552	0.531573
32	C	-0.978947	2.476054	-3.032667	C	-0.961339	2.467845	-2.991093

(*continued on next page*)

Table 9 (*continued*)

	Ground state geometry				Excited state geometry			
No.	Atom	X	Y	Z	Atom	X	Y	Z
33	S	-0.449544	2.490854	-1.375476	S	-0.410242	2.478492	-1.335899
34	C	-2.082176	2.482754	-0.758115	C	-2.043817	2.469775	-0.711330
35	C	-2.983367	2.471112	-1.817220	C	-2.967540	2.458975	-1.772111
36	C	-2.365928	2.467205	-3.082458	C	-2.364364	2.458252	-3.029162
37	H	-4.058976	2.464087	-1.659381	H	-4.036998	2.451996	-1.570065
38	H	-2.927531	2.454688	-4.015124	H	-2.929811	2.449255	-3.959533

Table 10
Molecular system 09: Cartesian coordinates of the optimized molecular structure at ground and excited states.

	Ground state geometry				Excited state geometry			
No.	Atom	X	Y	Z	Atom	X	Y	Z
1	C	1.119050	3.254786	16.711506	C	1.103203	3.032482	16.669131
2	C	2.256122	2.998577	17.481593	C	2.265553	2.863184	17.433841
3	C	3.491597	2.837736	16.849981	C	3.516006	2.850113	16.803105
4	C	3.594120	2.930110	15.462610	C	3.611967	3.006853	15.427216
5	C	2.455501	3.175840	14.672657	C	2.447539	3.168989	14.631747
6	C	1.218153	3.341574	15.324057	C	1.189985	3.175870	15.292522
7	H	0.150575	3.397689	17.194299	H	0.127645	3.059845	17.156457
8	H	2.180579	2.931394	18.568249	H	2.195796	2.742947	18.515982
9	H	4.386051	2.637259	17.442626	H	4.422513	2.710209	17.393609
10	H	4.563089	2.804830	14.981353	H	4.586320	2.990985	14.943949
11	H	0.328570	3.570216	14.734005	H	0.278800	3.339553	14.716767
12	N	4.706141	4.418693	13.053616	N	4.753004	4.386218	13.054925
13	C	3.635895	3.811920	12.491871	C	3.664658	3.831949	12.483686
14	C	3.667347	3.842288	11.038915	C	3.686293	3.898616	11.035108
15	C	2.529953	3.234134	13.198480	C	2.522480	3.305266	13.183707
16	C	2.603165	3.284737	10.264413	C	2.602775	3.398005	10.233408
17	C	1.509410	2.733527	12.400262	C	1.445117	2.920072	12.357140
18	S	5.617118	4.959339	11.823022	S	5.673382	4.941804	11.825708
19	C	1.541464	2.760227	10.985383	C	1.480782	2.961545	10.961813
20	H	0.710744	2.309803	10.438393	H	0.626823	2.575040	10.404656
21	N	4.746655	4.482333	10.540057	N	4.769971	4.530100	10.549193
22	H	0.654348	2.257998	12.883761	H	0.555315	2.499923	12.827629
23	S	5.652135	1.653152	7.250981	S	5.795595	1.831354	7.300712
24	C	3.683445	2.745472	8.022457	C	3.748352	2.857305	8.044526
25	H	0.660841	4.288889	6.158884	H	0.611966	4.230927	6.163556
26	H	2.226281	3.624425	0.483346	H	2.199297	3.500754	0.516325
27	C	3.659668	2.773432	6.569258	C	3.718089	2.851162	6.604159
28	C	3.527239	3.734306	2.208278	C	3.530605	3.491918	2.224839
29	C	2.550307	3.335964	5.855615	C	2.570116	3.340571	5.894363
30	N	4.741019	2.180065	6.014412	N	4.823572	2.299234	6.033610
31	C	1.250731	3.212051	3.723340	C	1.226984	3.332019	3.779077
32	C	3.623347	3.645895	3.596366	C	3.638325	3.433494	3.611682
33	C	1.543475	3.799906	8.062706	C	1.494773	3.783987	8.055380
34	N	4.768374	2.120585	8.528224	N	4.853739	2.289721	8.597713
35	H	0.360209	2.976147	4.309117	H	0.317192	3.234644	4.372747
36	H	4.588557	3.781392	4.082362	H	4.616565	3.435103	4.088042
37	C	2.483014	3.390824	4.380974	C	2.484995	3.363746	4.428365
38	C	1.519187	3.824773	6.647645	C	1.478083	3.804961	6.668280
39	C	1.158067	3.295209	2.335244	C	1.125515	3.375077	2.392989
40	C	2.296703	3.560440	1.570532	C	2.278194	3.463109	1.604421
41	H	0.193475	3.142400	1.847735	H	0.141642	3.332813	1.921604
42	H	4.422891	3.941977	1.619935	H	4.437131	3.556803	1.619814
43	C	2.607611	3.289669	8.790309	C	2.629834	3.349790	8.775482
44	H	0.703796	4.239914	8.604480	H	0.639528	4.183838	8.604319

Table 11
Molecular system 10: Cartesian coordinates of the optimized molecular structure at ground and excited states.

	Ground state geometry				Excited state geometry			
No.	Atom	X	Y	Z	Atom	X	Y	Z
1	C	1.344245	2.465934	-4.080816	C	1.339113	2.635824	-4.025443
2	C	-0.053473	2.558262	-4.208464	C	-0.062018	2.516324	-4.167806
3	C	-0.552765	2.801812	-5.507396	C	-0.557536	2.468564	-5.498932
4	N	0.206136	2.922577	-6.598628	N	0.204210	2.524063	-6.588671
5	C	1.535951	2.822353	-6.445898	C	1.532657	2.634829	-6.416733
6	C	2.146184	2.605018	-5.208577	C	2.138875	2.696317	-5.156606
7	H	1.793016	2.268166	-3.104729	H	1.788173	2.676344	-3.030894
8	H	-1.630081	2.919868	-5.659047	H	-1.633121	2.385474	-5.676776
9	H	2.136119	2.922905	-7.354898	H	2.135079	2.675271	-7.328421
10	H	3.232449	2.534419	-5.133989	H	3.222520	2.787152	-5.071194
11	C	-1.693255	2.146677	7.271492	C	-1.627714	2.185484	7.220952
12	C	-2.798646	2.740761	7.885472	C	-2.785149	2.666957	7.843454
13	C	-3.832186	3.248807	7.094835	C	-3.869952	3.074789	7.060695
14	C	-3.765889	3.166790	5.704689	C	-3.808948	3.002847	5.672711
15	C	-2.653498	2.580789	5.070826	C	-2.639792	2.539667	5.022950
16	C	-1.621747	2.068811	5.882060	C	-1.552989	2.130172	5.834492
17	H	-0.886276	1.731719	7.878138	H	-0.783194	1.845330	7.822865
18	H	-2.856944	2.801393	8.973556	H	-2.842799	2.715220	8.932385
19	H	-4.699969	3.715775	7.564353	H	-4.776885	3.449068	7.538885
20	H	-4.578921	3.565655	5.099821	H	-4.661692	3.299736	5.065969
21	H	-0.767258	1.576018	5.414460	H	-0.655027	1.724595	5.367100
22	N	-4.925749	2.085026	3.121064	N	-4.955682	2.203220	3.109657
23	C	-3.647776	2.284671	2.728170	C	-3.666491	2.348952	2.688125
24	C	-3.482400	2.212287	1.282180	C	-3.498228	2.306239	1.270903
25	C	-2.535822	2.516200	3.601294	C	-2.529515	2.496774	3.562436
26	C	-2.192268	2.382633	0.669878	C	-2.194664	2.434772	0.698227
27	C	-1.310291	2.668856	2.962090	C	-1.258307	2.611318	2.957065
28	S	-5.791524	1.845679	1.771310	S	-5.852881	2.034866	1.720133
29	C	-1.145780	2.604263	1.564263	C	-1.101069	2.590134	1.579427
30	H	-0.137031	2.742122	1.168714	H	-0.096465	2.708818	1.166664
31	N	-4.640136	1.969244	0.632363	N	-4.655230	2.127470	0.559643
32	C	-0.960429	2.418871	-3.075560	C	-0.956178	2.449380	-3.038123
33	S	-0.413787	2.674871	-1.445782	S	-0.368019	2.571858	-1.402458
34	C	-1.986315	2.335015	-0.767030	C	-1.975704	2.409231	-0.726989
35	C	-2.883026	2.046626	-1.789605	C	-2.919142	2.264056	-1.762443
36	C	-2.308438	2.094030	-3.075598	C	-2.351843	2.288633	-3.034452
37	H	-3.923312	1.802724	-1.590636	H	-3.975420	2.148277	-1.526871
38	H	-2.861061	1.868000	-3.986667	H	-2.936440	2.188958	-3.947690
39	H	-0.427399	2.874552	3.569697	H	-0.381883	2.773198	3.583168

Table 12
Molecular system 11: Cartesian coordinates of the optimized molecular structure at ground and excited states.

	Ground state geometry				Excited state geometry			
No.	Atom	X	Y	Z	Atom	X	Y	Z
1	C	-6.279332	2.275816	-0.036380	C	-6.257582	2.255336	-0.071315
2	C	-7.235954	1.305518	-0.354061	C	-7.198067	1.261329	-0.368502
3	C	-6.821227	0.005139	-0.647397	C	-6.767474	-0.042578	-0.632384
4	C	-5.467824	-0.330669	-0.624771	C	-5.412631	-0.360614	-0.601850
5	C	-4.493449	0.637523	-0.306077	C	-4.450940	0.632396	-0.303559
6	C	-4.928368	1.948502	-0.012810	C	-4.903929	1.948109	-0.039011
7	C	-3.045680	0.348410	-0.265666	C	-3.007964	0.359736	-0.256878
8	N	-2.226454	1.364545	0.014037	N	-2.221981	1.417631	0.031202
9	C	-0.889314	1.232295	0.081866	C	-0.892333	1.280456	0.097187

(*continued on next page*)

Table 12 (*continued*)

	Ground state geometry				Excited state geometry			
No.	Atom	X	Y	Z	Atom	X	Y	Z
10	C	-0.169008	0.042319	-0.124129	C	-0.191188	0.074294	-0.116129
11	C	-1.003951	-1.080915	-0.426378	C	-0.994028	-1.058008	-0.419343
12	C	-2.445311	-0.940111	-0.500404	C	-2.407411	-0.933876	-0.494001
13	N	-3.064885	-2.105544	-0.793944	N	-3.049787	-2.099597	-0.792516
14	S	-1.904782	-3.227989	-0.950920	S	-1.857419	-3.236813	-0.952865
15	N	-0.574723	-2.335675	-0.664229	N	-0.502510	-2.306570	-0.654175
16	C	1.269086	-0.038244	-0.037809	C	1.246082	-0.010407	-0.030627
17	S	2.125248	-1.532077	-0.282071	S	2.068769	-1.518854	-0.287915
18	C	3.698145	-0.870836	-0.031040	C	3.656429	-0.858631	-0.032433
19	C	3.585132	0.510459	0.243425	C	3.568304	0.525882	0.251202
20	C	2.216952	0.978375	0.239553	C	2.212370	1.009152	0.253317
21	N	1.926774	2.284623	0.485061	N	1.929732	2.306896	0.503604
22	C	2.960824	3.071810	0.720987	C	2.973119	3.091250	0.743499
23	C	4.305380	2.606523	0.724102	C	4.307906	2.612559	0.740827
24	N	4.626959	1.346784	0.490267	N	4.621324	1.348081	0.499651
25	C	4.880243	-1.682364	-0.110165	C	4.820731	-1.676466	-0.118708
26	S	4.797058	-3.390027	-0.472664	S	4.712618	-3.388858	-0.485044
27	C	6.503666	-3.562167	-0.378182	C	6.414706	-3.575635	-0.399321
28	C	7.119855	-2.366869	-0.081560	C	7.052905	-2.384665	-0.103350
29	C	6.206716	-1.298620	0.071462	C	6.160733	-1.308360	0.056475
30	H	-6.591392	3.295968	0.195306	H	-6.587171	3.275074	0.135981
31	H	-8.296614	1.562790	-0.372503	H	-8.262450	1.503325	-0.393878
32	H	-7.558430	-0.760138	-0.897407	H	-7.496494	-0.820978	-0.864624
33	H	-5.162343	-1.348912	-0.855183	H	-5.078248	-1.375996	-0.806828
34	H	-4.175497	2.696907	0.232861	H	-4.158676	2.708767	0.190206
35	H	-0.335781	2.141204	0.318233	H	-0.327642	2.182669	0.335442
36	H	2.748352	4.127103	0.920387	H	2.767234	4.145844	0.948492
37	H	5.124446	3.304125	0.925894	H	5.134942	3.300125	0.944491
38	H	6.956834	-4.534988	-0.546573	H	6.858748	-4.552418	-0.571092
39	H	8.198988	-2.262807	0.022818	H	8.134269	-2.299117	-0.006146
40	H	6.475241	-0.271264	0.306469	H	6.440587	-0.283948	0.291324

Table 13
Molecular system 12: Cartesian coordinates of the optimized molecular structure at ground and excited states.

	Ground state geometry				Excited state geometry			
No.	Atom	X	Y	Z	Atom	X	Y	Z
1	C	-0.804165	0.021982	1.381671	C	-0.798016	0.021941	1.370109
2	C	0.578491	0.037186	1.503358	C	0.574409	0.037773	1.490917
3	C	1.403526	0.017442	0.364040	C	1.411734	0.018304	0.336591
4	C	0.790378	-0.018376	-0.904498	C	0.788992	-0.017733	-0.951209
5	C	-0.590996	-0.033689	-1.026079	C	-0.581434	-0.033476	-1.071846
6	C	-1.416903	-0.013911	0.115806	C	-1.420190	-0.014203	0.087313
7	C	-2.868781	-0.031307	-0.046039	C	-2.840313	-0.031467	-0.063006
8	S	-3.972808	-0.013485	1.323717	S	-3.938856	-0.009524	1.358656
9	C	-5.301828	-0.049576	0.238924	C	-5.273187	-0.047912	0.284754
10	C	-4.842774	-0.072288	-1.056209	C	-4.830662	-0.073979	-1.036683
11	N	-3.487480	-0.061997	-1.208928	N	-3.496377	-0.064876	-1.228661
12	C	2.861356	0.033226	0.458474	C	2.836284	0.033439	0.436850
13	N	3.674479	0.015212	-0.578133	N	3.686683	0.016254	-0.595994
14	C	4.982025	0.037177	-0.190652	C	4.966670	0.037198	-0.173607
15	C	5.206725	0.073036	1.164672	C	5.170529	0.071765	1.204812
16	S	3.707956	0.079506	2.000065	S	3.668427	0.078617	2.028716
17	H	-1.417168	0.038487	2.285629	H	-1.417392	0.037315	2.269813

(*continued on next page*)

Table 13 (*continued*)

	Ground state geometry				Excited state geometry			
No.	Atom	X	Y	Z	Atom	X	Y	Z
18	H	1.023719	0.064897	2.500412	H	1.026650	0.065454	2.484896
19	H	1.426869	-0.033671	-1.789479	H	1.431569	-0.032385	-1.831680
20	H	-1.062713	-0.061462	-2.008508	H	-1.059880	-0.061078	-2.050931
21	H	-6.326386	-0.052226	0.599135	H	-6.296706	-0.049838	0.649159
22	H	-5.481558	-0.097229	-1.938646	H	-5.499902	-0.100711	-1.897678
23	H	5.765782	0.025780	-0.947607	H	5.776613	0.026609	-0.904222
24	H	6.152251	0.095386	1.698472	H	6.114356	0.092614	1.742532

Table 14
Molecular system 13: Cartesian coordinates of the optimized molecular structure at ground and excited states.

	Ground state geometry				Excited state geometry			
No.	Atom	X	Y	Z	Atom	X	Y	Z
1	C	-1.313758	0.626750	0.798389	C	-1.327445	0.622112	0.839584
2	C	-0.352808	0.001701	-0.005838	C	-0.367024	-0.017944	0.023927
3	C	-0.891623	-0.836055	-1.023356	C	-0.869412	-0.825515	-1.042338
4	C	-2.324990	-1.017791	-1.126520	C	-2.270515	-0.990006	-1.182160
5	C	-3.195626	-0.366193	-0.181087	C	-3.141365	-0.365265	-0.231577
6	N	-2.646377	0.453792	0.726414	N	-2.641959	0.475062	0.720831
7	C	-4.645200	-0.435971	-0.184168	C	-4.583517	-0.460610	-0.173050
8	N	-5.442018	-1.526462	-0.519779	N	-5.415739	-1.498200	-0.596232
9	C	-6.756332	-1.158086	-0.408325	C	-6.709649	-1.131846	-0.371471
10	C	-6.827423	0.172749	-0.016094	C	-6.747668	0.151023	0.176577
11	C	-5.505227	0.621880	0.142609	C	-5.420198	0.562582	0.324647
12	C	-5.028683	-2.905673	-0.740944	C	-5.041060	-2.870316	-0.927320
13	N	-2.686019	-1.765417	-2.190490	N	-2.639677	-1.717292	-2.290838
14	S	-1.308684	-2.202293	-2.933792	S	-1.207581	-2.149688	-3.019034
15	N	-0.199114	-1.479341	-1.987187	N	-0.101406	-1.420863	-1.984861
16	C	1.062386	0.245155	0.198305	C	1.026201	0.219465	0.235473
17	N	1.529682	1.027585	1.159129	N	1.512101	0.964445	1.241315
18	C	2.882510	1.087320	1.134311	C	2.847012	1.020227	1.198627
19	C	3.527232	0.351850	0.149886	C	3.486812	0.323202	0.154161
20	S	2.323398	-0.464132	-0.797228	S	2.274555	-0.444085	-0.823703
21	C	4.959185	0.236455	-0.116458	C	4.904620	0.228700	-0.113987
22	C	5.445613	-0.168138	-1.375438	C	5.393964	-0.447956	-1.258005
23	C	6.814225	-0.267001	-1.617073	C	6.757245	-0.534544	-1.508949
24	C	7.732865	0.041061	-0.610622	C	7.676412	0.050291	-0.629669
25	C	7.266056	0.443266	0.644086	C	7.213374	0.723317	0.507196
26	C	5.898705	0.534914	0.891877	C	5.851555	0.812929	0.764595
27	H	-0.964019	1.315505	1.571001	H	-0.977114	1.298487	1.623337
28	H	-7.543421	-1.883583	-0.591277	H	-7.516416	-1.825033	-0.592639
29	H	-7.738802	0.742828	0.134241	H	-7.645008	0.708908	0.425374
30	H	-5.164556	1.609798	0.434083	H	-5.046099	1.506371	0.705540
31	H	-5.861324	-3.564184	-0.465563	H	-5.942316	-3.393828	-1.267461
32	H	-4.169848	-3.148596	-0.102976	H	-4.647107	-3.382527	-0.036755
33	H	-4.746295	-3.077482	-1.786306	H	-4.279798	-2.869004	-1.715688
34	H	3.396427	1.718677	1.859353	H	3.372938	1.599200	1.958507
35	H	4.738749	-0.391176	-2.177480	H	4.687723	-0.903280	-1.954726
36	H	7.165664	-0.581081	-2.601523	H	7.109700	-1.060006	-2.397759
37	H	8.804513	-0.034975	-0.800904	H	8.746741	-0.018052	-0.829088
38	H	7.973747	0.677358	1.441451	H	7.923535	1.179862	1.198386
39	H	5.549920	0.820236	1.885503	H	5.512311	1.334931	1.659442

Table 15
System 14, cartesian coordinates of the optimized molecular structure at ground and excited states.

	Ground state geometry				Excited state geometry			
No.	Atom	X	Y	Z	Atom	X	Y	Z
1	C	-0.977609	1.095324	0.893178	C	-0.885036	1.438666	0.932032
2	C	0.388825	1.260922	1.037848	C	0.500509	1.516072	1.015497
3	C	1.319817	0.409126	0.401619	C	1.381260	0.524913	0.442320
4	C	0.773512	-0.614399	-0.385581	C	0.726900	-0.521170	-0.251602
5	C	-0.609448	-0.785235	-0.535341	C	-0.658267	-0.574477	-0.327776
6	C	-1.542300	0.066600	0.101371	C	-1.520299	0.372422	0.272172
7	C	-3.008995	0.016474	0.044278	C	-2.966491	0.191945	0.171523
8	S	-4.005297	-1.124984	-0.847279	S	-3.770528	0.134459	-1.511874
9	C	-5.406617	-0.338532	-0.261295	C	-5.237221	-0.225092	-0.773106
10	C	-5.059245	0.714798	0.554222	C	-5.105569	-0.211911	0.612488
11	N	-3.727095	0.905909	0.718796	N	-3.838298	-0.012995	1.104227
12	C	-0.821795	-1.948358	-1.426167	C	-1.033025	-1.708946	-1.134234
13	O	0.410618	-2.448856	-1.789322	O	0.065905	-2.386860	-1.532398
14	C	1.460808	-1.679376	-1.187372	C	1.248034	-1.705177	-1.012770
15	O	-1.842157	-2.460060	-1.832928	O	-2.173661	-2.066930	-1.487473
16	C	2.745164	0.653162	0.605983	C	2.795894	0.661791	0.593795
17	N	3.209660	1.634058	1.356756	N	3.373496	1.700150	1.218094
18	C	4.570546	1.648527	1.385123	C	4.721059	1.593551	1.204638
19	C	5.199539	0.670990	0.650842	C	5.259461	0.484352	0.584626
20	S	4.026615	-0.316663	-0.114079	S	3.986863	-0.511276	-0.027747
21	H	-1.663880	1.772091	1.400110	H	-1.489342	2.215425	1.404188
22	H	0.777519	2.068466	1.658464	H	0.967961	2.342502	1.548663
23	H	-6.399746	-0.681928	-0.538839	H	-6.135758	-0.453644	-1.340167
24	H	-5.762419	1.378909	1.056393	H	-5.932015	-0.344625	1.309837
25	H	2.077910	-2.354277	-0.570186	H	1.801139	-2.425554	-0.390748
26	H	2.098791	-1.272153	-1.990116	H	1.874113	-1.440816	-1.878632
27	H	5.086279	2.409729	1.969774	H	5.322757	2.373094	1.674331
28	H	6.262436	0.487180	0.524875	H	6.301596	0.207574	0.461223

Table 16
Molecular system 15: Cartesian coordinates of the optimized molecular structure at ground and excited states.

	Ground state geometry				Excited state geometry			
No.	Atom	X	Y	Z	Atom	X	Y	Z
1	N	-0.823572	1.042664	-0.451684	N	-0.823852	1.100034	-0.479630
2	C	0.524513	1.083143	-0.451241	C	0.505997	1.133076	-0.475666
3	C	1.385368	0.075505	-0.003189	C	1.346378	0.091774	-0.011907
4	C	0.725036	-1.091961	0.492542	C	0.710214	-1.091370	0.492306
5	C	-0.719837	-1.150341	0.497922	C	-0.698412	-1.139329	0.493204
6	C	-1.475298	-0.028221	0.002750	C	-1.434268	-0.014650	-0.004255
7	C	-2.919801	-0.027371	-0.016923	C	-2.868552	-0.014006	-0.023047
8	C	-3.878559	-0.946891	0.369532	C	-3.820273	-0.952567	0.371421
9	C	-5.142672	-0.358167	0.097015	C	-5.084762	-0.383694	0.109201
10	C	-4.878759	0.876526	-0.435534	C	-4.838282	0.862041	-0.427159
11	O	-3.541353	1.096343	-0.512938	O	-3.512455	1.104966	-0.515779
12	N	-1.206162	-2.307346	0.990906	N	-1.243510	-2.301657	0.989411
13	S	0.086889	-3.205105	1.396208	S	0.085596	-3.221219	1.406825
14	N	1.304374	-2.208985	0.982615	N	1.344422	-2.194985	0.979815
15	C	2.820421	0.204835	-0.038985	C	2.764076	0.223948	-0.048393
16	O	3.328826	1.384467	-0.545368	O	3.303216	1.398783	-0.551680
17	C	4.687691	1.293863	-0.485249	C	4.651210	1.276158	-0.477546
18	C	5.067883	0.091805	0.044075	C	5.009657	0.056198	0.059354
19	C	3.866189	-0.615551	0.334055	C	3.808236	-0.624001	0.336864

(*continued on next page*)

Table 16 (*continued*)

	Ground state geometry				Excited state geometry			
No.	Atom	X	Y	Z	Atom	X	Y	Z
20	H	0.958044	2.005272	-0.844971	H	0.961947	2.046673	-0.865728
21	H	-3.675586	-1.922533	0.795946	H	-3.574770	-1.921048	0.793902
22	H	-6.123117	-0.789831	0.271262	H	-6.060406	-0.824563	0.287763
23	H	-5.508045	1.683937	-0.794773	H	-5.487001	1.657920	-0.779877
24	H	5.232188	2.156778	-0.852833	H	5.222908	2.125132	-0.838675
25	H	6.086304	-0.246328	0.206754	H	6.023384	-0.293306	0.227449
26	H	3.762245	-1.605397	0.763602	H	3.652510	-1.609200	0.763323

Table 17
Molecular system 16: Cartesian coordinates of the optimized molecular structure at ground and excited states.

	Ground state geometry				Excited state geometry			
No.	Atom	X	Y	Z	Atom	X	Y	Z
1	C	1.500535	-0.982169	-0.958001	C	1.529904	-1.227541	-0.860956
2	C	2.878516	-1.041800	-0.788120	C	2.891059	-1.218769	-0.649396
3	C	3.477606	-0.304885	0.247737	C	3.476862	-0.293758	0.255533
4	N	2.748634	0.448027	1.093096	N	2.682900	0.602053	0.915858
5	C	1.427426	0.485133	0.926105	C	1.382370	0.582321	0.702850
6	C	0.726027	-0.198954	-0.088198	C	0.689973	-0.303311	-0.173387
7	C	-0.736945	-0.094238	-0.216338	C	-0.742121	-0.279054	-0.343183
8	C	-1.415180	1.113310	0.049438	C	-1.558535	0.761753	0.213853
9	N	-2.734875	1.276530	-0.031216	N	-2.854597	0.785905	0.053070
10	C	-3.486108	0.224042	-0.406461	C	-3.560191	-0.151785	-0.639301
11	C	-2.911324	-1.021387	-0.712246	C	-2.846975	-1.214689	-1.211681
12	C	-1.534442	-1.179855	-0.610410	C	-1.471061	-1.270894	-1.065049
13	C	-4.960053	0.430559	-0.477711	C	-4.952637	0.177452	-0.641545
14	N	-5.499929	1.281559	0.415177	N	-5.186021	1.322552	0.049755
15	C	-6.821010	1.478814	0.370461	C	-6.366461	1.876018	0.216565
16	C	-7.673093	0.859922	-0.549058	C	-7.507863	1.273198	-0.336981
17	C	-7.110771	-0.015820	-1.476689	C	-7.329908	0.089582	-1.059593
18	C	-5.735777	-0.236504	-1.441608	C	-6.063497	-0.465394	-1.220340
19	C	4.953827	-0.319929	0.449816	C	4.918962	-0.249784	0.507859
20	C	5.706193	-1.476909	0.183068	C	5.778511	-1.300610	0.096551
21	C	7.084147	-1.451490	0.386014	C	7.140492	-1.215867	0.346078
22	C	7.672510	-0.274002	0.845318	C	7.642793	-0.088522	1.007034
23	C	6.842444	0.825243	1.084621	C	6.723113	0.894909	1.389525
24	N	5.518906	0.816564	0.899320	N	5.412131	0.837948	1.160184
25	H	1.026972	-1.515125	-1.785264	H	1.114151	-1.925665	-1.589226
26	H	3.490985	-1.622113	-1.479666	H	3.516968	-1.908923	-1.215992
27	H	0.871927	1.078193	1.660448	H	0.817326	1.316494	1.290353
28	H	-0.841408	2.006158	0.320066	H	-1.126912	1.581842	0.788470
29	H	-3.541344	-1.868879	-0.986118	H	-3.376738	-1.990907	-1.766669
30	H	-1.079340	-2.153780	-0.802974	H	-0.935120	-2.111866	-1.503258
31	H	-7.224710	2.172238	1.115661	H	-6.408292	2.801221	0.794971
32	H	-8.744536	1.064699	-0.536484	H	-8.485460	1.728188	-0.194038
33	H	-7.731494	-0.513686	-2.223890	H	-8.193478	-0.406652	-1.505546
34	H	-5.263740	-0.896643	-2.170781	H	-5.916589	-1.384671	-1.786272
35	H	5.214086	-2.391284	-0.151614	H	5.376625	-2.189285	-0.391109
36	H	7.687111	-2.341538	0.196984	H	7.805996	-2.025150	0.038051
37	H	8.747281	-0.204968	1.019080	H	8.705505	0.023710	1.225123
38	H	7.266990	1.768291	1.444514	H	7.072862	1.791277	1.915913

Table 18
Molecular system 17: Cartesian coordinates of the optimized molecular structure at ground and excited states.

	Ground state geometry				Excited state geometry			
No.	Atom	X	Y	Z	Atom	X	Y	Z
1	C	-4.005228	-1.567560	2.506646	C	-3.926558	-1.415904	2.532926
2	C	-2.988091	-1.360100	1.556514	C	-2.928527	-1.077528	1.624999
3	C	-3.254288	-0.789772	0.312453	C	-3.241037	-0.608471	0.320323
4	C	-4.595010	-0.356971	0.012830	C	-4.631510	-0.350446	-0.001512
5	C	-5.631147	-0.606118	0.980178	C	-5.645219	-0.751169	0.936944
6	C	-5.307562	-1.219109	2.217864	C	-5.273018	-1.292875	2.189717
7	C	-6.963675	-0.210452	0.687259	C	-7.011216	-0.551094	0.606882
8	C	-7.274625	0.433233	-0.490676	C	-7.384678	0.066543	-0.578340
9	C	-6.250637	0.728148	-1.418085	C	-6.395560	0.530095	-1.456848
10	C	-4.947605	0.343752	-1.171236	C	-5.045570	0.331342	-1.165041
11	C	-2.166133	-0.680476	-0.650104	C	-2.179696	-0.450809	-0.621401
12	O	-0.900415	-0.532045	-0.126963	O	-0.889927	-0.405955	-0.091200
13	C	-0.002038	-0.543958	-1.167424	C	-0.002291	-0.335886	-1.129322
14	C	-0.689361	-0.705768	-2.352563	C	-0.707206	-0.364276	-2.338648
15	C	-2.065954	-0.789236	-2.023728	C	-2.070532	-0.437580	-2.013633
16	C	1.397286	-0.383256	-0.838909	C	1.399383	-0.251799	-0.807854
17	C	1.843917	-0.152372	0.474397	C	1.876451	-0.179256	0.526501
18	C	3.204347	-0.012704	0.715175	C	3.234478	-0.110131	0.752076
19	C	4.113580	-0.097266	-0.353197	C	4.149027	-0.114279	-0.340449
20	N	3.695664	-0.309973	-1.618485	N	3.685799	-0.170557	-1.627526
21	C	2.393309	-0.449191	-1.839156	C	2.379956	-0.235741	-1.827245
22	C	5.577975	0.051532	-0.135945	C	5.597486	-0.045346	-0.140845
23	C	6.176671	-0.375234	1.063246	C	6.185126	-0.231054	1.137864
24	C	7.550345	-0.218509	1.230465	C	7.561518	-0.151079	1.283834
25	C	8.290319	0.359313	0.199526	C	8.350547	0.115238	0.153765
26	C	7.609262	0.748649	-0.957650	C	7.688834	0.273174	-1.072370
27	N	6.292807	0.603969	-1.135693	N	6.371659	0.198229	-1.240552
28	H	-3.757426	-2.029421	3.463815	H	-3.648561	-1.804673	3.513788
29	H	-1.970823	-1.681794	1.780895	H	-1.882183	-1.226758	1.887225
30	H	-6.107509	-1.401504	2.938866	H	-6.054244	-1.582746	2.895093
31	H	-7.740327	-0.418825	1.426920	H	-7.770848	-0.882401	1.318353
32	H	-8.302770	0.733648	-0.699466	H	-8.440098	0.214162	-0.811325
33	H	-6.488768	1.275108	-2.332122	H	-6.676719	1.062895	-2.366306
34	H	-4.167576	0.611340	-1.882541	H	-4.294557	0.754611	-1.830289
35	H	-0.254682	-0.759305	-3.345642	H	-0.271751	-0.344526	-3.331482
36	H	-2.886214	-0.964721	-2.711284	H	-2.890764	-0.535822	-2.716635
37	H	1.124283	-0.070327	1.289440	H	1.174161	-0.157696	1.360953
38	H	3.557910	0.193106	1.726506	H	3.598662	-0.021826	1.775260
39	H	2.105640	-0.632880	-2.879930	H	2.065401	-0.287123	-2.877542
40	H	5.577738	-0.849656	1.841921	H	5.568827	-0.463404	2.007241
41	H	8.036403	-0.552623	2.149001	H	8.019807	-0.302029	2.263348
42	H	9.368459	0.503098	0.283405	H	9.436820	0.189711	0.216149
43	H	8.154791	1.206493	-1.789660	H	8.271170	0.474504	-1.980013

Table 19
Molecular system 18: Cartesian coordinates of the optimized molecular structure at ground and excited states.

	Ground state geometry				Excited state geometry			
No.	Atom	X	Y	Z	Atom	X	Y	Z
1	C	-3.825101	-2.323832	1.456824	C	-3.742356	-2.115609	1.573717
2	C	-2.738797	-1.770763	0.754849	C	-2.683519	-1.524447	0.879347
3	C	-2.931038	-0.897819	-0.316650	C	-2.908527	-0.747789	-0.276909
4	C	-4.271357	-0.508576	-0.673612	C	-4.268849	-0.480840	-0.686143
5	C	-5.372549	-1.110052	0.031493	C	-5.338861	-1.131234	0.019692

(*continued on next page*)

Table 19 (*continued*)

	Ground state geometry				Excited state geometry			
No.	Atom	X	Y	Z	Atom	X	Y	Z
6	C	-5.119211	-2.021195	1.088730	C	-5.049166	-1.951605	1.138668
7	C	-6.701606	-0.760439	-0.328093	C	-6.678561	-0.910499	-0.391205
8	C	-6.953853	0.166481	-1.316003	C	-6.975227	-0.051806	-1.433208
9	C	-5.874991	0.801435	-1.970164	C	-5.934308	0.638515	-2.081590
10	C	-4.571100	0.472449	-1.655716	C	-4.613680	0.431091	-1.711144
11	C	-1.759743	-0.439433	-1.048662	C	-1.758924	-0.294877	-1.011174
12	O	-0.579971	-0.419542	-0.343217	O	-0.567522	-0.320363	-0.315640
13	C	0.427995	-0.061412	-1.200642	C	0.438112	0.017020	-1.164139
14	C	-0.104466	0.143410	-2.461589	C	-0.095247	0.258962	-2.430717
15	C	-1.495144	-0.094956	-2.363577	C	-1.484687	0.064994	-2.330145
16	C	1.769698	0.046546	-0.685033	C	1.789494	0.071567	-0.644722
17	C	2.217324	-0.515376	0.553614	C	2.218994	-0.567912	0.552315
18	C	3.601371	-0.352668	0.953471	C	3.585997	-0.426559	0.933078
19	C	4.511868	0.362821	0.100239	C	4.471790	0.347973	0.106424
20	N	4.048609	0.869180	-1.047869	N	4.031586	0.953633	-1.019464
21	C	2.761499	0.724435	-1.404734	C	2.747354	0.804976	-1.360811
22	C	5.909701	0.572650	0.404488	C	5.868706	0.530305	0.401297
23	C	6.674319	0.178306	1.496514	C	6.651159	0.049291	1.449690
24	C	8.022218	0.593613	1.402528	C	7.994456	0.466064	1.362420
25	C	8.276005	1.298698	0.244337	C	8.229742	1.260014	0.253072
26	S	6.880061	1.462773	-0.738411	S	6.823237	1.506132	-0.690557
27	N	3.888624	-0.936992	2.135375	N	3.936068	-1.082531	2.073108
28	S	2.505405	-1.620236	2.645961	S	2.532515	-1.816870	2.582781
29	N	1.490134	-1.229371	1.440114	N	1.464836	-1.339520	1.389289
30	H	-3.633634	-3.013576	2.280542	H	-3.529006	-2.729937	2.449513
31	H	-1.720593	-2.045841	1.031913	H	-1.655954	-1.693275	1.203966
32	H	-5.967771	-2.468415	1.611251	H	-5.875026	-2.435826	1.664021
33	H	-7.525600	-1.236850	0.208382	H	-7.478322	-1.424353	0.146739
34	H	-7.980667	0.426797	-1.578357	H	-8.011002	0.110663	-1.734637
35	H	-6.072540	1.567784	-2.721884	H	-6.166158	1.354239	-2.871841
36	H	-3.755408	1.002025	-2.145346	H	-3.831393	1.016747	-2.190893
37	H	0.448586	0.402755	-3.358841	H	0.465791	0.508801	-3.324782
38	H	-2.210526	-0.081425	-3.178407	H	-2.198097	0.106322	-3.145881
39	H	2.490629	1.203618	-2.349923	H	2.442915	1.328439	-2.272872
40	H	6.257118	-0.390001	2.324524	H	6.227969	-0.578485	2.231038
41	H	8.779363	0.383235	2.156777	H	8.766037	0.198533	2.083306
42	H	9.219030	1.731390	-0.079907	H	9.171525	1.711689	-0.049716

Table 20
Molecular system 19: Cartesian coordinates of the optimized molecular structure at ground and excited states.

	Ground state geometry				Excited state geometry			
No.	Atom	X	Y	Z	Atom	X	Y	Z
1	C	-3.468010	-3.140455	-0.487757	C	-3.487389	-2.353251	-1.628337
2	C	-2.468696	-2.247243	-0.061297	C	-2.481362	-1.650484	-0.974622
3	C	-2.784848	-0.980641	0.431549	C	-2.779585	-0.738443	0.071030
4	C	-4.161285	-0.556069	0.448933	C	-4.167298	-0.434333	0.360568
5	C	-5.173996	-1.493777	0.040937	C	-5.184955	-1.203955	-0.296046
6	C	-4.797972	-2.782968	-0.415890	C	-4.820133	-2.163596	-1.272668
7	C	-6.538998	-1.102485	0.078256	C	-6.548457	-0.955298	-0.002407
8	C	-6.907416	0.166998	0.467334	C	-6.914872	0.049332	0.876727
9	C	-5.912504	1.107669	0.813919	C	-5.923196	0.853691	1.461199
10	C	-4.577401	0.754575	0.803268	C	-4.577177	0.622477	1.199242
11	C	-1.701119	-0.151276	0.936797	C	-1.693458	-0.220488	0.829560

(*continued on next page*)

Table 20 (*continued*)

	Ground state geometry				Excited state geometry			
No.	Atom	X	Y	Z	Atom	X	Y	Z
12	O	-0.458466	-0.398631	0.406507	O	-0.438233	-0.313455	0.266653
13	C	0.452328	0.394073	1.055640	C	0.474504	0.145846	1.170885
14	C	-0.208246	1.149534	2.010024	C	-0.194995	0.519525	2.337987
15	C	-1.576250	0.803585	1.933115	C	-1.555714	0.292904	2.133013
16	C	1.836974	0.323237	0.665728	C	1.885278	0.157824	0.793648
17	C	2.411987	-0.723988	-0.124435	C	2.713354	-0.958464	1.079156
18	C	3.829673	-0.692955	-0.437226	C	4.112830	-0.885706	0.697047
19	C	4.631656	0.387416	0.061702	C	4.582286	0.298143	0.050626
20	N	4.056047	1.343169	0.795261	N	3.742984	1.346571	-0.201908
21	C	2.742670	1.313608	1.069592	C	2.468823	1.266172	0.157861
22	C	6.059292	0.527243	-0.172526	C	5.946282	0.499219	-0.385173
23	N	6.838818	-0.282392	-0.858166	N	6.970425	-0.325385	-0.280489
24	C	8.123942	0.168714	-0.862443	C	8.098360	0.227019	-0.811784
25	C	8.348908	1.341091	-0.173468	C	7.965189	1.491306	-1.337799
26	S	6.891202	1.917894	0.517724	S	6.342667	2.038321	-1.167555
27	N	4.237491	-1.742550	-1.181236	N	4.811758	-1.996604	1.016800
28	S	2.917744	-2.651480	-1.424122	S	3.737243	-3.025522	1.742911
29	N	1.779176	-1.804103	-0.630985	N	2.339940	-2.101890	1.677293
30	H	-3.181656	-4.127638	-0.854166	H	-3.224000	-3.076357	-2.400142
31	H	-1.422626	-2.553932	-0.089804	H	-1.436722	-1.841357	-1.214615
32	H	-5.581061	-3.481390	-0.719442	H	-5.608098	-2.736212	-1.765553
33	H	-7.295127	-1.831424	-0.222774	H	-7.308682	-1.561629	-0.498536
34	H	-7.960187	0.453613	0.487355	H	-7.967431	0.234947	1.092103
35	H	-6.199636	2.126450	1.080332	H	-6.208452	1.679378	2.114121
36	H	-3.826255	1.507576	1.036156	H	-3.833811	1.302145	1.612384
37	H	0.246598	1.847114	2.706186	H	0.292152	0.885910	3.234573
38	H	-2.369771	1.163809	2.578289	H	-2.354728	0.413272	2.856677
39	H	2.374581	2.160216	1.655604	H	1.851764	2.143107	-0.068710
40	H	8.889091	-0.398413	-1.392166	H	9.027915	-0.343101	-0.795349
41	H	9.285910	1.876533	-0.046528	H	8.727556	2.108730	-1.804592

Table 21
Molecular system 20: Cartesian coordinates of the optimized molecular structure at ground and excited states.

	Ground state geometry				Excited state geometry			
No.	Atom	X	Y	Z	Atom	X	Y	Z
1	C	-6.710991	-0.056046	-0.663057	C	-6.285444	-0.255531	-0.929375
2	N	-5.377489	-0.084082	-0.745309	N	-5.017255	-0.133704	-0.580385
3	C	-4.671908	0.220494	0.360615	C	-4.619408	0.375634	0.606233
4	C	-5.292786	0.553008	1.577428	C	-5.585061	0.800573	1.524235
5	C	-6.683878	0.573488	1.646142	C	-6.932387	0.684006	1.181369
6	C	-7.416275	0.264972	0.500665	C	-7.301147	0.152543	-0.054542
7	C	-3.187185	0.185897	0.245867	C	-3.172932	0.376858	0.687997
8	N	-2.655151	-0.717114	-0.599719	N	-2.643589	-0.128922	-0.439780
9	C	-1.330474	-0.765049	-0.728306	C	-1.360640	-0.269426	-0.690835
10	C	-0.428199	0.071997	-0.035179	C	-0.388721	0.128770	0.274959
11	C	-1.000527	1.014689	0.835745	C	-0.921043	0.664419	1.468958
12	C	-2.380563	1.069877	0.982401	C	-2.290891	0.791325	1.683372
13	C	1.027923	-0.046112	-0.186136	C	1.046198	-0.019566	0.009151
14	C	1.684074	-0.395472	-1.405132	C	1.578649	-0.550570	-1.204806
15	C	3.127707	-0.475357	-1.443883	C	3.012087	-0.635261	-1.342206
16	C	3.894983	-0.205529	-0.259013	C	3.860003	-0.199136	-0.284756
17	N	3.244980	0.108631	0.863652	N	3.324177	0.299513	0.865286
18	C	1.896565	0.175034	0.883981	C	2.002528	0.371239	0.972528
19	C	5.345685	-0.253749	-0.206092	C	5.302037	-0.252311	-0.351953
20	S	6.366557	-0.625710	-1.567409	S	6.194215	-0.850424	-1.728267

(*continued on next page*)

Table 21 (*continued*)

	Ground state geometry				Excited state geometry		
No.	Atom	X	Y	Z	Atom	X	Y	Z
21	C	7.785794	-0.455342	-0.622240	C	7.697595	-0.546647	-0.954776
22	C	7.503935	-0.126780	0.688507	C	7.537518	-0.009162	0.307483
23	C	6.119021	-0.012210	0.925065	C	6.180820	0.158101	0.650171
24	N	3.617478	-0.797816	-2.657315	N	3.432771	-1.146692	-2.523190
25	S	2.327054	-0.969288	-3.630366	S	2.059929	-1.491342	-3.384557
26	N	1.109679	-0.653785	-2.602023	N	0.900934	-1.000725	-2.284363
27	H	-7.250360	-0.303250	-1.583500	H	-6.492512	-0.680825	-1.912862
28	H	-4.693296	0.764952	2.463985	H	-5.279438	1.212990	2.485290
29	H	-7.187284	0.817539	2.583433	H	-7.699556	1.010725	1.884652
30	H	-8.507186	0.267918	0.504510	H	-8.343761	0.049893	-0.349369
31	H	-0.944919	-1.521340	-1.416374	H	-1.047444	-0.691799	-1.647446
32	H	-0.365929	1.726231	1.367582	H	-0.248602	0.995188	2.258197
33	H	-2.831597	1.823164	1.629873	H	-2.672183	1.208976	2.615829
34	H	1.469535	0.409185	1.863931	H	1.661119	0.782623	1.927592
35	H	8.759223	-0.607170	-1.081660	H	8.626025	-0.780297	-1.469853
36	H	8.269661	0.024569	1.447959	H	8.370205	0.253466	0.959307
37	H	5.661314	0.236634	1.880433	H	5.810373	0.562580	1.589774

Table 22
Molecular system 21: Cartesian coordinates of the optimized molecular structure at ground and excited states.

	Ground state geometry				Excited state geometry		
No.	Atom	X	Y	Z	Atom	X	Y	Z
1	C	4.601892	-0.201461	-2.296752	C	4.556453	-0.188128	-2.330427
2	C	4.013346	-0.309822	-0.992876	C	4.001105	-0.215719	-1.005083
3	C	4.775098	-0.791396	0.064155	C	4.828813	-0.548927	0.070982
4	C	6.096912	-1.241205	-0.125963	C	6.160174	-0.950318	-0.118096
5	C	6.668500	-1.194766	-1.379469	C	6.696701	-0.987541	-1.391927
6	C	5.951039	-0.665555	-2.482959	C	5.924990	-0.591917	-2.513014
7	C	6.551633	-0.558076	-3.765971	C	6.496550	-0.555591	-3.811903
8	C	5.874356	0.009778	-4.822773	C	5.768944	-0.106055	-4.895615
9	C	4.564359	0.506169	-4.632148	C	4.441936	0.334546	-4.711717
10	C	3.946856	0.402692	-3.403038	C	3.851338	0.295148	-3.461578
11	C	2.615014	0.082054	-0.694549	C	2.594626	0.097981	-0.677992
12	C	1.481186	-0.434152	-1.407716	C	1.470036	-0.432676	-1.392109
13	C	0.143579	-0.044524	-1.017221	C	0.154750	-0.050497	-1.000286
14	C	-0.035544	0.852026	0.083346	C	0.008307	0.835343	0.100629
15	C	1.150948	1.240278	0.713389	C	1.179765	1.221988	0.767310
16	N	2.402966	0.876205	0.351847	N	2.425639	0.871345	0.412942
17	C	-1.331982	1.298720	0.521333	C	-1.294083	1.269137	0.554789
18	C	-2.624459	1.051368	0.098944	C	-2.586790	0.927531	0.175482
19	C	-3.481084	1.789808	0.950241	C	-3.455475	1.665661	1.000758
20	C	-2.681429	2.460315	1.856063	C	-2.672088	2.442590	1.849956
21	O	-1.365659	2.162717	1.595243	O	-1.346021	2.195328	1.568193
22	C	-3.016321	3.324589	2.981418	C	-3.032795	3.367497	2.896051
23	C	-4.201342	3.044958	3.660962	C	-4.329200	3.235705	3.429975
24	C	-4.629168	3.816453	4.756770	C	-4.792777	4.045495	4.469089
25	C	-3.862551	4.873634	5.197950	C	-3.966348	5.012829	5.017861
26	C	-2.652236	5.211888	4.540032	C	-2.658467	5.211651	4.513039
27	C	-2.213222	4.444304	3.403592	C	-2.170149	4.402948	3.425706
28	C	-1.027613	4.861355	2.740045	C	-0.881646	4.701421	2.914543
29	C	-0.300956	5.947438	3.185554	C	-0.101218	5.706700	3.463847
30	C	-0.717280	6.677400	4.320730	C	-0.568333	6.469064	4.551032
31	C	-1.872770	6.315802	4.977650	C	-1.828896	6.225823	5.059023
32	N	-0.822415	-0.628127	-1.758155	N	-0.857498	-0.611240	-1.724200
33	S	-0.048361	-1.586746	-2.822655	S	-0.067735	-1.593244	-2.828142

(*continued on next page*)

Table 22 (*continued*)

	Ground state geometry				Excited state geometry			
No.	Atom	X	Y	Z	Atom	X	Y	Z
34	N	1.501246	-1.323427	-2.425690	N	1.520964	-1.324987	-2.425784
35	H	4.321751	-0.833225	1.055424	H	4.400329	-0.517806	1.072731
36	H	6.658746	-1.634332	0.722983	H	6.764286	-1.240337	0.743206
37	H	7.689134	-1.550113	-1.539784	H	7.730457	-1.303436	-1.551451
38	H	7.572872	-0.924831	-3.894083	H	7.533416	-0.877642	-3.934071
39	H	6.349886	0.090700	-5.801757	H	6.220728	-0.079497	-5.888702
40	H	4.039202	0.979444	-5.463781	H	3.872171	0.708235	-5.564153
41	H	2.941912	0.803078	-3.274116	H	2.826587	0.639002	-3.342038
42	H	1.095062	1.899980	1.582190	H	1.104431	1.852080	1.657960
43	H	-2.897707	0.413891	-0.734362	H	-2.819081	0.224912	-0.617106
44	H	-4.563059	1.852493	0.892166	H	-4.540324	1.662588	0.962552
45	H	-4.792622	2.181562	3.352195	H	-4.975164	2.445752	3.046633
46	H	-5.558565	3.556631	5.266033	H	-5.800201	3.895160	4.859559
47	H	-4.175217	5.468270	6.059196	H	-4.313312	5.638700	5.842621
48	H	-0.686558	4.316601	1.862428	H	-0.495334	4.137429	2.070081
49	H	0.603543	6.245160	2.652173	H	0.885091	5.907625	3.042740
50	H	-0.129823	7.529310	4.667312	H	0.056953	7.253574	4.979803
51	H	-2.216884	6.880556	5.847328	H	-2.216397	6.820640	5.889175

Table 23
Molecular system 22: Cartesian coordinates of the optimized molecular structure at ground and excited states.

	Ground state geometry				Excited state geometry			
No.	Atom	X	Y	Z	Atom	X	Y	Z
1	C	4.408430	-3.318783	-1.248569	C	4.414145	-2.982796	-1.577326
2	C	5.756830	-3.786021	-1.406420	C	5.745181	-3.507119	-1.753085
3	C	6.823675	-3.020216	-0.867358	C	6.731700	-3.185435	-0.802526
4	C	5.312005	-1.464492	-0.084117	C	5.257966	-1.919904	0.428242
5	C	4.180480	-2.100285	-0.545081	C	4.189669	-2.163675	-0.444732
6	H	7.850094	-3.354599	-0.979421	H	7.747665	-3.572115	-0.922835
7	H	5.208624	-0.538507	0.470006	H	5.097245	-1.291724	1.311650
8	C	2.838141	-1.527513	-0.338333	C	2.849494	-1.572643	-0.214657
9	C	1.794992	-2.250685	0.310667	C	1.805748	-2.272663	0.471723
10	C	2.526765	-0.247418	-0.734025	C	2.520201	-0.303224	-0.664701
11	C	0.484968	-1.665953	0.505041	C	0.481204	-1.711444	0.655496
12	C	1.249085	0.325950	-0.552414	C	1.247082	0.270603	-0.465749
13	H	3.281075	0.341131	-1.241576	H	3.276230	0.263172	-1.207912
14	C	0.193541	-0.335223	0.051160	C	0.194330	-0.389548	0.175331
15	H	1.088240	1.324463	-0.938148	H	1.067907	1.268264	-0.874609
16	C	-1.101839	0.296411	0.236228	C	-1.088131	0.257931	0.335436
17	C	-2.388403	-0.216075	0.308402	C	-2.393129	-0.253127	0.523524
18	C	-2.920260	2.099332	0.470607	C	-2.905762	2.081719	0.464503
19	C	-3.372572	0.802037	0.428182	C	-3.364086	0.772448	0.578664
20	C	-3.132798	-1.448578	0.247334	C	-3.120732	-1.479713	0.616239
21	C	-4.431960	-1.094767	0.339850	C	-4.437073	-1.112026	0.723368
22	H	-2.749766	-2.449395	0.172566	H	-2.722798	-2.486340	0.628533
23	H	-5.337051	-1.678847	0.347367	H	-5.350504	-1.689105	0.823683
24	S	4.341359	-5.326135	-2.507577	S	4.394065	-4.295539	-3.594477
25	S	0.479057	-3.822550	1.508444	S	0.507723	-3.864851	1.667873
26	N	5.851179	-4.928550	-2.102538	N	5.897183	-4.278959	-2.868245
27	N	3.508147	-4.112083	-1.846323	N	3.516201	-3.327519	-2.526395
28	N	6.595782	-1.899871	-0.237725	N	6.497376	-2.407090	0.272829
29	N	1.906022	-3.472563	0.845809	N	1.933315	-3.501337	1.015024
30	N	-0.344034	-2.474531	1.174620	N	-0.359733	-2.522313	1.327387

(*continued on next page*)

Table 23 (*continued*)

	Ground state geometry				Excited state geometry			
No.	Atom	X	Y	Z	Atom	X	Y	Z
31	S	-1.185032	2.036937	0.354799	S	-1.161233	2.008767	0.288428
32	O	-4.620322	0.263717	0.453316	O	-4.612819	0.250660	0.704059
33	C	-3.656239	3.350455	0.598811	C	-3.632155	3.331732	0.485379
34	C	-3.015687	4.599465	0.575676	C	-2.985876	4.575018	0.315709
35	N	-4.987066	3.243107	0.740118	N	-4.968834	3.223451	0.678698
36	C	-3.776257	5.748097	0.705588	C	-3.750818	5.735449	0.349112
37	H	-1.942065	4.666512	0.455284	H	-1.907093	4.627972	0.158238
38	C	-5.702525	4.355985	0.860606	C	-5.681506	4.347718	0.705758
39	C	-5.153774	5.633522	0.851702	C	-5.127122	5.626761	0.547879
40	H	-3.300190	6.720882	0.691000	H	-3.279407	6.710406	0.220822
41	H	-6.774223	4.220590	0.971283	H	-6.757406	4.228213	0.862692
42	H	-5.786428	6.505046	0.955163	H	-5.765413	6.509927	0.580971

Table 24
Molecular system 23: Cartesian coordinates of the optimized molecular structure at ground and excited states.

	Ground state geometry				Excited state geometry			
No.	Atom	X	Y	Z	Atom	X	Y	Z
1	C	-2.556131	-1.174558	-0.008077	C	-2.265043	-0.909331	-1.152906
2	C	-1.150948	-1.404143	0.231080	C	-0.838073	-1.022159	-0.930411
3	C	-0.212581	-0.337805	0.028465	C	-0.235825	-0.079901	-0.081033
4	C	-1.990166	1.035667	-0.601236	C	-2.216853	1.005121	0.314197
5	C	-3.002837	0.107769	-0.438400	C	-2.981849	0.131759	-0.491644
6	H	-2.238155	2.029603	-0.957355	H	-2.714206	1.849428	0.798998
7	N	-0.678049	0.833937	-0.380548	N	-0.899394	0.926837	0.522482
8	N	-0.885969	-2.643986	0.645718	N	-0.230405	-2.052594	-1.576325
9	N	-3.303967	-2.258101	0.242853	N	-2.759459	-1.859217	-1.976447
10	S	-2.296315	-3.425629	0.721235	S	-1.461704	-2.808137	-2.416091
11	C	1.214170	-0.427473	0.234420	C	1.225110	-0.124762	0.206081
12	C	2.093225	-1.423864	0.646222	C	1.915172	-0.761635	1.223204
13	C	3.460692	-1.003251	0.694626	C	3.325799	-0.579935	1.233698
14	C	3.624727	0.324444	0.315381	C	3.742877	0.245766	0.154462
15	C	3.685292	-3.186874	1.378394	C	3.017642	-1.931118	3.076926
16	C	4.352028	-2.040416	1.119760	C	3.951923	-1.258282	2.304674
17	H	4.105897	-4.123322	1.713090	H	3.219875	-2.533453	3.960033
18	H	5.417353	-1.905944	1.216280	H	5.021589	-1.255657	2.498880
19	S	2.107534	1.035654	-0.092218	S	2.353354	0.733627	-0.789707
20	S	1.959609	-3.094232	1.130307	S	1.396530	-1.765166	2.538872
21	C	-4.412811	0.446892	-0.693380	C	-4.434932	0.330062	-0.619674
22	C	-4.926466	1.705149	-0.364770	C	-5.194332	0.890914	0.424111
23	C	-5.298001	-0.457767	-1.299477	C	-5.144303	-0.010279	-1.793981
24	C	-6.248946	2.001036	-0.653873	C	-6.559936	1.098317	0.254210
25	H	-4.300502	2.435400	0.133085	H	-4.717404	1.139593	1.374005
26	N	-6.568023	-0.181899	-1.580090	N	-6.456943	0.187883	-1.970720
27	H	-4.953884	-1.447378	-1.573375	H	-4.608556	-0.471380	-2.625371
28	C	-7.031682	1.026660	-1.260880	C	-7.146569	0.735701	-0.959151
29	H	-6.671299	2.965429	-0.402443	H	-7.165943	1.524692	1.055971
30	H	-8.073018	1.221169	-1.496775	H	-8.218132	0.884036	-1.127299
31	C	4.860524	1.064899	0.250087	C	5.062746	0.643430	-0.154895
32	S	4.937900	2.739019	-0.269825	S	5.447936	1.680053	-1.540526
33	C	7.024237	1.486328	0.413017	C	7.259700	0.811817	0.024984
34	C	6.636673	2.716810	-0.029277	C	7.092260	1.597258	-1.111763
35	H	8.043432	1.207624	0.641036	H	8.224144	0.610601	0.490358
36	H	7.244552	3.585465	-0.220710	H	7.855086	2.110282	-1.690698
37	N	6.031905	0.567687	0.567654	N	6.138116	0.285829	0.552498

Table 25
Molecular system 24: Cartesian coordinates of the optimized molecular structure at ground and excited states.

	Ground state geometry				Excited state geometry			
No.	Atom	X	Y	Z	Atom	X	Y	Z
1	C	4.873905	-0.655688	-0.101052	C	4.898684	-0.683838	-0.059567
2	C	6.279343	-0.912075	0.109558	C	6.312620	-0.909377	0.129589
3	C	6.905976	-0.527526	1.331581	C	6.967259	-0.484726	1.304645
4	C	6.146887	0.080136	2.275607	C	6.187967	0.154950	2.261756
5	C	4.749133	0.324367	2.077632	C	4.804656	0.356991	2.094572
6	C	4.099986	-0.018333	0.927970	C	4.105624	-0.042932	0.940484
7	C	4.596749	-1.113373	-1.360009	C	4.609331	-1.168315	-1.332609
8	C	6.726375	-1.507537	-1.036092	C	6.756312	-1.532925	-1.033088
9	H	7.958547	-0.718762	1.494006	H	8.033996	-0.648055	1.453530
10	H	6.590940	0.380919	3.215372	H	6.653559	0.496749	3.187189
11	H	4.183823	0.774375	2.884049	H	4.241930	0.821959	2.903968
12	H	3.714007	-1.135335	-1.972841	H	3.707067	-1.199049	-1.933411
13	H	7.682782	-1.879261	-1.358469	H	7.720819	-1.900697	-1.366602
14	O	5.712958	-1.624507	-1.910351	O	5.725626	-1.685102	-1.907631
15	C	2.676957	0.265511	0.762565	C	2.683592	0.216136	0.794367
16	C	1.973208	1.337157	1.236213	C	1.978974	1.300723	1.277079
17	N	0.638015	1.346010	0.984400	N	0.648958	1.348056	1.002013
18	H	2.421726	2.164891	1.767104	H	2.437180	2.130130	1.818079
19	C	0.280226	0.293714	0.308745	C	0.255184	0.289927	0.314991
20	S	1.583243	-0.785687	-0.057720	S	1.568177	-0.834907	-0.047518
21	C	-1.083655	0.025744	-0.099658	C	-1.097781	0.018841	-0.100541
22	C	-1.564305	-1.031249	-0.831309	C	-1.578107	-1.031938	-0.860188
23	S	-2.328265	1.113005	0.353741	S	-2.380258	1.101833	0.369574
24	C	-2.957152	-0.960582	-1.029027	C	-2.977092	-0.972711	-1.062970
25	H	-0.938145	-1.827506	-1.210116	H	-0.943903	-1.823943	-1.262748
26	C	-3.513338	0.150764	-0.441844	C	-3.551217	0.132616	-0.454508
27	H	-3.533638	-1.689925	-1.575334	H	-3.570972	-1.689382	-1.625594
28	C	-4.900082	0.592331	-0.402031	C	-4.956390	0.576953	-0.414156
29	C	-5.970323	-0.128825	-1.036883	C	-6.002182	-0.123014	-1.061096
30	C	-7.302346	0.382331	-0.935468	C	-7.339945	0.399543	-0.954196
31	C	-6.440647	2.170518	0.335463	C	-6.436268	2.179561	0.378342
32	C	-7.535440	1.579386	-0.217748	C	-7.544732	1.583711	-0.210456
33	H	-6.541357	3.090188	0.898690	H	-6.550106	3.097340	0.961861
34	H	-8.528767	1.991673	-0.120250	H	-8.542818	2.010670	-0.105848
35	N	-5.168173	1.695928	0.247500	N	-5.179663	1.700340	0.285713
36	N	-5.899384	-1.259966	-1.741213	N	-5.902667	-1.271068	-1.799354
37	N	-8.200016	-0.380559	-1.567165	N	-8.285398	-0.325426	-1.600006
38	S	-7.389752	-1.602256	-2.205619	S	-7.458013	-1.589623	-2.285666

Table 26
Molecular system 25: Cartesian coordinates of the optimized molecular structure at ground and excited states.

	Ground state geometry				Excited state geometry			
No.	Atom	X	Y	Z	Atom	X	Y	Z
1	C	3.284342	0.376354	-0.816108	C	3.317200	-0.065229	-0.915416
2	C	2.653923	-0.874152	-0.891077	C	2.630311	-1.277593	-0.953714
3	C	1.321429	-0.988514	-0.555282	C	1.285443	-1.298852	-0.593638
4	H	3.191347	-1.757110	-1.205463	H	3.144279	-2.189307	-1.261000
5	C	1.324840	1.345472	-0.097749	C	1.370850	1.064615	-0.180041
6	C	0.603834	0.140976	-0.141427	C	0.607581	-0.131474	-0.194302
7	H	0.816226	-1.942593	-0.605556	H	0.710498	-2.224796	-0.608974
8	H	0.840459	2.260065	0.213348	H	0.925192	2.014377	0.116000
9	C	-0.820127	0.006349	0.217823	C	-0.819002	-0.173309	0.184910
10	C	-1.677116	1.082591	0.633600	C	-1.568587	0.956119	0.596723

(*continued on next page*)

Table 26 (*continued*)

	Ground state geometry				Excited state geometry			
No.	Atom	X	Y	Z	Atom	X	Y	Z
11	C	-3.056791	0.808097	0.959194	C	-2.950859	0.771605	0.938462
12	C	-2.635269	-1.452053	0.454016	C	-2.666354	-1.560614	0.431479
13	C	-3.572854	-0.519796	0.871856	C	-3.533532	-0.528552	0.858249
14	H	-2.930323	-2.489736	0.350964	H	-3.053954	-2.579845	0.349053
15	S	-2.696920	3.144821	1.255472	S	-2.453699	3.121454	1.236085
16	N	-1.369461	2.380356	0.768922	N	-1.135060	2.248409	0.717282
17	N	-3.733659	1.906907	1.326932	N	-3.592408	1.906470	1.321585
18	N	-1.350075	-1.202011	0.150382	N	-1.386321	-1.398977	0.112998
19	N	2.606762	1.457785	-0.420373	N	2.641727	1.031463	-0.529992
20	C	4.724011	0.563713	-1.168716	C	4.690925	0.283001	-1.221442
21	C	5.516917	-0.498435	-1.623710	C	5.758166	-0.508681	-1.656494
22	N	5.228946	1.795974	-1.031881	N	4.888290	1.605325	-1.028660
23	C	6.847778	-0.270596	-1.937645	C	6.995504	0.097201	-1.876999
24	H	5.109432	-1.492311	-1.737032	H	5.613805	-1.576629	-1.816524
25	C	6.503856	2.003687	-1.335100	C	6.048473	2.204333	-1.229591
26	C	7.362586	1.009240	-1.792752	C	7.157022	1.466541	-1.665432
27	H	7.471028	-1.082996	-2.290981	H	7.839508	-0.504767	-2.216460
28	H	6.863545	3.020611	-1.206562	H	6.093797	3.278374	-1.041797
29	H	8.395090	1.235339	-2.025326	H	8.109928	1.966254	-1.828938
30	C	-4.938917	-0.871283	1.185063	C	-4.912075	-0.781293	1.189412
31	C	-5.588119	-2.103139	1.169998	C	-5.682152	-1.956708	1.185178
32	N	-5.873415	0.060720	1.580877	N	-5.747505	0.237209	1.606498
33	C	-6.924287	-1.892183	1.562042	C	-6.984752	-1.616549	1.606295
34	H	-5.143845	-3.048428	0.906110	H	-5.331325	-2.945633	0.907002
35	C	-7.070739	-0.541648	1.810942	C	-6.994637	-0.246622	1.860875
36	H	-5.659210	1.041574	1.680119	H	-5.390993	1.196740	1.684890
37	H	-7.696052	-2.638269	1.654340	H	-7.831098	-2.287891	1.715873
38	H	-7.929170	0.024623	2.130741	H	-7.794185	0.403830	2.200568

Table 27
Molecular system 26: Cartesian coordinates of the optimized molecular structure at ground and excited states.

	Ground state geometry				Excited state geometry			
No.	Atom	X	Y	Z	Atom	X	Y	Z
1	C	0.508377	-0.126563	0.644344	C	0.490607	0.081645	0.738669
2	C	1.948117	0.008690	0.722265	C	1.946120	0.121897	0.764147
3	C	2.684257	0.678307	-0.300517	C	2.671495	0.683499	-0.323438
4	C	0.524430	1.050621	-1.414376	C	0.501801	1.079401	-1.430796
5	C	-0.235382	0.396609	-0.462352	C	-0.272919	0.560042	-0.387523
6	H	0.034518	1.489720	-2.272560	H	0.001611	1.428621	-2.333290
7	N	2.456142	-0.517823	1.845490	N	2.474327	-0.377364	1.907286
8	N	-0.009259	-0.757172	1.703855	N	-0.034086	-0.434703	1.865566
9	S	1.219747	-1.121111	2.684943	S	1.202473	-0.829101	2.830019
10	C	-8.149375	-0.975000	0.970105	C	-8.070450	-1.395727	0.758609
11	C	-7.100002	-1.663465	1.629151	C	-6.983925	-1.969880	1.454250
12	C	-5.739342	-1.409971	1.242071	C	-5.652018	-1.520098	1.151405
13	C	-6.599294	0.140386	-0.326750	C	-6.658459	-0.031954	-0.439379
14	C	-5.471471	-0.467824	0.201038	C	-5.484082	-0.516201	0.161184
15	H	-6.482721	0.899773	-1.090007	H	-6.587017	0.752561	-1.198096
16	S	-5.715466	-3.028838	2.978751	S	-5.477761	-3.203800	2.861177
17	N	-7.216653	-2.569007	2.611524	N	-7.051219	-2.934949	2.410891
18	N	-4.857343	-2.135000	1.942669	N	-4.674958	-2.123113	1.867073
19	N	-7.887108	-0.106773	0.028547	N	-7.912191	-0.442604	-0.168225

(*continued on next page*)

Table 27 (*continued*)

	Ground state geometry				Excited state geometry			
No.	Atom	X	Y	Z	Atom	X	Y	Z
20	C	1.928219	1.183957	-1.334641	C	1.907429	1.164448	-1.380563
21	H	2.434638	1.702049	-2.139564	H	2.421105	1.601951	-2.240710
22	H	-9.184406	-1.156584	1.239518	H	-9.091289	-1.727654	0.970153
23	C	-4.137405	-0.151138	-0.289132	C	-4.172441	0.005055	-0.227601
24	C	-3.820416	0.407580	-1.512107	C	-3.887195	0.946153	-1.217402
25	S	-2.699557	-0.406932	0.645837	S	-2.713146	-0.503089	0.560868
26	C	-2.449352	0.639437	-1.679807	C	-2.519188	1.227731	-1.343805
27	H	-4.554126	0.618447	-2.276871	H	-4.654020	1.414320	-1.831033
28	C	-1.682175	0.267113	-0.590286	C	-1.719590	0.521983	-0.449689
29	H	-2.033809	1.051873	-2.587419	H	-2.125927	1.950097	-2.059551
30	C	4.149674	0.875661	-0.248841	C	4.146291	0.822267	-0.330359
31	C	5.069437	-0.226396	-0.175575	C	5.034509	-0.260892	-0.082089
32	C	4.669457	2.144054	-0.310217	C	4.748463	2.055925	-0.627811
33	C	6.494129	0.035816	-0.151182	C	6.461744	-0.082995	-0.132104
34	C	4.801009	-1.584377	-0.160136	C	4.697482	-1.593965	0.210908
35	C	6.069917	2.397169	-0.280224	C	6.141517	2.225755	-0.698849
36	H	3.990896	2.986983	-0.357590	H	4.100691	2.914714	-0.805420
37	C	6.968993	1.376451	-0.197872	C	7.017653	1.174360	-0.445891
38	C	7.238259	-1.131237	-0.102321	C	7.144318	-1.280506	0.142180
39	H	3.843882	-2.076833	-0.164958	H	3.701218	-2.010917	0.316771
40	H	6.414151	3.423329	-0.316830	H	6.541791	3.209852	-0.945995
41	H	8.034101	1.571183	-0.171847	H	8.097718	1.313886	-0.489936
42	H	8.310896	-1.233914	-0.077353	H	8.219944	-1.434944	0.181883
43	S	6.231415	-2.499250	-0.098770	S	6.071576	-2.581706	0.436511

Table 28
Molecular system 27: Cartesian coordinates of the optimized molecular structure at ground and excited states.

	Ground state geometry				Excited state geometry			
No.	Atom	X	Y	Z	Atom	X	Y	Z
1	C	-6.505023	3.334368	2.605318	C	-6.560963	3.709026	2.008821
2	C	-5.846273	4.287232	1.792166	C	-5.366409	4.183173	2.580756
3	C	-4.601278	3.945331	1.149491	C	-4.108825	3.642872	2.121709
4	C	-4.823070	1.820857	2.171706	C	-5.431399	2.269677	0.617667
5	C	-4.049821	2.635225	1.349187	C	-4.171156	2.654476	1.105820
6	H	-4.491298	0.809572	2.376349	H	-5.489370	1.507488	-0.167271
7	S	-5.150908	6.187664	0.565307	S	-3.601217	5.270507	3.819059
8	N	-6.259685	5.535984	1.534283	N	-5.241893	5.127397	3.556246
9	N	-4.112749	4.957653	0.421900	N	-3.006492	4.145107	2.712779
10	N	-5.990708	2.144146	2.775066	N	-6.598117	2.767944	1.041785
11	C	-0.812409	0.603351	0.224963	C	-0.895980	0.561606	0.103420
12	C	-0.795101	1.839908	-0.369142	C	-1.037480	1.662795	-0.751885
13	C	-1.871587	2.721556	-0.090764	C	-2.149715	2.494883	-0.519732
14	C	-2.804556	2.157802	0.774790	C	-2.938560	2.068965	0.550662
15	C	-0.407303	3.667141	-1.487066	C	-0.960187	3.273164	-2.233481
16	C	-1.571342	3.912075	-0.851151	C	-2.073607	3.540946	-1.502653
17	H	0.187397	4.266960	-2.155350	H	-0.485467	3.768623	-3.073229
18	H	-2.148437	4.815025	-0.903795	H	-2.750125	4.378024	-1.636697
19	S	-2.260068	0.540827	1.188826	S	-2.250651	0.635581	1.231394
20	O	0.101770	2.415031	-1.221407	O	-0.298704	2.119411	-1.795574
21	H	-7.440872	3.577199	3.096493	H	-7.520812	4.106483	2.350067
22	C	0.120322	-0.504617	0.147014	C	0.088786	-0.463676	0.143823
23	C	1.286811	-0.425024	-0.634666	C	1.167361	-0.488747	-0.800479
24	C	-0.076151	-1.710694	0.836239	C	0.074883	-1.511253	1.100389
25	N	2.177272	-1.398592	-0.747387	N	2.116157	-1.405606	-0.828112

(*continued on next page*)

Table 28 (*continued*)

	Ground state geometry				Excited state geometry		
No.	Atom	X	Y	Z	Atom	X	Y	Z
26	H	1.500962	0.478082	-1.193202	H	1.230210	0.294644	-1.559637
27	C	0.845256	-2.728804	0.724164	C	1.061368	-2.471602	1.077582
28	H	-0.951089	-1.850760	1.459449	H	-0.713911	-1.554142	1.852728
29	C	1.979932	-2.550902	-0.082910	C	2.083462	-2.404385	0.098289
30	H	0.689436	-3.657201	1.257908	H	1.052902	-3.277579	1.813602
31	C	2.998386	-3.578493	-0.251986	C	3.146027	-3.368548	0.010529
32	C	4.145647	-3.532582	-1.000432	C	4.208670	-3.424772	-0.884662
33	C	4.840307	-2.547369	-1.897648	C	4.721381	-2.630072	-2.045059
34	C	4.922297	-4.727786	-0.937500	C	5.071984	-4.528982	-0.670126
35	C	4.370247	-5.691039	-0.140102	C	4.674124	-5.331356	0.396985
36	C	6.071810	-3.320261	-2.318412	C	5.950276	-3.405800	-2.447155
37	H	5.086163	-1.615740	-1.378645	H	4.947698	-1.585502	-1.771084
38	H	4.218877	-2.252044	-2.748739	H	3.981757	-2.551986	-2.860115
39	C	6.105966	-4.547005	-1.771076	C	6.140857	-4.490796	-1.652979
40	H	6.821163	-2.911232	-2.982639	H	6.590963	-3.111079	-3.277097
41	H	6.880977	-5.285896	-1.918948	H	6.951974	-5.211823	-1.732649
42	S	2.888450	-5.136207	0.540946	S	3.249325	-4.731589	1.130870
43	H	4.730281	-6.680742	0.091399	H	5.140875	-6.233495	0.784695

Table 29
Molecular system 28: Cartesian coordinates of the optimized molecular structure at ground and excited states.

	Ground state geometry				Excited state geometry		
No.	Atom	X	Y	Z	Atom	X	Y	Z
1	C	-3.956467	1.291876	1.668732	C	-3.919214	1.301850	1.646445
2	C	-4.523958	2.573672	2.004362	C	-4.482314	2.586503	1.983515
3	C	-5.866342	2.625553	2.532473	C	-5.829024	2.637587	2.516321
4	C	-5.947261	0.274283	2.356469	C	-5.909875	0.267944	2.331855
5	C	-6.592417	1.428885	2.709557	C	-6.556136	1.440162	2.692122
6	H	-6.444574	-0.683094	2.466126	H	-6.420732	-0.692234	2.444197
7	S	-5.054095	4.852912	2.415541	S	-5.014094	4.873662	2.400239
8	N	-3.963437	3.782041	1.894434	N	-3.908119	3.798067	1.868419
9	N	-6.277704	3.872363	2.804430	N	-6.249292	3.891975	2.795538
10	N	-4.690243	0.207387	1.859978	N	-4.658804	0.193571	1.835176
11	C	0.259520	-1.248232	-0.214863	C	0.241415	-1.302209	-0.212565
12	C	0.027292	-2.609127	-0.259641	C	-0.003366	-2.678612	-0.240413
13	C	2.081154	-2.665843	-1.059005	C	2.051243	-2.736192	-1.047108
14	N	1.031539	-3.382091	-0.724456	N	0.984598	-3.468660	-0.696554
15	H	-0.896923	-3.077231	0.050393	H	-0.941033	-3.134221	0.084562
16	S	1.870061	-0.949707	-0.806444	S	1.864222	-1.006717	-0.819064
17	C	-2.627296	1.070623	1.128123	C	-2.606038	1.072104	1.112521
18	C	-1.568396	1.880394	0.780320	C	-1.521988	1.868922	0.760649
19	C	-0.447041	1.161732	0.276038	C	-0.419205	1.131873	0.263717
20	C	-0.629334	-0.209099	0.229341	C	-0.634305	-0.270880	0.221804
21	C	0.173250	3.355035	0.216071	C	0.242744	3.311664	0.200519
22	C	0.604604	2.113155	-0.059604	C	0.653179	2.043031	-0.073745
23	H	0.740604	4.263577	0.068494	H	0.833519	4.214155	0.050887
24	H	1.573581	1.861824	-0.464393	H	1.623453	1.762499	-0.478314
25	S	-2.218063	-0.609114	0.822762	S	-2.233231	-0.636163	0.813444
26	H	-7.598908	1.432997	3.102363	H	-7.569968	1.444621	3.089855
27	C	-1.228915	3.349411	0.770455	C	-1.156298	3.326898	0.748439
28	H	-1.282233	3.795153	1.766920	H	-1.213136	3.783907	1.750369
29	H	-1.919930	3.931779	0.155708	H	-1.845024	3.928799	0.132421
30	C	3.284772	-3.243923	-1.583616	C	3.256544	-3.285162	-1.566734
31	C	4.475223	-2.631518	-1.980426	C	4.413251	-2.608613	-1.957236
32	C	5.457235	-3.571064	-2.457419	C	5.429591	-3.495086	-2.433458

(*continued on next page*)

Table 29 (*continued*)

	Ground state geometry				Excited state geometry		
No.	Atom	X	Y	Z	Atom	X	Y	Z
33	C	4.998719	-4.875438	-2.415412	C	4.992725	-4.835819	-2.383626
34	C	5.912284	-0.939270	-2.359814	C	5.788669	-0.858858	-2.336442
35	H	5.525731	-5.767612	-2.711522	H	5.567184	-5.708770	-2.686393
36	C	6.888795	-1.872567	-2.834018	C	6.783060	-1.731177	-2.802773
37	H	6.152133	0.119579	-2.342454	H	5.993316	0.216704	-2.319517
38	H	7.854191	-1.504116	-3.168578	H	7.738924	-1.319785	-3.138593
39	N	4.728134	-1.298284	-1.939753	N	4.571594	-1.242197	-1.896196
40	N	6.682818	-3.160150	-2.888344	N	6.646926	-3.078277	-2.870873
41	S	3.411895	-4.946746	-1.809328	S	3.415039	-5.006866	-1.783409

Table 30
Molecular system 29: Cartesian coordinates of the optimized molecular structure at ground and excited states.

	Ground state geometry				Excited state geometry		
No.	Atom	X	Y	Z	Atom	X	Y	Z
1	C	-0.240416	2.508444	-0.344980	C	-0.675430	2.348670	-0.191083
2	C	-0.128482	1.158070	-0.850330	C	-0.532998	0.975084	-0.643622
3	C	-0.125421	0.038085	0.041499	C	0.011562	-0.006016	0.227834
4	C	-0.435161	1.646250	1.868311	C	0.235863	1.736835	1.929324
5	C	-0.368883	2.752763	1.054611	C	-0.248685	2.751550	1.115384
6	H	-0.566594	1.796440	2.931808	H	0.520232	2.002054	2.947424
7	N	-0.109191	1.101331	-2.186456	N	-1.002675	0.743185	-1.888935
8	N	-0.298669	3.424653	-1.320234	N	-1.293518	3.121387	-1.110512
9	S	-0.211538	2.619613	-2.715478	S	-1.593826	2.185773	-2.389740
10	C	-0.480871	4.108781	1.632082	C	-0.355889	4.136351	1.637708
11	C	0.426464	5.167273	1.295626	C	0.086216	5.268046	0.908903
12	C	0.248183	6.458770	1.901605	C	-0.033588	6.569844	1.536876
13	C	-1.575282	5.546157	3.096799	C	-0.936266	5.442500	3.459672
14	C	-0.805857	6.642786	2.823612	C	-0.576356	6.637671	2.837181
15	H	-2.386852	5.614079	3.812086	H	-1.342768	5.462903	4.476070
16	S	2.164062	6.570261	0.512630	S	0.992303	6.900804	-0.612945
17	N	1.497978	5.104594	0.494805	N	0.674697	5.292160	-0.316159
18	N	1.173583	7.353222	1.522091	N	0.425687	7.599905	0.792263
19	N	-1.422021	4.318860	2.524375	N	-0.822468	4.224917	2.907053
20	C	-0.305704	0.326870	1.379261	C	0.363769	0.392598	1.505927
21	H	-0.313498	-0.486469	2.094119	H	0.768742	-0.341104	2.206683
22	C	-0.793570	-5.173125	-0.693588	C	-0.918750	-5.065349	-0.985483
23	C	-1.571991	-5.806254	0.241447	C	-2.178368	-5.535863	-0.564351
24	C	-1.755135	-7.140572	-0.216544	C	-2.267586	-6.872041	-0.971606
25	H	-1.948331	-5.374158	1.153920	H	-2.925837	-4.957361	-0.030486
26	C	-1.077466	-7.232757	-1.389898	C	-1.076028	-7.158817	-1.615444
27	H	-2.308515	-7.927775	0.267430	H	-3.095514	-7.556719	-0.822493
28	C	0.940669	-1.881196	-1.325016	C	1.225169	-2.000419	-0.958145
29	C	2.752407	-1.920774	-2.666584	C	3.248437	-2.100062	-1.939750
30	C	0.766461	-3.298757	-1.525398	C	0.984144	-3.365461	-1.306298
31	C	0.013913	-1.329173	-0.443929	C	0.149731	-1.390394	-0.251426
32	C	2.564051	-3.322299	-2.885528	C	3.006040	-3.459506	-2.290922
33	H	3.587362	-1.414938	-3.143213	H	4.192162	-1.623935	-2.219199
34	C	-0.298388	-3.827829	-0.788208	C	-0.293876	-3.814874	-0.857225
35	H	3.251752	-3.857673	-3.533907	H	3.766369	-4.020972	-2.841811
36	S	-1.052147	-2.565126	0.100816	S	-1.113178	-2.509981	-0.039875
37	H	-0.977662	7.598505	3.298562	H	-0.687006	7.596531	3.344878
38	N	1.973890	-1.207920	-1.902691	N	2.373309	-1.363381	-1.275501
39	N	1.605839	-4.008056	-2.326498	N	1.891604	-4.108068	-1.984027
40	O	-0.490191	-6.049371	-1.695975	O	-0.254708	-6.085075	-1.632303
41	H	-0.918778	-8.031583	-2.093041	H	-0.690718	-8.053369	-2.093842

Table 31
Molecular system 30: Cartesian coordinates of the optimized molecular structure at ground and excited states.

	Ground state geometry				Excited state geometry			
No.	Atom	X	Y	Z	Atom	X	Y	Z
1	C	-2.781485	-1.002420	0.612715	C	-2.784046	-0.968408	1.104864
2	C	-1.341359	-0.998580	0.596308	C	-1.336281	-0.951501	1.049794
3	C	-0.644452	0.137375	0.076082	C	-0.678780	0.046363	0.267662
4	C	-2.692336	1.164178	-0.320703	C	-2.723504	1.023284	-0.263836
5	C	-3.499595	0.125783	0.113557	C	-3.483422	0.036966	0.389237
6	H	-3.153440	2.061756	-0.717232	H	-3.238094	1.844114	-0.777005
7	S	-2.038781	-3.005801	1.643750	S	-2.006538	-2.746786	2.515860
8	N	-3.293478	-2.100894	1.181391	N	-3.321606	-1.934186	1.870672
9	N	-0.807450	-2.084862	1.168969	N	-0.766288	-1.897474	1.830714
10	N	-1.339907	1.177636	-0.330432	N	-1.395636	1.041981	-0.328018
11	C	0.828009	0.229360	0.031754	C	0.776990	0.136628	0.127974
12	C	1.662125	-0.801329	-0.493765	C	1.644846	-0.987420	-0.071769
13	C	1.466160	1.364168	0.472092	C	1.402902	1.381601	0.143984
14	C	3.102726	-0.653710	-0.503838	C	3.091000	-0.816511	-0.149657
15	C	2.873207	1.503613	0.468208	C	2.800121	1.542151	0.068671
16	H	0.863761	2.177154	0.855754	H	0.770692	2.263230	0.255249
17	C	3.729523	0.528795	0.004006	C	3.693054	0.479915	-0.056411
18	H	3.291958	2.413662	0.878344	H	3.203782	2.552828	0.156995
19	N	1.250131	-1.935063	-1.074815	N	1.250362	-2.257863	-0.291881
20	N	3.723290	-1.695129	-1.076957	N	3.748172	-1.974566	-0.388690
21	S	2.573802	-2.721801	-1.550853	S	2.603396	-3.123763	-0.521227
22	C	5.195274	0.717390	0.016578	C	5.151602	0.700463	-0.111424
23	C	6.068462	-0.327839	0.341876	C	6.062839	-0.209659	0.458668
24	C	5.744126	1.972667	-0.276308	C	5.673763	1.858484	-0.721198
25	C	7.439894	-0.117088	0.388390	C	7.434413	0.039731	0.432984
26	H	5.669234	-1.306841	0.564480	H	5.685727	-1.117667	0.927134
27	C	7.116055	2.179772	-0.236428	C	7.045462	2.104860	-0.748607
28	H	5.090044	2.786388	-0.563442	H	4.992028	2.561087	-1.204205
29	C	7.970355	1.135506	0.099818	C	7.934979	1.197306	-0.168107
30	H	8.097202	-0.936866	0.650998	H	8.118899	-0.678129	0.889445
31	H	7.518302	3.156210	-0.476885	H	7.422531	3.006164	-1.236160
32	H	9.041064	1.295054	0.130609	H	9.009616	1.387140	-0.190803
33	C	-4.952001	0.213763	0.088803	C	-4.949043	0.065914	0.384744
34	C	-5.935433	-0.734914	-0.123019	C	-5.864823	-0.503681	-0.474803
35	C	-7.268740	-0.201743	-0.164587	C	-7.241046	-0.286825	-0.171488
36	C	-7.293261	1.155409	0.049943	C	-7.387837	0.494686	0.983397
37	C	-7.691186	-2.423322	-0.629813	C	-7.382678	-1.592326	-2.083251
38	C	-8.253402	-1.208914	-0.451819	C	-8.103238	-0.916948	-1.101828
39	H	-8.198587	-3.349517	-0.853859	H	-7.793752	-2.159656	-2.915103
40	H	-9.315134	-1.020721	-0.522165	H	-9.191199	-0.892874	-1.072690
41	S	-5.952891	-2.452312	-0.436493	S	-5.686977	-1.484426	-1.902970
42	S	-5.716969	1.768460	0.281834	S	-5.868879	0.919422	1.637961
43	H	-8.144815	1.815568	0.087154	H	-8.313506	0.816352	1.455119

Table 32
Molecular system 31: Cartesian coordinates of the optimized molecular structure at ground and excited states.

No.	Ground state geometry				Excited state geometry			
	Atom	X	Y	Z	Atom	X	Y	Z
1	C	-1.047881	-1.082317	-0.876364	C	-0.959303	-0.596600	-1.162635
2	C	-2.489665	-1.050486	-0.902082	C	-2.411133	-0.606461	-1.258894
3	C	-3.177153	-0.056219	-0.129495	C	-3.173759	-0.082329	-0.165510
4	C	-1.125168	0.796153	0.560718	C	-1.220758	0.422486	1.013062
5	C	-0.333556	-0.134817	-0.083814	C	-0.368671	-0.070107	0.011469
6	H	-0.656254	1.559253	1.172458	H	-0.789856	0.839357	1.930822
7	S	-1.774328	-2.734638	-2.405203	S	-1.503966	-1.552956	-3.291645

(*continued on next page*)

Table 32 (*continued*)

No.	Ground state geometry				Excited state geometry			
	Atom	X	Y	Z	Atom	X	Y	Z
8	N	-0.524790	-2.001193	-1.696211	N	-0.297634	-1.090632	-2.223159
9	N	-3.014708	-1.952895	-1.743279	N	-2.850015	-1.130016	-2.428216
10	N	-2.475771	0.835831	0.536342	N	-2.543941	0.418859	0.938282
11	C	2.010234	-1.158743	0.258239	C	1.978543	-1.028239	0.680685
12	C	2.667245	-3.261532	0.743812	C	2.571833	-2.968748	1.660274
13	C	3.383745	-0.729292	0.294602	C	3.353682	-0.656242	0.596714
14	C	4.035595	-2.842015	0.740488	C	3.944079	-2.599277	1.569483
15	H	2.430794	-4.300616	0.954248	H	2.296981	-3.928009	2.107627
16	H	4.819630	-3.569231	0.929135	H	4.717499	-3.276055	1.944177
17	S	2.001063	1.350636	-0.168474	S	1.991666	1.281473	-0.432792
18	C	-4.654733	0.040857	-0.046202	C	-4.645341	-0.030660	-0.124729
19	C	-5.256110	1.275012	0.225027	C	-5.296865	0.495197	1.016742
20	C	-6.687041	-1.007395	-0.120812	C	-6.678655	-0.437776	-1.134569
21	C	-6.637016	1.338057	0.311539	C	-6.683479	0.539511	1.047360
22	H	-4.637153	2.149270	0.364879	H	-4.689808	0.853282	1.846837
23	C	-7.374846	0.173964	0.134628	C	-7.405332	0.063070	-0.052090
24	H	-7.226627	-1.939876	-0.254555	H	-7.202461	-0.821666	-2.017808
25	H	-7.130813	2.280808	0.513241	H	-7.201555	0.941644	1.921045
26	H	-8.455505	0.176330	0.194332	H	-8.496277	0.078090	-0.071861
27	C	1.118691	-0.119316	0.008631	C	1.090989	-0.049339	0.142527
28	C	3.550990	0.641997	0.080754	C	3.549979	0.620741	-0.001279
29	N	1.671007	-2.452324	0.514085	N	1.585007	-2.199065	1.226978
30	N	4.394219	-1.604799	0.531069	N	4.351391	-1.449768	1.047325
31	N	-5.362982	-1.080858	-0.213745	N	-5.345486	-0.490310	-1.185966
32	C	4.758656	1.425132	0.040948	C	4.758549	1.298624	-0.242304
33	C	4.870732	2.789251	-0.144058	C	4.932747	2.567579	-0.841581
34	S	6.340735	0.715631	0.223562	S	6.318986	0.611012	0.195739
35	C	6.204524	3.252004	-0.141227	C	6.269316	2.950610	-0.933892
36	H	4.015360	3.437886	-0.276716	H	4.094900	3.168209	-1.192702
37	C	7.105424	2.241174	0.046622	C	7.130487	1.988247	-0.410799
38	H	6.482850	4.288189	-0.271241	H	6.611875	3.889451	-1.364263
39	H	8.180603	2.311129	0.094116	H	8.215785	2.036811	-0.360455

Table 33
Molecular system 32: Cartesian coordinates of the optimized molecular structure at ground and excited states.

No.	Ground state geometry				Excited state geometry			
	Atom	X	Y	Z	Atom	X	Y	Z
1	C	-2.528786	0.198152	-0.018322	C	-2.569932	0.177286	-0.577759
2	C	-1.099576	0.373502	0.040502	C	-1.142401	0.364750	-0.498409
3	C	-0.237589	-0.763876	-0.099596	C	-0.320754	-0.702608	-0.081046
4	C	-2.119697	-2.103476	-0.321725	C	-2.157729	-2.065300	0.177716
5	C	-3.071433	-1.104352	-0.218862	C	-3.104425	-1.102163	-0.244814
6	H	-2.448812	-3.129976	-0.438729	H	-2.523109	-3.045551	0.498363
7	S	-2.087952	2.516116	0.290582	S	-2.092753	2.445719	-1.261088
8	N	-3.194224	1.356580	0.110355	N	-3.241262	1.277057	-0.997010
9	N	-0.730624	1.646385	0.215475	N	-0.708484	1.600898	-0.856147
10	N	-0.779706	-1.951370	-0.271731	N	-0.837512	-1.902163	0.263634
11	C	-4.514198	-1.393864	-0.314342	C	-4.536378	-1.439535	-0.310986
12	C	-4.977407	-2.373840	-1.202901	C	-4.952709	-2.765654	-0.557485
13	C	-5.452133	-0.726000	0.483732	C	-5.539257	-0.465700	-0.121594
14	C	-6.327907	-2.683503	-1.282894	C	-6.303393	-3.106276	-0.593131
15	H	-4.275603	-2.879608	-1.853846	H	-4.204187	-3.535169	-0.752622
16	C	-6.801534	-1.041799	0.405823	C	-6.889757	-0.810588	-0.155021

(*continued on next page*)

Table 33 (*continued*)

No.	Ground state geometry				Excited state geometry			
	Atom	X	Y	Z	Atom	X	Y	Z
17	H	-5.120754	0.039418	1.170665	H	-5.243477	0.569172	0.043850
18	C	-7.246160	-2.020739	-0.476118	C	-7.282804	-2.130982	-0.387163
19	H	-6.664064	-3.436634	-1.984811	H	-6.593293	-4.139628	-0.795037
20	H	-7.508919	-0.520935	1.039369	H	-7.644157	-0.036169	-0.000124
21	H	-8.300304	-2.260569	-0.538875	H	-8.341303	-2.396050	-0.418835
22	C	1.220349	-0.668995	-0.063378	C	1.132845	-0.545859	-0.002375
23	C	3.588657	-0.019920	0.064898	C	3.435407	0.283948	-0.060686
24	C	3.310921	-1.361504	-0.133169	C	3.272718	-1.025475	0.332112
25	H	4.065394	-2.130945	-0.230416	H	4.085965	-1.698448	0.609733
26	N	2.012669	-1.704150	-0.202113	N	1.990768	-1.472185	0.367861
27	S	2.088965	0.837972	0.166905	S	1.892147	1.005630	-0.431477
28	C	4.868841	0.624451	0.177457	C	4.685627	1.016382	-0.186773
29	C	5.193288	1.945552	0.417380	C	5.361197	1.819966	0.709543
30	C	6.599790	2.216030	0.464545	C	6.588322	2.384826	0.253524
31	C	7.349407	1.083789	0.254850	C	6.871385	1.991895	-1.062314
32	C	5.743577	4.327906	0.856138	C	6.455898	3.224789	2.411362
33	C	6.875190	3.604202	0.719994	C	7.207572	3.190953	1.240423
34	H	5.664029	5.386464	1.051172	H	6.698894	3.765891	3.322965
35	H	7.867461	4.025232	0.796069	H	8.148408	3.725303	1.121350
36	S	6.349261	-0.283048	0.006433	S	5.650749	0.972166	-1.681549
37	S	4.267516	3.398732	0.686880	S	5.016069	2.305558	2.346197
38	H	8.422068	0.978622	0.232605	H	7.735105	2.263316	-1.665190

Table 34
Molecular system 33: Cartesian coordinates of the optimized molecular structure at ground and excited states.

No.	Ground state geometry				Excited state geometry			
	Atom	X	Y	Z	Atom	X	Y	Z
1	C	-0.001029	-0.850739	0.153016	C	0.008694	-0.794648	0.164930
2	C	0.820960	-1.992877	0.481033	C	0.789422	-1.924263	0.485352
3	C	2.244463	-1.826752	0.618386	C	2.231036	-1.768419	0.619282
4	C	1.963013	0.445280	0.122100	C	2.021839	0.494394	0.132595
5	C	0.585897	0.436271	-0.036146	C	0.633514	0.465007	-0.020389
6	H	2.504992	1.375641	-0.003378	H	2.557956	1.439443	0.000770
7	N	2.731366	-0.613621	0.427662	N	2.792480	-0.562612	0.436819
8	N	0.098010	-3.113853	0.620338	N	0.077196	-3.079921	0.638609
9	N	-1.304525	-1.154544	0.059251	N	-1.349309	-1.025922	0.055364
10	S	-1.442928	-2.737178	0.361213	S	-1.505745	-2.664022	0.371245
11	C	3.201867	-2.901982	0.957714	C	3.159878	-2.859818	0.949395
12	C	4.567393	-2.582959	1.046736	C	4.544067	-2.571512	1.035543
13	C	2.817010	-4.228875	1.199971	C	2.735253	-4.187589	1.186049
14	C	5.506160	-3.549236	1.366027	C	5.461108	-3.566850	1.343964
15	H	4.872095	-1.563461	0.860708	H	4.866217	-1.547256	0.852644
16	C	3.763930	-5.193902	1.520440	C	3.662358	-5.178793	1.495253
17	H	1.777756	-4.508939	1.139240	H	1.674401	-4.422244	1.122599
18	C	5.109998	-4.862515	1.606083	C	5.025210	-4.877424	1.575856
19	H	6.553002	-3.278002	1.428754	H	6.523722	-3.325333	1.405205
20	H	3.442972	-6.211910	1.704443	H	3.317886	-6.198561	1.675548
21	H	5.844396	-5.618043	1.856727	H	5.746671	-5.660180	1.818411
22	C	-0.172527	1.621522	-0.360747	C	-0.113538	1.659155	-0.350405
23	C	0.237500	2.936437	-0.574212	C	0.280319	3.001270	-0.578342
24	N	-1.537714	1.606039	-0.514528	N	-1.474575	1.603323	-0.497406
25	C	-0.902951	3.699868	-0.857519	C	-0.873777	3.727912	-0.861362

(*continued on next page*)

Table 34 (*continued*)

No.	Ground state geometry				Excited state geometry			
	Atom	X	Y	Z	Atom	X	Y	Z
26	H	1.250557	3.299545	-0.528314	H	1.294871	3.383839	-0.537720
27	C	-2.010302	2.854446	-0.817185	C	-1.980583	2.838826	-0.808809
28	H	-2.076260	0.759244	-0.413098	H	-1.944701	0.687775	-0.366487
29	H	-0.921984	4.755990	-1.067193	H	-0.926992	4.789038	-1.083198
30	C	-3.422248	3.131783	-1.032525	C	-3.385461	3.081713	-1.021550
31	C	-3.858459	4.428488	-1.356608	C	-3.855456	4.378534	-1.350274
32	C	-4.416626	2.151164	-0.932591	C	-4.360467	2.064918	-0.918571
33	N	-5.124414	4.764528	-1.566244	N	-5.132919	4.687671	-1.562383
34	H	-3.135953	5.232065	-1.449897	H	-3.143790	5.204100	-1.444212
35	C	-5.741682	2.493088	-1.150769	C	-5.694502	2.379807	-1.138640
36	H	-4.168140	1.126232	-0.685206	H	-4.078378	1.040628	-0.668647
37	C	-6.052100	3.810027	-1.464678	C	-6.037004	3.698229	-1.456886
38	H	-6.524646	1.749147	-1.077924	H	-6.467425	1.613527	-1.064795
39	H	-7.078848	4.112586	-1.641082	H	-7.079473	3.976257	-1.635355

Table 35
Electronic excitations giving rise the absorption spectra in OPV systems

System	Electronic transition (eV)				ΔEexc	Contribution (%)
1	HOMO -1	-5.52	LUMO +2	-2.13	3.39	68.4
2	HOMO	-4.44	LUMO +3	-1.34	3.10	68.4
3	HOMO	-4.76	LUMO +2	-0.83	3.93	46.6
4	HOMO	-4.59	LUMO +2	-1.75	2.84	63.6
5	HOMO	-4.68	LUMO +1	-2.00	2.68	92.4
6	HOMO	-5.42	LUMO +1	-1.90	3.52	90.9
7	HOMO	-5.56	LUMO +1	-2.09	3.47	66.4
8	HOMO	-5.26	LUMO +1	-2.66	2.60	80.0
9	HOMO	-5.41	LUMO	-3.30	2.11	92.8
10	HOMO	-5.16	LUMO +1	-2.47	2.69	55.2
11	HOMO	-4.89	LUMO	-3.77	1.12	91.0
12	HOMO	-5.38	LUMO	-2.84	2.54	96.8
13	HOMO	-4.97	LUMO +1	-2.38	2.59	84.7
14	HOMO	-5.63	LUMO	-3.18	2.45	93.8
15	HOMO	-5.05	LUMO +1	-2.02	3.03	73.6
16	HOMO -2	-5.84	LUMO	-2.74	3.10	41.1
17	HOMO	-4.99	LUMO	-2.70	2.29	92.4
18	HOMO	-4.86	LUMO +1	-2.44	2.42	78.0
19	HOMO	-4.99	LUMO +1	-2.50	2.49	81.9
20	HOMO	-5.41	LUMO +1	-2.47	2.94	87.3
21	HOMO	-4.99	LUMO +1	-2.49	2.50	80.6
22	HOMO -3	-6.20	LUMO +1	-3.34	2.86	44.5
23	HOMO	-5.01	LUMO	-3.68	1.33	93.2
24	HOMO	-5.01	LUMO +1	-2.72	2.29	80.4
25	HOMO	-5.09	LUMO +1	-2.45	2.64	88.8
26	HOMO -1	-5.33	LUMO	-3.60	1.73	83.5
27	HOMO	-4.94	LUMO +1	-2.74	2.20	81.4
28	HOMO	-4.92	LUMO	-3.62	1.30	92.8
29	HOMO	-5.01	LUMO +2	-3.05	1.96	52.7
30	HOMO	-5.03	LUMO	-3.51	1.52	96.7
31	HOMO	-5.04	LUMO	-3.53	1.51	71.9
32	HOMO	-4.98	LUMO +1	-2.56	2.42	79.3
33	HOMO	-4.99	LUMO +1	-2.27	2.72	90.2

Table 36
Dihedral angles $\boldsymbol{\theta}_1$, $\boldsymbol{\theta}_2$ and $\boldsymbol{\theta}_3$ in degrees (°); $\boldsymbol{\lambda}$ maximum absorption wavelength in nm; Δ is the difference between ground and excited state values.

System	Ground State				Excited State				Δ Avg	$\Delta\lambda$ Max
	θ_1	θ_2	θ_3	λ Max	θ_1	θ_2	θ_3	λ Max	Degree (°)	(nm)
1	49.7	42.9	-	337.3	40.2	41.0	-	422.5	5.7	85.2
2	43.2	37.8	40.7	375.3	35.8	15.2	76.7	336.3	2.0	-39.0
3	43.4	38.4	-	271.0	68.5	0.0	-	301.1	27.6	30.1
4	0.0	1.6	42.6	390.8	0.0	90.1	41.7	689.7	23.3	298.9
5	0.0	0.0	-	394.0	0.0	0.0	-	430.7	0.0	36.7
6	36.0	37.4	-	321.5	20.5	21.5	-	355.6	15.7	34.1
7	0.0	36.5	-	325.2	0.0	23.2	-	352.5	13.3	27.3
8	0.0	0.0	0.0	410.2	0.0	0.0	0.0	434.4	0.0	24.2
9	36.3	53.2	36.1	526.1	25.8	45.5	25.4	575.3	9.6	49.2
10	36.6	4.8	21.1	403.2	27.9	-	-	438.2	7.1	35.0
11	0.0	0.0	0.0	792.7	0.0	0.0	0.0	940.3	0.0	147.6
12	0.0	0.0	-	386.9	0.0	0.0	-	422.7	0.0	35.8
13	37.2	0.0	21.4	426.8	30.0	0.0	0.0	451.5	0.7	24.7
14	0.0	0.0	-	403.8	61.7	0.0	-	366.0	61.7	-37.8
15	0.0	0.0	-	347.0	0.0	0.0	-	366.4	0.0	19.4
16	33.9	36.8	33.8	356.4	13.7	8.3	0.0	419.2	23.8	62.8
17	35.9	0.0	31.9	455.7	24.3	0.0	12.1	512.7	15.7	57.0
18	32.6	16.4	0.0	457.5	26.1	19.8	0.0	476.6	6.6	19.1
19	32.4	15.2	0.0	446.3	25.5	91.8	0.0	415.0	34.9	-31.3
20	33.1	35.3	0.0	397.4	0.0	0.0	0.0	718.3	34.2	320.9
21	54.1	0.0	33.0	450.5	46.5	0.0	19.9	483.8	10.4	33.3
22	55.7	28.0	0.0	426.1	86.6	23.3	0.0	439.6	13.1	13.5
23	0.0	0.0	37.2	696.2	0.0	90.8	29.7	444.4	23.1	-251.8
24	35.0	0.0	0.0	481.5	34.6	0.0	0.0	540.6	0.4	59.1
25	0.0	0.0	0.0	432.2	0.0	0.0	0.0	442.4	0.0	10.2
26	21.1	6.1	57.6	630.5	0.0	18.6	51.5	736.7	6.8	106.2
27	2.5	0.2	0.2	478.4	88.8	0.0	0.0	479.3	88.8	0.9
28	0.0	0.0	0.0	756.0	0.0	0.0	0.0	500.8	0.0	-255.2
29	47.5	48.0	20.0	617.0	46.0	90.1	0.0	642.4	29.6	25.4
30	32.0	46.4	39.1	714.7	92.1	38.2	34.7	618.3	15.8	-96.4
31	26.6	47.5	0.0	694.4	0.0	91.5	0.0	475.6	54.5	-218.8
32	2.7	0.0	37.4	438.4	87.4	0.0	28.9	661.5	20.8	223.1
33	0.0	0.0	0.0	397.4	0.0	0.0	0.0	424.8	0.0	27.4

dihedral angle ϕ was evaluated by considering Eq. 1, in which ϕ stands for the dihedral angle in ground (θGrd) and excited (θExc) states.

$$cos\phi = \frac{|n_1 \cdot n_2|}{\|n_1\|\|n_2\|} \tag{1}$$

In Eq. 1, n_1 and n_2 represent normal vectors perpendicular to the planes 1 and 2, respectively (see Fig. 1 in [1]).

Ethics Statement

Not applicable.

Declaration of Competing Interest

The authors declare that they have no known competing financial interests or personal relationships which have, or could be perceived to have, influenced the work reported in this article.

Acknowledgments

The authors would like to acknowledge the financial support given by DGAPA (Dirección General de Asuntos del Personal Académico) under Project No. PAPIIT-IA102820 and PAPIIT-IN109319. C.D. wants to acknowledge the PhD. scholarships provided by Consejo Nacional de Ciencia y Tecnología (CONACYT) with No. 633818. J.M. would like to acknowledge the computational infrastructure provided by Laboratorio Nacional de Conversión y Almacenamiento de Energía (CONACYT) under project No. 270810, the Supercomputing Department of Universidad Nacional Autónoma de México for the computing resources under Project No. LANCAD-UNAM-DGTIC-370 and LANCAD-UNAM-DGTIC-310, and the support given by Fondo Sectorial de Investigación para la Educación-CONACYT under Project No. A1-S-13294.

Supplementary Materials

Supplementary material associated with this article can be found in the online version at doi:10.1016/j.dib.2021.106952.

References

[1] C. Delesma, M. Robles, C. Amador-bedolla, J. Muñiz, The role of photoisomerization in the opto-electronic properties of organic photovoltaic materials: A DFT study, J. Photochem. Photobiol. A. 409 (2021) 113155, doi:10.1016/j.jphotochem.2021.113155.
[2] J.P. Perdew, K. Burke, M. Ernzerhof, Generalized gradient approximation made simple, Phys. Rev. Lett. 77 (1996) 18, doi:10.1103/PhysRevLett.77.3865.
[3] F. Weigend, M. Häser, H. Patzelt, R. Ahlrichs, RI-MP2: optimized auxiliary basis sets and demonstration of efficiency, Chem. Phys. Lett. 294 (1998) 1, doi:10.1016/S0009-2614(98)00862-8.
[4] F. Weigend, R. Ahlrichs, Balanced basis sets of split valence, triple zeta valence and quadruple zeta valence quality for H to Rn: design and assessment of accuracy, Phys. Chem. Chem. Phys. 7 (2005) 18, doi:10.1039/B508541A.
[5] TURBOMOLE V7.3 2018, a development of University of Karlsruhe and Forschungszentrum Karlsruhe GmbH, 1989-2007, TURBOMOLE GmbH, since 2007; available from http://www.turbomole.com.
[6] C. Steffen, K. Thomas, U. Huniar, A. Hellweg, O. Rubner, A. Schroer, TmoleX—A graphical user interface for TURBOMOLE, J. Comput. Chem. 31 (2010) 16, doi:10.1002/jcc.21576.
[7] G. Rossum, Python Reference Manual, CWI (Centre for Mathematics and Computer Science), 1995 Amsterdam, The Netherlands, The Netherlands.